A NEW TAKE ON A DECADES-OLD TECHNIQUE: THE APPLICATIONS OF ^{87}Sr/^{86}Sr AND δ^2H TO ESTABLISH PATTERNS IN MIGRATION AND DISPERSAL OF TERRESTRIAL WILDLIFE SPECIES

by © Caralie Brewer

A Thesis submitted to the School of Graduate Studies in partial fulfillment of the

requirements for the degree of

Master of Science in Boreal Ecosystems and Agricultural Sciences,

School of Science and the Environment

Memorial University of Newfoundland (Grenfell Campus)

Approved by Research Advisors: Dr. Erin E. Fraser

Dr. Vaughan Grimes

March 2024

Corner Brook, Newfoundland and Labrador

TABLE OF CONTENTS

ABSTRACT

A thorough body of literature establishes the use of intrinsic marking techniques for studying continent scale, seasonal migrations of organisms. However, there is great potential for these techniques to infer movements across a smaller landscape and greater range of timescales than previously demonstrated. Here, we used multiple tissues (bones, teeth, fur) and several isotopic systems (δ^2H, δ^{34}S, ^{87}Sr/^{86}Sr) to predict seasonal and lifetime movements of *Myotis lucifugus* in Newfoundland, Canada. Using regional ^{87}Sr/^{86}Sr estimates calculated from the fur of known origin individuals, we inferred movements of unknown origin individuals relative to three geologically distinct regions. Additionally, although the δ^{34}S results were inconclusive, using a newly developed δ^2H in precipitation (δ^2H$_p$) isoscape, we determined probabilistic summer residency locations for the same individuals. These inferences and predictions, combined with the absolute difference between ^{87}Sr/^{86}Sr values of teeth and bones ($|^{87}$Sr/^{86}Sr$_T$-^{87}Sr/^{86}Sr$_B|$), provided evidence that *M. lucifugus* in Newfoundland exhibit a high rate of migratory movements within and between regions, but rarely disperse on the regional level, and don't appear to have sex-biased dispersal. Employing these results as a case study, we establish the potential for these techniques to illuminate many unanswered questions related to migratory theory and the protection of imperiled species.

Keywords: seasonal migration; dispersal; philopatry; bats; *Myotis lucifugus;* intrinsic markers; strontium isotopes; ^{87}Sr/^{86}Sr; stable hydrogen isotopes; δ^2H; stable sulfur isotopes; δ^{34}S; keratinous tissues; calciferous tissues; isoscape; probabilistic assignment; Newfoundland, Canada

GENERAL SUMMARY

Migratory organisms are notoriously difficult to study but increasingly imperiled. Intrinsic markers – chemical signatures that vary predictably across the landscape and are incorporated into the tissues of organisms – are frequently used to deduce continental-scale migrations. By combining the stable isotopes of hydrogen (δ^2H) and the radiogenic isotopes of strontium (^{87}Sr/^{86}Sr), we increased the precision with which we could predict migratory movements of little brown bats, *Myotis lucifugus*, in Newfoundland, Canada. Additionally, by comparing the ^{87}Sr/^{86}Sr values in fur, teeth, and bone of *M. lucifugus*, we inferred birthplace and compared it to habitat use during the summer preceding death. Our results showed that *M. lucifugus* in Newfoundland exhibit a high rate of migratory movements within and between regions but rarely disperse on the regional level. This study reveals the power of strontium isotope analysis for understanding the movements of modern migratory vertebrates, particularly when used in combination with other intrinsic markers.

CO-AUTHORSHIP STATEMENT

The introduction and literature review were written by me and reviewed by Dr. Erin Fraser and Dr. Vaughan Grimes. The data chapters were originally conceived by Dr. Erin Fraser and Dr. Vaughan Grimes, while I conducted all project planning, sample collection, and sample preparation for these chapters. Jessica Humber, our primary contact with the Department of Fisheries, Forestry, and Agriculture of Newfoundland and Labrador, provided the bat carcasses from which all tissue samples were extracted for this study. I performed all sample preparation and analysis for the radiogenic isotopes of strontium ($^{87}Sr/^{86}Sr$), under the advice and supervision of Dr. Vaughan Grimes; this data was then used in the data chapters. Dr. Fred Longstaffe and colleagues at the Laboratory for Stable Isotope Science at the University of Western Ontario performed all necessary pretreatment and analysis of fur samples for the stable isotopes of hydrogen (δ^2H); this data used then in the second data chapter. The strontium isoscape of Atlantic Canada used in the second data chapter was constructed by Dr. Mael Le Corre. I conducted data analysis, interpretation, and manuscript preparation for the data chapters with the collaboration of Dr. Erin Fraser and Dr. Vaughan Grimes.

ACKNOWLEDGEMENTS

LIST OF ABBREVIATIONS AND SYMBOLS

CBS	Caribou hoof standard
CV	Column Volume
CWHC	Canadian Wildlife Health Center
DI	Deionized
ECCC	Department of Environment and Climate Change Canada
g	Gram
GNIP	Global Network for Isotopes in Precipitation
H	Hydrogen
HCl	Hydrochloric acid
He	Helium
HNO_3	Nitric acid
H_2O	Water
H_2O_2	Hydrogen peroxide
IAEA	International Atomic Energy Agency
ICARUS	International Cooperation for Animal Research Using Space
IQR	Inter-Quartile Range
KHS	Kudu Horn Standard
M	Molar
MAE	Mean Absolute Error
MC-ICP-MS	Multi-Collector Inductively Coupled Plasma Mass Spectrometer
μL	Microliter

mg	Milligram
mL	Milliliter
min	Minute
MSE	Mean Squared Error
MSR	Mean Square of Regression
MUN	Memorial University of Newfoundland
n	Sample size
NIES	National Institute for Environmental Studies
NIST	National Institute of Standards and Technology
ng	Nanogram
p	p-value; Probability of obtaining observed results
PIT	Passive integrated transponder
ppb	Parts per billion
r	Pearson correlation coefficient
RMSE	Root Mean Square Error
r^2	Coefficient of determination
S	Sulfur
SD	Standard Deviation
SO_2	Sulfur dioxide
Sr	Strontium
SRM	Strontium Reference Material
TC/EA	Temperature Conversion Elemental Analyzer
TIMS	Thermal Ionization Mass Spectrometry

V	Volts
VCDT	Vienna Canyon Diablo Troilite
VSMOW	Vienna Standard Mean Ocean Water
WNS	White-nose syndrome
^{87}Sr/^{86}Sr	Ratio of ^{87}Sr to ^{86}Sr, commonly referred to as "the radiogenic isotopes of strontium"
^{87}Sr/^{86}Sr$_B$	^{87}Sr/^{86}Sr value of bone
^{87}Sr/^{86}Sr$_{bio}$	^{87}Sr/^{86}Sr value of biologically available materials
^{87}Sr/^{86}Sr$_{corr}$	^{87}Sr/^{86}Sr value corrected for analytical error
^{87}Sr/^{86}Sr$_F$	^{87}Sr/^{86}Sr value of fur
^{87}Sr/^{86}Sr$_{feather}$	^{87}Sr/^{86}Sr value of feather
^{87}Sr/^{86}Sr$_{iso}$	^{87}Sr/^{86}Sr value predicted in an isoscape
^{87}Sr/^{86}Sr$_T$	^{87}Sr/^{86}Sr value of teeth
$|^{87}$Sr/^{86}Sr$_T$-^{87}Sr/^{86}Sr$_B|$	Absolute difference of ^{87}Sr/^{86}Sr values between teeth and bone
$|^{87}$Sr/^{86}Sr$_T$-^{87}Sr/^{86}Sr$_F|$	Absolute difference of ^{87}Sr/^{86}Sr values between teeth and fur
^{88}Sr$_v$	Voltage of ^{88}Sr recorded in a sample or standard
δ^{13}C	Ratio of ^{13}C to ^{12}C relative to PeeDee Belemnite, commonly referred to as "the stable isotopes of carbon"
δ^2H	Ratio of deuterium (^{2}H) to protium (^{1}H) relative to Vienna Standard Mean Ocean Water, commonly referred to as "the stable isotopes of hydrogen"
δ^2H$_{fur}$	δ^2H value of fur
δ^2H$_p$	δ^2H value of precipitation

δ^2H_{sw}	δ^2H value of surface waters
δ^2H_{tissue}	δ^2H value of a tissue
$\delta^{15}N$	Ratio of ^{15}N to ^{14}N relative to atmosphperic N_2, commonly referred to as "the stable isotopes of nitrogen"
$\delta^{18}O$	Ratio of ^{18}O to ^{16}O relative to Vienna Standard Mean Ocean Water, commonly referred to as "the stable isotopes of oxygen"
$\delta^{34}S$	Ratio of ^{34}S to ^{32}S relative to Vienna Canyon Diablo Troilite, commonly referred to as "the stable isotopes of sulfur"
$\delta^{34}S_{fur}$	$\delta^{34}S$ value of fur
$\delta^{34}S_{iso}$	$\delta^{34}S$ value predicted in an isoscape

LIST OF TABLES

LIST OF FIGURES

CHAPTER I: Introduction and literature review

I. INTRODUCTION

A. Overview

Insectivorous bats are increasingly imperiled by biological and anthropological stressors, and because they are notoriously cryptic, can be difficult to study. Nocturnal behavior, small body size, and high mobility contribute to a relatively minimal understanding of life histories and migratory behaviors for many bat species worldwide (Popa-Lisseanu et al., 2009; Krauel & McCracken, 2013). Basic biological and behavioral information about bats is increasingly relevant as hibernating and latitudinally migrating bat species face severe population declines (Arnett & Baerwald, 2013; Kurta & Smith, 2020). Many hibernating species are heavily impacted by white-nose syndrome (WNS), a lethal fungal pathogen; *Myotis lucifugus*, *M. septentrionalis*, and *Perimyotis subfavus* (three hibernating species) face a mortality rate greater than 90 % from this fungal infection (Kurta & Smith, 2020; Cheng et al., 2021). In addition, wind energy facilities threaten populations of migratory bat species worldwide (e.g., Arnett & Baerwald, 2013; Lehnert et al., 2014; Frick et al., 2017).

With so many species facing extinction, developing methods to study regional bat movements has never been more critical. Not only will an understanding of migratory bat movements provide information about important habitat use areas, but it can also shed light on the connectivity of seemingly genetically distinct populations (Moussy et al., 2013). Furthermore, as migratory species across taxa are increasingly imperiled, the adaptation of migration itself may soon be lost to an increasingly anthropogenic world (Brower &

1

Malcolm, 1991; Wilcove, 2008; Albers et al., 2023). A better understanding of the evolutionary trends of migration requires rapid advancement of effective monitoring techniques before these species are lost to the "sixth mass extinction" (Ceballos et al., 2015 but see Briggs, 2017).

Intrinsic marking techniques – i.e., biochemical signatures incorporated into an organism's tissues that vary predictably across the landscape, (e.g., stable and radiogenic isotopes, trace elements) – have been successful at tracking long-term movements of species but are limited by relatively coarse gradients in isotopic variation. Previously, multi-isotope approaches have successfully addressed this limitation, as each isotopic system provides a different perspective on the study area and the combination of probability surfaces generated with these systems allows a finer resolution for identifying probable origin (Figure 1.1; e.g., Popa-Lisseanu et al., 2012; Bataille et al., 2021).
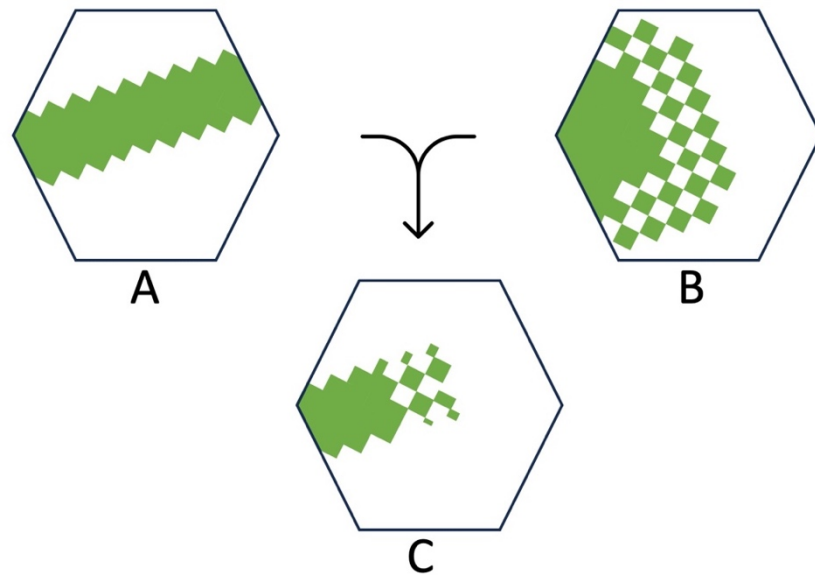
Figure 1.1. *Simplistic example of how the combination of two isotopic systems could increase the precision of migratory origin assignments. Where A and B show examples of probable origin surfaces for two separate isotope systems, and C shows the overlap between the two surfaces.*

Building on this trend, in the subsequent document we aim to broaden the scope of intrinsic marking techniques by using a combination of multiple isotopic systems to make origin assignments of migratory animals and further, to develop a novel approach to infer movements at various life stages through the analysis of multiple tissue types. The overarching research goals of this study are twofold: (i) develop a theoretical framework for future investigations of migratory movements and (ii) contribute to a better understanding of the natural history and movement behavior of an endangered species of bat in a northern island habitat.

Therefore, for this project, we attempted to make origin assignments using three isotope systems [stable hydrogen (δ^2H), stable sulfur ($\delta^{34}S$), and strontium ($^{87}Sr/^{86}Sr$)] and the population of *M. lucifugus* in Newfoundland and Labrador, Canada as a case study. Although the former (δ^2H) is a well-understood method for identifying bat movement pathways (e.g., Cryan et al., 2004; Cryan et al., 2014; Pylant et al., 2014; Fraser et al., 2017), the latter ($\delta^{34}S$, $^{87}Sr/^{86}Sr$) have reportedly been conducted only once each in bats (Cryan et al., 2012; Kruszynski et al., 2020).

B. Research questions, objectives, and hypotheses

The following section details the overarching research question addressed by this project, and its associated objectives and hypotheses, grouped by chapter.

Research Question: How can the combined use of δ^2H, $\delta^{34}S$, and $^{87}Sr/^{86}Sr$ improve our understanding of relatively small landscape-level movements of species?

Chapter II: Using strontium isotope techniques to elucidate lifetime movements of wild animals: A case study of *Myotis lucifugus* in insular Newfoundland, Canada

(O₁): Evaluate whether bat fur can be reliably sampled for Sr analysis and the difference between ^{87}Sr/^{86}Sr values across teeth, fur, and bone in juvenile bats.

> **(H₁.₁):** Bat fur contains high enough concentrations of elemental Sr to be analyzed for ^{87}Sr/^{86}Sr (Bentley, 2006; Kruszynski et al., 2020).

> **(H₁.₂):** Each tissue sampled from juvenile bats will have similar ^{87}Sr/^{86}Sr values, as these individuals will have formed all three tissues at the same location (van Zyll de Jong, 1983).

(O₂): Correlate the variation in ^{87}Sr/^{86}Sr values between geologically distinct regions in Newfoundland with the isotopic signatures in the fur of known origin individuals.

> **(H₂):** If ^{87}Sr/^{86}Sr is known to vary with underlying geology (Faure & Powell, 1972), and is incorporated into bat fur with minimal discrimination, then known origin fur samples collected from geologically distinct regions of the island will have ^{87}Sr/^{86}Sr values that are significantly different.

(O₃): Identify patterns in lifetime movements of adult *M. lucifugus* in Newfoundland.

> **(H₃):** If adult female *M. lucifugus* in Newfoundland are more likely to exhibit natal philopatry while adult males are more likely to disperse from their natal grounds (Dixon, 2011; Johnson et al., 2015), then female individuals will be more likely to have similar ^{87}Sr/^{86}Sr values in their calciferous and fur tissues compared to males.

Chapter III: Advancing the use of intrinsic markers for studying the migratory movements of modern wildlife: A case study of *Myotus lucifugus* in Newfoundland, Canada

(O$_1$): Correlate the variation in δ^2H, δ^{34}S, and ^{87}Sr/^{86}Sr across the landscape with the isotopic signatures in bat fur sampled from individuals collected during the period of fur growth.

(H$_{1.1}$): If δ^2H, ^{87}Sr/^{86}Sr, and δ^{34}S vary predictably across the Newfoundland landscape and are incorporated predictably into the fur of bats, then the stable or radiogenic isotope signature of fur will correspond to the underlying landscape signature. When overlaid, these will provide a fine resolution isoscape for this region.

(H$_{1.2}$): Fur sampled from the dorsal and ventral surfaces of a single individual will reflect similar ^{87}Sr/^{86}Sr values, as *M. lucifugus* is known to replace the fur across its body in a period of two months, during which individuals of this species are largely sedentary (Fraser et al., 2013).

(O$_2$): Identify seasonal movements of *M. lucifugus* in Newfoundland.

(H$_2$): If *M. lucifugus* is known to migrate > 500 km among sites of summer residency, swarming sites, and hibernacula (Fenton 1969; Norquay et al., 2013), the δ^2H, δ^{34}S, and ^{87}Sr/^{86}Sr fur values of bats collected outside of the period of fur growth (summer) will be distinct from those of the location where the bat carcass was found.

II.   LITERATURE REVIEW

A. Rationale for studying the migratory movements of bats

Migratory behavior is present in many taxa, from aphids to raptors to fishes, but what movements are classified as migratory? For the remainder of this document, migration is defined as a persistent, anticipatory movement away from an individual's home range which necessitates a change in energy investment and storage and is not altered by encounters with favorable resources (Dingle, 2014). This behavior differs from other biological movements (e.g., dispersal) which are halted when suitable habitat is encountered, and which actively seek to expand the distance between individuals (whereas migration may result in either aggregation or scattering of individuals across the landscape depending on the time of year and environmental conditions) (Dingle, 2014). Despite being such a widespread phenomenon, much of what we understand about terrestrial migration comes from the extensive research of ornithologists on migratory bird species (McGuire & Guglielmo, 2009). Although this research provides a solid basis for theories of migratory behavior, there is growing evidence that these theories do not explain migratory decision-making in bats (McGuire, 2022). For migratory bats in North America, this knowledge gap is exacerbated by WNS and bat mortality at wind energy facilities, which are both contributors to severe declines in many populations. Thus, we classify the need for a better understanding of migratory behaviors into the following categories: [1] applied research for the protection and conservation of imperiled species, and [2] theoretical research for a better understanding of the adaptive and evolutionary pressures that lead to migratory decision making in bats. Research that addresses questions related to either category often begins with fundamental questions – where and how far are bats moving across the

landscape (e.g., Cryan et al., 2014; Ijäs et al., 2017; Bach et al., 2022) ? Once a basic understanding of a species' migratory movements is established, more complex questions can be addressed.

Subsequent research may seek to understand migratory connectivity (e.g., Britzke et al., 2012; Sullivan et al., 2012; Segers & Broders, 2015), population-level (e.g., sex-biased) trends in migratory movements (e.g., Norquay et al., 2013; Fraser et al., 2012; Jonasson & Guglielmo, 2016; Fraser et al., 2017), morphological and physiological characteristics related to migration (e.g., Lehnert et al., 2018; Clerc et al., 2021; Rogers et al., 2021), or weather/climatic conditions that predict migration (e.g., Dechmann et al., 2017; Pettit & O'Keefe, 2017; Roby et al., 2019), among others. Much of this research contributes to a better understanding of migratory bat species, their adaptive pressures, and decision-making, with broader theories of the evolutionary history of this behavior (i.e., the physiological, behavioral, and ecological factors that drive migration in individuals and populations) [category 2]. Simultaneously, many of these studies are addressing the conservation of imperiled bat species in some way [category 1] (i.e., the increasing erection of wind energy facilities, implications for the spread of WNS, or a need for protected migratory corridors). Reflecting these trends in the literature, the subsequent document will provide results that address both pressing conservation concerns for *M. lucifugus* in Newfoundland and an important theoretical framework for future investigations of various terrestrial migratory species and taxa.

B. Methods for studying the migratory movements of bats

Several methods have been developed and used for the study of migratory movements in bats. In general, these methods can be divided into three categories:

extrinsic marking techniques, intrinsic marking techniques, and passive monitoring

techniques. Extrinsic marking techniques attach a physical device [i.e., wing band,

Passive Integrated Transponder (PIT) tag, radio transmitter] to the bat upon initial

capture, and recover information about that individual when it is recaptured, or the radio

frequency is manually detected or "reheard". These techniques can generate specific

geospatial information about the individual; however, they may introduce bias, especially

if the movement data is inferred by the individual's recapture at a specific location

(Hobson et al., 2019). Additionally, although radio/satellite transmitters are frequently

innovated, the current technology can offer information about movements during a single

season, but not across years or the lifetime of an individual (O'Mara et al., 2014).

Alternatively, intrinsic marking techniques (i.e., stable and radiogenic isotopes, trace

elements, contaminants) use chemical signatures that are incorporated into the tissues of a

bat and vary predictably across the landscape. Similarly, genetics (another intrinsic

marking technique) use molecular markers that vary between breeding populations to

track dispersal to, or movements between, these sites (Broquet & Petit, 2009). The use of

intrinsic marking techniques to infer movements involve a single capture and tissue

sampling event but require a number of inferences and typically offer information about

movements across a wide spatial scale (e.g., latitudinally, or between breeding

populations) (Hobson et al., 2019). Finally, passive monitoring techniques (i.e., acoustic

monitoring) do not require a capture event; instead, they use receivers to detect bat

presence across the landscape, though are unable to make detections to the level of

individuals. These techniques can determine the presence or absence of bat species in a

study area and identify movement corridors (e.g., Furmankiewicz & Kucharska, 2009;

Ijäs et al., 2017; Cortes & Gillam, 2020). While they show promise for decreasing bias associated with extrinsic marking techniques, these techniques are not always feasible, as they require considerable time and monetary investments, as well as a high level of training (Ross et al., 2023). Additionally, these techniques are limited by the location and number of receivers erected on the landscape, and therefore cannot completely eliminate bias associated with receiver locations.

Bat biologists have used extrinsic marking, intrinsic marking, and passive monitoring techniques to ask various questions about migration. In general, each of these techniques can address fundamental questions related to bat migration (i.e., distance and direction traveled) (e.g., Cryan et al., 2014; Samoray et al., 2019; Bach et al., 2022). However, each technique ultimately has strengths and limitations, and more complex questions require careful selection of the most informative technique. For example, stable isotope analysis (i.e., intrinsic marking techniques) can make inferences about migratory origin that are not biased towards capture or recapture location, but typically produce origin assignments at relatively low resolution (Hobson et al., 2019). Specifically, stable isotope analyses of bat fur have been used to identify patterns of migration (e.g., the first case of leapfrog migration in bats; Fraser et al., 2017), ascertain catchment and connectivity of migratory bats (e.g., Baerwald et al., 2014), and better understand morphological and physiological adaptations to migration (e.g., Rogers et al., 2021). Alternatively, radio transmitters (i.e., extrinsic marking techniques) allow individual bats to be traced to precise locations, but are limited by cost, battery life, and transmitter size relative to the bat species of interest (Hobson et al., 2019). Radio transmitters and telemetry have been used to identify specific roosting sites (e.g., Johnson & Gates, 2008),

determine weather and climatic conditions that influence migration (e.g., Dechmann et al., 2017), and elucidate the role foraging and stopover play in migration (e.g., Roby et al., 2019). Finally, acoustic monitoring (i.e., passive monitoring techniques) can identify the presence of species in relation to important habitat characteristics but are limited to making inferences within the array of receiver stations, by researchers with knowledge and expertise in acoustic call identification, and can only provide an index of bat activity as opposed to movements of individual bats (Ross et al., 2023). Acoustic monitoring has been used to identify migratory corridors (e.g., Furmankiewicz & Kucharska, 2009, but see Cortes & Gillam, 2020), determine anthropogenic structure use during the migratory period (e.g., Jameson & Willis, 2014), and understand the role of coastlines in the migratory movements of bats (e.g., Ijäs et al., 2017).

C. The stable isotopes of hydrogen

The stable isotopes of hydrogen (δ^2H) describe the ratio of deuterium (^2H) to protium (^1H) relative to the international standard for δ^2H, Vienna Standard Mean Ocean Water (VSMOW) (Wassenaar, 2019). In mathematical terms, the reported δ^2H for a sample is as follows:

$$\delta^2H\ (‰) = \frac{R_{sample}}{R_{VSMOW}} - 1 \qquad \textbf{(Equation 1)}$$

Where R is the ratio of the heavy to the light isotope (e.g., ^2H / ^1H) (Wassenaar, 2019). Equal treatment of experimental samples and standards is important when conducting δ^2H analysis of organic tissues, as a fraction of H in the samples may exchange with ambient moisture in the air (Soto et al., 2017). By using the comparative equilibrium approach, whereby experimental samples are left to equilibrate with laboratory air for a minimum of

96 hours alongside standards with known compositions of non-exchangeable δ^2H,

researchers are able to measure the non-exchangeable δ^2H composition of the

experimental samples (Wassenaar & Hobson, 2003).

Variation in the δ^2H composition of meteoric water across the landscape is well

characterized and has been used to track the migratory movements of terrestrial species

for many years (e.g., Wassenaar & Hobson, 1998; Meehan et al., 2001; Cryan et al.,

2004). Rayleigh Distillation, which describes the preferential condensation of deuterium,

results in the increasing enrichment of protium as cloud masses move across the

landscape and preferentially release protium (^{1}H) in the form of precipitation (Bowen &

West, 2019). Therefore, precipitation is depleted of deuterium with increasing latitude,

altitude, and distance from the coast, at lower temperatures, and in areas with higher

relative humidity (Rubenstein & Hobson, 2004). A worldwide isoscape, or map of

isotopic distribution, for δ^2H in precipitation (δ^2H$_p$) was first published in 2013 using a

50-year dataset from the Global Network for Isotopes in Precipitation (GNIP; Terzer et

al., 2013). To date, there are a variety of ways to obtain a δ^2H isoscape for a study area,

including waterisotopes.org, IsoMAP (though recently retired) (Bowen, 2003; Bowen et

al., 2014), R packages (e.g., IsoriX) (Courtiol et al., 2019), and previously published

studies (e.g., Timsic & Patterson, 2014).

δ^2H is incorporated into animal tissues via diet and drinking water, although

physiological fractionation of δ^2H may complicate the organism's δ^2H$_{tissue}$ value (Vander

Zanden et al., 2016). Further, understanding the diet of an organism and how it relates to

its δ^2H$_{tissue}$ value becomes increasingly complex when considering differences between

terrestrial and aquatic food sources (Voigt et al., 2015; Vander Zanden et al., 2016). This

distinction between food sources is an additional source of variation in $\delta^2 H_{tissue}$ for organisms that consume both terrestrial and aquatic insects (i.e., *M. lucifugus*) for two main reasons: (i) emergent aquatic insects may reflect $\delta^2 H$ values of aquatic-sourced or terrestrial-sourced benthic organic matter, and (ii) $\delta^2 H_{tissue}$ values reflect a composite of both aquatic emergent insects and terrestrial insects (Voigt et al., 2015; Vander Zanden et al., 2016). Additionally, as *M. lucifugus* forages over open bodies of water (e.g., ponds, lakes, streams), the organism's $\delta^2 H_{tissue}$ value may be more accurately approximated by $\delta^2 H$ in surface waters ($\delta^2 H_{sw}$) than $\delta^2 H$ in precipitation ($\delta^2 H_p$) (Britzke et al., 2009; Sullivan et al., 2012).

The relationship between $\delta^2 H_p$ and $\delta^2 H$ in *M. lucifugus* fur tissue ($\delta^2 H_{fur}$) (i.e., transfer function) is well documented (Britzke et al., 2009; Sullivan et al., 2012). Britzke et al. (2009) developed the first transfer function using a general linear model to relate $\delta^2 H_p$ to $\delta^2 H_{fur}$ for male, female, and juvenile *M. lucifugus* in the eastern United States. The published transfer function reflecting all sexes and age groups is as follows:

$$\delta^2 H_{fur} = \left(0.52 \times \delta^2 H_p\right) - 30.82 \qquad \textbf{(Equation 2)}$$

$$r^2 = 0.17, p = 0.002$$

In 2012, Sullivan et al. (2012) supplemented the Britzke et al. (2009) data with 80 additional *M. lucifugus* individuals collected in the midwestern United States. The authors then mirrored the methodology in Britzke et al. (2009) and, using the combined data, developed a transfer function for *M. lucifugus* (Sullivan et al., 2012):

$$\delta^2 H_{fur} = \left(2.69 \times \delta^2 H_p\right) + 96.93 \qquad \textbf{(Equation 3)}$$

$$r^2 = 0.63, p < 0.001$$

Fundamentally, the differences between the published transfer functions of these two studies largely stem from Sullivan et al. (2012) supplementing new experimental data with the data previously collected and published in Britzke et al. (2009). While it is common to supplement experimental δ^2H_{fur} data with publicly available data for the same study species (e.g., Pylant et al., 2016; Campbell et al., 2020; Măntoiu et al., 2020), researchers must exercise caution when doing so. Samples taken from outside the study area may not reflect differences in diet or behavior of *M. lucifugus* between populations. Additionally, slight differences in δ^2H_p variation across the landscape, and the covariates that explain this variation (e.g., latitude, longitude, elevation), may exist between study areas. Lastly, and perhaps most importantly, Soto et al. (2017) presented revised non-exchangeable δ^2H values of VSMOW in two widely used keratin calibration standards [Caribou Hoof Standard (CBS) and Kudu Horn Standard (KBS)]. These revised values mean that any δ^2H values of keratinous tissues published prior to 2017 were corrected with inaccurate standard values and therefore need to be retroactively adjusted using the values published by Soto et al. (2017).

Ultimately, it is up to the researchers to decide whether to develop a new transfer function or supplement a previously developed transfer function with new experimental data, depending on the respective study area. In the case of this study, we believe the environmental conditions of Newfoundland to be distinct from the eastern and midwestern United States due to its high latitude and boreal climate. These conditions have the potential to impact both the behavior of *M. lucifugus* and the covariates incorporated into our δ^2H_p model, warranting the development of a transfer function unique to this area.

δ^2H has been extensively used to track the migratory movements of bat species in North America and Europe (e.g., Cryan et al., 2014; Fraser et al., 2017; Măntoiu et al., 2019; Wright et al., 2020). However, few studies exist which use δ^2H to understand the migratory movements of *M. lucifugus* (but see Britzke et al., 2009; Sullivan et al., 2012; Fraser et al., 2015). This is likely because (i) the relatively small migratory movements of *M. lucifugus* may not be detectable at the resolution generated in δ^2H_p isoscapes, and (ii) the diet of *M. lucifugus* complicates the development of a robust transfer function. This project addresses those complications by using multiple isotopes to understand the movements of *M. lucifugus* in Newfoundland. More broadly, the following document will present a muti-isotope technique for understanding the movements of any organism which migrates on a scale too small to detect using δ^2H analyses of tissues alone.

D. The radiogenic isotopes of strontium

The radiogenic isotopes of strontium (^{87}Sr/^{86}Sr) describe the ratio of the heavy (^{87}Sr) to the light (^{86}Sr) isotope. The radioactive decay of ^{87}Rb forms ^{87}Sr, whereas ^{86}Sr is a naturally occurring, non-radiogenic stable isotope of Sr (Faure & Powell, 1972). As ^{87}Sr, ^{86}Sr, and ^{87}Rb are known to occur in minerals naturally, the variation in ^{87}Sr/^{86}Sr values across the landscape primarily relates to the underlying geology (Faure & Powell, 1972). Specifically, ^{87}Sr/^{86}Sr values of underlying bedrock depend on the relative age of the mineral, as well as its initial ^{87}Sr, ^{86}Sr, and ^{87}Rb concentration (Faure & Powell, 1972). Over time, the radioactive decay of ^{87}Rb will form ^{87}Sr while ^{86}Sr will remain unchanged, thus increasing the ^{87}Sr/^{86}Sr value of a mineral (Faure & Powell, 1972). Therefore, an older rock formation will typically have greater ^{87}Sr/^{86}Sr values than a

younger rock formation, given the initial concentrations of ^{87}Sr, ^{86}Sr, and ^{87}Rb are the same (Faure & Powell, 1972).

The isotopes of Sr are not reported relative to an international standard but are instead corrected after analysis for any mass bias that may influence the $^{87}Sr/^{86}Sr$ value of the experimental sample (Bataille et al., 2020). This correction is done by analyzing a standard with a known $^{87}Sr/^{86}Sr$ value alongside experimental samples; the National Institute of Standards and Technology's Strontium Reference Material 987 (NIST SRM 987) is a common international certified standard used for experimental sample correction (Avanzinelli et al., 2005).

The earth's mantle is typically depleted in ^{87}Sr compared to other rock formations ($^{87}Sr/^{86}Sr = 0.702 - 0.704$) (Faure & Powell, 1972; Bentley, 2006). Limestone and dolomite are slightly more enriched in ^{87}Sr than mantle rock, reflecting oceanic $^{87}Sr/^{86}Sr$ values ($0.707 - 0.709$) (Faure & Powell, 1972; Bentley, 2006). Alternatively, geological formations derived from continental crust may have more variance; relatively old granites are comparatively enriched in ^{87}Sr ($^{87}Sr/^{86}Sr = 0.710 - 0.740$), while relatively young basalts are comparatively depleted in ^{87}Sr ($^{87}Sr/^{86}Sr = 0.703 - 0.704$) (Faure & Powell, 1972; Bentley, 2006). Additional sources of variation in $^{87}Sr/^{86}Sr$ values across the landscape include atmospheric dust, pollution, sea spray, and ocean water (modern seawater $^{87}Sr/^{86}Sr = 0.7092$), surface waters (variable – related to soil and bedrock), soil (variable – related to bedrock), and agricultural fertilizers ($^{87}Sr/^{86}Sr = 0.7034 - 0.7152$) (Faure & Powell, 1972; Vitória et al., 2004; Bentley, 2006; Bataille et al., 2020).
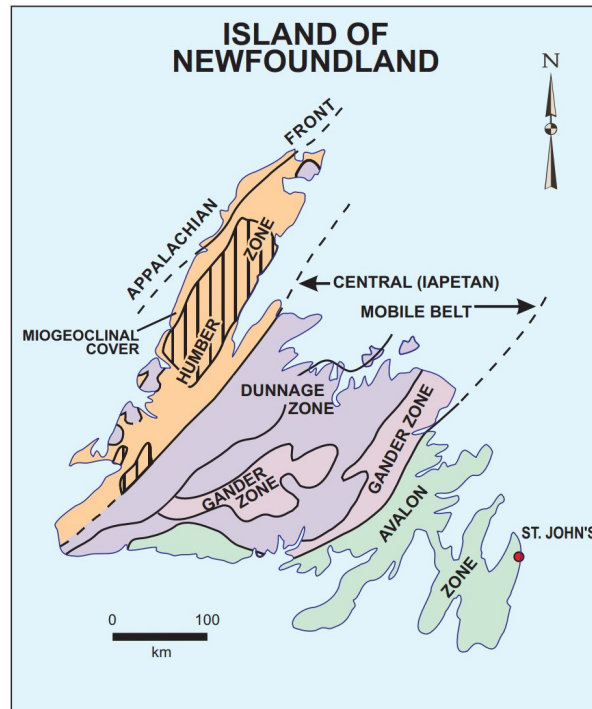
Figure 1.2. *Simplified geological map of insular Newfoundland showing four tectonic zones: Humber, Dunnage, Gander, and Avalon (Colman-Sadd et al., 2000).*

The island of Newfoundland has a unique geologic history, contributing to diverse $^{87}Sr/^{86}Sr$ values across the landscape. The island is typically divided into four tectonic zones: Humber, Dunnage, Gander and Avalon (Figure 1.2; Hild, 2012). While portions of the Humber and Avalon zones were formed up to 1,500 and 700 million years ago, respectively, and are composed of relatively old rock formations, the Dunnage and Gander zones are relatively young; the oldest rock formations are approximately 510 and 540 million years old, respectively (Bell & Liverman, 1999; Hild, 2012). The Humber zone is made up of the oldest rocks in Newfoundland; ancient gneiss in this zone was formed 1,500 million years ago, while other formations date back 540 – 460 million

years, during which the Humber zone was part of the continent Laurentia (Bell &

Livermann, 1999; Hild, 2012). Key characteristics of the Humber zone include ancient

granitic gneiss, a carbonate shelf, and melanges composed of ocean crust, ocean

sediments, and mantle (Hild, 2012). This zone is also famously known for the presence of

ultra-mafic peridotite in an area called the Tablelands, although similar ultramafic

ophiolite complexes can also be found in nearby rock formations (i.e., around the Bay of

Islands) and the northern tip of the Northern Peninsula (Hild, 2012). The Dunnage zone

was once a collection of island arcs formed in the Iapetus Ocean and became part of

Newfoundland when Laurentia and Gondwana collided (subduction beginning about 470

million years ago); the oldest formation in this zone dates back 510 million years (Bell &

Livermann, 1999; Hild, 2012). The Dunnage zone includes sedimentary rock, ocean crust,

and mantle formed in the Iapetus Ocean floor, as well as granitic and volcanic intrusions,

and red sandstone river deposits (primarily formed during the Ordovician and Silurian

periods; Bell & Livermann, 1999; Hild, 2012). The Gander zone is primarily composed of

sediments originating in the Iapetus Ocean that were deposited along the continental slope

of Gondwana; the oldest formations in this zone date back 540 million years (Hild, 2012).

This zone was similarly affected by the collision between Gondwana and Laurentia (Hild,

2012). Key features of the Gander zone include sediments, crust, and mantle formed in

the Iapetus Ocean, sandstone and siltstone formed along the continental margin of

Gondwana, Schist and gneiss formed by metamorphism approximately 420 million years

ago, and post-tectonic granites formed 385 million years ago (Hild, 2012). The Avalon

zone began forming with the supercontinent Rodinia, and later belonged to the continent

Gondwana before its collision with Laurentia (Hild, 2012); the oldest rock formations in

this zone date back 760 million years (Hild, 2012). Notably, the Avalon zone includes

ancient volcanic arcs and ocean sediment, sedimentary layers formed through deposition

by rivers approximately 550 million years ago, and Iapetus Ocean sediments (Hild, 2012).
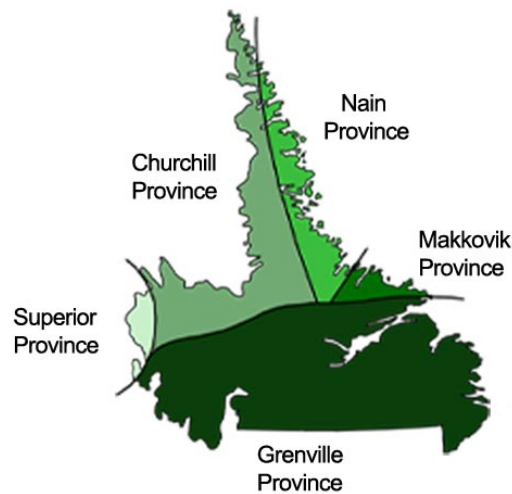
Figure 1.3. *Simplified geological map of Labrador showing four geologic zones or provinces: Superior, Nain (with Makkovik sub-zone), Churchill, and Grenville (Wijayawardhana, 1998).*

Labrador is located northwest of the island of Newfoundland and forms the

remainder of the province, as well as the easternmost section of the Canadian Shield

(Greene, 1974). Though a detailed summary of the geology of Labrador is beyond the

scope of this review, it should be noted that this portion of the province is composed of

much older geological formations than the island of Newfoundland (Bell & Livermann,

1997). Labrador is divided into four major geologic zones (or provinces): Superior, Nain,

Churchill, and Grenville (Figure 1.3; Greene, 1974). The Superior zone is primarily made

up of metamorphic orogenic belts formed during the Archean eon (4,000 – 2,500 million

years ago) (Greene, 1974). Similarly, the Nain zone is generally composed of Archean

metamorphic orogenic belts with Proterozic volcanic intrusions, although sedimentary

and volcanic formations formed during the Proterozoic eon (2,500 – 542 million years

ago) are also present in the southeastern section of the Nain zone, sometimes known as

the Makkovik zone or sub-zone (Greene, 1974). The Churchill zone was broadly formed

during the early Proterozoic eon; the western section of this zone is made up of

sedimentary and volcanic formations while the eastern is composed of metamorphic rock

with volcanic intrusions (Greene, 1974). Finally, the Grenville zone is primarily

composed of metamorphic gneiss with large volcanic intrusions, all dating back to the

middle Proterozoic (approximately 1010 million years ago) (Greene, 1974). This

incredible diversity in geologic age and rock types throughout Newfoundland and

Labrador will likely translate to a diverse landscape of $^{87}Sr/^{86}Sr$ values once a

bioavailable Sr isoscape is developed.

In 2020, Bataille et al. published the first global bioavailable Sr isoscape (i.e., an

isoscape modeled with $^{87}Sr/^{86}Sr$ values of plants and local animals). This isoscape

increased the power to make inferences using Sr isotope techniques for studying

migratory movements of organisms, as a previous barrier to these studies was the

construction of a regional bioavailable Sr isoscape. Bataille et al. (2020) used random

forest regression, a machine learning algorithm, to model bioavailable Sr isotopes using

previously published and unpublished data from 278 studies and a host of covariate

models (e.g., bedrock age, soil properties, agricultural activity). Random forest regression

uses bootstrapping to create a "forest" of decision trees which are each constructed of a

random subset of the calibration dataset (Bataille et al., 2018; Bataille et al., 2020). Each

branch (or "node") of a tree is created by the predictor variables which partition the data

19

by optimizing a pre-defined threshold [e.g., Root Mean Square Error (RMSE)] (Bataille et al., 2018; Bataille et al., 2020). The algorithm then aggregates the mean bioavailable Sr value at each terminal branch to predict variation in bioavailable Sr using the predictor variables (Bataille et al., 2018; Bataille et al., 2020). An advantage of this method for modeling isotopic distribution is its robust nature – it does not require normality or homoscedasticity of the calibration dataset or residuals, nor does it restrict the predictor variables to be either categorical or continuous (Bataille et al., 2020). Further, the data used by the variables can be either measured or modeled (Holt et al., 2021). However, random forest regression requires a calibration dataset and predictor variables, which can each be influenced by limitations (e.g., biases towards specific sampling locations, low accuracy of predictor distribution maps) (Holt et al., 2021). Much of the data used to construct the global bioavailable Sr model is concentrated in Europe and the United States, and under-studied regions (e.g., much of Africa, Polynesia, South America) may not be well represented (Bataille et al., 2020). For the context of this project, no samples taken in Newfoundland and Labrador were included in the model (Bataille et al., 2020).

The isotopes of Sr are incorporated into animal tissues primarily via diet, although drinking water may also contribute to tissue $^{87}Sr/^{86}Sr$ values (Bentley, 2006). As elemental Sr (Sr^{2+}) is known to substitute for calcium (Ca^{2+}) in calciferous tissues (Faure & Powell, 1972), bones and teeth have historically been sampled and analyzed for the isotopes of Sr (e.g., Hope et al., 1999; Britton et al., 2009; Copeland et al., 2016). However, Sr analysis of keratinous tissues (e.g., fur, feathers) is an increasingly common approach to elucidating animal movements across the landscape (e.g., Sellick et al., 2009; Kruszynski et al., 2020; Crowley et al., 2021). Measuring the $^{87}Sr/^{86}Sr$ value in keratinous

tissues presents challenges. Keratin has low quantities of Sr, meaning large samples are required (Brewer et al., 2021). Additionally, it remains unclear exactly how Sr is incorporated into keratin (but see Font et al. 2012). Finally, contamination of keratin samples is expected, as atmospheric, lithospheric, and hydrospheric particles that contain Sr may become trapped in the structure of the fur or feathers, known broadly as "exogenous Sr" (e.g., Font et al., 2007). As such, the $^{87}Sr/^{86}Sr$ value of exogenous material has the potential to mix with, or mask entirely, the endogenous $^{87}Sr/^{86}Sr$ value, resulting in tissue $^{87}Sr/^{86}Sr$ values that reflect locations of origin other than where the tissue was originally formed. Several methodologies have been proposed to remove the exogenous Sr physically or chemically; however, a widely accepted protocol has yet to be developed (Font et al. 2007; Tipple et al. 2013; Shin et al. 2020).

The discrimination of ^{87}Sr across trophic levels has been contested (Bentley, 2006; Kruszynski et al., 2020); however, laboratory studies report minimal fractionation when Sr isotopes are incorporated into animal tissues (e.g., Flockhart et al., 2015). For highly mobile species, lengthy movements of organisms during tissue formation may lead to tissues with isotopic values that integrate the signature of multiple locations, potentially adding noise to transfer functions or quantifications of fractionation and further complicating differences between bioavailable and tissue $^{87}Sr/^{86}Sr$ values (Fraser et al., 2013). Recently, Kruszynski et al. (2020) conducted the first study using $^{87}Sr/^{86}Sr$ values recorded in fur to understand the migratory movements of bat species. The authors reported a discrimination factor of 0.0028 ± 0.0002 ($n = 10$) between their modeled bioavailable Sr and the $^{87}Sr/^{86}Sr$ values of fur sampled from known origin *Pipistrellus nathusii* individuals at a single location (Kruszynski et al., 2020). Additionally, Crowley

et al. (2021) used ^{87}Sr/^{86}Sr values recorded in raptor feathers to delineate their natal origin during autumn migration. The authors also reported discrimination between their modeled bioavailable Sr (^{87}Sr/^{86}Sr$_{bio}$) and the ^{87}Sr/^{86}Sr value in the feathers of known origin individuals (^{87}Sr/^{86}Sr$_{feather}$) (Crowley et al., 2021). However, this relationship was very close to ^{87}Sr/^{86}Sr$_{feather}$ = ^{87}Sr/^{86}Sr$_{bio}$, and their reported transfer function is as follows:

$$^{87}\text{Sr}/^{86}\text{Sr}_{feather} = (1.27 \times \,^{87}\text{Sr}/^{86}\text{Sr}_{bio}) - 0.19 \qquad \textbf{(Equation 4)}$$

$$r^2 = 0.90$$

The present project continues the investigation into discrimination of ^{87}Sr/^{86}Sr in keratinous tissues by comparing ^{87}Sr/^{86}Sr values in the fur of known origin *M. lucifugus* individuals to a regional modelled bioavailable Sr isoscape. It contributes to a growing body of literature that uses the isotopes of Sr to understand movements of modern migratory species, while developing a novel method to identify lifetime movements of organisms. Using the *M. lucifugus* population in a geologically diverse landscape, the resulting origin analysis will shed light on the applicability of this technique for a variety of cryptic and mobile species whose movements are otherwise difficult to elucidate.

E. The stable isotopes of sulfur

The stable isotopes of sulfur (δ^{34}S) describe the ratio of the heavy (^{34}S) to the light (^{32}S) isotope relative to the international δ^{34}S standard, Vienna Canyon Diablo Troilite (VCDT) (Wassenaar, 2019). In mathematical terms, the reported δ^{34}S value for a sample is described as follows:

$$\boldsymbol{\delta^{34}S} \text{ (‰)} = \frac{R_{sample}}{R_{VCDT}} - \mathbf{1} \qquad \textbf{(Equation 5)}$$

Where R is the ratio of the heavy to the light isotope (^{34}S / ^{32}S) (Wassenaar, 2019).

Variation in δ^{34}S across the landscape is driven by the cycling of S from marine and

terrestrial water sources, the introduction of S via anthropogenic sources, and the sulfuric

content of underlying bedrock and minerals (Peterson & Fry, 1987; Nehlich, 2015).

Oceanic water and sea spray have a distinct and consistent δ^{34}S value of approximately

+20 ‰ (Ault & Kulp, 1959; Thode et al., 1961; Nielsen, 1974; Nehlich, 2015). Likewise,

marine-derived precipitation tends to have a δ^{34}S value of +16 to +20 ‰, and marine-

derived sediments can range from +10 to +35 ‰ (Ault & Kulp, 1959; Claypool et al.,

1980; Nehlich, 2015). Terrestrial sources of S tend to be more complex and variable,

depending on weathering processes which oxidize or reduce sulfur-containing compounds

in minerals (Kaplan, 1975; Krouse, 1980; Böttcher, 2001; Nehlich, 2015). However,

terrestrial sources of S are generally depleted in ^{34}S compared to marine sources, with

most bedrock δ^{34}S values clustering around 0 ‰ and ranging from –20 to +30 ‰ (Ault &

Kulp, 1959; Thode et al., 1961; Krouse, 1980; Nehlich, 2015). Terrestrial water sources

also vary in their δ^{34}S value but generally reflect a range of 0 to +10 ‰ (Nriagu et al.,

1991; Nehlich, 2015). Similarly, anthropogenic δ^{34}S values tend to be complex depending

on the presence of various pollutants; sources include atmospheric pollution (–3 to –6 ‰

in North America) and agricultural amendments (i.e., organic and inorganic fertilizers, +1

to +23 ‰) (Case & Krouse, 1980; Caron et al., 1986; Vitória et al., 2004). The wide

variation between marine and anthropogenic sources of S and their resulting δ^{34}S values

make the island of Newfoundland an ideal study site; several industrial areas in

Newfoundland introduce atmospheric S pollution (predicted δ^{34}S values around –3 to

–6 ‰), in contrast to large expanses of coastlines (predicted δ^{34}S values around +16 to +20 ‰). Wadleigh and Blake (1999) reportedly observed a +13 ‰ range in the δ^{34}S values of lichen on the island of Newfoundland.

The incorporation of δ^{34}S into animal tissues and the resulting discrimination of ^{34}S in those tissues is well-documented; there have been several controlled feeding studies that reported δ^{34}S values in animal tissues compared to a laboratory food source (McCutchan et al., 2003; Richards et al., 2003; Pinzone et al., 2017; Webb et al., 2017). Keratin contains a relatively high S composition (up to 5 %), and its sources include cysteine and methionine, both essential amino acids ultimately derived from an organism's diet (Richards et al., 2003; Nehlich, 2015). As methionine cannot be metabolized, it is entirely derived from the animal's dietary protein source and thus reflects the same δ^{34}S value without discrimination (Richards et al., 2003; Nehlich, 2015). Cysteine is metabolized from dietary methionine, therefore introducing a slight discrimination of ^{34}S in the organism's tissues (Richards et al., 2003; Nehlich, 2015). While both essential amino acids are present in fur keratin, cysteine is more abundant in the head, tail, and rod domains of α keratin and thus more common in the fur keratin of mammals (Bragulla & Homberger, 2009). Despite the relative abundance of cysteine in fur, the difference in δ^{34}S between an organism's diet and fur keratin is typically only +1 ‰ (Richards et al., 2003; Pinzone et al., 2017; Webb et al., 2017; but see McCutchan et al., 2003). While there is minimal information regarding δ^{34}S values of emergent aquatic insects in Newfoundland, which is the primary protein source for *M. lucifugus*,

δ^{34}S values of epiphytic lichen throughout the island have been well documented and used to model the distribution of δ^{34}S across the landscape (Wadleigh & Blake, 1999).

To date, there are no published studies which use δ^{34}S to track the migratory movements of bats. However, several studies have used δ^{34}S to elucidate diet and habitat use (e.g., Cryan et al., 2012; Dechmann et al., 2014). Additionally, δ^{34}S has been used to study the movements of other modern migratory vertebrates, including voles (Crumsey et al., 2019), domestic sheep (Zazzo et al., 2011), waterfowl (Hebert & Wassenaar, 2005; Fox et al., 2016; Asante et al., 2017), domestic cattle (Kabalika et al., 2020), and raptors (Lott et al., 2003; Crowley et al., 2021). This project, therefore, presents the first application of the use of δ^{34}S to study the migratory movements of bat species.

Figure 1.4. *Geographic distribution of*
Myotis lucifugus *(Naughton, 2012).*

F. Little brown myotis (*Myotis lucifugus*) biology and behavior

Myotis lucifugus is a globally endangered species of bat whose habitat ranges from northern Canada to the southern U.S. and Mexico (Figure 1.4; Solari, 2021). Despite the wide range of this species, its habitat use is confined by the suitability of hibernacula,

maternity sites, and water bodies for foraging (van Zyll de Jong, 1983; Solari, 2021). *Myotis lucifugus* typically hibernate in caves and abandoned mines during winter, seeking sites with optimal microclimate conditions, including high humidity levels (≥ 90 %) and moderate temperatures (≥ 0 °C) (Fenton & Barclay, 1980). The timeline of hibernation for this species is variable; depending on the weather conditions, *M. lucifugus* in Newfoundland may be active on the landscape through early October, with juveniles entering hibernation after adults (J. Humber, personal communication, May 27, 2021; van Zyll de Jong, 1983). In Newfoundland, individuals may emerge from hibernacula by mid-to-late April (J. Humber, personal communication, May 27, 2021). Upon emergence, *M. lucifugus* individuals will undergo a spring migration to summer roosting or maternity colonies. These migratory movements have been recorded as great as 800 km one-way (Fenton, 1969), however, they are more frequently within the 200 – 500 km range (Norquay et al., 2013).

The time between spring and fall migration is known as the summer residency period. During this time, *M. lucifugus* individuals will occupy summer roosts. Roosting typically occurs in buildings or artificial structures, tree cavities, rockpiles, woodpiles, or (rarely) caves (Fenton & Barclay, 1980; Randall et al., 2014; Johnson et al., 2019). In Newfoundland, *M. lucifugus* roosts have been identified in River of Ponds (Northern Peninsula), Notre Dame (North Central), Jipujikuei Kuespe (South Central), and Salmonier (Avalon Peninsula) (Park & Broders, 2012). Maternity roosts are more commonly found in buildings or bat boxes where available (van Zyll de Jong, 1983), and females appear to exhibit fidelity to their maternity roost (van Zyll de Jong, 1983, but see Slough & Jung, 2020). From May to August, pregnant females will occupy these

maternity roosts and give birth to a single pup (Wimsatt, 1945). The newborn pups will remain in maternity roosts, while their mothers forage, for about two weeks, and will begin to fly 18 days after birth (van Zyll de Jong, 1983). Juveniles will be weaned, adept at flying, and fully grown three weeks after birth (van Zyll de Jong, 1983).

Meanwhile, during the summer residency period, males and nonreproductive females will recover fat stores depleted during hibernation. *Myotis lucifugus* is known to occupy a wide dietary niche, foraging in both aquatic and terrestrial ecosystems, although variation exists between provinces in Atlantic Canada (Broders et al., 2014). In Nova Scotia, *M. lucifugus* has been documented primarily consuming insects from the orders Diptera, Lepidoptera, Ephemeroptera, Trichoptera, and Coleoptera (Clare et al., 2014). Foraging over open water bodies and consuming emergent aquatic insects may complicate analyses which relate δ^2H values in precipitation to δ^2H values in tissues collected from *M. lucifugus* individuals (Britzke et al., 2009; Fraser et al., 2015; Voigt et al., 2015, but see Sullivan et al., 2012).

After summer residency and before hibernation, typically in mid-to-late August, *M. lucifugus* individuals will undergo a fall migration and congregate at hibernacula for swarming and mating (J. Humber, personal communication, May 27, 2021). There is evidence that *M. lucifugus* individuals will travel far distances during this time; in Newfoundland, there is a record of a female traveling 375 km between July 28 and August 1 (Sunga et al., 2021). Swarming appears to be an important behavior to increase genetic diversity of populations and acquaint young of the year to hibernation sites (Fenton, 1969; van Zyll de Jong, 1983).

The timeline for tissue formation in *M. lucifugus* is of particular interest for this study, as we used $^{87}Sr/^{86}Sr$ values recorded in teeth, bone, and fur to elucidate patterns in movements of individuals throughout their lives. *Myotis lucifugus* is an ideal candidate for this comparison, as tissue growth occurs rapidly in adolescence. Juveniles will grow their coat, form adult dentition, and ossify their metacarpal-phalangeal joint 4 – 14, 14 – 21, and 29 days after birth, respectively (Fenton, 1970; van Zyll de Jong, 1983). Fur growth in adult *M. lucifugus* typically occurs in late summer; Sullivan et al., (2012) estimate the molt period for *M. lucifugus* in the midwestern USA to occur from July 1 to August 23. There is evidence that molting occurs later for reproductive females, possibly during swarming and fall migration (Fraser et al., 2013). Likewise, juvenile *M. lucifugus* individuals may molt in the late summer or fall (Fraser et al., 2013). Additionally, the growth of new fur is asynchronous across a single individual, and if captured before molt is completed, fur collected from the dorsal or ventral surface of a single individual may represent two different seasons (Fraser et al., 2013). These irregular molting patterns observed in juvenile and reproductive females have the potential to complicate stable isotope analyses of fur tissues.

While the preceding section details the wide breadth of knowledge available on *M. lucifugus*, there is minimal information about this species in Newfoundland. Particularly, the response of *M. lucifugus* to WNS, and the connectivity of white nose-prolific populations to those in white nose-absent areas of Newfoundland has yet to be studied. To address this knowledge gap, this project will identify important habitat use areas for *M. lucifugus* in Newfoundland, as well as identify patterns in this population's natal philopatry and inter-year fidelity to roosting sites.

III.   REFERENCES

Albers, H. J., Lee, K. D., Martínez-Salinas, A., Middleton, A., Murphy, M., Newbold, S., & Stoellinger, T. (2023). *Review of Environmental Economics and Policy, 17*(1), 91-110. https://doi-org.qe2a-proxy.mun.ca/10.1086/723886.

Arnett, E. B., & Baerwald, E. F. (2013). Impacts of wind energy development on bats: Implications for conservation. In Adams, R. A., & Pedersen, S. C. (Eds.), *Bat Evolution, Ecology, and Conservation* (pp. 435-456). Springer Science and Business Media. https://doi.org/10.1007/978-1-4614-7397-8_21.

Asante, C. K., Jardine, T. D., Van Wilgenburg, S. L., & Hobson, K. A. (2017). Tracing origins of waterfowl using the Saskatchewan River Delta: Incorporating stable isotope approaches in continent-wide waterfowl management and conservation. *The Condor, 119*(2), 261-274. https://doi.org/10.1650/CONDOR-16-179.1.

Ault, W. U., & Kulp, J. L. (1959). Isotopic geochemistry of sulfur. *Geochimica et Cosmochimica Acta, 16*, 201-235.

Avanzinelli, R., Boari, E., Conticelli, S., Francalanci, L., Guarnieri, L., Perini, G., Petrone, C. M., Tommasini, S., & Ulivi, M. (2005). High precision Sr, Nd, and Pb isotopic analyses using the new generation Thermal Ionisation Mass Spectrometer ThermoFinnigan Triton-Ti. *Periodico di Mineralogia, 74*(3), 147-166.

Bach, P., Voigt, C. C., Göttsche, M., Bach, L., Brust, V., Hill, R., Hüppop, O., Lagerveld, S., Schmaljohann, H., & Seebens-Hoyer, A. (2022). Offshore and coastline migration of radio-tagged Nathusius' pipistrelles. *Conservation Science and Practice, 4*(10), e12783. https://doi.org/10.1111/csp2.12783.

Baerwald, E. F., Patterson, W. P., & Barclay, R. M. R. (2014). Origins and migratory

patterns of bats killed by wind turbines in southern Alberta: Evidence from stable isotopes. *Ecosphere, 5*(9), 118. https://doi.org/10.1890/ES13-00380.1.

Bataille, C. P., von Holstein, I. C. C., Laffoon, J. E., Willmes, M., Liu, X.-M., Davies, G. R. (2018). A bioavailable strontium isoscape for Western Europe: A machine learning approach. *PLoS One, 13*(5), Article e0197386. https://doi.org/10.1371/journal.pone.0197386.

Bataille, C. P., Crowley, B. E., Wooller, M. J., & Bowen, G. J. (2020). Advances in global bioavailable strontium isoscapes. *Palaeogeography, Palaeoclimatology, Palaeoecology, 55,* 109849. https://doi.org/10.1016/j.palaeo.2020.109849.

Bataille, C. P., Jaouen, K., Milano, S., Trost, M., Steinbrenner, S., Crubézy, É., & Colleter, R. (2021). Triple sulfur-oxygen-strontium isotopes probabilistic geographic assignment of archaeological remains using a novel sulfur isoscape of western Europe. *PLoS One, 16*(5), e0250383. https://doi.org/10.1371/journal.pone.0250383.

Bell, T., & Liverman, D. (1999). *The Newfoundland story.* Newfoundland and Labrador heritage. https://www.heritage.nf.ca/articles/environment/newfoundland-story.php.

Bell, T., & Liverman, D. (1997). *Landscape.* Newfoundland and Labrador heritage. https://www.heritage.nf.ca/articles/environment/landscape.php.

Bentley, R. A. (2006). Strontium isotopes from the earth to the archaeological skeleton: A review. *Journal of Arcaheological Method and Theory, 13*(3), 135-187. https://doi.org/10.1007/s10816-006-9009-x.

Böttcher, M. E. (2001). Sulfur Isotope Fractionation in the Biogeochemical Sulfur Cycle

of Marine Sediments. *Isotopes in Environmental and Health Studies, 37*(2), 97-99.

    https://doi.org/10.1080/10256010108033286.

Bowen, G. J. (2003). Waterisotopes.org.

    https://wateriso.utah.edu/waterisotopes/index.html.

Bowen, G. J., Liu, Z., Vander Zanden, H. B., Zhao, L., & Takahashi, G. (2014).

    Geographic assignment with stable isotopes in IsoMAP. *Methods in Ecology and*

    Evolution, 5(3), 201-206. https://doi.org/10.1111/2041-210X.12147.

Bowen, G. J., & West, J. B. (2019). Isoscapes for terrestrial migration research. In K. A.

    Hobson & L. I. Wassenaar (Eds.), *Tracking animal migration with stable isotopes*

    (pp. 53-84). Academic Press. https://doi.org/10.1016/B978-0-12-814723-8.00003-

    9.

Bragulla, H. H., & Homberger, D. G. (2009). Structure and functions of keratin proteins

    in simple, stratified, keratinized and cornified epithelia. *Journal of Anatomy,*

    214(4), 516-559. https://doi.org/10.1111/j.1469-7580.2009.01066.x.

Brewer, C. T., Rauch-Davis, W. A., & Fraser, E. E. (2021). The use of intrinsic markers

    for studying the migratory movements of bats. *Animals, 11*(12)*,* 3477.

    https://doi.org/10.3390/ani11123477.

Briggs, J. C. (2017). Emergence of a sixth mass extinction? *Biological Journal of the*

    Linnean Society, 122(2) 243-248. https://doi.org/10.1093/biolinnean/blx063.

Britton, K., Grimes, V., Dau, J., & Richards, M. P. (2009). Reconstructing faunal

    migrations using intra-tooth sampling and strontium and oxygen isotope analyses:

    A case study of modern caribou (*Rangifer tarandus granti*). *Journal of*

Archaeological Science, 36(5), 1163-1172.

https://doi.org/10.1016/j.jas.2009.01.003.

Britzke, E. R., Loeb, S. C., Hobson, K. A., Romanek, C. S., & Vonhof, M. J. (2009).

Using hydrogen isotopes to assign origin of bats in the eastern United States.

Journal of Mammalogy, 90(3), 743-751.

Britzke, H. G., Loeb, S. C., Romanek, C. S., Hobson, K. A., & Vonhof, M. J. (2012).

Variation in catchment areas of Indiana bat (*Myotis sodalis*) hibernacula inferred

from stable hydrogen (δ^2H) jisotope analysis. *Canadian Journal of Zoology,*

90(10), 1243-1250. https://doi.org/10.1139/z2012-093.

Broders, H. G., Farrow, L. J., Hearn, R. N., Lawrence, L. M., & Forbes, G. J. (2014).

Stable isotopes reveal that little brown bats have a broader dietary niche than

northern long-eared bats. *Acta Chiropterologica, 16*(2), 315-325.

https://doi.org/10.3161/150811014X687279.

Broquet, T., & Petit, E. J. (2009). Molecular estimation of dispersal for ecology and

population genetics. *Annual Review of Ecology, Evolution, and Systematics, 40*,

193-216. https://doi.org/10.1146/annurev.ecolsys.110308.120324.

Brower, L. P, & Malcolm, S. B. (1991). Animal migrations: Endangered phenomena.

American Zoologist, 31(1), 265-276. https://doi.org/10.1093/icb/31.1.265.

Campbell, C. J., Fitzpatrick, M. C., Vander Zanden, H. B., & Nelson, D. M. (2020).

Advancing interpretation of stable isotope assignment maps: Comparing and

summarizing origins of known-provenance migratory bats. *Animal Migration,*

7(1), 27-41. https://doi.org/10.1515/ami-2020-0004.

Caron, F., Tessier, A., Kramer, J. R., Schwarcz, H. P., & Rees, C. E. (1986). Sulfur and

oxygen isotopes of sulfate in precipitation and lake water, Quebec, Canada. *Applied Geochemistry, 1*(5), 601-606. https://doi.org/10.1016/0883-2927(86)90067-3.

Case, J. W., & Krouse, H. R. (1980). Variations in sulphur content and stable sulphur isotope composition of vegetation near a SO_2 source at Fox Creek, Alberta, Canada. *Oecologia, 44*, 248-257. https://doi.org/10.1007/BF00572687.

Ceballos, G., Ehrlich, P. R., Barnosky, A. D., García, A., Pringle, R. M., & Palmer, T. M. (2015). Accelerated modern human-induced species losses: Entering the sixth mass extinction. *Science Advances, 1*(5), e1400253. https://doi.org/10.1126/sciadv.1400253.

Cheng, T. L., Reichard, J. D., Coleman, J. T. H., Weller, T. J., Thogmartin, W. E., Reichard, B. E., Bennett, A. B., Broders, H. G., Campbell, J., Etchison, K., Feller, D. J., Geboy, R., Hemberger, T., Herzog, C., Hicks, A. C., Houghton, S., Humber, J., Kath, J. A., King, R. A.,… Frick, W. F. (2021). The scope and severity of white-nose syndrome on hibernating bats in North America. *Conservation Biology, 35*(5), 1586-1597. https://doi.org/10.1111/cobi.13739.

Clare, E. L., Symondson, W. O. C., Broders, H., Fabianek, F., Fraser, E. E., MacKenzie, A., Boughen, A., Hamilton, R., Willis, C. K. R., Martinez-Nuñez, F., Menzies, A. K., Norquay, K. J. O., Brigham, M., Poissant, J., Rintoul, J., Barclay, R. M. R., & Reimer, J. P. (2014). The diet of *Myotis lucifugus* across Canada: Assessing foraging quality and diet variability. *Molecular Ecology,* 23(15), 3618-3632. https://doi.org/10.1111/mec.12542.

Claypool, G. E., Holser, W. T., Kaplan, I. R., Sakai, H, & Zak, I. (1980). The age curves

of sulfur and oxygen isotopes in marine sulfate and their mutual interpretation. *Chemical Geology, 28*, 199-260. https://doi.org/10.1016/0009-2541(80)90047-9.

Clerc, J., Rogers, E. J., & McGuire, L. P. (2021). Testing predications of optimal migration theory in migratory bats. *Frontiers in Ecology and Evolution, 9*, 686379. https://doi.org/10.3389/fevo.2021.686379.

Colman-Sadd, S. P., Hayes, J. P., & Knight, I. (2000). *Geology of the island of Newfoundland*. Newfoundland Department of Mines and Energy, Geological Survey, Map 2000-30, scale 1:1,000,000.

Copeland, S. R., Cawthra, H. C., Fisher, E. C., Lee-Thorp, J. A., Cowling, R. M., le Roux, P. J., Hodgkins, J., & Marean, C. W. (2016). Strontium isotope investigation of ungulate movement patterns on the Pleistocene Paleo-Agulhas Plain of the Greater Cape Floristic Region, South Africa. *Quaternary Science Reviews, 141*, 65-84. https://doi.org/10.1016/j.quascirev.2016.04.002.

Cortes, K. M., & Gillam, E. H. (2020). Assessing the use of rivers as migratory corridors for temperate bats. *Journal of Mammalogy, 101*(2), 448-454. https://doi.org/10.1093/jmammal/gyz211.

Courtiol, A., Rousset, F., Rohwäder, M.-S., Soto, D. X., Lehnert, L. S., Voigt, C. C., Hobson, K. A., Wassenaar, L. I., & Kramer-Schadt, S. (2019). Isoscape computation and inference of spatial origins with mixed models using the R package IsoriX. In K. A. Hobson & L. I. Wassenaar (Eds.), *Tracking animal migration with stable isotopes* (pp. 207-236). Academic Press. https://doi.org/10.1016/B978-0-12-814723-8.00009-X.

Crowley, B. E., Bataille, C. P., Haak, B. A., & Sommer, K. M. (2021). Identifying nesting

grounds for juvenile migratory birds with dual isotope: An initial test using North American raptors. *Ecosphere, 12*(10), e03765. https://doi.org/10.1002/ecs2.3765.

Crumsey, J. M., Searle, J. B., & Sparks, J. P. (2019). Isotope values of California vole (*Microtus californicus*) hair relate to historical drought and land use patterns in California, USA. *Oecologia, 190*, 769-781. https://doi.org/10.1007/s00442-019-04457-2.

Cryan, P. M., Bogan, M. A., Rye, R. O., Landis, G. P., & Kester, C. L. (2004). Stable hydrogen isotope analysis of bat hair as evidence for seasonal molt and long-distance migration. *Journal of Mammalogy, 85*(5), 995-1001. https://doi.org/10.1644/BRG-202.

Cryan, P. M., Stricker, C. A., & Wunder, M. B. (2012). Evidence of cryptic individual specialization in an opportunistic insectivorous bat. *Journal of Mammalogy, 93*(2), 381-389. https://doi.org/10.1644/11-MAMM-S-162.1.

Cryan, P. M., Stricker, C. A., & Wunder, M. B. (2014). Continental-scale, seasonal movements of a heterothermic migratory tree bat. *Ecological Applications, 24*(4), 602-616. https://doi.org/10.1890/13-0752.1.

Dechmann, D. K. N., Wikelski, M., Varga, K., Yohannes, E., Fiedler, W., Safi, K., Burkhard, W.-D., & O'Mara, M. T. (2014). Tracking post-hibernation behavior and early migration does not reveal the expected sex-differences in a "female-migrating" bat. *PLoS One, 9*(12), e114810. https://doi.org/10.1371/journal.pone.0114810.

Dechmann, D. K. N., Wikelski, M., Ellis-Soto, D., Safi, K., & O'Mara, M. T. (2017).

Determinants of spring migration departure decision in a bat. *Biology Letters, 13*(9), 20170395. https://doi.org/10.1098/rsbl.2017.0395.

Dixon, M. D. (2011). Population genetic structure and natal philopatry in the widespread North American bat *Myotis lucifugus*. *Journal of Mammalogy, 92*(6), 1343-1351. https://doi.org/10.1644/10-MAMM-A-426.1.

Dingle, H. (2014). Migration: Definition and scope. In H. Dingle (Ed.), *migration* (pp. 13-23). Oxford University Press.

Faure, G., & Powell, J. L. (1972). *Strontium Isotope Geology* (W. von Engelhardt, T. Hahn, R. Roy, & P. J. Wyllie, Eds.). Springer.

Fenton, M. B. (1969). Summer activity of *Myotis lucifugus* (Chiroptera:Vespertilionidae) at hibernacula in Ontario and Quebec. *Canadian Journal of Zoology, 47*(4), 597-602. https://doi.org/10.1139/z69-103.

Fenton, M. B. (1970). The deciduous dentition and its replacement in *Myotis lucifugus* (Chiroptera: Vespertilionidae). *Canadian Journal of Zoology, 48*(4), 817-820. https://doi.org/10.1139/z70-143.

Fenton, M. B., & Barclay, R. M. R. (1980). *Myotis lucifugus*. *Mammalian Species, 142*, 1-8. https://doi.org/10.2307/3503792.

Flockhart, D. T. T., Kyser, T. K., Chipley, D., Miller, N.G., & Norris, D.R. (2015). Experimental evidence shows no fractionation of strontium isotopes (^{87}Sr/^{86}Sr) among soil, plants, and herbivores: Implications for tracking wildlife and forensic science. *Isotopes in Environmental and Health Studies, 51*(3), 372-381. https://doi.org/10.1080/10256016.2015.1021345.

Font, L., Nowell, G. M., Pearson, D. G., Ottley, C. J., & Willis, S. G. (2007). Sr isotope

analysis of bird feathers by TIMS: A tool to trace bird migration paths and breeding sites. *Journal of Analytical Atomic Spectrometry, 22*(5), 513-522. https://doi.org/10.1039/b616328a.

Font, L., van der Peijl, G., van Wetten, I., Vroon, P., van der Wagt, B., & Davies, G. (2012). Strontium and lead isotope ratios in human hair: Investigating a potential tool for determining recent human geographical movements. *Journal of Analytical Atomic Spectrometry, 27*(5), 719-732. https://doi.org/10.1039/c2ja10361c.

Fox, A. D., Hobson, K. A., De Jong, A., Kardynal, K. J., Koehler, G., & Heinicke, T. (2016). Flyway population delineation in Taiga Bean Geese *Anser fabalis fabalis* revealed by multi-element feather stable isotope analysis. *International Journal of Avian Science, 159*(1), 66-75. https://doi.org/10.1111/ibi.12417.

Fraser, E. E., McGuire, L. P., Eger, J. L., Longstaffe, F. J., & Fenton, M. B. (2012). Evidence of latitudinal migration in tri-colored bats, *Perimyotis subflavus*. *Public Library of Science One, 7*(2), e31419. https://doi.org/10.1371/journal.pone.0031419.

Fraser, E. E., Longstaffe, F. J., & Fenton, M. B. (2013). Moulting matters: The importance of understanding moulting cycles in bats when using fur for endogenous marker analysis. *Canadian Journal of Zoology, 91*(8), 533-544. https://doi.org/10.1139/cjz-2013-0072.

Fraser, E. E., Miller, J. F., Longstaffe, F. J., & Fenton, M. B. (2015). Systematic variation in the stable hydrogen isotope (δ^2H) composition of fur from summer populations of two species of temperate insectivorous bats. *Mammalian Biology, 80*(4), 278-284. https://doi.org/10.1016/j.mambio.2015.03.006.

Fraser, E. E., Brooks, D., & Longstaffe, F. J. (2017). Stable isotope investigation of the migratory behavior of silver-haired bats (*Lasionycteris noctivagans*) in eastern North America. *Journal of Mammalogy, 98*(5), 1225-1235. https://doi.org/10.1093/jmammal/gyx085.

Frick, W. F., Baerwald, E. F., Barclay, R. M. R., Szymanski, J. A., Weller, T. J., Russell, A. L., Loeb, S. C., Medellin, R. A., & McGuire, L. P. (2009). Fatalities at wind turbines may threaten population viability of a migratory bat. *Biological Conservation, 209*, 172-177. https://doi.org/10.1016/j.biocon.2017.02.023.

Furmankiewicz, J., & Kucharska, M. (2009). Migration of bats along a large river valley in southwestern Poland. *Journal of Mammalogy, 90*(6), 1310-1317. https://doi.org/10.1644/09-MAMM-S-099R1.1.

Greene, B. A. (1974). An Outline of the Geology of Labrador. *Geoscience Canada, 1*(3), 36-40. Retrieved from https://journals.lib.unb.ca/index.php/GC/article/view/2844.

Hebert, C. E., & Wassenaar, L. I. (2005). Feather stable isotopes in western North American waterfowl: Spatial patterns, underlying factors, and management applications. *Wildlife Society Bulletin, 33*(1), 92-102. https://doi.org/10.2193/0091-7648(2005)33[92:FSIIWN]2.0.CO;2.

Hild, M. H. (2012). *Geology of Newfoundland: field guide*. Boulder Publications.

Hobson, K. A., Norris, D. R., Kardynal, K. J., & Yohannes, E. (2019). Animal migration: A context for using new techniques and approaches. In K. A. Hobson & L. I. Wassenaar (Eds.), *Tracking animal migration with stable isotopes* (pp. 1-23). Academic Press. https://doi.org/1016/B978-0-12-814723-8.00001-5.

Holt, E., Evans, J. A., & Madgwick, R. (2021). Strontium (^{87}Sr/^{86}Sr) mapping: A critical

review of methods and approaches. *Earth-Science Reviews, 216*, Article 103593.

https://doi.org/10.1016/j.earscirev.2021.103593.

Hoppe, K. A., Koch, P. L., Carlson, R. W., & Webb, S. D. (1999). Tracking mammoths

and mastodons: Reconstruction of migratory behavior using strontium isotope

ratios. *Geology, 27*(5), 439-442. https://doi.org/10.1130/0091-

7613(1999)027<0439:TMAMRO>2.3.CO;2.

Ijäs, A., Kahilainen, A., Vasko, V. V., & Lilley, T. M. (2017). Evidence of the migratory

bat, *Pipistrellus nathusii*, aggregating to the coastlines in the Northern Baltic Sea.

Acta Chiropterologica, 19(1), 127-139.

https://doi.org/10.3161/15081109ACC2017.19.1.010.

Jameson, J. W., & Willis, C. K. R. (2014). Activity of tree bats at anthropogenic tall

structures: Implications for mortality of bats at wind turbines. *Animal Behaviour,
97*, 145-152. https://doi.org/10.1016/j.anbehav.2014.09.003.

Johnson, J. B., & Gates, J. E. (2008). Spring migration and roost selection of female

Myotis leibii in Maryland. *Northeastern Naturalist, 15*(3), 453-460.

https://doi.org/10.1656/1092-6194-15.3.453.

Johnson, L. N. L., McLeod, B. A., Burns, L. E., Arseneault, K., Frasier, T. R., & Broders,

H. G. (2015). Population genetic structure within and among seasonal site types in the

little brown bat (*Myotis lucifugus*) and the northern long-eared bat (*M.

septentrionalis*). *Public Library of Science One, 10*(7), e0133457.

https://doi.org/10.1371/journal.pone.0126309.

Johnson, J. S., Treanor, J. J., Slusher, A. C., & Lacki, M. J. (2019). Buildings provide

vital habitat for little brown myotis (*Myotis lucifugus*) in a high-elevation

landscape. *Ecosphere, 10*(11), e02925. https://doi.org/10.1002/ecs2.2925.

Jonasson, K. A., & Guglielmo, C. G. (2016). Sex differences in spring migration timing

and body composition of silver-haired bats *Lasionycteris noctivagans*. *Journal of*

Mammalogy, 97(6), 1535-1542. https://doi.org/10.1093/jmammal/gyw119.

Kabalika, Z., Morrison, T. A., McGill, R. A. R., Munishi, L. K., Ekwem, D., Mahene, W.

L., Lobora, A. L., Newton, J., Morales, J. M., Haydon, D. T., & Hopcraft, G. G. J.

C. (2020). Tracking animal movements using biomarkers in tail hairs: A novel

approach for animal geolocating from sulfur isoscapes. *Movement Ecology, 8*, 37.

https://doi.org/10.1186/s40462-020-00222-w.

Kaplan, I. R. (1975). Stable isotopes as a guide to biogeochemical processes. *Proceedings*

of the Royal Society B, 189(1095), 183-211.

https://doi.org/10.1098/rspb.1975.0052.

Krauel, J. J., & McCracken, G. F. (2013). Recent advances in bat migration research. In

Adams, R. A., & Pedersen, S. C. (Eds.), *Bat Evolution, Ecology, and*

Conservation (pp. 293-313). Springer Science and Business Media.

https://doi.org/10.1007/978-1-4614-7397-8_15.

Krouse, H. R. (1980). Sulfur isotopes in our environment. In P. Fritz & J. C. Fontes

(Eds.), *Handbook of Environmental Isotope Geochemistry* (pp. 435-471). Elsevier

Science Ltd.

Kruszynski, C., Bailey, L. D., Courtiol, A., Bach, L., Bach, P., Göttsche, Ma., Göttsche,

Mi., Hill, R., Lindecke, O., Matthes, H., Pommeranz, H., Popa-Lisseanu, A. G.,

Seebens-Hoyer, A., Tichomirowa, M., & Voigt, C. C. (2020). Identifying

migratory pathways of Nathusius' pipistrelles (*Pipistrellus nathusii*) using stable

hydrogen and strontium isotopes. *Rapid Communications in Mass Spectrometry,*

35(6). https://doi.org/10.1002/rcm.9031.

Kurta, A., & Smith, S. M. (2020). Changes in population size and clustering behavior of

hibernating bats in the Upper Peninsula of Michigan after arrival of white-nose

syndrome. *Northeastern Naturalist, 27*(4), 763-772.

https://doi.org/10.1656/045.027.0415.

Lehnert, L. S., Kramer-Schadt, S., Schönborn, S., Lindecke, O., Niermann, I., & Voigt, C.

C. (2014). Wind farm facilities in Germany kill noctule bats from near and far.

Public Library of Science One, 9(8), e103106.

https://doi.org/10.1371/journal.pone.0103106.

Lehnert, L. S., Kramer-Schadt, S., Teige, T., Hoffmeister, U., Popa-Lisseanu, A.,

Bontadina, F., Ciechanowski, M., Dechmann, D. K. N., Kravchenko, K.,

Presetnik, P., Starrach, M., Straube, M., Zoephel, U., & Voigt, C. C. (2018).

Variability and repeatability of noctule bat migration in Central Europe: Evidence

for partial and differential migration. *Proceedings of the Royal Society B,*

285(1893), 20182174. https://doi.org/10.1098/rspb.2018.2174.

Lott, C. A., Meehan, T. D., & Heath, J. A. (2003). Estimating the latitudinal origins of

migratory birds using hydrogen and sulfur stable isotopes in feathers: Influence of

marine prey base. *Oecologia, 134*, 505-510. https://doi.org/10.1007/s00442-002-

1153-8.

Măntoiu, D. S., Kravchenko, K., Lehnert, L. S., Vlaschenko, A., Moldovan, O. T., Mirea,

I. C., Stanciu, R. C., Zaharia, R., Popescu-Mirceni, R., Nistorescu, M. C., & Voigt, C. C. (2020). Wildlife and infrastructure: Impact of wind turbines on bats in the Black Sea coast region. *European Journal of Wildlife Research, 66*, 44. https://doi.org/10.1007/s10344-020-01378-x.

McCutchan, J. H., Lewis, W. M., Kendall, C., & McGrath, C. C. (2003). Variation in trophic shift for stable isotope ratios of carbon, nitrogen, and sulfur. *Oikos, 102*(2), 378-390. https://doi.org/10.1034/j.1600-0706.2003.12098.x.

McGuire, L. P., & Guglielmo, C. G. (2009). What can birds tell us about the migration physiology of bats? *Journal of Mammalogy, 90*(6), 1290-1297. https://doi.org/10.1644/09-MAMM-S-084R.1.

McGuire, L. P. (2022, Aug. 11). *Migration ecophysiology: The influence of heterothermy in migrating bats and birds* [Oral presentation]. North American Symposium for Bat Research, Austin, TX, United States.

Meehan, T. D., Lott, C. A., Sharp, Z. D., Smith, R. B., Rosenfield, R. N., Stewart, A. C., & Murphy, R. K. (2001). Using hydrogen isotope geochemistry to estimate the natal latitudes of immature Cooper's Hawks migrating through the Florida Keys. *The Condor, 103*(1), 11-20. https://doi.org/10.1093/condor/103.1.11.

Moussy, C., Hosken, D. J., Mathews, F., Smith, G. C., Aegerter, J. N., & Bearhop, S. (2013). Migration and dispersal of bats and their influence on genetic structure. *Mammal Review, 43*(3), 183-195. https://doi-org.qe2a-proxy.mun.ca/10.1111/j.1365-2907.2012.00218.x.

Naughton, D. (2012). *The natural history of Canadian mammals* (pp. 784). University of Toronto Press.

Nehlich, O. (2015). The application of sulphur isotope analyses in archaeological

    research: A review. *Earth-Science Reviews, 142*, 1-17.

    https://doi.org/10.1016/j.earscirev.2014.12.002.

Nielsen, H. (1974). Isotopic composition of the major contributors to atmospheric sulfur.

    Tellus, 26(1-2), 213-221. https://doi.org/10.1111/j.2153-3490.1974.tb01969.x.

Norquay, K. J. O., Martinez-Nuñez, F., Dubois, J. E., Monson, K. M., & Willis, C. K. R.

    (2013). Long-distance movements of little brown bats (*Myotis lucifugus*). *Journal*

    of Mammalogy, 94(2), 506-515. https://doi.org/10.1644/12-MAMM-A-065.1.

Nriagu, J. O., Rees, C. E., Mekhtiyeva, V. L., Lein, A. Y., Fritz, P., Drimmie, R. J.,

    Pankina, R. G., Robinson, R. W., Krouse, H. R. (1991). Hydrosphere. In H. R.

    Krouse (Ed.), *Stable isotopes: Natural and Anthropogenic sulphur in the*

    environment (pp. 177-265). Scientific Committee on Problems of the Environment

    (SCOPE).

O'Mara, M. T., Wikelski, M., & Dechmann, D. K. N. (2014). 50 years of bat tracking:

    Device attachment and future directions. *Methods in Ecology and Evolution, 5*(4),

    311-319. https://doi.org/10.1111/2041-210X.12172.

Park, A. C., & Broders, H. G. (2012). Distribution and roost selection of bats on

    Newfoundland. *Northeastern Naturalist, 19*(2), 165-176.

    https://doi.org/10.1656/045.019.0203.

Peterson, B. J., & Fry, B. (1987). Stable isotopes in ecosystem studies. *Annual Review of*

    Ecology, Evolution, and Systematics, 18, 293-320.

Pettit, J. L., & O'Keefe, J. M. (2017). Day of year, temperature, wind, and precipitation

predict timing of bat migration. *Journal of Mammalogy, 98*(5), 1236-1248. https://doi.org/10.1093/jmammal/gyx054.

Pinzone, M., Acquarone, M., Huyghebaert, L., Sturaro, N., Michel, L. N., Siebert, U., & Das, K. (2017). Carbon, nitrogen, and sulphur isotopic fractionation in captive juvenile hooded seal (*Cystophora cristata*): Application for diet analysis. *Rapid Communications in Mass Spectrometry, 31*(20), 1720-1728. https://doi.org/10.1002/rcm.7955.

Popa-Lisseanu, A. G., & Voigt, C. C. (2009). Bats on the move. *Journal of Mammalogy, 90*(6), 1283-1289. https://doi.org/10.1644/09-MAMM-S-130R2.1.

Popa-Lisseanu, A. G., Sörgel, K., Luckner, A., Wassenaar, L.I., Ibáñez, C., Kramer-Schadt, S., Ciechanowski, M., Görföl, T., Niermann, I., Beuneux, G., Mysłajek, R. W., Juste, J., Fonderflick, J., Kelm, D. H., & Voigt, C. C. (2012). A triple-isotope approach to predict the breeding origins of European bats. *PLoS One, 7*(1), e30388. https://doi.org/10.1371/journal.pone.0030388.

Pylant, C. L., Nelson, D. M., & Keller, S. R. (2014). Stable hydrogen isotopes record the summering grounds of eastern red bats (*Lasiurus borealis*). *PeerJ,* e629. https://doi.org/10.7717/peerj.629.

Pylant, C. L., Nelson, D. M., Fitzpatrick, M. C., Gates, J. E., & Keller, S. R. (2016). Geographic origins and population genetics of bats killed at wind-energy facilities. *Ecological Applications, 26*(5), 1381-1395. https://doi.org/10.1890/15-0541.

Randall, L. A., Jung, T. S., & Barclay, R. M. R. (2014). Roost-site selection and

movements of little brown myotis (*Myotis lucifugus*) in Southwestern Yukon. *Northwestern Naturalist, 95*(3), 312-317. https://doi.org/10.1898/13-02.1.

Richards, M. P., Fuller, B. T., Sponheimer, M., Robinson, T., & Ayliffe, L. (2003). Sulphur isotopes in palaeodietary studies: A review and results from a controlled feeding experiment. *International Journal of Osteoarchaeology, 13*(1-2), 37-45. https://doi.org/10.1002/oa.654.

Roby, P. L., Gumbert, M. W., & Lacki, M. J. (2019). Nine years of Indiana bat (*Myotis sodalis*) spring migration behavior. *Journal of Mammalogy, 100*(5), 1501-1511. https://doi.org/10.1093/jmammal/gyz104.

Rogers, E. J., McGuire, L., Longstaffe, F. J., Clerc, J., Kunkel, E., & Fraser, E. (2021). Relating wing morphology and immune function to patterns of partial and differential bat migration using stable isotopes. *Journal of Animal Ecology, 91*(4), 858-869. https://doi.org/10.1111/1365-2656.13681.

Ross, S. R. P.-J., O'Connell, D. P., Deichmann, J. L., Desjonquéres, C., Gasc, A., Phillips, J.N., Sethi, S. S., Wood, C. M., Burivalova, Z. (2023). Passive acoustic monitoring provides a fresh perspective on fundamental ecological questions. *Functional Ecology, 37*(4), 959-975. https://doi.org/10.1111/1365-2435.14275.

Rubenstein, D. R., & Hobson, K. A. (2004). From birds to butterflies: Animal movement patterns and stable isotopes. *Trends in Ecology and Evolution, 19*(5), 256-263. https://doi.org/10.1016/j.tree.2004.03.017.

Samoray, S. T., Cotham, S. N., & Gumbert, M. W. (2019). Spring migration behavior of a *Perimyotis subflavus* (Tri-colored bat) from Tennessee. *Southeastern Naturalist, 18*(3), 16-20. https://doi.org/10.1656/058.018.0302.

Segers, J. L., & Broders, H. G. (2015). Carbon (δ^{13}C) and nitrogen (δ^{15}N) stable isotope

signatures in bat fur indicate swarming sites have catchment areas for bats from

different summering areas. *PLoS One, 10*(4), e0125755.

https://doi.org/10.1371/journal.pone.0125755.

Sellick, M. J., Kyser, T. K., Wunder, M. B., Chipley, D., & Norris, D. R. (2009).

Geographic variation of strontium and hydrogen isotopes in avian tissue:

Implications for tracking migration and dispersal. *PLoS One, 4*(3), e4735.

https://doi.org/10.1371/journal.pone.0004735.

Shin, W.-J., Jung, M., Ryu, J-S., Hwang, J., & Lee, K.-S. (2020). Revisited digestion

methods for trace element analysis in human hair. *Journal of Analytical Science

and Technology, 11*, 1. https://doi.org/10.1186/s40543-019-0200-6.

Slough, B. G., & Jung, T. S. (2020). Little brown bats utilize multiple maternity roosts

within foraging areas: Implications for identifying summer habitat. *Journal of

Fish and Wildlife Management, 11*(1), 311-320. https://doi.org/10.3996/052019-

JFWM-039.

Solari, S. (2021). *Myotis lucifugus*. The IUCN Red List of Threatened Species.

https://doi.org/10.2305/IUCN.UK.2021-3.RLTS.T14176A208031565.en.

Soto, D. X., Koehler, G., Wassenaar, L. I., & Hobson, K. A. (2017). Re-evaluating of the

hydrogen stable isotopic composition of keratin calibration standards for wildlife

and forensic science applications. *Rapid Communications in Mass Spectrometry,

31*(14), 1193-1203. https://doi.org/10.1002/rcm.7893.

Sullivan, A. R., Bump, J. K. Kruger, L. A., & Peterson, R. O. (2012). Bat-cave catchment

areas: Using stable isotopes (δD) to determine the probable origins of hibernating bats. *Ecological Applications, 22*(5), 1428-1434. https://doi.org/10.1890/11-1438.1.

Sunga, J. S., Humber, J., Rodrigues, B., McGuire, L., & Broders, H. (2021). Long-distance movement over a period of days by a female *Myotis lucifugus* in Newfoundland, Canada. *Northeastern Naturalist, 28*(2), 24-26. https://doi.org/10.1656/045.028.0214.

Terzer, S., Wassenaar, L. I., Araguás-Araguás, L. J., & Aggarwal, P. K. (2013). Global isoscapes for δ^{18}O and δ^2H in precipitation: Improved prediction using regionalized climatic regression models. *Hydrology and Earth System Sciences, 17*(11), 4713-4728. https://doi.org/10.5194/hess-17-4713-2013.

Thode, H.G., Monster, J., & Dunford, H. B. (1961). Sulfur isotope geochemistry. *Geochimica et Cosmochimica Acta, 25*(3), 159-174. https://doi.org/10.1016/0016-7037(61)90074-6.

Timsic, S., & Patterson, W. P. (2014). Spatial variability in stable isotope values of surface waters of Eastern Canada and New England. *Journal of Hydrology, 511*, 594-604. https://doi.org/10.1016/j.jhydrol.2014.02.017.

Tipple, B. J., Chau, T., Chesson, L. A., Fernandez, D. P., & Ehleringer, J. R. (2013). Isolation of strontium pools and isotope ratios in modern human hair. *Analytica Chimica Acta, 798*, 64-73. https://doi.org/10.1016/j.aca.2013.08.054.

Vander Zanden, H. B., Soto, D. X., Bowen, G. J., & Hobson, K. A. (2016). Expanding the

isotopic toolbox: Applications of hydrogen and oxygen stable isotope ratios to food web studies. *Frontiers in Ecology and Evolution, 4*, 20. https://doi.org/10.3389/fevo.2016.00020.

Van Zyll de Jong, C. G. (1983). *Handbook of Canadian Mammals: Bats* (2nd Ed.). Canadian Museum of Natural Sciences.

Vitória, L., Otero, N., Soler, A., & Canals, Á. (2004). Fertilizer characterization: Isotopic data (N, S, O, C, and Sr). *Environmental Science and Technology, 38*(12), 3254-3262. https://doi.org/10.1021/es0348187.

Voigt, C. C., Lehmann, D., & Greif, S. (2015). Stable isotope ratios of hydrogen separate mammals of aquatic and terrestrial food webs. *Methods in Ecology and Evolution, 6*(11), 1332-1340. https://doi.org/10.1111/2041-210X.12414.

Wadleigh, M. A., & Blake, D. M. (1999). Tracing sources of atmospheric sulphur using epiphytic lichens. *Environmental Pollution, 106*(3), 265-271. https://doi.org/10.1016/S0269-7491(99)00114-1.

Wassenaar, L. I., & Hobson, K. A. (1998). Natal origins of migratory monarch butterflies at wintering colonies in Mexico: New isotopic evidence. *Proceedings of the National Academy of Sciences of the United States of America, 95*(26), 15436-15439. https://doi.org/10.1073/pnas.95.26.15436.

Wassenaar, L. I., & Hobson, K. A. (2003). Comparative equilibration and online technique for determination of non-exchangeable hydrogen of keratins for use in animal migration studies. *Isotopes in Environmental and Health Studies, 39*(3), 211-217. https://doi.org/10.1080/1025601031000096781.

Wassenaar, L. I. (2019). Introduction to conducting stable isotope measurements for

animal migration. In K. A. Hobson & L. I. Wassenaar (Eds.), *Tracking animal migration with stable isotopes* (pp. 25-51). Academic Press. https://doi.org/1016/B978-0-12-814723-8.00002-7.

Webb, E. C., Newton, J., Lewis, J., Stewart, A., Miller, B., Tarlton, J. F., & Evershed, R. P. (2017). Sulphur-isotope compositions of pig tissues from a controlled feeding study. *Science and Technology of Archaeological Research, 3*(1), 71-79. https://doi.org/10.1080/20548923.2017.1368821.

Wijayawardhana, D. (1998). *Geological zones of Newfoundland and Labrador* [Map]. Newfoundland and Labrador heritage. https://www.heritage.nf.ca/articles/environment/landscape.php.

Wilcove, D. S. (2008). Animal migration: An endangered phenomenon? *Issues in Science and Tecchnology, 24*(3), 71-78.

Wimsatt, W. A. (1945). Notes on breeding behavior, pregnancy, and parturition in some Vespertilionid bats of the Eastern United States. *Journal of Mammalogy, 26*(1), 23-33. https://doi.org/10.2307/1375029.

Wright, P. G. R., Newton, J., Agnelli, P., Budinski, I., Di Salvo, I., Flaquer, C., Fulco, A., Georgiakakis, P., Martinoli, A., Mas, M., Mazija, M., Mucedda, M., Papadatou, E., Petrov, B., Rodrigues, L., Mathews, F., & Russo, D. (2020). Hydrogen isotopes reveal evidence of migration of *Miniopterus schreibersii* in Europe. *BMC Ecology, 20,* 52. https://doi.org/10.1186/s12898-020-00321-7.

Zazzo, A., Monahan, F. J., Moloney, A. P., Green, S., & Schmidt, O. (2011). Sulphur isotopes in animal hair track distance to sea. *Rapid Communications in Mass Spectrometry, 25*(17), 2371-2378. https://doi.org/10.1002/rcm.5131.

CHAPTER II: Using strontium isotope techniques to elucidate lifetime movements of wild animals: A case study of *Myotis lucifugus* in insular Newfoundland, Canada

I.   ABSTRACT

The analysis of animal tissues for biochemical markers is commonly used to infer landscape-level movements by terrestrial organisms. However, given that most applications of this technique investigate seasonal migrations at a continental scale; our ability to study regional movements across a range of timescales remains limited. We addressed this limitation by using multiple tissues (bones, teeth, fur) and strontium isotope techniques to infer movements of an endangered bat species, *Myotis lucifugus*, in insular Newfoundland, Canada. We found significant differences in the $^{87}Sr/^{86}Sr$ values of fur sampled from geologically distinct regions of the island. Thus, we used regional $^{87}Sr/^{86}Sr$ estimates calculated from the fur of known origin individuals and the absolute difference between $^{87}Sr/^{86}Sr$ values of teeth and bones ($|^{87}Sr/^{86}Sr_T-^{87}Sr/^{86}Sr_B|$) to infer movements relative to natal region. In total, we interpreted movements for 21 individuals and found that male and female *M. lucifugus* in insular Newfoundland are equally likely to disperse from their natal region. This comparative study illustrates the applications of strontium isotopes incorporated into fur, teeth, and bone for investigations of lifetime movements of terrestrial species, expanding the breadth of applications of intrinsic markers to study animal mobility.

Keywords: migration; bats; *Myotis lucifugus;* intrinsic markers; strontium isotopes; $^{87}Sr/^{86}Sr$; calciferous tissues; bones; teeth; dispersal; philopatry; Newfoundland, Canada

II. GENERAL SUMMARY

Understanding the movements and life histories of organisms can help us to safeguard their needs in a changing climate. However, our ability to identify movements of individuals to specific habitats, and relate those movements to birthplace, is limited. In this study, we used intrinsic markers – chemical signatures incorporated into an organism's tissues that vary predictably across the landscape – to infer regional occupancy up to three times in an individual's life. By comparing the $^{87}Sr/^{86}Sr$ values in fur, teeth, and bone of little brown bats, *Myotis lucifugus*, we inferred birthplace ($^{87}Sr/^{86}Sr$ values of teeth, bone) and compared it to residency location during the summer preceding death ($^{87}Sr/^{86}Sr$ values of fur). Our results indicated that *M. lucifugus* males and females are equally likely to disperse to new regions after birth. This study paves the way for researchers interested in using intrinsic markers to investigate lifetime movements of species.

III. INTRODUCTION

Movements of organisms to or from natal areas (philopatry or dispersal) is a facet of natural history that is minimally understood and understudied for many species, and evolutionary inferences about this behavior in mammals is often based on a small group of well-studied, diurnal species (Clutton-Brock, 2021). However, at its core, the protection of imperiled species requires a fundamental understanding of how and why organisms disperse or return to natal areas; this information is crucial to decisions regarding protections of, and restorations to, essential breeding habitat and stopover sites. As researchers, it is vital to gain a better understanding of these behaviors by asking

several critical questions: Where and how far are these species moving across the landscape? What habitat characteristics are key predictors of movement corridors for these species? Which demographics of these populations tend to disperse to new habitats? Understanding this fundamental information will benefit researchers, policymakers, and community members who seek to protect imperiled species.

Intrinsic markers show promise for answering these crucial biological and behavioral questions. These techniques use chemical signatures incorporated into an organism's tissues that vary predictably across the landscape (Hobson et al., 2019). The chemical composition of these tissues can then be used to infer habitat use during the time that the tissue was grown (Hobson et al., 2019), and tissues grown at various times in an individual's life can provide information from multiple time-points. However, analyses of intrinsic markers are not without their limitations. The most common approach, which uses stable hydrogen isotope values (δ^2H) incorporated in fur or feathers and compared to predicted δ^2H values in the precipitation of the study area (e.g., Hobson & Wassenaar, 1996; Cryan et al., 2004), offers information about large-scale movements across the landscape in a single year of the individual's life. For species that migrate or disperse regionally, however, these movements may go unnoticed due to the resolution of the technique (Hobson et al., 2019). Researchers have addressed this limitation by combining intrinsic marking techniques with extrinsic marking techniques (e.g., von Rönn et al., 2020), morphological characteristics (e.g., Clem et al., 2022; Rogers et al., 2021), or species distribution models (e.g., Wieringa et al., 2023). Additional methods for addressing this limitation include overlaying data from multiple isotopes (e.g., Horacek, 2011; Popa-Lisseanu et al., 2012; Hobson et al., 2022), including introducing

underutilized isotopic systems [e.g., $^{87}Sr/^{86}Sr$ (Kruszynski et al., 2020; Crowley et al., 2021; Reich et al., 2021)]. While each solution improves the scale at which movements can be identified, they do not improve the timeline when only individual tissues are being considered. The tissue analyzed, commonly fur, feathers, or insect wing membrane, restricts movement or habitat use predictions to the time of formation. Therefore, when fur or feathers are analyzed for stable isotopes, movements can be identified in a single year. However, identifying patterns in lifetime movements of extant organisms using intrinsic markers alone is still in its infancy, thus there is a need for further investigations using multiple tissues to address this limitation.

The underlying principle behind using multiple tissues to study animal movements is that each tissue is formed during a unique period in the organism's life and represents the local environment during tissue formation (Brewer et al., 2021). When compared, the isotopic values of each tissue can infer movements throughout the organism's lifetime and can be used to answer questions about the natural histories and movements of single organisms or populations. The analysis of multiple tissues for stable isotopes has been used primarily for questions related to diet (e.g., Frick et al., 2014; Voigt et al., 2016), while only a few studies use a comparison between tissues to infer movements (but see Fraser et al., 2010; Wright et al., 2020; Hamilton et al., 2021). The use of an organism's tissues for intrinsic marker analysis requires a basic understanding of a few underlying biological concepts: (1) whether the tissue is metabolically active (continuously forming) or inert (fixed after formation), (2) the timing of formation for metabolically inert tissues or the tissue turnover rate (i.e., the rate an intrinsic marker is replaced in a given tissue) for metabolically active tissues; and (3) the relative quantity of a given intrinsic marker in

the tissue(s) of interest (Brewer et al., 2021). While much of this information is available for commonly used tissues (e.g., fur, feather), our understanding of these concepts may be rudimentary for lesser-used tissues (e.g., liver, muscle, bone).

The radiogenic isotopes of strontium ($^{87}Sr/^{86}Sr$) are an intrinsic marker that can be used to infer regional movements of species, are incorporated into a number of tissues, and have a thorough body of literature detailing their use in studies of both modern (e.g., Kruszynski et al., 2020; Crowley et al., 2021; Reich et al., 2021) and prehistoric organisms (e.g., Britton et al., 2011; Copeland et al., 2016; Price et al., 2017). The ratio of these isotopes is known to vary predictably with underlying bedrock type and age (depending on the concentrations of ^{87}Rb, ^{87}Sr, and ^{86}Sr at the time of rock formation) (Faure & Powell, 1972; Bentley, 2006). Additionally, as Sr^{2+} is known to substitute for calcium (Ca^{2+}) in biological tissues, these isotopes are abundant in the calciferous tissues of organisms (Faure & Powell, 1972; Bentley, 2006). Therefore, this isotopic system is particularly well suited for study areas with diverse geologic histories and analyses of calciferous tissues. Several studies have also used $^{87}Sr/^{86}Sr$ values in fur or feathers to infer migratory movements of organisms (e.g., Font et al., 2007; Kruszynski et al., 2020; Crowley et al., 2021). Despite the proliferation of this technique, analysis of keratinous tissues for $^{87}Sr/^{86}Sr$ values requires initial method development to ensure no external ("exogenous") contamination exists in the tissue, and the $^{87}Sr/^{86}Sr$ value generated during analysis is not skewed by the relatively low concentration of Sr isotopes in the tissue (Font et al., 2007; Font et al., 2012; Tipple et al., 2013; Shin et al., 2020).

To our knowledge, only one study has used Sr isotopes incorporated into bat fur to infer movements. Kruszynski et al. (2020) used a combination of δ^2H and $^{87}Sr/^{86}Sr$ values

in the fur of *Pipistrellus nathusii* to infer seasonal movements in Europe. This investigation reported a discrimination factor of 0.0028 ± 0.0002 between predicted bioavailable Sr isotope values and those in local bat fur. However, previous studies have reported little to no fractionation of ^{87}Sr across trophic levels (Flockhart et al., 2015). Therefore, Sr isotope analysis of bat fur requires additional investigation to better understand the applications of this technique in movement studies.

Here, we build on the currently available literature by using multiple tissues (bones, teeth, fur), the distribution of ^{87}Sr/^{86}Sr in Newfoundland, and the regional movements of *M. lucifugus* to advance the field of movement studies using intrinsic marker analyses. To do this, we first evaluate whether the fur of *M. lucifugus* contains great enough concentrations of Sr to be analyzed for ^{87}Sr/^{86}Sr, and how the ^{87}Sr/^{86}Sr values differ among teeth, fur, and bone in juvenile bats. We predict that *M. lucifugus* fur contains high enough concentrations of Sr to be analyzed for ^{87}Sr/^{86}Sr. Further, we predict that fur, bone, and teeth will have a similar ^{87}Sr/^{86}Sr values in juvenile bats, as these individuals will have formed all three tissues at the same location (van Zyll de Jong, 1983). Next, we correlate the variation in ^{87}Sr/^{86}Sr values between geologically distinct regions in insular Newfoundland with the isotopic signatures in the fur of known origin individuals. We predict that known origin fur samples collected from geologically distinct regions of the island would have ^{87}Sr/^{86}Sr values that are significantly different. Finally, we identify lifetime movements for adult *M. lucifugus* individuals in Newfoundland. We predict that, when comparing calciferous and fur tissues, adult female individuals would be more likely to have similar ^{87}Sr/^{86}Sr values than males, as females are known to

55

exhibit some degree of natal philopatry while males may be more likely to disperse from their natal regions (Dixon, 2011; Johnson et al., 2015).

IV.   MATERIALS & METHODS

A. Study species

Myotis lucifugus is a small (7 – 10 g), insectivorous, globally endangered species of bat whose habitat ranges from northern Canada to the southern U.S. (Fenton, 1970; Solari, 2021). From September to May, individuals of this species will hibernate in caves or abandoned mines, after which they will undergo spring migratory movements, typically 200 – 500 km (Fenton et al., 1969; Norquay et al., 2013; Sunga et al., 2021), to summer roosting habitats [typically buildings or artificial structures, tree cavities, rockpiles or woodpiles (Fenton & Barclay, 1980; Norquay et al., 2013)]. During this time, parous females will congregate to maternity roosts where they will give birth and raise young while nonreproductive females and males will recover fat stores depleted during hibernation, foraging in both terrestrial and aquatic ecosystems (Wimsatt, 1945; van Zyll de Jong, 1983; Broders et al., 2014). After summer residency and before hibernation, typically in August, M. lucifugus will undergo a fall migration and congregate at hibernacula for swarming and mating; however, the specifics around swarming, especially regarding distance traveled to swarming sites and movement behavior during the swarming season, are still being unraveled (e.g., Davis & Hitchcock, 1965; Fenton, 1969; Norquay et al., 2013; Gallant & Broders, 2015; Fraser & McGuire, 2023). Likewise, sex-biased patterns in dispersal in this species are still under investigation (Dixon, 2011; Norquay et al., 2013; Burns et al., 2014; Johnson et al., 2015).

Myotis lucifugus rapidly grows calciferous tissues early in life (Fenton, 1970; van Zyll de Jong, 1983), and its fur tissue is annually replaced (Sullivan et al., 2012). Specifically, adult dentition in *M. lucifugus* is formed 14 – 21 days after birth, and is considered metabolically inert (Brewer et al., 2021; Fenton, 1970). Likewise, the metacarpal-phalangeal joint (representative of bone tissue) in *M. lucifugus* is calcified 29 days after birth and is considered metabolically active but is known to slowly turnover after calcification, although the specific timeframe of turnover is unclear (Kunz & Anthony, 1982; van Zyll de Jong, 1983; Voigt et al., 2003). In rats, the turnover rate of bone tissue has been reported anywhere from 500 days to the full lifespan of the organism (Thompson & Ballou, 1956). Finally, fur tissue in *M. lucifugus* is thought to be replaced in early July to late August, and is considered metabolically inert (Voigt et al., 2003; Sullivan et al., 2012). Therefore, the $^{87}Sr/^{86}Sr$ value associated with bone and teeth will reflect habitat occupancy in early life (i.e., natal location) while the $^{87}Sr/^{86}Sr$ value associated with fur will reflect habitat occupancy during either the previous summer [for those individuals found outside of the summer residency period ("unknown origin individuals")] or the location of mortality [for those individuals found at the location of fur replacement ("known origin individuals")].

B. Study area

The island of Newfoundland is an ideal location for this study, as distinct geologic regions exist across the island, each with unique bedrock types and formation times (Figure 1.2, pg. 16). The Western region (Humber tectonic zone) dates back 1,500 million years and is characteristically made up of ancient granitic gneiss, a carbonate shelf, and melanges composed of ocean crust, ocean sediments, and mantle (Hild, 2012). The

Central region (Dunnage and Gander tectonic zones) dates back 540 million years and is predominantly composed of island formations with granitic, and volcanic intrusions (Hild, 2012). The Eastern region (Avalon tectonic zone) is characteristically composed of ancient volcanic arcs and ocean sediment, and sedimentary layers formed through deposition by rivers; it dates back 760 million years (Hild, 2012).

C. Sample acquisition

Due to the nature of the tissues used in this study (both bone and teeth require lethal and destructive sampling), we restricted tissue collection to pre-deceased *M. lucifugus* carcasses from which we could obtain all three tissues. To obtain tissue samples from this endangered bat species, we accessed carcasses collected throughout Newfoundland and Labrador that had been submitted to the Wildlife Division of the Department of Fisheries, Forestry, and Agriculture as part of a long-term disease monitoring effort. Carcasses were submitted by members of the general public, as the provincial government actively solicits these submissions. Each carcass had associated metadata, including the time and location of either mortality or discovery, as well as any general commentary (e.g., frequency of access to the collection site, condition of the carcass, presence of other bat carcasses). In some cases, the submission dates were not necessarily representative of the date the individual died; for example, some carcasses were found in cabins unoccupied since the previous summer. For those individuals, the structure associated with the carcass was used as a proxy for the season (i.e., cave or mine likely indicates hibernation, bat box or building likely indicates summer residency). We sampled fur, teeth, and bone from 21 *M. lucifugus* individuals collected from various locations across the province (Table & Figure 2.1). All work was conducted with

appropriate permits, granted by the Wildlife Division of the Department of Fisheries, Forestry, and Agriculture of Newfoundland and Labrador (Endangered Species Permit Number: 2022/23-02).

To elucidate regional $^{87}Sr/^{86}Sr$ tissue growth patterns, we sampled fur from an additional ten individuals that we classified as having died within the summer residency and molting period of this species and to therefore have fur with a chemical composition representative of the location of collection. A thorough body of literature supports the assumption that many temperate bat species molt their coat during the summer residency period, when these species occupy summer roosts and forage in nearby habitats (Fraser et al., 2013). Previous studies have documented molting in *M. lucifugus* occurring in late June to August but note that molting typically occurs later in parous females and juveniles (Jones & Genoways, 1967; Davis & Barbour, 1970; Sullivan et al., 2012; Fraser et al., 2013). Sullivan et al. (2012) estimate the molting period for *M. lucifugus* to be July 1 to August 23 based on known parturition, weaning, and fall migration dates in Michigan, USA. This timeline served as a guideline for our study.

We included individuals with known mortality dates between June 1 and August 23, as well as individuals with submission dates during the same time period, as long as the carcasses were found within structures indicative of summer roosting habitat (i.e., residences, bat boxes) (Fenton & Barclay, 1980; Randall et al., 2014; Johnson et al., 2019). For these individuals, we assume the $^{87}Sr/^{86}Sr$ values recorded in their fur tissues are representative of the location where the individuals were found. Including individuals sampled for all three tissues, we analyzed fur from 23 presumed known origin individuals (Table 2.1).

Those individuals that were found or died outside of this time period, or were found within this time period but at a location not indicative of summer residency (i.e., known hibernaculum), were classified as unknown origin. For these individuals, we assume the $^{87}Sr/^{86}Sr$ values associated with their fur is representative of the previous summer. This assumption provides an additional source of information for these carcasses – we have a physical location associated with where the carcass was found, and two implied locations based on the $^{87}Sr/^{86}Sr$ values associated with their fur and calciferous tissues. We analyzed fur, teeth, and bone from eight presumed unknown origin individuals (Table 2.1).
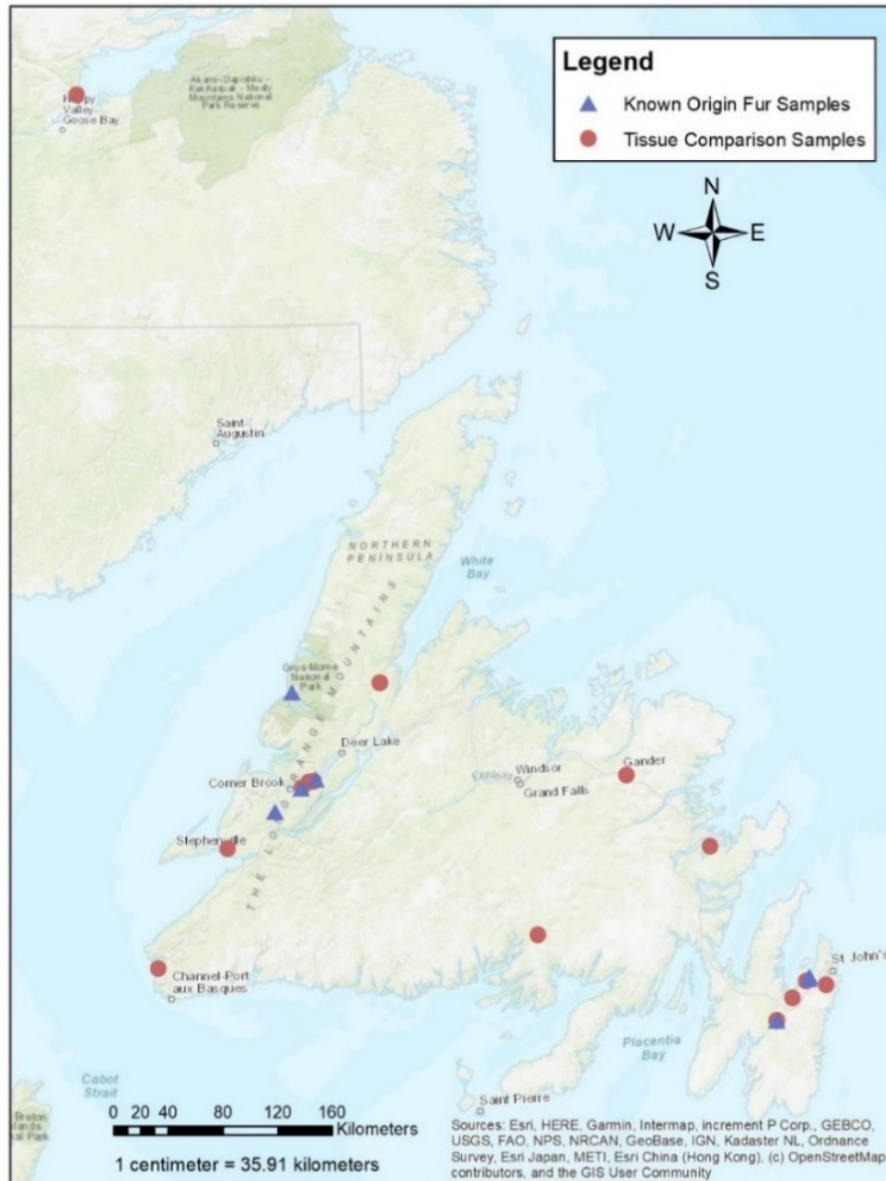
Figure 2.1. *Geographic distribution of samples. Red circles show individuals sampled for all three tissues (n = 21). Blue triangles show additional fur samples taken from known-origin individuals and used for regional $^{87}Sr/^{86}Sr$ estimates (n = 10).*

Table 2.1. *Age, sex, mortality region, $^{87}Sr/^{86}Sr$ value results, and classification of carcasses sampled and analyzed for $^{87}Sr/^{86}Sr$ (n = 31). Bolded rows are those assumed to be known origin individuals; summer residency of these individuals is presumed based on date and structure where the carcass was found. Unknown origin individuals have likely molted their coat the previous summer and therefore offer a unique opportunity to infer movements in the last year of their life by comparing fur $^{87}Sr/^{86}Sr$ values and location of mortality. Asterisk (*) next to date signifies known date of mortality. Individuals used in the tissue comparison were sampled for fur, teeth, and bone (F/T/B), while individuals used for the regional $^{87}Sr/^{86}Sr$ estimates were only sampled for fur (F).*

Sample #	Age Class	Sex	Region	Date	Structure	$^{87}Sr/^{86}Sr_F$	$^{87}Sr/^{86}Sr_T$	$^{87}Sr/^{86}Sr_B$	Classification
44	juvenile	male	Eastern	08/01/18	residence	0.710554	0.710253	0.710383	-
88	juvenile	female	Eastern	-	-	0.713456	0.710422	0.710421	-
78	juvenile	male	Labrador	07/17/19	bat box	0.710065	-	-	-
43	juvenile	male	Labrador	06/23/18	residence	0.707023	0.706834	0.707104	-
41	adult	male	Eastern	06/08/18*	-	0.710642	0.709999	0.710279	Indeterminate
42	adult	male	Eastern	07/10/18*	-	0.710237	0.710054	0.710148	Philopatric
81	adult	male	Eastern	07/22/19	bat box	0.709915	-	-	-
66	adult	female	Eastern	08/02/19	-	0.709364	0.709231	0.709342	Indeterminate
69	adult	female	Eastern	06/28/18*	bat box	0.709484	-	-	-
79	adult	female	Eastern	07/19/19	bat box	0.709601	0.708691	0.709006	Indeterminate
82	adult	female	Eastern	07/24/19	road	0.709738	-	-	-
83	adult	female	Eastern	07/25/19	-	0.709730	0.709657	0.709643	Philopatric
76	adult	male	Central	06/17/19*	residence	0.715323	0.715244	0.715142	Philopatric
37	adult	female	Central	06/17/18	bat box	0.713227	0.713555	0.713400	Philopatric
38	adult	female	Central	06/17/18	bat box	0.712907	0.712907	0.712556	Philopatric
40	adult	male	Western	06/01/18	residence	0.711416	0.712389	0.712142	Indeterminate
39	adult	female	Western	06/17/18*	residence	0.711518	-	-	-
75	adult	female	Western	06/17/19*	residence	0.712084	0.711540	0.711840	Indeterminate
84	adult	female	Western	08/01/19	residence	0.712034	-	-	-
85	adult	female	Western	08/01/19	residence	0.711844	-	-	-

Sample #	Age Class	Sex	Region	Date	Structure	$^{87}Sr/^{86}Sr_F$	$^{87}Sr/^{86}Sr_T$	$^{87}Sr/^{86}Sr_B$	Classification
86	**adult**	**female**	**Western**	**08/01/19**	**residence**	**0.711243**	**-**	**-**	**-**
87	**adult**	**female**	**Western**	**08/05/19**	**residence**	**0.711586**	**-**	**-**	**-**
97	**adult**	**female**	**Western**	**06/04/20**	**residence**	**0.713401**	**-**	**-**	**-**
67	adult	female	Eastern	05/30/18*	residence	0.710668	0.708854	0.708679	Indeterminate
16	adult	male	Western	07/05/17	hibernaculum	0.713208	0.710918	0.710775	Indeterminate
95	adult	male	Western	01/16/20*	hibernaculum	0.714787	0.711772	0.711590	Dispersed
96	adult	male	Western	05/17/20	hibernaculum	0.711478	0.711400	0.711688	Philopatric
14	adult	female	Western	05/11/17	residence	0.709898	0.709494	0.709508	Indeterminate
17	adult	female	Western	03/04/18	-	0.709450	0.709317	0.709351	Philopatric
18	adult	female	Western	03/18/18	-	0.713392	0.712352	0.712159	Indeterminate
60	adult	female	Western	03/13/19*	hibernaculum	0.712860	0.711780	0.711781	Dispersed

D. Tissue collection

i. Fur tissue

To collect tissues from the frozen, pre-deceased *M. lucifugus* carcasses, we initially thawed and patted dry the fur tissue using paper towels. Then, using curved dissection scissors, we carefully trimmed fur from the full body of the individual, placing it in a 1-dram glass vial. When large enough samples could be obtained, we removed fur from the dorsal and ventral surfaces of the individual and stored each in separated vials. We then placed the vials containing fur samples in a laboratory oven and heated them to 60 °C for 30 minutes as per our biosafety protocol to neutralize possible *Pseudogymnoascus destructans* and rabies virus present on the sample (Turner & Kaplan, 1967; CWHC, 2016). All surfaces and dissection tools were cleaned with 70 % isopropyl alcohol between individuals to avoid cross-contamination.

ii. Calciferous tissues

Using bone cutting shears, we separated the entire skull from the first cervical vertebrae and placed it in a glass petri dish. We then trimmed both wings from connective membranes, separated the humerus from the scapula at the glenohumeral joint, and placed both wings in a glass petri dish. Once dissected, the skull and wings were fed to a dermestid beetle colony for 1 – 3 days until flesh was removed. We then transferred the de-fleshed bones to aluminum weighing dishes and decontaminated them in a laboratory oven at 60 °C for 30 minutes. We stored the decontaminated wing bones and skull samples in 1-dram glass vials. All surfaces and dissection tools were cleaned with 70 % isopropyl alcohol between individuals to avoid cross-contamination.

E. Tissue pre-treatment, digestion, and analysis

i. Fur tissue – Pre-treatment

Previously trimmed bat fur samples were finely chopped using dissection scissors. 12.3 ± 0.2 mg of each sample (with the exception of samples number 39 and 69, which were limited to 4.0 and 4.7 mg, respectively) and standard [IAEA 086 (International Atomic Energy Agency, Vienna, Austria), NIES 13 (National Institute for Environmental Studies, Tsukuba-City, Japan)] were weighed into 2 mL centrifuge tubes. Samples, standards, and blanks (empty 2 mL centrifuge tubes) were pre-treated using the recommended IAEA treatment protocol (treatment (2) outlined in the pre-treatment experiment; Appendix I, pg. 167). After pre-treatment, we moved all samples to a clean hood, added 250 µL of deionized water (DI H_2O), and transferred the solution to pre-weighed and acid cleaned 3 mL Savillex vials (Minnetonka, USA). The acid cleaning protocol used is as follows: 8 M HNO_3 for 24 hours; 6 M HCl for 24 hours; DI H_2O for 24 hours; all heated to sub-boiling temperatures. We covered each Savillex vial loosely with its cap, and left samples on a hotplate set to 100 °C until dry. We then weighed the dried samples in their Savillex vials to recover the final mass of sample used in analysis. Samples were stored with caps secured until digestion.

ii. Tooth tissue – Extraction and pre-treatment

To extract teeth for analysis, we added the entire mandible to a 2 mL centrifuge tube with 1 mL of DI H_2O. We then heated the tube to 70 °C for 10 – 15 minutes on an Analog heat block to soften connective tissues. We removed all teeth from the mandible using forceps and a small dental pick and transferred them to a clean 2 mL centrifuge tube. When small quantities of teeth could be recovered from the mandible, we

supplemented with teeth extracted from the maxilla. We cleaned the extracted teeth by ultrasonicating them in 1 mL of DI H_2O for 10 minutes and decanted the waste solution using a 1 mL pipette. After cleaning, teeth samples were transferred to a clean hood, covered with parafilm fitted with condensation release holes, and dried on a hotplate overnight at 100 °C. Once dry, teeth samples, alongside ~5 – 10 mg of the bone ash standards [NIST 1400 (National Institute of Standards and Technology, Gaithersburg, USA)] and blanks were added to pre-weighed and acid cleaned 3 mL Savillex vials and weighed to recover the final mass of sample used in analysis. Samples, standards, and blanks were stored with caps secured until digestion.

iii. Bone tissue – Pre-treatment

We identified the humerus as the most appropriate bone for analysis, as it is the largest of the wing bones and was the least likely to be degraded at the joint during the de-fleshing process. We transferred each humerus bone to a clean 1-dram glass vial and pre-treated them with 2 – 3 mL of 30 % hydrogen peroxide (enough to cover the bone) in an ultrasonic bath for 10 minutes. We then decanted the waste solution and rinsed samples by ultrasonication for 10 minutes in DI H_2O. We decanted the waste solution again, transferred samples to a clean hood, and dried them overnight on a hotplate at 100 °C. Once dried, we cut the adult humerus bones in half and used the entire humerus for juvenile bats to account for weight discrepancies between the two. The sampled humerus bones, alongside the bone ash standards (NIST 1400) and blanks, were transferred to pre-weighed and acid cleaned 3 mL Savillex vials and weighed to recover the final mass of the sample used in the analysis. We stored samples, standards, and blanks with caps secured until digestion.

iv. Fur tissue – Strontium digestion, elution, and $^{87}Sr/^{86}Sr$ analysis

Following the procedure outlined by Shin et al. (2020), we first digested fur samples, standards (IAEA 086, NIES 13), and blanks in 1 mL of 16 M HNO_3 at 160 °C for 24 hours. We removed the samples from the hotplate and left them to cool slightly before adding 400 µL of 30 % hydrogen peroxide (H_2O_2). We left the samples to react at room temperature for 30 minutes and then dried samples to a small drop on a hotplate set to 90 – 100 °C. Once dried, we added 1 mL of 8 M HNO_3 to each sample and stored the samples with caps secured until Sr extraction and elution.

We extracted Sr from the digested samples, standards, and blanks using the column chemistry procedure outlined by Chau et al. (2017). Using 1 mL pre-conditioned BioRad columns (Hercules, USA), we rinsed the columns with 2 Column Volumes (CV) of DI water, 1 CV of 6 M HCl, and finally, 1 CV of 8 M HNO_3. Then, we added 200 µL of clean Sr-Spec Resin and rinsed the resin with 1 CV of DI water and 2 CV of 8 M HNO_3. Next, we loaded the samples suspended in 8 M HNO_3 in four 250 µL aliquots to the columns. We then washed the samples using 1 CV of 8 M HNO_3 and 1 CV of 3 M HNO_3. Finally, we eluted the samples from the resin using 1 mL of DI H_2O and collected the samples in 2 mL centrifuge tubes. Finally, we acidified the samples with 75 µL of 8 M HNO_3. Alongside every 17 samples, we included two standards (IAEA 086, NIES 13) and one blank.

We analyzed $^{87}Sr/^{86}Sr$ for all keratinous samples (including appropriate standards and blanks) using a Neptune Multi-Collector Inductively Coupled Plasma Mass Spectrometer [MC-ICP-MS (Thermo Fisher Scientific, Bremen, Germany)] fitted with a 50 µL/min nebulizer and measuring solution values every 4 seconds for a total of 100

measurements per sample or standard. We analyzed a 20, 50, or 100 ppb Sr carbonate solution standard [NIST SRM 987 (Gaithersburg, USA)] after every five samples for quality control. Additionally, we recorded the 0.3 M HNO_3 ^{88}Sr baseline before and after analysis to ensure quality control of background Sr levels. We corrected all measurements to an accepted SRM 987 ^{87}Sr/^{86}Sr value of 0.710248 (Avanzinelli et al., 2005). Due to the potential for samples with low Sr concentration to bias results, in conjunction with the small number of solution standard measurements associated with a single analysis session, we corrected experimental samples using a linear function that related ^{88}Sr intensity (measured in V) to the ^{87}Sr/^{86}Sr correction factor of all SRM 987 measurements collected across keratinous tissue sessions (^{87}Sr/^{86}Sr$_{corr}$ = -0.00002(^{88}Sr$_v$) + 0.0002; r^2 = 0.2131). The average and standard deviation of uncorrected SRM 987 ^{87}Sr/^{86}Sr values across all analysis sessions was 0.710352 ± 0.000063 (n = 45). The long-term average and 95 % confidence interval of uncorrected SRM 1400 ^{87}Sr/^{86}Sr values for the facility was 0.717315 ± 0.000008 (n = 101). Detailed analysis results can be found in Appendix II (pg. 173).

v. Bone and teeth tissue – Strontium digestion, elution, and ^{87}Sr/^{86}Sr analysis

We digested calciferous tissues in 1 mL of 8 M HNO_3 on a hotplate set to 90 – 100 °C for 30 – 60 minutes. We then extracted Sr from the digested calciferous tissue samples using the column chemistry protocol previously outlined by Madgwick et al. (2017) and modified from Deniel and Pin (2001), Copeland et al. (2008). Using 1 mL pre-conditioned BioRad columns (Hercules, USA), we rinsed the columns with 2 CVs of DI H_2O, 1 CV of 6 M HCl, and finally, 1 CV of 8 M HNO_3. Then, we added 400 µL of clean Sr-Spec Resin and rinsed the resin with 3 CVs of 6 M HCl, 3 CVs of DI water, and 3 CVs

of 8 M HNO$_3$. Next, we loaded the samples suspended in 8 M HNO$_3$ in a single 1 mL aliquot to the columns. We then washed the samples using 3 CVs of 8 M HNO$_3$. Finally, we eluted the samples from the resin using 2 mL of DI H$_2$O and collected the samples in 2 mL centrifuge tubes. Finally, we acidified the samples with 150 µL 0.3 M HNO$_3$. Alongside every 17 samples, we included two standards [NIST 1400 (Gaithersburg, USA)] and one blank.

A Neptune Multi-Collector Inductively Coupled Plasma Mass Spectrometer [MC-ICP-MS (Thermo Fisher Scientific, Bremen, Germany)] in combination with a 100 µL/min nebulizer, measuring solution values every 2 seconds for a total of 50 measurements per sample was used to analyze ^{87}Sr/^{86}Sr for all calciferous samples (including appropriate standards and blanks). We analyzed a 200 ppb Sr carbonate solution standard [NIST SRM 987 (Gaithersburg, USA)] after every six samples for quality control. The same quality control measures were used for these samples as with the keratinous samples. All measurements were corrected to an accepted SRM 987 ^{87}Sr/^{86}Sr value of 0.710248 (Avanzinelli et al., 2005).

F. Statistical analyses

We conducted all subsequent statistical analyses and graphical comparisons in R-Studio version 4.1.3 (R Core Team, 2022). Data manipulation was done using the dplyr package (Wickham et al., 2022), statistics were conducted using the rstatix package (Kassambara, 2023), and graphics were made using the ggplot2 package (Wickham, 2016) and the RColorBrewer package (Neuwirth, 2014).

i. Known origin fur tissue

Due to a lack of sample availability (Figure 2.1), we were unable to make any

meaningful inferences about movement behavior in Labrador, and therefore excluded

Labrador in the following geographical analyses. However, as the singular individual

sampled from this region of the province was a juvenile (Table 2.1), we included the

^{87}Sr/^{86}Sr data associated with its tissues in the subsequent juvenile tissue comparison. For

known origin individuals sampled from insular Newfoundland, we grouped fur samples

by geologically distinct region (Western, Central, Eastern; Figure 1.2, pg. 16). First, we

visually checked all three distributions for outliers by plotting each region's boxplot.

Then, as the small sample size of our data necessitated non-parametric statistics, we used

the median, inter-quartile range (IQR), and range to quantify the distribution of ^{87}Sr/^{86}Sr

values in each region of Newfoundland. Finally, we conducted a Wilcoxon Rank Sum test

to determine if the median ^{87}Sr/^{86}Sr values for each region were significantly different

from one another. We considered results significant if the *p* value was less than or equal

to 0.05.

ii. Tissue comparisons

We tested differences between the ^{87}Sr/^{86}Sr values in fur (^{87}Sr/^{86}Sr$_F$), bone

(^{87}Sr/^{86}Sr$_B$), and teeth (^{87}Sr/^{86}Sr$_T$) tissues by first graphically comparing the measured

^{87}Sr/^{86}Sr values for each individual. Then, as teeth and bones are theoretically formed at

virtually the same time period in a bat's life (14 – 21 and 29 days, respectively), we used

the absolute difference of ^{87}Sr/^{86}Sr values between teeth and bones to quantify intra-

individual variation in ^{87}Sr/^{86}Sr values ($|^{87}$Sr/^{86}Sr$_T$-^{87}Sr/^{86}Sr$_B|$). We calculated the mean

and 95 % confidence interval of $|^{87}$Sr/^{86}Sr$_T$-^{87}Sr/^{86}Sr$_B|$ for all 21 individuals and compared

the absolute difference of $^{87}Sr/^{86}Sr$ values between teeth and fur ($|^{87}Sr/^{86}Sr_T-^{87}Sr/^{86}Sr_F|$) for juvenile and adult bats separately. If the $|^{87}Sr/^{86}Sr_T-^{87}Sr/^{86}Sr_F|$ value fell within the 95 % confidence interval of $|^{87}Sr/^{86}Sr_T-^{87}Sr/^{86}Sr_B|$, we considered this individual's fur value to be representative of the same location as the calciferous tissues. To further interpret the regional origin of tissues, we graphically compared all tissue $^{87}Sr/^{86}Sr$ values to the established regional $^{87}Sr/^{86}Sr$ value distributions (developed using Sr isotope composition of known origin fur tissue). If a tissue $^{87}Sr/^{86}Sr$ value fell within a region's distribution, we treated it as evidence for tissue growth within that region. For unknown origin individuals, we compared all three tissues' formation regions to the region where the unknown origin individual was found. This comparison allowed us to infer movements across multiple seasons in a single year and relate these movements to the regional occupancy of that individual throughout its life in insular Newfoundland.

To investigate the likelihood of adult *M. lucifugus* to disperse or return to their natal region, we used a combination of the tissue absolute difference and regional comparison data. Individuals could be classified into one of three categories: dispersed, philopatric, or indeterminate. To be classified as dispersed, an individual had to meet two criteria: (1) the $|^{87}Sr/^{86}Sr_T-^{87}Sr/^{86}Sr_F|$ for this individual fell outside of the 95 % confidence interval of $|^{87}Sr/^{86}Sr_T-^{87}Sr/^{86}Sr_B|$, and (2) the $^{87}Sr/^{86}Sr$ values of the fur and one or both calciferous tissues fell within separate regional $^{87}Sr/^{86}Sr$ estimates. Similarly, to be classified as philopatric, an individual had to meet two criteria: (1) the $|^{87}Sr/^{86}Sr_T-^{87}Sr/^{86}Sr_F|$ for the individual fell within the 95 % confidence interval of $|^{87}Sr/^{86}Sr_T-^{87}Sr/^{86}Sr_B|$, and (2) the $^{87}Sr/^{86}Sr$ values of its fur and one or both calciferous tissues fell within a single regional $^{87}Sr/^{86}Sr$ estimate. Finally, to be classified as indeterminate, an

individual met a single criterion of being dispersed or philopatric [e.g., (1) or (2) above], but not both.

To address our prediction that females are more likely to return to their natal region than males, we calculated the proportion of male and female individuals that were classified as dispersed or philopatric. Finally, we conducted two post-hoc Wilcoxon Rank Sum tests upon observing patterns in our data. The first compared $|{}^{87}Sr/{}^{86}Sr_T - {}^{87}Sr/{}^{86}Sr_F|$ values of adult males and females, which allowed us to make inferences about sex biases in our sample population. The second compared $|{}^{87}Sr/{}^{86}Sr_T - {}^{87}Sr/{}^{86}Sr_F|$ values of known-origin and unknown-origin adults, which we used to elucidate patterns or biases in ${}^{87}Sr/{}^{86}Sr$ values for these two groups of individuals.

V.   RESULTS

A. Strontium analysis of bat fur

We recorded ${}^{87}Sr/{}^{86}Sr$ values for all 31 fur samples analyzed. The mean and standard deviation of ${}^{88}Sr$ intensity associated with these samples was 1.6 ± 1.1 V ($n = 31$). The ${}^{88}Sr$ intensity can be used as a proxy for Sr concentration in the sample, as ${}^{88}Sr$ is the most abundant isotope of Sr (Faure & Powell, 1972; Bentley, 2006). For reference, the mean and standard deviation of ${}^{88}Sr$ intensity associated with the teeth and bone samples analyzed for this study were 24.7 ± 7.6 V ($n = 21$) and 24.0 ± 4.9 V ($n = 21$), respectively.

B. Known origin fur tissue

We observed two extreme outliers in ${}^{87}Sr/{}^{86}Sr$ distributions of known origin fur samples for the Western and Eastern regions of Newfoundland (97: ${}^{87}Sr/{}^{86}Sr = 0.713401$,

Western; 88: $^{87}Sr/^{86}Sr = 0.713457$, Eastern; Figure 2.2). However, because our sample

sizes were small, and non-parametric statistics are not heavily affected by outliers, they

were not removed from the distributions. The median $^{87}Sr/^{86}Sr$ value for each region is as

follows – Western: 0.711844 ($n = 8$) / Central: 0.713227 ($n = 3$) / Eastern: 0.709915 ($n =$

11). According to the Wilcoxon Rank Sum test, the median $^{87}Sr/^{86}Sr$ value of each region

was significantly different (Western/Central: p value = 0.04, effect size $r = 0.61$;

Western/Eastern: p value = 0.002, effect size $r = 0.69$; Central/Eastern: p value = 0.03,

effect size $r = 0.60$).
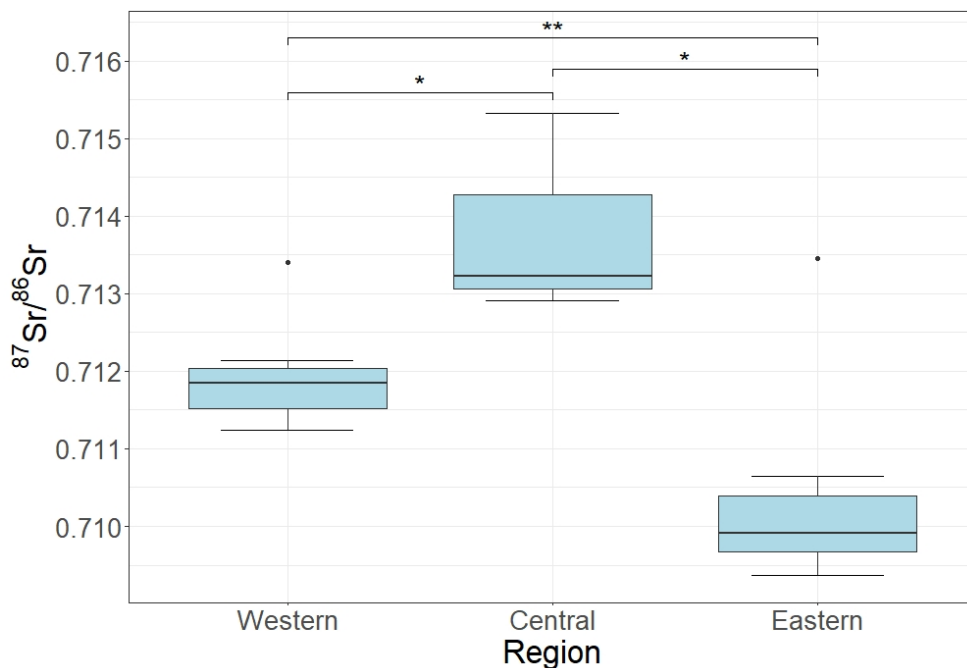
Figure 2.2. *Regional distributions of the $^{87}Sr/^{86}Sr$ values of fur samples taken from* M. lucifugus *with known origin. Sample sizes for each region are as follows: Central: n=3 / Eastern: n=10 / Western: n=9. Median $^{87}Sr/^{86}Sr$ values for each region area as follows: Western: 0.711844 / Central: 0.713227 / Eastern: 0.709915. Significant differences between medians calculated using a Wilcox Rank Sum Test and denoted with an asterisk depending on the significance level; p ≤ 0.005 is signified with "**" while p ≤ 0.05 is signified with "*".*

C. Juvenile tissue comparison

Two juvenile individuals' $|^{87}Sr/^{86}Sr_T-^{87}Sr/^{86}Sr_F|$ values fell within the range representative of intra-individual variation (0.000162 ± 0.000225); however, one individual's $|^{87}Sr/^{86}Sr_T-^{87}Sr/^{86}Sr_F|$ value fell outside this range (88; Figure 2.3). Furthermore, while the $^{87}Sr/^{86}Sr$ values of this individual's calciferous tissues fell within value of its fur fells within the $^{87}Sr/^{86}Sr$ distribution of Central Newfoundland (Figure the distribution of $^{87}Sr/^{86}Sr$ values representing its region of origin (Eastern), the $^{87}Sr/^{86}Sr$ 2.4). This individual is also represented as an outlier in Figure 2.2.
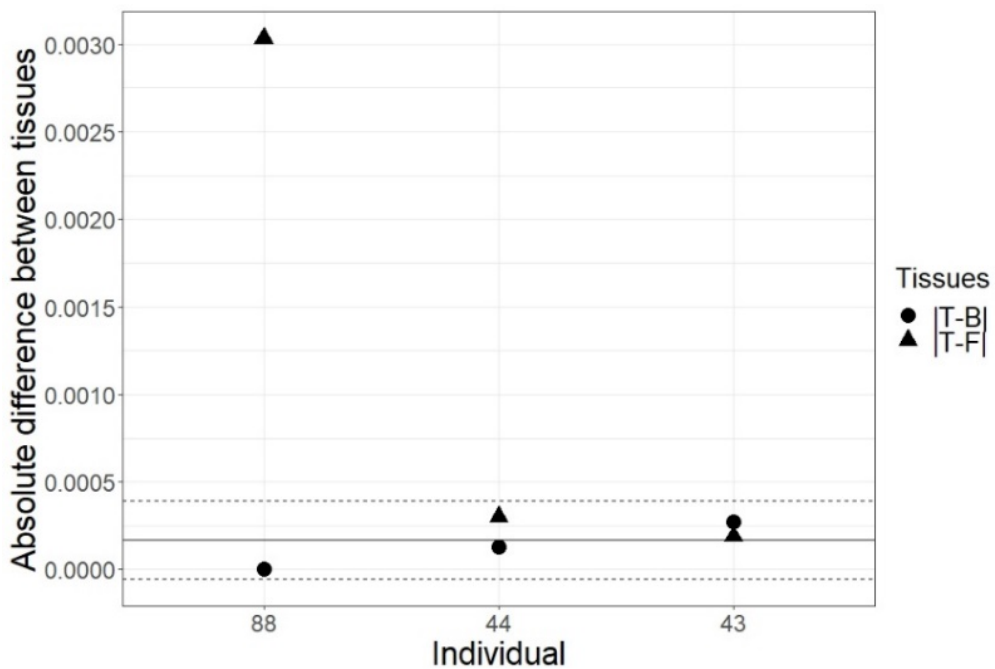
Figure 2.3. *$^{87}Sr/^{86}Sr$ values in the tissues of juvenile bats, compared using absolute differences of teeth and bones ($|^{87}Sr/^{86}Sr_T-^{87}Sr/^{86}Sr_B|$) and teeth and fur ($|^{87}Sr/^{86}Sr_T-^{87}Sr/^{86}Sr_F|$). Solid line represents mean absolute difference between teeth and bones for all 21 bats sampled. Dashed line represents 95% confidence interval around the mean. Notice individual 88, which had a distinct $^{87}Sr/^{86}Sr$ fur value compared to its calciferous tissues.*
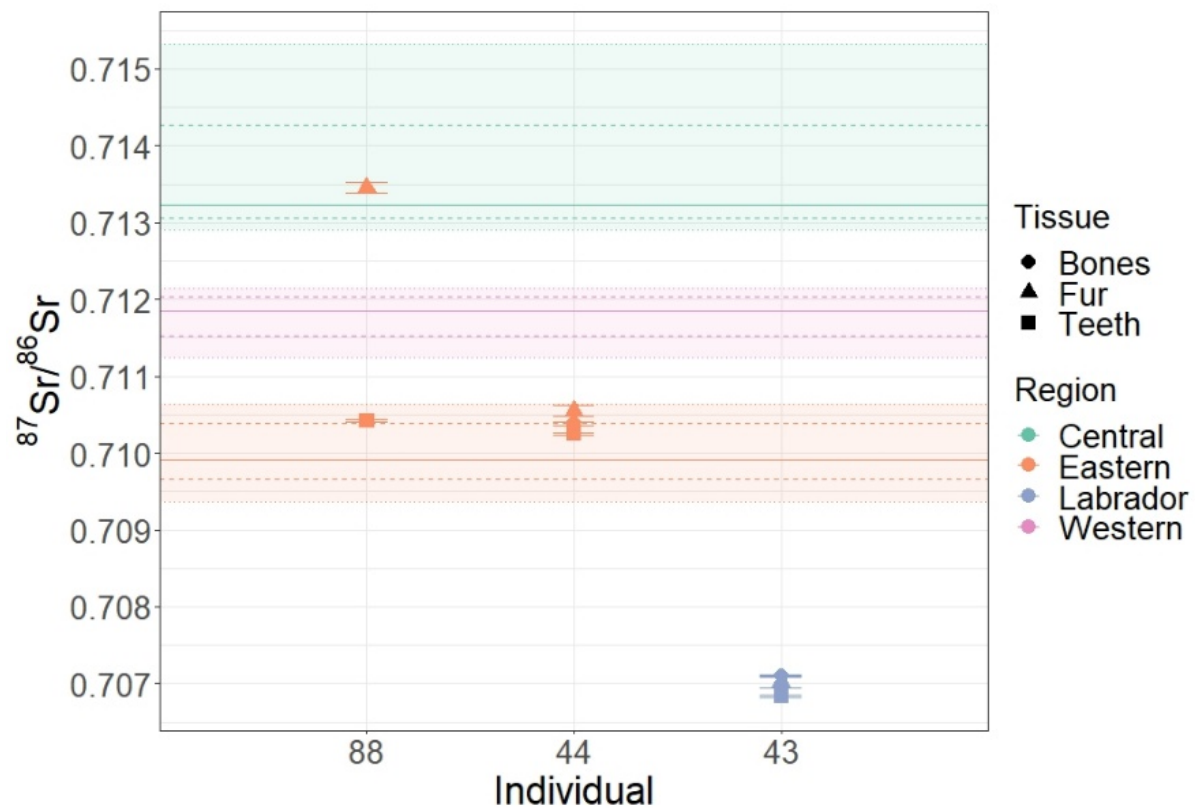
Figure 2.4. *$^{87}Sr/^{86}Sr$ values in the tissues of juvenile bats compared with regional estimates of $^{87}Sr/^{86}Sr$ values in the fur of known origin individuals. Solid lines represent the median, dashed lines represent the intra-quartile range, and shading represents the range of the known origin fur data. Points associated with each individual are color-coded based on region of mortality. Notice individual 88 which shows a distinct $^{87}Sr/^{86}Sr$ fur value that falls within the distribution of $^{87}Sr/^{86}Sr$ values representative of Central Newfoundland.*

D. Adult tissue comparisons

By comparing the absolute differences between pairs of tissues, we found four known origin adults (40 %) had $|^{87}Sr/^{86}Sr_T-^{87}Sr/^{86}Sr_F|$ values that fell outside of the range representative of intra-individual variation (Figure 2.5). However, after cross-validation using the regional $^{87}Sr/^{86}Sr$ estimates, none of these individuals were classified as dispersed (Table 2.2; Figure 2.6). Alternatively, six known origin adults (60 %) had $|^{87}Sr/^{86}Sr_T-^{87}Sr/^{86}Sr_F|$ values that fell within the range representative of intra-individual variation (Figure 2.5). Five of these individuals (50 % of all known origin adults) were classified as philopatric upon consulting the regional $^{87}Sr/^{86}Sr$ estimates (Table 2.2; Figure 2.6). Finally, 50 % of all known origin adults were classified as indeterminate (Table 2.2; Figures 2.5 & 2.6).

In total, six unknown origin adults (75 %) had $|^{87}Sr/^{86}Sr_T-^{87}Sr/^{86}Sr_F|$ values that fell outside of the range representative of intra-individual variation (Figure 2.5). After consulting the regional $^{87}Sr/^{86}Sr$ estimates, we classified two individuals as dispersed (25 % of all unknown origin individuals; Table 2.2, Figure 2.6). Notably, both of these individuals appear to have dispersed from Western (their natal region) to Central Newfoundland (where they spent the previous summer) but returned to Western for hibernation (both carcasses were found in the winter at a known hibernaculum in Western Newfoundland). Alternatively, two unknown origin adults (25 %) had $|^{87}Sr/^{86}Sr_T-^{87}Sr/^{86}Sr_F|$ values that fell within the 95 % confidence interval of $|^{87}Sr/^{86}Sr_T-^{87}Sr/^{86}Sr_B|$; based on the regional $^{87}Sr/^{86}Sr$ estimates, we classified both of these as philopatric (Table 2.2, Figures 2.5 & 2.6). One of these individuals likely hibernated and spent its summer residency in its natal region (96; Figure 2.6). Meanwhile, the second individual likely

spent its summer in its natal region (Eastern) and migrated to Western Newfoundland

after molting and before its death in early March 2018 (17; Table 2.2, Figure 2.6).
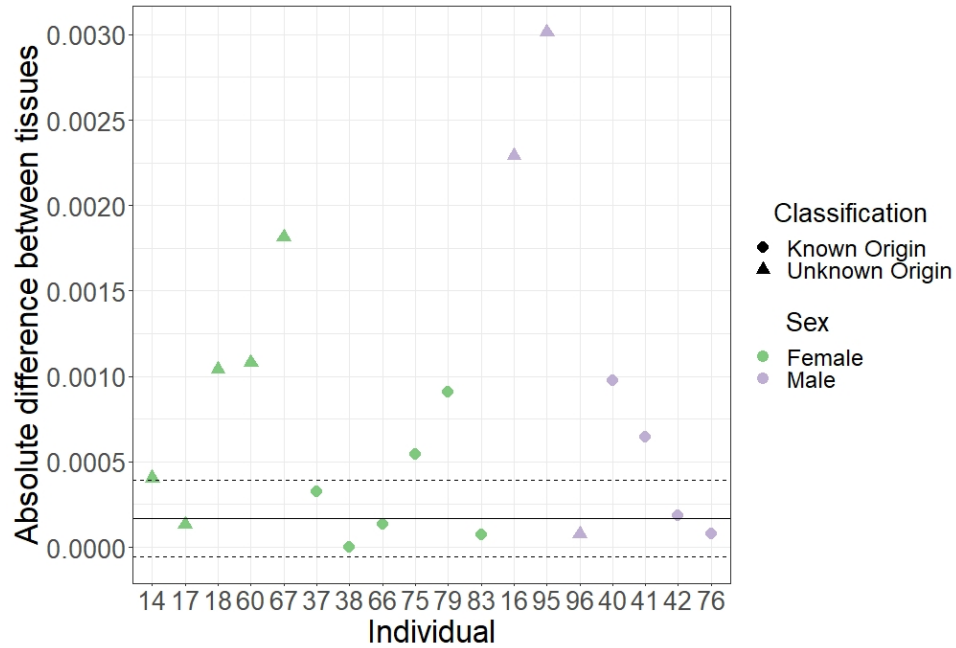
Figure 2.5. *$^{87}Sr/^{86}Sr$ values in the tissues of adult bats, compared using absolute differences of teeth and bones ($|^{87}Sr/^{86}Sr_T$-$^{87}Sr/^{86}Sr_B|$) (indicated by solid and dashed lines) and teeth and fur ($|^{87}Sr/^{86}Sr_T$-$^{87}Sr/^{86}Sr_F|$) (indicated by colored points). Solid line represents mean absolute difference between $^{87}Sr/^{86}Sr$ values of teeth and bones for all 21 bats sampled while dashed line represents the 95% confidence interval around the mean. Notice the relative proportions of females and males (55% and 57%, respectively) whose $|^{87}Sr/^{86}Sr_T$-$^{87}Sr/^{86}Sr_F|$ value falls outside of the 95% confidence interval compared to the relative proportions of females and males whose $|^{87}Sr/^{86}Sr_T$-$^{87}Sr/^{86}Sr_F|$ value falls within of the 95% confidence interval (45% and 43%, respectively).*
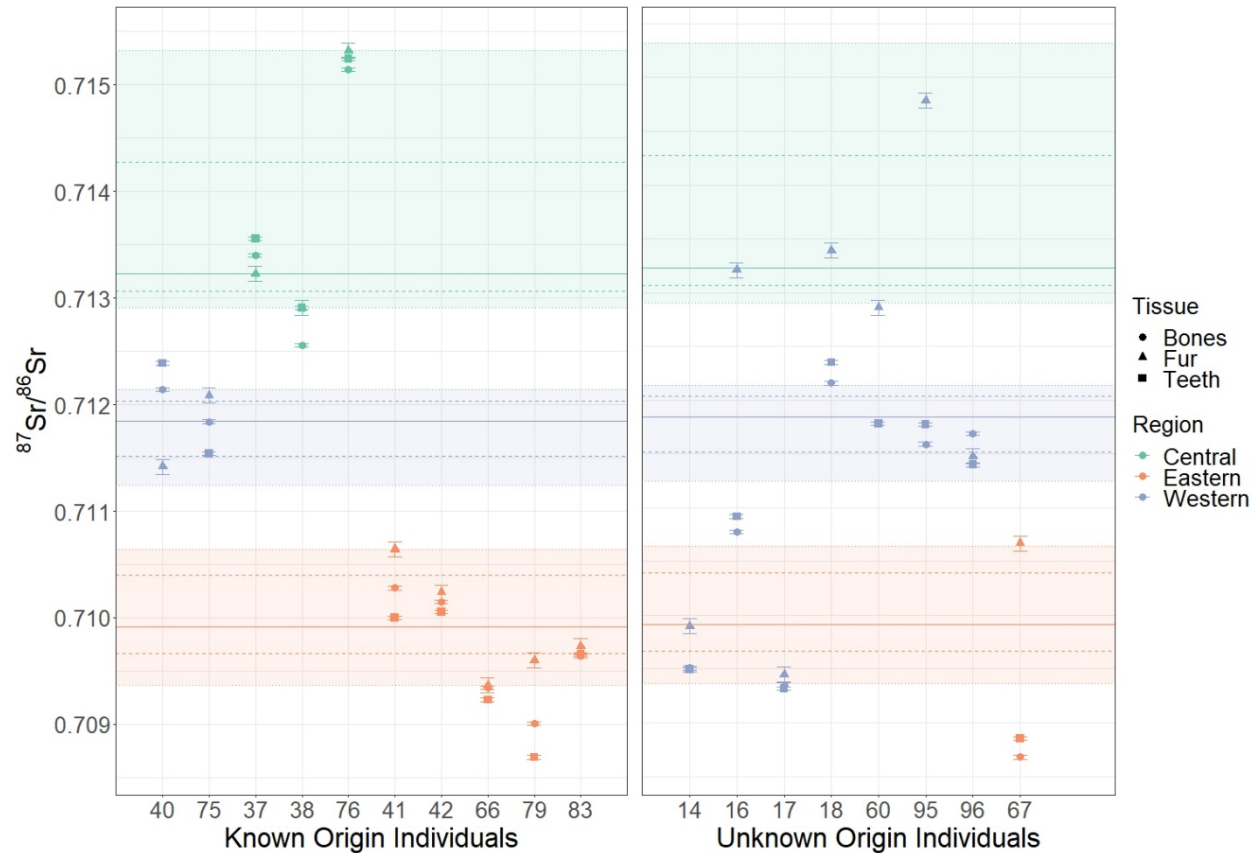
Figure 2.6. *$^{87}Sr/^{86}Sr$ values in the tissues of adult bats compared with regional estimates of $^{87}Sr/^{86}Sr$ values in the fur of known origin individuals. Solid lines represent the median, dashed lines represent the intra-quartile range, and shading represents the range of the known origin fur data. Points associated with each individual are color-coded based on region of mortality. Keep in mind that the $^{87}Sr/^{86}Sr$ values in the fur tissue of the known origin individuals were used in the regional $^{87}Sr/^{86}Sr$ estimates.*

Fifty percent of all unknown origin adults were classified as indeterminate (Table 2.2, Figures 2.5 & 2.6). One of these individuals behaved similarly to individual 17 – it likely spent its summer in Eastern Newfoundland (its natal region) and migrated to Western Newfoundland after molting and before death, between late summer and mid-May 2017 (14; Table 2.1, Figure 2.6). The $^{87}Sr/^{86}Sr$ values in the calciferous tissues of the remaining three individuals did not fall within a known regional $^{87}Sr/^{86}Sr$ distribution (Figure 2.6). However, by comparing the $^{87}Sr/^{86}Sr$ value of the fur and the location of mortality, we can make inferences about movements in the last year of these individuals' lives. Two of these individuals (16 and 18) likely occupied summer roosts in Central Newfoundland according to their $^{87}Sr/^{86}Sr_F$ values and migrated to Western Newfoundland before death – individual 18 died in a residential area in mid-March 2018 while individual 16 was found in early July 2017 at a known hibernaculum (Table 2.1, Figure 2.6).

Ultimately, 25 % of all unknown origin individuals were classified as dispersed while none of the known origin individuals fit into this classification. Consequently, 9 % of all adult females and 14 % of all adult males exhibited evidence for dispersal from their natal region. Alternatively, 50 % of known origin individuals and 25 % of unknown origin individuals were classified as philopatric – 36 % of females and 43 % of males. Finally, 50 % of both known and unknown origin individuals were classified as indeterminate – 55 % of females and 43 % of males. Our Wilcoxon Rank Sum test showed no significant difference between $|^{87}Sr/^{86}Sr_T$-$^{87}Sr/^{86}Sr_F|$ values in male and female adults (p value = 0.59, effect size r = 0.14). Similarly, according to our Wilcoxon Rank

Sum test, there is no significant difference between the $|^{87}Sr/^{86}Sr_T - ^{87}Sr/^{86}Sr_F|$ values in unknown origin and known origin adult individuals (p value = 0.06, effect size r = 0.45).

VI.   DISCUSSION

Despite the relatively low concentration of Sr in fur tissue, we found significant differences between the median $^{87}Sr/^{86}Sr$ values in fur samples tied to three geologically distinct regions in Newfoundland. Thus, our results show that bone, teeth, and fur can be sampled in *M. lucifugus*, and the $^{87}Sr/^{86}Sr$ values of each tissue may be tied to variation in the underlying geology of Newfoundland. A comparison between the $^{87}Sr/^{86}Sr$ values of tissues in juvenile bats indicated fur, teeth, and bone tissue may not always reflect the same location of formation. In adult bats, a comparison between the $^{87}Sr/^{86}Sr$ values of tissues indicated no evidence for sex-biased dispersal in the *M. lucifugus* population of Newfoundland. Finally, by comparing the $^{87}Sr/^{86}Sr$ values in bone, teeth, and fur of unknown origin individuals, we provide anecdotal evidence of movements between regions in a single year and relate those movements to natal region.

A. Strontium analysis of bat fur

Keratinous tissue analysis for $^{87}Sr/^{86}Sr$ has been used in studies of modern wildlife migration and human residence for many years (e.g., Sellick et al., 2009; Tipple et al., 2018; Kruszynski et al., 2020, Crowley et al., 2021). However, a thorough body of literature detailing methods for digestion and analysis of keratinous samples for $^{87}Sr/^{86}Sr$ illustrates the complexity of this objective (e.g., Font et al., 2007; Font et al., 2012; Tipple et al., 2013; Shin et al., 2020). Difficulties with analyzing keratinous tissues for $^{87}Sr/^{86}Sr$ primarily relate to the relatively low concentration of Sr in keratinous tissues (Brewer et

al., 2021). We quantified the amount of Sr in our samples by using the intensity of ^{88}Sr as a proxy for concentration, and the ^{88}Sr intensity of our keratinous samples was low compared to that of the calciferous samples analyzed in this study. The mean ^{88}Sr intensity reported by Font et al. (2007) in sedge warbler (*Acrocephalus schoenobaenus*) feathers was similar to the intensity of keratinous tissues reported in the present study (0.79 – 2.7 V). A question that arises from these results is whether exogenous Sr has the potential to mask endogenous Sr in samples with relatively low concentrations of Sr. Our method for pre-treatment of fur samples appears to have addressed this question, as we do not have evidence for exogenous contamination in our samples. The $^{87}Sr/^{86}Sr_F$ values of all individuals were not biased towards a specific value, which would suggest contamination of the reagents used in processing the samples. Additionally, the $^{87}Sr/^{86}Sr$ values in the fur of unknown origin individuals were not biased towards the location of mortality; if this bias was present, we would expect all or most individuals of unknown origin to have $^{87}Sr/^{86}Sr_F$ values that were reflective of their region of mortality. However, only 25 % of unknown origin individuals had $^{87}Sr/^{86}Sr_F$ values that fell within the distribution of values associated with their region of mortality (Figure 2.6). Ultimately, our results satisfy the prediction that *M. lucifugus* fur contains large enough concentrations of Sr to be analyzed for $^{87}Sr/^{86}Sr$.

B. Juvenile tissue comparisons

Contrary to our prediction, all juvenile tissue $^{87}Sr/^{86}Sr$ values were not reflective of the same location – we present evidence that one individual's fur value was distinct from its calciferous tissues and the $^{87}Sr/^{86}Sr$ baseline of its region of mortality (88; Figures 2.3, 2.4). However, our estimates of $^{87}Sr/^{86}Sr$ baseline values for each region

assume that Sr isotopes are homogenous across each region when they are known to be heterogeneous (Faure & Powell, 1972; Bentley, 2006; Bataille et al., 2020). A geological pocket may exist near the location of mortality with a value enriched in ^{87}Sr compared to the rest of the Eastern region – in fact, the Holyrood area (where this individual was found) is home to several granitic intrusions that were formed 730 – 580 million years ago and may be enriched in ^{87}Sr compared to surrounding turbidites derived from the deep ocean and siliclastic sediments formed approximately 555 million years ago (Faure & Powell, 1972; Hild, 2012). Further, there is evidence that *M. lucifugus* populations in northern latitudes tend to have higher rates of movements among maternity colonies than in southern latitudes (Norquay et al., 2013; Slough & Jung, 2020). It is therefore feasible that this individual moved from its place of birth to a location within a nearby geological pocket where it spent the rest of the summer and grew its coat. Alternatively, there is evidence that some juvenile bats will molt their coat during the first year of life, and it is not uncommon for molting to take place in the late summer or fall for these individuals (Fraser et al., 2013). It is also possible that the ^{87}Sr/^{86}Sr value of this individual's fur is an integrated signal indicative of multiple locations, as it incorporated Sr while moving through the landscape during its fall migration or the swarming season. At this time, further investigations comparing ^{87}Sr/^{86}Sr values in the fur, teeth, and bones of juvenile bats will aid in a better understanding of this technique. Though beyond the scope of this study, incorporation of a bioavailable Sr isoscape for Newfoundland would allow more robust and precise estimates of the location of formation for each tissue.

C. Sex biases in dispersal or philopatry

Ultimately, there was no significant difference between the median $|^{87}Sr/^{86}Sr_T$-$^{87}Sr/^{86}Sr_F|$ value of adult male or female individuals in this study. Although this is contrary to our prediction, it is not unusual for males and females of this species to both disperse to new areas and return to their natal territory. Previous studies seeking to elucidate patterns of sex-biased dispersal or philopatry in *M. lucifugus* have shown conflicting results (Dixon, 2011; Norquay et al., 2013; Burns et al., 2014; Johnson et al., 2015). According to Dixon (2011), the population genetic structure of *M. lucifugus* is largely facilitated by female philopatry, although both males and females engage in some degree of dispersal. Likewise, Norquay et al. (2013) observed high fidelity of both male and female *M. lucifugus* to summer roosting sites, but also found that females were more likely to relocate than males (at least between hibernacula). Alternatively, Burns et al. (2014) observed high genetic connectivity in *M. lucifugus* at swarming sites, suggesting dispersal by both sexes with a possibility of male-biased dispersal. Finally, Johnson et al. (2015), found a high degree of year-to-year fidelity to maternity roosts by female *M. lucifugus*, with evidence that fidelity to swarming sites is somewhat uncommon but varies among individuals.

Intriguingly, according to our results, both male and female *M. lucifugus* individuals in Newfoundland were more likely to be classified as philopatric (43 % and 45 %, respectively) than dispersed (14 % and 9 %, respectively) relative to their natal region. Studies that sought to elucidate philopatric behavior of *M. lucifugus* to summer roosting sites suggest that this behavior may vary depending on the individual (e.g., Johnson et al., 2015; Norquay et al., 2013). However, it is generally understood that *M.*

lucifugus exhibits high year-to-year fidelity to summering grounds; in other words, if an individual disperses to a new summer roost after birth, it will likely return to that roost in subsequent years (Dixon, 2011; Johnson et al., 2015; Norquay et al., 2013; Slough & Jung, 2020). Building on this body of literature, our results indicate that individuals dispersing from their natal area in Newfoundland rarely do so on the regional level (e.g., traveling distances greater than 100 – 200 kilometers). However, we classified a high percentage of both sexes as indeterminate (55 % and 43 % of females and males, respectively) and, therefore, may be under-classifying dispersed individuals. Future investigations can verify this pattern using a bioavailable Sr isoscape to make more precise predictions of natal area and infer yearly movements relative to natal region.

Curiously, most individuals that exhibited evidence for philopatry to their natal region were of known origin (50 % of known origin compared with 25 % of unknown origin); these known origin individuals were found where they grew their fur, which was also likely where they were born. Alternatively, 25 % of all unknown origin individuals showed evidence for dispersal from their natal region while none of the known origin individuals were classified as dispersed; these unknown origin individuals were found outside of the summer residency period, had likely grown their fur at a distinct location from where they were found, and had not returned to their natal region the previous summer. Although this pattern of philopatric known origin and dispersed unknown origin individuals emerged after categorizing bats based on regional $^{87}Sr/^{86}Sr$ estimates and intra-individual variation in $^{87}Sr/^{86}Sr$, there was no significant difference between the median $|^{87}Sr/^{86}Sr_T-^{87}Sr/^{86}Sr_F|$ values of the two origin groups. Further investigation is necessary to determine if this pattern is truly coincidental. While it is difficult to deduce

an underlying reason for this pattern, we propose one possible explanation: the molting

timeline for *M. lucifugus* in Newfoundland extends past the summer residency period. If

individuals captured during their summer residency had grown most, but not all, of their

new coat, the $^{87}Sr/^{86}Sr$ value of their fur would reflect the location of capture. However,

after those individuals began their fall migration, if fur growth was still occurring, the

$^{87}Sr/^{86}Sr$ value of their fur would integrate more noise; this value would become an

average of $^{87}Sr/^{86}Sr$ values associated with multiple locations as opposed to the location

of summer residency exclusively. As the distribution of Sr across the landscape is

heterogenous, even individuals moving relatively short distances across geological

pockets or towards coastlines (where sea-spray may influence $^{87}Sr/^{86}Sr$ values) would

have $^{87}Sr/^{86}Sr$ values of their fur that do not reflect the underlying geology of their

summer location.

Further, bats at northern latitudes face increased energetic challenges compared to

bats at southern latitudes (but see Boyles et al., 2016). These challenges are likely

exacerbated by exposure to the fungus that causes white-nose syndrome (WNS), which

can have more devastating effects in regions with extreme winters (Boyles & Willis,

2009). There is evidence that increased energetic demands delay molting, as the fur

growth process itself is energetically costly, and parous females often undergo molting

after males (Fraser et al., 2013). Likewise, Davis (1963) reported variation in the timing

of the juvenile molt cycle across latitudes for *Perimyotis subflavus*, with molting

occurring later for juveniles at northern latitudes compared with those at southern

latitudes (as cited in Fraser et al., 2013). Finally, our estimate for molt timeline was based

on the parturition and weaning dates of *M. lucifugus* in the midwestern and northeastern

United States (Cagle & Cockrum, 1943 as cited in Sullivan et al., 2012; Davis & Hitchcock, 1965). It is not unlikely that this timeline is different for *M. lucifugus* in northern Canada (see Slough & Jung, 2008). Additionally, the increased energetic demands introduced by WNS have the potential to further alter the molt timeline of this species. Investigations into the timing of molting for hibernating bats at northern latitudes and in the context of WNS could contribute to a better theoretical understanding of how energetic costs influence the physiology and behavior of hibernating bats. Additionally, future investigations using $^{87}Sr/^{86}Sr$ isotopes to understand the movements of bats at northern latitudes can incorporate a greater sample size and a bioavailable Sr isoscape to confirm or deny the presence of this pattern.

D. A Case study of *Myotis lucifugus*

As a case study, Sr isotope analysis of fur, teeth, and bone tissues in *M. lucifugus* offers insight into the possibilities of this technique by inferring movements for a single individual up to three times in its life (natal region, summer residency region, location of mortality) and identifying habitat occupancy at a regional level. From my perspective, an exciting facet of this technique is the possibility to elucidate movements between summering and wintering grounds (i.e., maternity colonies and hibernacula) or summering and mating grounds (i.e., maternity colonies and swarming sites) and relate them to habitat use in early life. We present two cases in which *M. lucifugus* individuals dispersed to a distinct region (where they spent their summer residency period) but returned to their natal region to hibernate. Likewise, we present evidence that individuals migrate between regions (in some cases from one side of the island to the other) despite exhibiting philopatry to their natal region in the summer. These movements are

particularly insightful in the context of WNS, as it is currently exclusive to the Western region of Newfoundland. Individuals dispersing from the Western region to either Central or Eastern Newfoundland may be inadvertently spreading the fungus to their summer residency colony. In the broader context of the introduction and continental spread of WNS, this technique has the potential to predict at-risk populations in white nose absent regions of the United States and Canada (given there are geological distinctions between regions). These at-risk populations can then be targeted for WNS mitigation measures (i.e., vaccinations, habitat improvement projects). Thus, the analysis of multiple tissues for ^{87}Sr/^{86}Sr is particularly useful for gathering habitat use information for understudied species and taxa, offers a unique opportunity to illuminate natural history of increasingly imperiled species, and has the potential to predict regions at risk for the spread of infectious diseases.

VII. CONCLUSION

The overarching purpose of this study was to introduce a novel use of intrinsic markers to identify the lifetime movements of species. This study, which used the *M. lucifugus* population in Newfoundland as a case study, showed the applications of Sr isotopes incorporated into fur, teeth, and bone for investigations seeking to identify lifetime movements of species. We analyzed 32 *M. lucifugus* fur samples for Sr and recorded ^{87}Sr/^{86}Sr values for each sample analyzed despite the relatively low ^{88}Sr intensity associated with these samples. Our results showed fur, teeth, and bone samples taken from juvenile *M. lucifugus* do not always reflect similar ^{87}Sr/^{86}Sr values. Further, using comparisons between ^{87}Sr/^{86}Sr values in the tissues of adult bats, we provide

evidence that adult *M. lucifugus* male and female individuals in insular Newfoundland are more likely to exhibit philopatric behavior towards (than disperse from) their natal region. Ultimately, we found no evidence of *M. lucifugus* in Newfoundland engaging in sex-biased dispersal, as both male and female individuals in our study were equally likely to disperse from their natal region. Finally, we present evidence for seasonal movements between white nose prolific and white nose absent regions of Newfoundland. Future investigations can seek to understand how $^{87}Sr/^{86}Sr$ values differ in the tissues of juvenile bats, determine whether molting timeline changes with northern latitudes and in the context of WNS, or compare $^{87}Sr/^{86}Sr$ values in the tissues of known origin and unknown origin adult bats. Future investigations would also be improved with a greater sample size and a bioavailable Sr isoscape for Newfoundland, which could be used to identify the probable locations of tissue formation. As intrinsic markers continue to advance, and the analysis of samples for Sr isotopes becomes more affordable, this technique will become increasingly accessible, and we are excited for the many insights into the natural history of imperiled species that will be illuminated using this technique.

VIII. REFERENCES

Avanzinelli, R., Boar, E., Conticelli, S., Francalanci, L., Guarnier, L., Perini, G., Petrone,
C. M., Tommasini, S., & Ulivi, M. (2005). High precision Sr, Nd, and Pb isotopic
analyses using the new generation Thermal Ionisation Mass Spectrometer
ThermoFinnigan Triton-Ti®. *Periodico di Mineralogia, 74*(3), 147-166.

Bataille, C. P., Crowley, B. E., Wooller, M. J., & Bowen, G. J. (2020). Advances in
global bioavailable strontium isoscapes. *Palaeogeography, Palaeoclimatology,
Palaeoecology, 55*, Article 109849. https://doi.org/10.1016/j.palaeo.2020.109849.

Bentley, R. A. (2006). Strontium isotopes from the earth to the archaeological skeleton: A
review. *Journal of Arcaheological Method and Theory, 13*(3), 135-187.
https://doi.org/10.1007/s10816-006-9009-x.

Boyles, J. G., & Willis, C. K. R. (2009). Could localized warm areas inside cold caves
reduce mortality of hibernating bats affected by white-nose syndrome? *Frontiers
in Ecology and the Environment, 8*(2), 92-98. https://doi.org/10.1890/080187.

Boyles, J. G., McGuire, L. P., Boyles, E., Reimer, J. P., Brooks, C. A. C., Rutherford, R.
W., Rutherford, T. A., Whitaker, J. O. Jr., & McCracken, G. F. (2016).
Physiological and behavioral adaptations in bats living at high latitudes.
Physiology & Behavior, 165, 322-327.
https://doi.org/10.1016/j.physbeh.2016.08.016.

Brewer, C. T., Rauch-Davis, W. A., & Fraser, E. E. (2021). The use of intrinsic markers
for studying the migratory movements of bats. *Animals, 11*(12), 3477.
https://doi.org/10.3390/ani11123477.

Britton, K., Grimes, V., Niven, L., Steele, T. E., McPherron, S., Soressi, M., Kelly, T. E.,

Jaubert, J., Hublin, J.-J., & Richards, M. P. (2011). Strontium isotope evidence for migration in late Pleistocene *Rangifer*: Implications for Neanderthal hunting strategies in the Middle Palaeolithic site of Jonzac, France. *Journal of Human Evolution, 61*(2), 176-185. https://doi.org/10.1016/j.jhevol.2011.03.004.

Broders, H. G., Farrow, L. J., Hearn, R. N., Lawrence, L. M., & Forbes, G. J. (2014). Stable isotopes reveal that little brown bats have a broader dietary niche than northern long-eared bats. *Acta Chiropterologica, 16*(2), 315-325. https://doi.org/10.3161/150811014X687279.

Burns, L. E., Frasier, T. R., & Broders, H. G. (2014). Genetic connectivity among swarming sites in the wide ranging and recently declining little brown bat (*Myotis lucifugus*). *Ecology and Evolution, 4*(21), 4130-4149. https://doi.org/10.1002/ece3.1266.

Cagle, F. R., & Cockrum, L. (1943). Notes on a summer colony of *Myotis lucifugus lucifugus*. *Journal of Mammalogy, 24*, 474-492.

Chau, T. H., Tipple, B. J., Hu, L., Fernandez, D. P., Cerling, T. E., Ehleringer, J. R., & Chesson, L. A. (2017). Reconstruction of travel history using coupled δ^{18}O and ^{87}Sr/^{86}Sr measurements of hair. *Rapid Communications in Mass Spectrometry, 31*(6), 583-589. https://doi.org/10.1002/rcm.7822.

Clem, C. S., Hobson, K. A., & Harmon-Threatt, A. N. (2022). Do Nearctic hover flies (Diptera: Syrphidae) engage in long-distance migration? An assessment of evidence and mechanisms. *Ecological Monographs, 92*(4). https://doi.org/10.1002/ecm.1542.

Clutton-Brock, T. (2021). Social evolution in mammals. *Science, 373*(6561).

https://doi.org/10.1126/science.abc9699.

Copeland, S. R., Sponheimer, M., le Roux, P. J., Grimes, V., Lee-Throp, J. A., de Ruiter, D. J., & Richards, M. P. (2008). Strontium isotope ratios (^{87}Sr/^{86}Sr) of tooth enamel: A comparison of solution and laser ablation multicollector inductively coupled plasma mass spectrometry methods. *Rapid Communications in Mass Spectrometry, 22*(20), 3187-3194. https://doi.org/10.1002/rcm.3717.

Copeland, S. R., Cawthra, H. C., Fisher, E. C., Lee-Thorp, J. A., Cowling, R. M., le Roux, P. J., Hodgkins, J., & Marean, C. W. (2016). Strontium isotope investigation of ungulate movement patterns on the Pleistocene Paleo-Agulhas Plain of the Greater Cape Floristic Region, South Africa. *Quaternary Science Reviews, 141*, 65-84. https://doi.org/10.1016/j.quascirev.2016.04.002.

Crowley, B. E., Bataille, C. P., Haak, B. A., & Sommer, K. M. (2021). Identifying nesting grounds for juvenile migratory birds with dual isotope: An initial test using North American raptors. *Ecosphere, 12*(10), e03765. https://doi.org/10.1002/ecs2.3765.

Cryan, P. M., Bogan, M. A., Rye, R. O., Landis, G. P., & Kester, C. L. (2004). Stable hydrogen isotope analysis of bat hair as evidence for seasonal molt and long-distance migration. *Journal of Mammalogy, 85*(5), 995-1001. https://doi.org/10.1644/BRG-202.

Canadian Wildlife Health Center (CWHC). (2016). *Canadian national white-nose syndrome decontamination protocol for entering bat hibernacula*. http://www.cwhc-rcsf.ca/docs/WNS_Decontamination_Protocol-Nov2016.pdf.

Davis, W. H. (1963). Aging bats in winter. *Transactions of the Kentucky Academy of Science, 24*, 28-30.

Davis, W. H., & Hitchcock, H. B. (1965). Biology and migration of the bat, *Myotis lucifugus*, in New England. *Journal of Mammalogy, 46,* 255-265.

Davis, W.H., & Barbour, R.W. (1970). Life history data on some southwestern Myotis. *The Southwestern Naturalist, 15*(2), 261-273. https://doi.org/10.2307/3670354.

Deniel, C., & Pin, C. (2001). Single-stage method for the simultaneous isolation of lead and strontium from silicate samples for isotopic measurements. *Analytica Chimica Acta, 426*(1) 95-103. https://doi.org/10.1016/S0003-2670(00)01185-5.

Dixon, M. D. (2011). Population genetic structure and natal philopatry in the widespread North American bat *Myotis lucifugus*. *Journal of Mammalogy, 92*(6), 1343-1351. https://doi.org/10.1644/10-MAMM-A-426.1.

Faure, G., & Powell, J. L. (1972). *Strontium Isotope Geology* (W. von Engelhardt, T. Hahn, R. Roy, & P. J. Wyllie, Eds.). Springer.

Fenton, M. B. (1969). Summer activity of *Myotis lucifugus* (Chiroptera:Vespertilionidae) at hibernacula in Ontario and Quebec. *Canadian Journal of Zoology, 47*(4), 597-602. https://doi.org/10.1139/z69-103.

Fenton, M. B. (1970). The deciduous dentition and its replacement in *Myotis lucifugus* (Chiroptera: Vespertilionidae). *Canadian Journal of Zoology, 48*(4), 817-820. https://doi.org/10.1139/z70-143.

Fenton, M. B., & Barclay, R. M. R. (1980). *Myotis lucifugus. Mammalian Species, 142*, 1-8. https://doi.org/10.2307/3503792.

Flockhart, D. T. T., Kyser, T. K., Chipley, D., Miller, N.G., & Norris, D.R. (2015). Experimental evidence shows no fractionation of strontium isotopes (^{87}Sr/^{86}Sr) among soil, plants, and herbivores: Implications for tracking wildlife and forensic

science. *Isotopes in Environmental and Health Studies, 51*(3), 372-381. https://doi.org/10.1080/10256016.2015.1021345.

Font, L., Nowell, G. M., Pearson, D. G., Ottley, C. J., & Willis, S. G. (2007). Sr isotope analysis of bird feathers by TIMS: A tool to trace bird migration paths and breeding sites. *Journal of Analytical Atomic Spectrometry, 22*(5), 513-522. https://doi.org/10.1039/b616328a.

Font, L., van der Peijl, G., van Wetten, I., Vroon, P., van der Wagt, B., & Davies, G. (2012). Strontium and lead isotope ratios in human hair: Investigating a potential tool for determining recent human geographical movements. *Journal of Analytical Atomic Spectrometry, 27*(5), 719-732. https://doi.org/10.1039/c2ja10361c.

Fraser, E. E., Longstaffe, F. J., & Fenton, M. B. (2013). Moulting matters: The importance of understanding moulting cycles in bats when using fur for endogenous marker analysis. *Canadian Journal of Zoology, 91*(8), 533-544. https://doi.org/10.1139/cjz-2013-0072.

Fraser, E. E., & McGuire, L. P. (2023). Prehibernation swarming in temperate bats: A critical transition between summer activity and hibernation. *Canadian Journal of Zoology, 101*(6), 408-422. https://doi.org/10.1139/cjz-2022-0129.

Fraser, K. C., McKinnon, E. A., & Diamond, A. W. (2010). Migration, diet, or molt? Interpreting stable-hydrogen isotope values in Neotropical bats. *Biotropica, 42*(4), 512-517. https://doi.org/10.1111/j.1744-7429.2009.00608.x.

Frick, W. F., Shipley, J. R., Kelly, J. F., Heady, P. A. III, & Kay, K. M. (2014). Seasonal reliance on nectar by an insectivorous bat revealed by stable isotopes. *Oecologia, 174*, 55-65. https://doi.org/10.1007/s00442-013-2771-z.

Gallant, A. J., & Broders, H. G. (2015). Body condition explains little of the

    interindividual variation in the swarming behaviour of adult male little brown

    myotis (*Myotis lucifugus*) in Nova Scotia, Canada. *Canadian Journal of Zoology,*

    93(6), 469-476. https://doi.org/10.1139/cjz-2014-0249.

Hamilton, M. I., Fernandez, D. P., & Nelson, S. V. (2021). Using strontium isotopes to

    determine philopatry and dispersal in primates: A case study from Kibale National

    Park. *Royal Society Open Science, 8*(2), Article 200760.

    https://doi.org/10.1098/rsos.200760.

Hild, M. H. (2012). *Geology of Newfoundland: field guide*. Boulder Publications.

Hobson, K. A., & Wassenaar, L. (1996). Linking breeding and wintering grounds of

    neotropical migrant songbirds using stable hydrogen isotopic analysis of feathers.

    Oecologia, 109, 142-148. https://doi.org/10.1007/s004420050068.

Hobson, K. A., Norris, D. R., Kardynal, K. J., & Yohannes, E. (2019). Animal migration:

    A context for using new techniques and approaches. In K. A. Hobson & L. I.

    Wassenaar (Eds.), *Tracking animal migration with stable isotopes* (pp. 1-23).

    Academic Press. https://doi.org/1016/B978-0-12-814723-8.00001-5.

Hobson, K. A., Kusack, J. W., Gootgarts, J., Longstaffe, F. J., & McNeil, J. N. (2022).

    Using stable isotopes (δ^2H, δ^{13}C) to identify natal origins and larval host plant use

    by western bean cutworm, *Striacosta albicosta* (Lepidoptera: Noctuidae) captured

    in southern Ontario. *Ecological Entomology, 47*(3), 347-356.

    https://doi.org/10.1111/een.13120.

Horacek, M. (2011). Backtracking the movements of a migratory bird: A case study of a

white-fronted goose (*Anser albifrons*). *Rapid Communications in Mass Spectrometry, 25*(20), 3146-3150. https://doi.org/10.1002/rcm.5209.

Johnson, L. N., McLeod, B. A., Burns, L. E., Arseneault, K., Frasier, T. R., & Broders, H. G. (2015). Population genetic structure within and among seasonal site types in the little brown bat (*Myotis lucifugus*) and the northern long-eared bat (*M. septentrionalis*). *Public Library of Science ONE, 10*(5). https://doi.org/10.1371/journal.pone.0126309.

Johnson, J. S., Treanor, J. J., Slusher, A. C., & Lacki, M. J. (2019). Buildings provide vital habitat for little brown myotis (*Myotis lucifugus*) in a high-elevation landscape. *Ecosphere, 10*(11), e02925. https://doi.org/10.1002/ecs2.2925.

Jones, J.K., Jr., & Genoways, H.H. (1967). Annotated checklist of bats from South Dakota. *Transactions of the Kansas Academy of Science, 70*(2), 184-196. https://doi.org/10.2307/3627117.

Kassambara, A. (2023). *rstatix: Pipe-friendly framework for basic statistical tests*. R package version 0.7.2. https://rpkgs.datanovia.com/rstatix.

Kruszynski, C., Bailey, L. D., Courtiol, A., Bach, L., Bach, P., Göttsche, Ma., Göttsche, Mi., Hill, R., Lindecke, O., Matthes, H., Pommeranz, H., Popa-Lisseanu, A. G., Seebens-Hoyer, A., Tichomirowa, M., & Voigt, C. C. (2020). Identifying migratory pathways of Nathusius' pipistrelles (*Pipistrellus nathusii*) using stable hydrogen and strontium isotopes. *Rapid Communications in Mass Spectrometry, 35*(6). https://doi.org/10.1002/rcm.9031.

Kunz, T. H., & Anthony, E. L. P. (1982). Age estimation and post-natal growth in the bat *Myotis lucifugus, 63*(1), 23-32. https://doi.org/10.2307/1380667.

Madgwick, R., Lewis, J., Grimes, V., & Guest, P. (2017). On the hoof: Exploring the supply of animals to the Roman legionary fortress at Caerleon using strontium (^{87}Sr/^{86}Sr) isotope analysis. *Archaeological and Anthropological Sciences, 11*, 223-235. https://doi.org/10.1007/s12520-017-0539-9.

Neuwirth, E. (2014). *RColorBrewer: ColorBrewer palettes*. R package version 1.1-2. https://CRAN.R-project.org/package=RColorBrewer.

Norquay, K. J. O., Martinez-Nuñez, F., Dubois, J. E., Monson, K. M., & Willis, C. K. R. (2013). Long-distance movements of little brown bats (*Myotis lucifugus*). *Journal of Mammalogy, 94*(2), 506-515. https://doi.org/10.1644/12-MAMM-A-065.1.

Popa-Lisseanu, A. G., Sörgel, K., Luckner, A., Wassenaar, L.I., Ibáñez, C., Kramer-Schadt, S., Ciechanowski, M., Görföl, T., Niermann, I., Beuneux, G., Mysłajek, R. W., Juste, J., Fonderflick, J., Kelm, D. H., & Voigt, C. C. (2012). A triple-isotope approach to predict the breeding origins of European bats. *PLoS One, 7*(1), e30388. https://doi.org/10.1371/journal.pone.0030388.

Price, G. J., Ferguson, K. J., Webb, G. E., Feng, Y., Higgins, P., Nguyen, A. D., Zhao, J., Joannes-Boyau, R., & Louys, J. (2017). Seasonal migration of marsupial megafauna in Pleistocene Sahul (Australia – New Guinea). *Proceedings of the Royal Society B, 284*(1863), Article 20170785. http://doi.org/10.1098/rspb.2017.0785.

R Core Team (2022). *R: A language and environment for statistical computing*. R Foundation for Statistical Computing, Vienna, Austria. https://www.R-project.org.

Randall, L. A., Jung, T. S., & Barclay, R. M. R. (2014). Roost-site selection and

movements of little brown myotis (*Myotis lucifugus*) in Southwestern Yukon.
Northwestern Naturalist, 95(3), 312-317. https://doi.org/10.1898/13-02.1.

Reich, M. S., Flockhart, D. T. T., Norris, D. R., Hu, L., & Bataille, C. P. (2021).
Continuous-surface geographic assignment of migratory animals using strontium
isotopes: A case study with monarch butterflies. *Methods in Ecology and
Evolution, 12*(12), 2445-2457. https://doi.org/10.1111/2041-210X.13707.

Rogers, E. J., McGuire, L., Longstaffe, F. J., Clerc, J., Kunkel, E., & Fraser, E. (2021).
Relating wing morphology and immune function to patterns of partial and
differential bat migration using stable isotopes. *Journal of Animal Ecology, 91*(4),
858-869. https://doi.org/10.1111/1365-2656.13681.

Sellick, M. J., Kyser, T. K., Wunder, M. B., Chipley, D., & Norris, D. R. (2009).
Geographic variation of strontium and hydrogen isotopes in avian tissue:
Implications for tracking migration and dispersal. *PLoS One, 4*(3).
https://doi.org/10.1371/journal.pone.0004735.

Shin, W.-J., Jung, M., Ryu, J-S., Hwang, J., & Lee, K.-S. (2020). Revisited digestion
methods for trace element analysis in human hair. *Journal of Analytical Science
and Technology, 11*, Article 1. https://doi.org/10.1186/s40543-019-0200-6.

Slough, B. G., & Jung, T. S. (2008). Observations on the natural history of bats in the
Yukon. *The Northern Review, 29,* 127-150.

Slough, B. G., & Jung, T. S. (2020). Little brown bats utilize multiple maternity roosts
within foraging areas: Implications for identifying summer habitat. *Journal of
Fish and Wildlife Management, 11*(1), 311-320. https://doi.org/10.3996/052019-
JFWM-039

Solari, S. (2021). *Myotis lucifugus*. The IUCN Red List of Threatened Species.

 https://doi.org/10.2305/IUCN.UK.2021-3.RLTS.T14176A208031565.en.

Sullivan, A. R., Bump, J. K. Kruger, L. A., & Peterson, R. O. (2012). Bat-cave catchment

 areas: Using stable isotopes (δD) to determine the probable origins of hibernating

 bats. *Ecological Applications, 22*(5), 1428-1434. https://doi.org/10.1890/11-

 1438.1.

Sunga, J. S., Humber, J., Rodrigues, B., McGuire, L., & Broders, H. (2021). Long-

 distance movement over a period of days by a female *Myotis lucifugus* in

 Newfoundland, Canada. *Northeastern Naturalist, 28*(2), 24-26.

 https://doi.org/10.1656/045.028.0214.

Thompson, R.C., & Ballou, J.E. (1956). Studies of metabolic turnover with tritium as a

 tracer V. The predominantly non-dynamic state of body constituents in the rat.

 Journal of Biological Chemistry, *223*, 795-809.

Tipple, B. J., Chau, T., Chesson, L. A., Fernandez, D. P., & Ehleringer, J. R. (2013).

 Isolation of strontium pools and isotope ratios in modern human hair. *Analytica

 Chimica Acta, 798*, 64-73. https://doi.org/10.1016/j.aca.2013.08.054.

Tipple, B. J., Valenzuela, L. O., & Ehleringer, J. R. (2018). Strontium isotope ratios of

 human hair record intra-city variations in tap water source. *Scientific Reports, 8*,

 3334. https://doi.org/10.1038/s41598-018-21359-0.

Turner, G. S., & Kaplan, C. (1967). Some properties of fixed rabies virus. *Journal of

 General Virology, 1*(4), 537-551. https://doi.org/10.1099/0022-1317-1-4-537.

van Zyll de Jong, C. G. (1983). *Handbook of Canadian Mammals: Bats* (2nd Ed.).

 Canadian Museum of Natural Sciences.

Voigt, C.C., Matt, F., Michener, R., & Kunz, T.H. (2003). Low turnover rates of carbon isotopes in tissues of two nectar-feeding bat species. *Journal of Experimental Biology, 206*(8), 1419-1427. https://doi.org/10.1242/jeb.00274.

Voigt, C. C., Lindecke, O., Schönborn, S., Kramer-Schadt, S., & Lehmann, D. (2016). Habitat use of migratory bats killed during autumn at wind turbines. *Ecological Applications, 26*(3), 771-783. https://doi.org/10.1890/15-0671.

von Rönn, J. A. C., Grüebler, M. U., Fransson, T., Köppen, U., & Korner-Nievergelt, F. (2020). Integrating stable isotopes, parasite, and ring-reencounter data to quantify migratory connectivity – A case study with Barn Swallows breeding in Switzerland, Germany, Sweden, and Finland. *Ecology and Evolution, 10*(4), 2225-2237. https://doi.org/10.1002/ece3.6061.

Wickham, H. (2016). *ggplot2: Elegant graphics for data analysis*. Springer-Verlag New York. https://ggplot2.tidyverse.org.

Wickham, H., François, R., Henry, L., & Müller, K. (2022). *dplyr: A grammar of data manipulation*. R package version 1.0.8. https://CRAN.R-project.org/package=dplyr.

Wieringa, J. G., Nagel, J., Campbell, C. J., Nelson, D. M., Carstens, B. C., & Gibbs, H. L. (2023). Combining stable isotopes, trace elements, and distribution models to assess the geographic origins of migratory bats. *Ecosphere, 14*(6). https://doi.org/10.1002/ecs2.4588.

Wimsatt, W. A. (1945). Notes on breeding behavior, pregnancy, and parturition in some Vespertilionid bats of the Eastern United States. *Journal of Mammalogy, 26*(1), 23-33. https://doi.org/10.2307/1375029.

Wright, P. G. R., Newton, J., Agnelli, P., Budinski, I., Di Salvo, I., Flaquer, C., Fulco, A.,

    Georgiakakis, P., Martinoli, A., Mas, M., Mazija, M., Mucedda, M., Papadatou,

    E., Petrov, B., Rodrigues, L., Mathews, F., & Russo, D. (2020). Hydrogen

    isotopes reveal evidence of migration of *Miniopterus schreibersii* in Europe. *BMC*

    Ecology, 20, Article 52. https://doi.org/10.1186/s12898-020-00321-7.

CHAPTER III: Advancing the use of intrinsic markers for studying the migratory movements of modern wildlife: A case study of *Myotis lucifugus* in Newfoundland and Labrador, Canada

I.   ABSTRACT

The analysis of keratinous tissues for the stable isotopes of hydrogen (δ^2H) has been used to study the migratory movements of organisms for decades. More recently, researchers have enhanced this technique by using additional biochemical markers which increase the accuracy and precision of inferences. We contributed to this body of literature by exploring a combination of δ^2H, δ^{34}S, and ^{87}Sr/^{86}Sr to infer the seasonal movements of *Myotis lucifugus* in Newfoundland and Labrador, Canada. We used previously published ^{87}Sr/^{86}Sr isoscapes, and developed new δ^{34}S and δ^2H isoscapes, to evaluate the distribution of each isotope across the province. The δ^2H isoscape exclusively explained variation in the fur of known origin individuals; using it, we determined probabilistic summer residency locations for unknown origin individuals. Alternatively, using regional ^{87}Sr/^{86}Sr estimates, we inferred the region of summer residency for the same individuals; no pattern was evident for δ^{34}S, limiting its use in further analyses. Using a combination of δ^2H and ^{87}Sr/^{86}Sr, we reveal *M. lucifugus* exhibits a high rate of migratory movements within and between regions of Newfoundland. This study illustrates the applications of this technique for inferring the movements of species in areas of the world with limited bioavailable ^{87}Sr/^{86}Sr data.

Keywords: seasonal migration; bats; *Myotis lucifugus;* intrinsic markers; strontium isotopes; ^{87}Sr/^{86}Sr; stable hydrogen isotopes; δ^2H; stable sulfur isotopes; δ^{34}S; keratinous tissues; metabolically inert tissues; isoscape; probabilistic assignment; Newfoundland, Canada

II.   GENERAL SUMMARY

Migratory species across taxa are increasingly imperiled, and thus the adaptation of migration itself is becoming increasingly rare. Identifying the migratory movements of organisms can help us to safeguard their habitats and movement pathways, while simultaneously understanding the evolutionary drivers of migration. In this study, we advance the methods for studying migratory movements by using multiple intrinsic markers, or chemical signatures, incorporated into the tissues of organisms that predictably vary across the landscape. By combining the stable isotopes of hydrogen (δ^2H) and the radiogenic isotopes of strontium (^{87}Sr/^{86}Sr), we make increasingly accurate and precise predictions of the migratory movements of *Myotis lucifugus* in Newfoundland and Labrador, Canada. This study contributes to a growing number of investigations using multiple intrinsic markers to infer habitat use of migratory organisms and reveals the power of combing isotopic systems to understand the migratory movements of modern vertebrates.

III.   INTRODUCTION

Intrinsic markers have been used for many years to infer the movements of terrestrial migratory organisms. Specifically, the incorporation of stable hydrogen isotopes (δ^2H) into keratinous tissues (e.g., fur, feathers) has been a staple for inferring migratory movements across continents for close to three decades (e.g., Hobson & Wassenaar, 1996; Wassenaar & Hobson, 2000; Cryan et al., 2004). Less prolific but equally informative are the use of the stable isotopes of elements such as carbon (δ^{13}C), nitrogen (δ^{15}N), sulfur (δ^{34}S), radiogenic isotopes of elements such as strontium

(^{87}Sr/^{86}Sr), or trace elements to infer migratory movements of terrestrial organisms on regional scales (e.g., Farmer et al., 2004; Horacek, 2011; Wieringa et al., 2020; Bataille et al., 2021; Crowley et al., 2021; Hobson et al., 2022). The most appropriate isotopic system for inferring movements will depend on the organism of interest, study area, and research question (Wunder & Norris, 2019). However, ^{87}Sr/^{86}Sr is a particularly useful system that is often overlooked in studies of modern migratory vertebrates for several reasons, including high analytical cost, few preliminary investigations establishing the use of this system for modern vertebrates (but see Chamberlain et al., 1997; Blum et al., 2001; Evans & Bullman, 2009; Sellick et al., 2009; Kruszynski et al., 2020; Crowley et al., 2021), and a relatively minimal understanding of the incorporation of Sr into keratinous tissues and possible consequent fractionation (but see Font et al., 2012; Flockhart et al., 2015). Likewise, δ^{34}S has been used primarily to differentiate marine from terrestrial origin (e.g., Lott et al., 2003; Zazzo et al., 2011; Fox et al., 2016) but rarely in continuous-surface probabilistic origin assignments (but see Kabalika et al., 2020; Bataille et al., 2021). However, there is evidence that δ^{34}S varies on local scales in a similar way to ^{87}Sr/^{86}Sr, and the combination of these isotopic systems has shown promise in studies investigating the geographic origins of prehistoric vertebrates (e.g., Madgwick et al., 2019; Linglin et al., 2020; Rand et al., 2020; Bataille et al., 2021).

A thorough body of literature supports the claim that using the isotopes of multiple elements improves the precision and accuracy of probabilistic origin assignments (e.g., Popa-Lisseanu et al., 2012; Bataille et al., 2021; Crowley et al., 2021; Reich et al., 2021). Every isotope varies differently across the landscape and when overlaid, the combination of isoscapes will predict migratory origin in greater detail than any singular

isotope (Figure 1.1, pg. 3; Hobson, 2019). In 2012, Popa-Lisseanu et al. quantified the

accuracy of origin assignments of two species of European bats (*Eptesicus serotinus, E.

isabellinus*) using a combination of up to three isotopes (δ^2H, δ^{13}C, δ^{15}N). The researchers

found that the accuracy of assignments improved from 47.4 % (single) to 86 – 89.5 %

(dual) to 93 % (triple) (Popa-Lisseanu et al., 2012). More recently, and of particular

interest for this study, Bataille et al. (2021) used a combination of δ^{18}O, ^{87}Sr/^{86}Sr, and

δ^{34}S to predict the probabilistic origin of local (i.e., known origin) human and animal

remains from an archaeological site in Rennes, France. The results showed precision

increases with all three isotopes compared to single and dual-isotope assignments

(Bataille et al., 2021).

In the subsequent study, we sought to employ a triple isotopic approach to infer

the movements of an endangered migratory bat species, *Myotis lucifugus* in

Newfoundland, Canada. Simultaneous to the theoretical framework established above,

this study aims to contribute to a better understanding of the movements of an endangered

species of bat impacted by the recent introduction of *Pseudogymnoascus destructans*, the

fungus which causes white-nose syndrome (WNS), to Newfoundland. WNS is a fungal

pathogen that has devastating effects on hibernating bat species in North America; *M.

lucifugus* has faced severe population declines due to the fungus (Kurta & Smith, 2020;

Cheng et al., 2021). In brief, *P. destructans* increases arousal frequency during

hibernation, which causes premature consumption of fat stores and, in many cases,

subsequent mortality (Cryan et al., 2010; Reeder et al., 2012). Infected individuals that

survive the winter months may emerge with increased energetic demands as they recover

from infection; these energetic demands may be compounded in northern habitats by long

winters and cold spring temperatures (Wilcox & Willis, 2016). In Newfoundland, WNS was detected in 2017 on the western side of the island, but has yet to spread easterly (CBC News, 2018). Thus, movement data for this species will support targeted conservation efforts in Newfoundland as researchers respond to the effects of WNS on the local *M. lucifugus* population.

Our objectives to address these underlying theoretical and applied motives are twofold. Firstly, we seek to understand the distribution of isotopes across our study area and their incorporation into the fur of resident bats. Secondly, we aim to apply the theoretical concepts established in the first objective to the case study of the migratory *M. lucifugus* population in Newfoundland. Detailed research questions and predictions can be found below:

Question: Is the variation in environmental (e.g., water, soil, bedrock, atmospheric pollution, and dust) δ^2H, δ^{34}S, and ^{87}Sr/^{86}Sr values across Newfoundland correlated with the isotopic signatures in bat fur?

> *Prediction:* δ^2H, δ^{34}S, and ^{87}Sr/^{86}Sr will vary predictably across Newfoundland, and each will be incorporated predictably into the fur of bats (Flockhart et al., 2015). Further, when the three isoscape are overlaid, they will provide a fine resolution isoscape with which to identify regional movements of bats in the province.

> *Prediction:* Fur sampled from the dorsal and ventral surfaces of a single individual will reflect similar ^{87}Sr/^{86}Sr values, as *M. lucifugus* is known to replace the fur across its body in a period of two months, during which individuals of this species are largely sedentary (Fraser et al., 2013).

Question: What seasonal movements of *M. lucifugus* in Newfoundland can be identified using data from all three isotope systems?

> *Prediction:* As *M. lucifugus* is known to regularly migrate $200 - 500$ km (Fenton, 1969; Norquay et al., 2013; Sunga et al., 2021), the δ^2H, ^{87}Sr/^{86}Sr, and δ^{34}S fur values of bats found outside of the period of fur replacement will indicate locations of summer residency that are distinct from where the carcass was found.

IV.   MATERIALS & METHODS

A. Sample acquisition & tissue collection

All fur samples obtained for this chapter were taken from the same collection of pre-deceased carcasses and used the same methods as described in the previous chapter. When large enough samples could be obtained, we removed fur from the dorsal and ventral surfaces of the individual and stored each in separated vials. We classified individuals as known origin (i.e., the location of mortality was the same as fur growth) based on date and structure associated with the carcass (Table 3.1); see the previous chapter for more details about this classification procedure (pg. $60 - 61$). All other individuals were classified as unknown origin (i.e., the location of mortality was distinct from that of fur growth). In total, we sampled fur from 43 *M. lucifugus* individuals collected throughout the province; 23 of these were of known origin and 20 were of unknown origin (Table & Figure 3.1). Due to budgetary constraints and sample availability, we analyzed fur from all 43 individuals for δ^2H and ^{87}Sr/^{86}Sr but restricted our analysis for δ^{34}S to 36 of these individuals (16 of known origin, 20 of unknown

origin). Known origin individuals were prioritized for δ^{34}S analysis based on mortality

location with respect to distance from the coast.
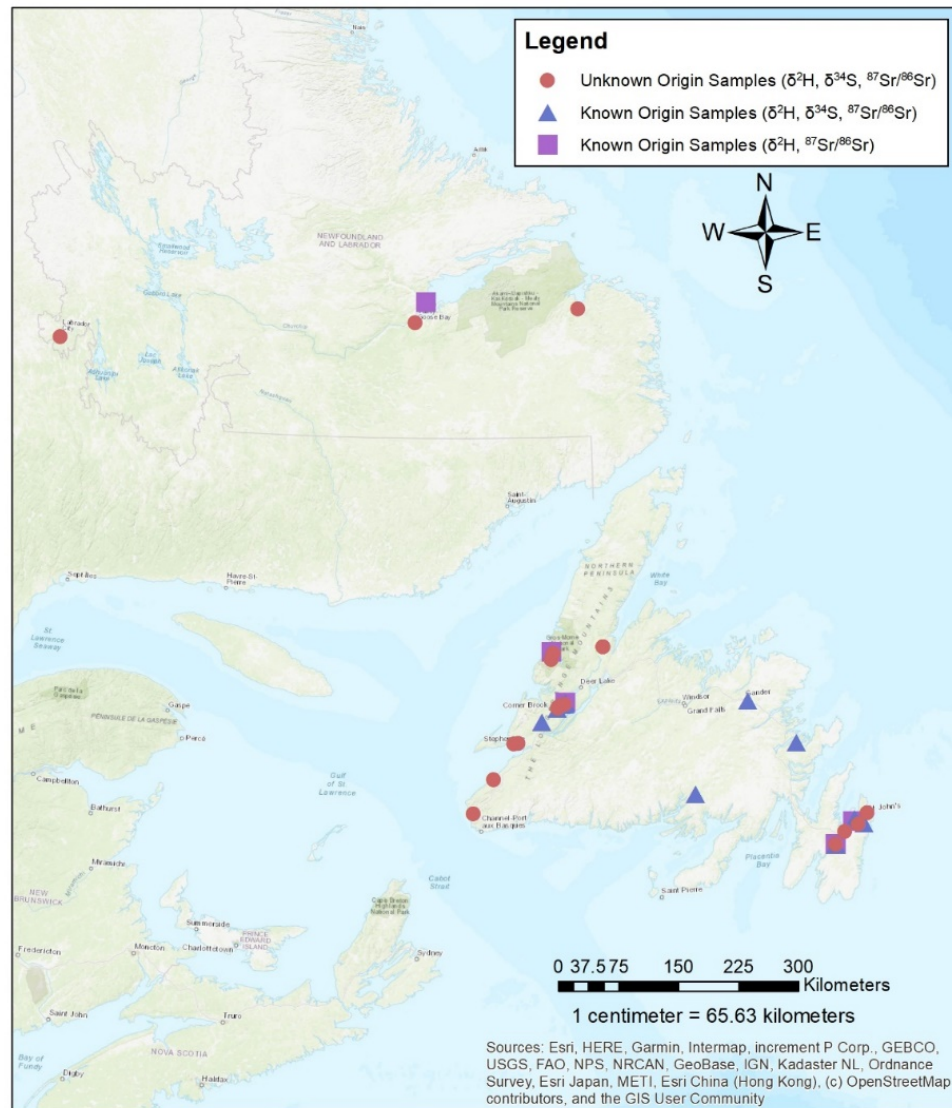
Figure 3.1. *Geographic distribution of samples. Blue triangles show known-origin individuals sampled and analyzed for δ^2H, δ^{34}S, ^{87}Sr/^{86}Sr (n = 15). Purple squares show additional known-origin individuals sampled and analyzed for δ^2H and ^{87}Sr/^{86}Sr only (n = 7). Red circles show unknown-origin individuals sampled and analyzed for δ^2H, δ^{34}S, ^{87}Sr/^{86}Sr (n = 21).*

Table 3.1. *Age, sex, and regional distribution of carcasses sampled and analyzed for δ^2H, ^{87}Sr/^{86}Sr, δ^{34}S with corresponding isotopic analysis results. Bolded rows are those assumed to be known origin individuals; summer residency of these individuals is presumed based on date and structure where the carcass was found. Asterisk (*) next to date signifies known date of mortality. ^{87}Sr/^{86}Sr values are reported alongside the corresponding surface [dorsal (D) or ventral (V)] where applicable.*

Sample ID	Sex	Region	Date	Structure	δ^2H (‰)	^{87}Sr/^{86}Sr	δ^{34}S (‰)
41	**male**	**Eastern**	**6/08/2018 ***	**-**	**−29.6**	**0.710642**	**+12.0**
42	**male**	**Eastern**	**7/10/2018 ***	**-**	**−38.2**	**0.710237**	**+11.0**
44	**male**	**Eastern**	**8/01/2018**	**residence**	**−42.4**	**0.710554**	**-**
81	**male**	**Eastern**	**7/22/2019**	**bat box**	**−50.4**	**0.709915**	**+11.1**
66	**female**	**Eastern**	**8/02/2019**	**-**	**−41.6**	**0.709364**	**+11.8**
69	**female**	**Eastern**	**6/28/2018 ***	**bat box**	**−30.1**	**0.709484**	**-**
79	**female**	**Eastern**	**7/19/2019**	**bat box**	**−36.6**	**0.709601**	**+12.5**
82	**female**	**Eastern**	**7/24/2019**	**road**	**−53.6**	**0.709738**	**+10.2**
83	**female**	**Eastern**	**7/25/2019**	**-**	**−45.5**	**0.709730**	**-**
88	**female**	**Eastern**	**-**	**-**	**−36.6**	**0.713456**	**+14.0**
76	**male**	**Central**	**6/17/2019 ***	**residence**	**−57.7**	**0.715323**	**+12.4**
37	**female**	**Central**	**6/17/2018**	**bat box**	**−47.4**	**0.713227**	**+9.8**
38	**female**	**Central**	**6/17/2018**	**bat box**	**−52.7**	**0.712907**	**+8.4**
40	**male**	**Western**	**6/01/2018**	**residence**	**−51.7**	**0.711416**	**+10.9**
39	**female**	**Western**	**6/17/2018 ***	**residence**	**−47.9**	**0.711518**	**-**
75	**female**	**Western**	**6/17/2019 ***	**residence**	**−40.3**	**0.712140 (D) 0.712028 (V)**	**+10.9**
78	**female**	**Western**	**7/17/2019**	**bat box**	**−43.4**	**0.710065**	**+14.8**
84	**female**	**Western**	**8/01/2019**	**residence**	**−51.0**	**0.712034**	**-**
85	**female**	**Western**	**8/01/2019**	**residence**	**−55.1**	**0.711844**	**-**
86	**female**	**Western**	**8/01/2019**	**residence**	**−43.7**	**0.711243**	**+10.4**
87	**female**	**Western**	**8/05/2019**	**residence**	**−55.1**	**0.711586**	**+10.6**
97	**female**	**Western**	**6/04/2020**	**residence**	**−51.5**	**0.713401**	**+11.4**
43	**male**	**Labrador**	**6/23/2018**	**residence**	**−76.2**	**0.707023**	**-**
67	female	Eastern	5/30/2018 *	residence	−26.4	0.710668	+13.0
90	female	Eastern	5/24/2020	forested area	−48.2	0.711833	+11.2
91	female	Eastern	5/18/2020	residence	−48.3	0.709422 (D) 0.710160 (V)	+11.9
15	male	Western	4/5/2017	residence	−59.2	0.711094	+8.7
16	male	Western	7/05/2017	hibernaculum	−63.9	0.713208	+11.9
95	male	Western	1/16/2020 *	hibernaculum	−48.2	0.714787	+9.9
96	male	Western	5/17/2020	hibernaculum	−43.9	0.711478	+10.5
14	female	Western	5/11/2017	residence	−38.4	0.709898	+8.8
17	female	Western	3/04/2018	-	−43.6	0.709450	+8.1
18	female	Western	3/18/2018	-	−52.6	0.713392	+9.1
19	female	Western	5/11/2018	residence	−35.5	0.711193	+11.0
20	female	Western	5/11/2018 *	residence	−42.2	0.709844	+11.3
60	female	Western	3/13/2019 *	hibernaculum	−54.8	0.712860	+11.4
74	female	Western	5/14/2019	residence	−46.6	0.711747 (D) 0.713147 (V)	+10.7

Sample ID	Sex	Region	Date	Structure	δ^2H (‰)	$^{87}Sr/^{86}Sr$	$\delta^{34}S$ (‰)
100	-	Western	5/4/2021	residence	–58.2	0.712176 (D) 0.711733 (V)	+10.8
101	-	Western	5/14/2021	residence	–41.5	0.714315 (D) 0.712507 (V)	+10.5
102	-	Western	4/30/2021	residence	–43.0	0.712422 (D) 0.713338 (V)	+10.3
50	female	Labrador	6/30/2018	-	–58.3	0.712514 (D) 0.712662 (V)	+9.3
98	-	Labrador	5/13/2021	hibernaculum	–88.1	0.720056 (D) 0.716555 (V)	+5.5
99	-	Labrador	5/18/2021	bat box	–74.7	0.716015 (D) 0.716141 (V)	+9.6

B. Sample pre-treatment & analysis

i. Analysis of fur for δ^2H

Analysis of fur samples for δ^2H was conducted at the Laboratory for Stable Isotope Science at the University of Western Ontario in London, Ontario. Raw fur samples were shipped directedly to the Laboratory for Stable Isotope Science, where pre-treatment, subsampling, microbalance weighing, and analysis occurred. To remove surface oils, fur samples were left to soak in a 2 : 1 chloroform : methanol solution overnight, rinsed with the same solution, and dried under a fume hood. Approximately 0.34 ± 0.02 mg of samples and standards were weighed into silver capsules, loosely closed, and left to equilibrate with ambient water vapor for > 96 hours (Wassenaar & Hobson, 2003). On the morning of analysis, all capsules were folded securely closed before loading. Samples and standards were combusted at 1120 °C using a Thermo Scientific High Temperature Conversion Elemental Analyzer (TC/EA) equipped with a newly packed chromium reactor, and the resulting gas analyzed for δ^2H with an interfaced Delta^Plus XL Isotope Ratio Mass Spectrometer operating in continuous flow mode.

Results are reported in parts per thousand (‰) using standard δ notation relative to VSMOW (Vienna Standard Mean Ocean Water), which was calibrated using two internationally accepted keratin standards: Caribou Hoof Standard [CBS; –157.0 ± 0.9 ‰ (Soto et al., 2017)] and Kudu Horn Standard [KHS; –35.3 ± 1.1 ‰ (Soto et al., 2017)]. Sample δ^2H values are reported according to Equation 1 (pg. 11). Experimental samples were analyzed with a 10 % duplication rate, and the mean ± standard deviation difference between duplicates was +3.0 ± 3.7 ‰ ($n = 4$). Quality assurance was verified using an internal laboratory standard, Spectrum-1; the δ^2H value of this standard across both sessions was –56.0 ± 1.8 ‰ ($n = 14$). The accepted value for this standard is –57 ‰. The average reproducibility for CBS and KHS across both sessions was +1.9 ‰ (SD, $n = 11$) and +2.0 ‰ (SD, $n = 11$), respectively.

ii. Analysis of fur for $\delta^{34}S$

To remove surface oils, fur samples were left to soak in a 2 : 1 chloroform : methanol solution overnight, rinsed with the same solution, and dried under a fume hood. Approximately 1.0 ± 0.01 mg of samples were weighed into tin capsules and folded securely closed. These tin capsules were then shipped to the Ján Veizer Stable Isotope Laboratory at the University of Ottawa in Ottawa, Ontario for $\delta^{34}S$ analysis. There, samples were loaded into an Elemental Analyser Isotope Cube in S mode and flash combusted at 1800 °C. The resulting gases were He-swept, SO_2 isolated using a trap and purge column, and analyzed for $\delta^{34}S$ using a Thermo Scientific Delta^{PLUS} XP isotope ratio mass spectrometer via a Conflo IV interface. Long term analytical precision of the lab is ± 0.3 ‰.

Results are reported in parts per thousand (‰) using standard δ notation relative to VCDT (Vienna Canyon Diablo Troilite), which was calibrated using three internationally accepted sulphide standards: IAEA-S1 (–0.3 ‰), IAEA-S2 (+22.7 ‰), and IAEA-S3 (–32.6 ‰). Sample $\delta^{34}S$ values are reported according to Equation 5 (pg. 23). Experimental samples were analyzed with a 10 % duplication rate, and the average difference between duplicates was +0.1 ± 0.1 ‰ ($n = 3$). The percent S of our experimental samples was as expected (4.0 ± 0.9 %, $n = 39$). Quality assurance was verified using an internal argentite standard, AG-2; the $\delta^{34}S$ value of this standard was –0.8 ± 0.01 ‰ ($n = 5$). The accepted value for this standard is –0.6 ‰.

iii. Analysis of fur for $^{87}Sr/^{86}Sr$

See the previous chapter for the $^{87}Sr/^{86}Sr$ pre-treatment, digestion, and analysis procedure of fur samples (pg. 64, 66 – 67). Fur sampled from the dorsal and ventral surfaces of nine individuals were analyzed separately to compare differences in $^{87}Sr/^{86}Sr$ values across the body of a single individual. We calculated the mean absolute difference between dorsal and ventral $^{87}Sr/^{86}Sr$ values for these individuals to quantify variation in $^{87}Sr/^{86}Sr$ values across the body of a single individual. A more detailed breakdown of $^{87}Sr/^{86}Sr$ analysis results can be found in Appendix II (pg. 173).

C. Statistical analyses

We conducted all subsequent statistical analyses, geographic modeling, and graphical comparisons in R-Studio version 4.1.3 (R Core Team, 2022). R codes used in relevant analyses can be found in Appendices III – VII (pg. 175 – 224). Data manipulation was done using the dplyr package (Wickham et al., 2022), origin assignments were predicted using the AssignR package (Ma et al., 2020), random forest

regression modeling was conducted using the VSURF (Genuer et al., 2019) and randomForest (Liaw & Wiener, 2002) packages, raster file extraction and manipulation was done using the raster package (Hijmans & van Etten, 2012), transfer functions were made using the smatr package (Warton et al., 2012), and graphics were made using the ggplot2 package (Wickham, 2016) and the RColorBrewer package (Neuwirth, 2014). We considered results significant if the *p* value was less than or equal to 0.05.

i. δ^2H isoscape & transfer function

δ^2H varies predictably across the landscape with the preferential condensation of deuterium (and preferential release of protium) as cloud masses move across continents (Bowen & West, 2019). This process, known as Rayleigh Distillation, drives the patterns that we see in the isotopic distribution of δ^2H in many parts of the world: precipitation is depleted of deuterium with increasing latitude, altitude, and distance from the coast, lower temperatures, and higher relative humidity (Rubenstein & Hobson, 2004). Generally, distance to the open ocean (i.e., the Eastern region of the province) and changes in elevation (the majority of topographic relief being present in the Western region) have the potential to influence the isotopic distribution of δ^2H on the island of Newfoundland. Similarly, distance to the Atlantic Ocean, latitude, and altitude have the potential to influence the isotopic distribution of δ^2H across both Newfoundland and Labrador.

We modeled the distribution of δ^2H in precipitation (δ^2H$_p$) across our study area using IsoMAP, a recently decommissioned publicly available resource for the construction of δ^2H and δ^{18}O isoscapes worldwide (Bowen et al., 2014). Our model used a 30-year average of δ^2H$_p$ during the growing season (May – August, 1988 – 2018),

interpolated with latitude^2, |latitude|, longitude, longitude^2, and elevation to generate a mean and standard deviation δ^2H_p isoscape (job # 86,948). IsoMAP generates two models: one using a multiple linear regression and the other using a geostatistical model. Because the p value of Moran's I for this model was not significant ($p = 0.55$) we used the multiple linear regression model in our subsequent analysis (Moran, 1948).

Physiological fractionation of δ^2H is well documented, and therefore, the relationship between δ^2H_p and δ^2H_{fur} needs to be established prior to estimates of probable origin (Hobson, 1999; Hobson, 2005; Voigt et al., 2015; Vander Zanden et al., 2016). To demonstrate this relationship in the form of a transfer function, we extracted δ^2H_p values at the location of mortality for all individuals classified as known origin ($n = 23$) and calculated the mean δ^2H_{fur} value for individuals whose geographic coordinates fell within the same raster cell (i.e., individuals with the same δ^2H_p value). We then related δ^2H_p and δ^2H_{fur} ($n = 17$) using a Standardized Major Axis Regression (McArdle, 1988; Smith, 2009; Pylant et al., 2014; Campbell et al., 2020).

ii. Summer residency predictions & migratory classifications using δ^2H

We used the AssignR package (Ma et al., 2020) to predict the location of summer residency for all individuals of unknown origin ($n = 20$) based on their respective δ^2H_{fur} value. To do so, we loaded the mean and standard deviation δ^2H_p isoscapes built in IsoMAP (Bowen et al., 2014), and adapted the "calRaster" function to rescale the δ^2H_p isoscape to the equivalent δ^2H_{fur} values using our newly developed δ^2H transfer function. AssignR requires a metric of analytical precision alongside each δ^2H_{fur} to quantify intra-individual variation – we used the standard deviation of the absolute difference between all duplicates analyzed for δ^2H, as well as all individuals whose geographic coordinates

fell within the same raster cell ($n = 8$; $SD = 3.89$). We then mapped probability density surfaces using the "pdRaster" function. This function calculates probability of origin for each cell in the rescaled δ^2H isoscape. Then, we calculated the location of summer residency for each individual with 50 % and 75 % probability thresholds using the "qtlRaster" function. These probability thresholds are a proxy for accuracy of the assigned location of summer residency and are somewhat arbitrary (but 0.5 and 0.75 are typical, e.g., Pylant et al., 2016; Fraser et al., 2017; but see Campbell et al., 2020); they are used to calculate the smallest area within which the probability values of each cell sum to 0.50 or 0.75. Finally, we used the "distanceFromPoints" function in the Raster package to determine migratory status (Hijmans, 2022). This function calculates the distance from a point, in this case the geographic coordinate associated with the individual's mortality location, to the closest numerical cell of a raster (i.e., the closest cell with a value other than 'NA') (Hijmans, 2022). After applying this function to our raster, we masked all cells outside of the area of probable origin and determined the minimum value present in the newly masked area. Finally, because this function calculates the distance to the closest cell, but does not include the cell that contains the geographic coordinate, the output is almost always > 0. Therefore, to determine migratory status, we made calculations for three probability thresholds – 50 %, 75 %, and 90 % – to ensure that the minimum value generated in analyses was truly the smallest value that could be generated for that geographic coordinate. Individuals were classified as migratory if their minimum distance value was greater than that of the 90 % probability threshold. Likewise, individuals were classified as non-migratory if their minimum distance value was equal to that of the 90 % probability threshold.

iii. δ^{34}S isoscape & transfer function

δ^{34}S has a distinct and consistent oceanic signature (+ 20.3 ‰); in the terrestrial environment, δ^{34}S varies with lithology (depending on the sulfuric content of minerals), atmospheric pollution, sea spray, surface waters, marine or terrestrial influenced rain, and with the breakdown of biological materials (terrestrial sources are highly variable but cluster around 0 ‰) (Nehlich, 2015). Variations in bedrock geology (e.g., tectonic zones), proximity to the coast, and proximity to industrial areas (e.g., atmospheric sources of pollution) have the potential to be significant predictors of variation in δ^{34}S across our study area.

We know of one previously developed δ^{34}S isoscape in Newfoundland, which used δ^{34}S values of lichen sampled throughout the island interpolated with the gridding methods established by Smith and Wessel (1990) (Wadleigh & Blake, 1999). This method of interpolation is a form of contour mapping that applies tension to minimum-curvature gridding methods to prevent large oscillations between known data points, and relies on a good distribution of measured data to extrapolate variation across the landscape (Smith & Wessel, 1990; Holt et al., 2021). However, there are several disadvantages to modeling isotopic surfaces with contour mapping. Primarily, it can increase uncertainty by interpolating values beyond the limits of the measured data, which can be especially problematic when data is not evenly collected throughout the landscape or when there is bias in sampling locations (Holt et al., 2021). Additionally, contour mapping can smooth variation in δ^{34}S across the landscape, which tends to create homogeneity in the model and can be problematic in areas where the distribution of δ^{34}S varies with underlying geology and is thus heterogeneous in nature (Holt et al., 2021).

Both of these disadvantages can be remedied by using random forest regression in place of contour mapping (e.g., Bataille et al., 2018; Holt et al., 2021). An advantage of random forest regression is its ability to use both measured and modeled data, as well as categorical and continuous variables, to predict variation in isotope distribution across the landscape (Holt et al., 2021). Additionally, it does not rely on assumptions of normality or homoscedasticity for the calibration dataset or residuals (Bataille et al., 2020). However, random forest regression is still a model which relies on a calibration dataset and predictors and can be affected by limitations of that dataset (i.e., biases towards specific sampling locations) and the predictors (i.e., low accuracy of bedrock distribution maps) (Holt et al., 2021).

Considering the tradeoffs between using these two methods for modeling the distribution of δ^{34}S across our study area, we ultimately used δ^{34}S values of lichen sampled throughout insular Newfoundland and published by Wadleigh and Blake (1999) as our calibration dataset ($n = 76$), and the random forest regression methodology outlined by Bataille et al. (2021) to develop a new δ^{34}S isoscape for Newfoundland. We adapted the methods of Bataille et al. (2021) to our calibration dataset by including distance to pollutants as an additional covariate, as industrial areas influence the δ^{34}S values recorded in this dataset (Wadleigh & Blake, 1999). We created a raster file using the distanceFromPoints function in the raster package (Hijmans, 2022) to quantify distance to the closest of four industrial areas that, at the time of the Wadleigh and Blake (1999) publication, represented the majority of anthropogenic sulfur dioxide (SO_2) sources on the island. These sources include the Corner Brook Pulp and Paper Mill, Buchans Mine,

Come by Chance Refinery, and Holyrood Thermal Generating Station (Wadleigh &

Blake, 1999).

Physiological fractionation of δ^{34}S is well understood thanks to several

investigations reporting δ^{34}S values of animal tissues compared to a laboratory food

source (McCutchan et al., 2003; Richards et al., 2003; Pinzone et al., 2017; Webb et al.,

2017). Fur keratin is composed of approximately 5 % S, and has a reported +1 ‰

discrimination factor, likely due to the high concentration of metabolized cycsteine in α

keratin (Richards et al., 2003; Nehlich, 2015; Pinzone et al., 2017; Webb et al., 2017; but

see McCutchan et al., 2003). Thus, to evaluate whether our newly developed δ^{34}S

isoscape (δ^{34}S$_{iso}$) explained variation in δ^{34}S values associated with modern *M. lucifugus*

fur (δ^{34}S$_{fur}$), we developed a transfer function using the same methods as δ^2H. We

extracted δ^{34}S$_{iso}$ values at each location of mortality for the individuals of known origin (*n*

= 16) and calculated the mean δ^{34}S$_{fur}$ value for individuals sampled from the same raster

cell (*n* = 7). We then related the δ^{34}S$_{iso}$ to δ^{34}S$_{fur}$ values using a Standardized Major Axis

Regression (McArdle, 1988; Smith, 2009). We acknowledge two limitations of using this

approach: (1) a more than 20-year difference between our fur samples and the lichen

samples published by Wadleigh and Blake (1999), and (2) the greater sensitivity of lichen

to atmospheric sources of S (e.g., SO$_2$ pollution) relative to our study species (Krouse,

1977). Based on the results of this transfer function we did not move forward with

probabilistic summer residency predictions using δ^{34}S.

iv. ^{87}Sr/^{86}Sr isoscape & transfer function

^{87}Sr/^{86}Sr is known to vary predictably with bedrock type and age, making it

particularly well-suited for study areas with heterogeneity in underlying bedrock (Bataille

et al., 2020). Additional sources of variation in $^{87}Sr/^{86}Sr$ include atmospheric dust or pollution, sea spray, and soil or surface waters (Bataille et al., 2020). As with $\delta^{34}S$, variations in underlying geology, adjacent coastlines and their resulting sea spray, and the presence of atmospheric pollutants/dust have the potential to be significant predictors of variation in $^{87}Sr/^{86}Sr$ across our study area.

We know of two isoscapes that have been constructed for our study region – one as part of a global Sr model (Bataille et al., 2020), and the other as part of a regional model for Atlantic Canada (Le Corre, 2023). Both isoscapes use the previously described random forest regression methodology (first developed by Bataille et al., 2018), paired with up to 20 covariates that were selected for importance using the VSURF package, to predict variation in $^{87}Sr/^{86}Sr$ across the landscape (Bataille et al., 2020; Le Corre, 2023).

Physiological fractionation of $^{87}Sr/^{86}Sr$ is still under investigation (Bentley, 2006; Flockhart et al., 2015), particularly in regards to the relationship between dietary $^{87}Sr/^{86}Sr$ values and those incorporated into bat fur (Kruszynski et al., 2020). Therefore, we tested the relationship between these isoscapes and the $^{87}Sr/^{86}Sr$ isotopes recorded in the fur of our known origin individuals using the same methodology as we used for the δ^2H and $\delta^{34}S$ fur data. Fur sampled from the dorsal and ventral surfaces of one known origin individual (75) was analyzed separately; we calculated the mean $^{87}Sr/^{86}Sr$ fur value for this individual and used it in our transfer function. Based on the results of these transfer functions we did not move forward with probabilistic summer residency predictions using $^{87}Sr/^{86}Sr$.

v. Predictions of summer residency region & migratory classifications using $^{87}Sr/^{86}Sr$

To predict the region of summer residency for all individuals of unknown origin based on their respective $^{87}Sr/^{86}Sr_F$ values, we used the same regional $^{87}Sr/^{86}Sr$ estimates as the previous chapter (pg. 69 – 72). Using this approach, we classified individuals into one of three categories: migratory, non-migratory, and indeterminate. If an individual's $^{87}Sr/^{86}Sr_F$ value fell within the regional $^{87}Sr/^{86}Sr$ estimate corresponding to its mortality location, we classified it as non-migratory. Alternatively, if an individual's $^{87}Sr/^{86}Sr_F$ value fell within a regional $^{87}Sr/^{86}Sr$ estimate distinct from the individual's mortality region, we classified it as migratory. Finally, we designated individuals as indeterminate in two ways: (1) an individual's $^{87}Sr/^{86}Sr_F$ value fell outside of a regional $^{87}Sr/^{86}Sr$ estimate, or (2) the $^{87}Sr/^{86}Sr_F$ values of the dorsal and ventral surfaces of an individual were not in agreement (i.e., the $^{87}Sr/^{86}Sr_F$ values of the dorsal and ventral surfaces of a single individual did not fall within the same regional $^{87}Sr/^{86}Sr$ estimate).

vi. Dual isotope (δ^2H, $^{87}Sr/^{86}Sr$) migratory classifications

We combined the $^{87}Sr/^{86}Sr$ regional estimates and the δ^2H probabilistic assignments to further determine migratory status for all individuals of unknown origin. Based on the combination of these isotope systems, we classified individuals into the same three categories: (1) migratory, (2) non-migratory, or (3) indeterminate. Cases where an individual's migratory classification was the same for δ^2H and $^{87}Sr/^{86}Sr$ were straightforward. Those individuals maintained their migratory status as long as there was an overlap between summer residency predictions according to both isotope systems. If the migratory classifications conflicted (e.g., an individual was classified as migratory according to one isotope system and non-migratory according to the other), we

determined migratory status by manually comparing the predicted region and probabilistic assignment. The overlap between summer residency predictions according to both isotope systems determined migratory status. Specifically, an individual was classified as migratory if its location of mortality fell outside of the overlap between summer residency predictions and non-migratory if it fell within this combined summer residency prediction. Finally, an individual was classified as indeterminate if there was disagreement between the two predictions (e.g., an individual's summer residency prediction according to δ^2H fell within Eastern Newfoundland, but its prediction according to ^{87}Sr/^{86}Sr fell within Western Newfoundland). Individuals classified as indeterminate according to ^{87}Sr/^{86}Sr were reclassified based on their δ^2H migratory status. Cases where dorsal and ventral ^{87}Sr/^{86}Sr values indicated separate summer residency regions presented an extra complication. In these cases, we compared the δ^2H probabilistic assignment and the predicted region of summer residency according to ^{87}Sr/^{86}Sr values of the dorsal surface for that individual. Ultimately, we classified these individuals as indeterminate but noted the migratory classification of the dorsal surface.

V.   RESULTS

A. δ^2H results

The δ^2H$_p$ isoscape constructed using IsoMAP performed well for predicted δ^2H$_p$ values in our study area (Figure 3.2; $r^2 = 0.97$, $MSE = 13.53$, $MSR = 16.37$). To establish our transfer function, we first excluded one outlier (individual 43), as it was the only individual of known origin sampled from Labrador and disproportionately affected the relationship between δ^2H$_{fur}$ and δ^2H$_p$. After removing this individual, we observed a

moderately strong and significant linear relationship between δ^2H_{fur} and δ^2H_p (Figure 3.2; $p < 0.05$, $r^2 = 0.35$), with the standard deviation of the residuals being +7.06 ‰. The δ^2H transfer function equation used in all subsequent analyses is as follows:

$$\delta^2H_{fur} = \left(0.94 \times \delta^2H_p\right) + 3.51 \qquad \textbf{Equation 6}$$

Figure 3.3 shows a subset of our results, and results for all individuals can be found in Appendices VIII and IX (pg. 225 – 230). According to the predictions made using 50 % probability, 25 % ($n = 5$) and 75 % ($n = 15$) of unknown origin individuals were classified as non-migratory and migratory, respectively (Table 3.2). Comparatively, according to the predictions made using 75 % probability, 35 % ($n = 7$) and 65 % ($n = 13$) of unknown origin individuals were classified as non-migratory and migratory, respectively (Table 3.2). Most individuals migrated within the island; the majority of these movements occurred between neighboring regions, with some individuals migrating between Western and Eastern Newfoundland. Individuals whose mortality locations were in Labrador, for the most part, remained on the mainland; however, one individual may have migrated to the Northern Peninsula of Newfoundland (individual 50; Figure 3.3). The farthest migratory estimates generated with these probability surfaces were made by individuals 50, 19, and 67 (Figure 3.3), who likely migrated several hundred kilometers.
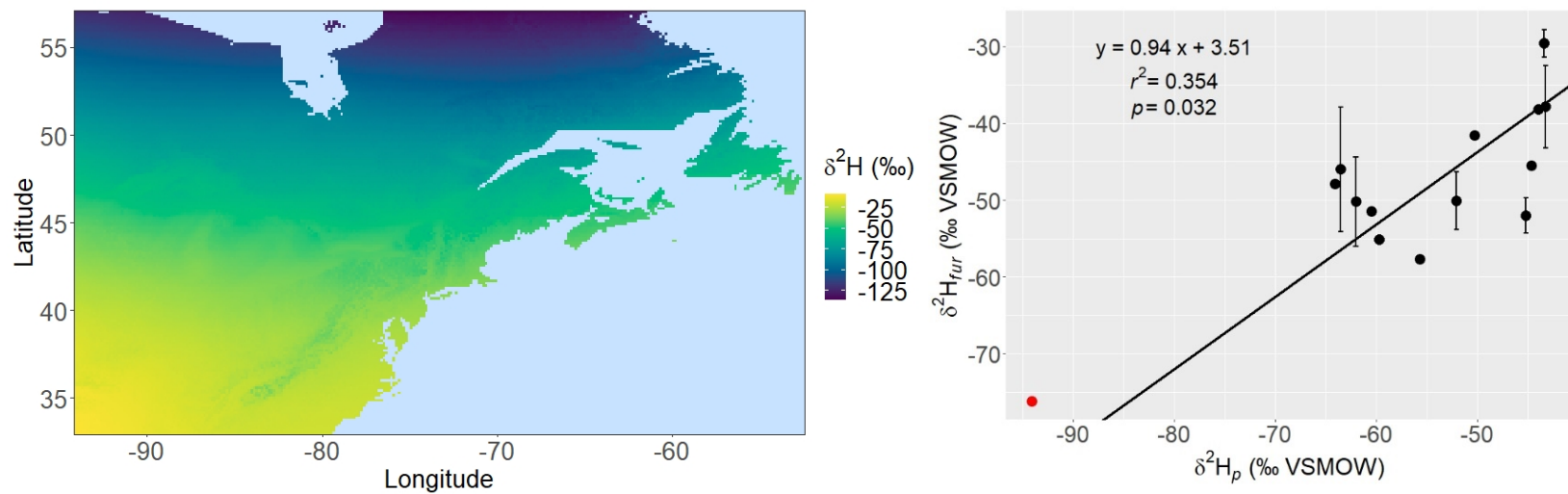
Figure 3.2. (Left) *30-year average of growing season δ^2H precipitation values (δ^2H_p May-August, 1988-2018) interpolated with latitude^2, |latitude|, longitude, longitude^2, and elevation using a multiple linear regression (IsoMAP job # 86,948; Bowen et al., 2014).* ***(Right)*** *Linear relationship between δ^2H values of* Myotis lucifugus *fur (δ^2H_{fur}) and δ^2H_p in insular Newfoundland. Variation in δ^2H_{fur} values of individuals sampled within the same raster cell is illustrated with error bars ($\pm$ 1 SD). δ^2H values reported relative to Vienna Standard Mean Ocean Water (VSMOW). Outlier excluded from calculations is plotted in red.*
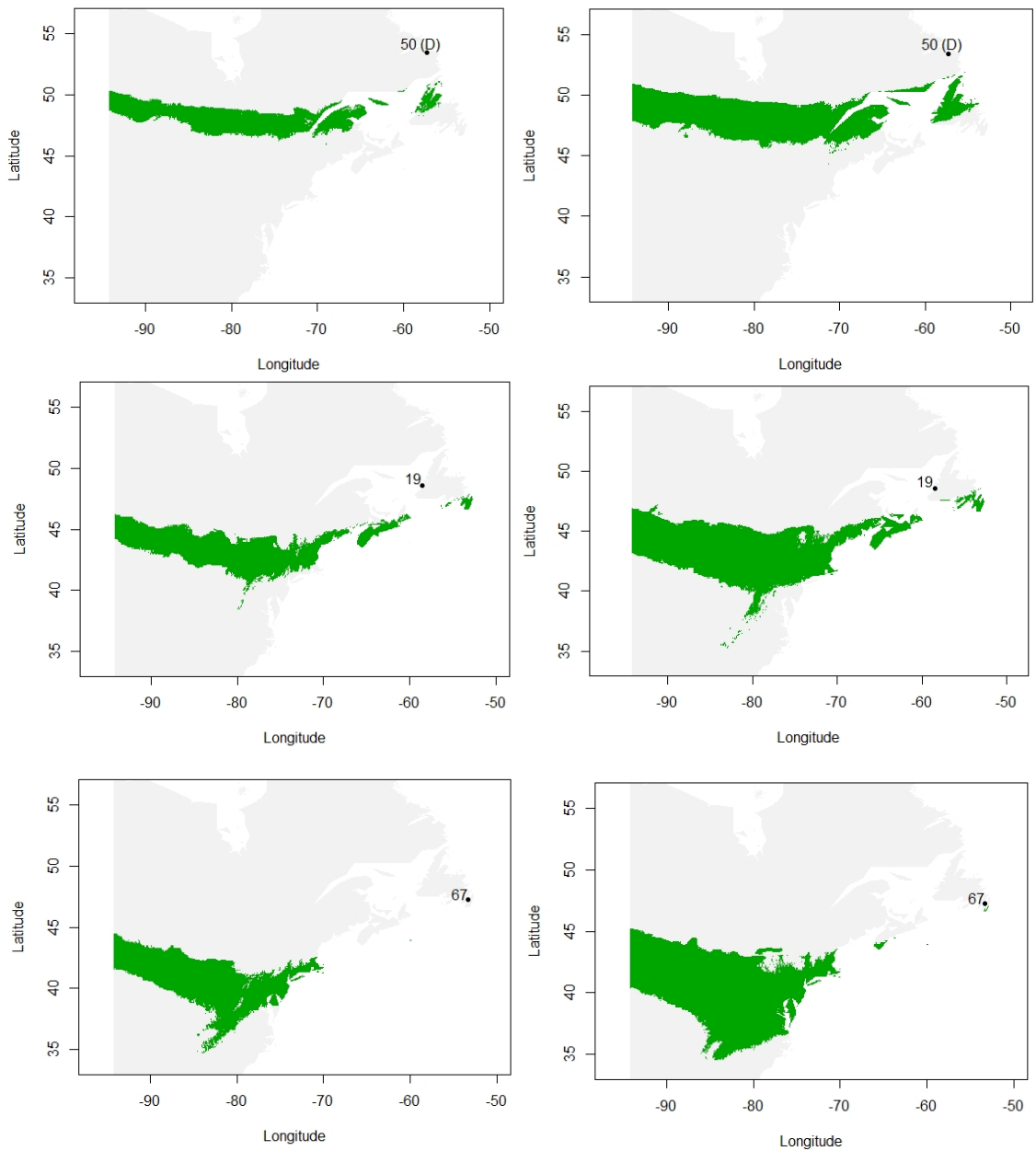
Figure 3.3. *Summer residency predictions for a subset of individuals of unknown origin based on $\delta^2 H_{fur}$ values and using the "qtlRaster" function in AssignR (Ma et al., 2020). Results indicate 50% (left) and 75% (right) probability of origin. Point denotes location of mortality with label specifying sample ID.*

Table 3.2. *Region of mortality, regional summer residency prediction (according to* $^{87}Sr/^{86}Sr_F$ *values), and migratory classification according to each isotopic prediction. Migratory status was determined for* δ^2H *using 50 % and 75 % probability thresholds. The combined migratory status (using* δ^2H *and* $^{87}Sr/^{86}Sr$*) is based on manual vetting of summer residency predictions for each isotope. Combined migratory status did not differ with predictions made using 50 % or 75 % probability thresholds with the exception of individual 67. This individual's dual isotope migratory status was considered* indeterminate *when the* $^{87}Sr/^{86}Sr$ *prediction was combined with the 50 % threshold, and* migratory *when it was combined with the 75 % threshold.*

Sample ID	Region of Mortality	Predicted region - $^{87}Sr/^{86}Sr$	Migratory Status - $^{87}Sr/^{86}Sr$	Migratory status - δ^2H (50 % Accuracy)	Migratory status - δ^2H (75 % Accuracy)	Migratory status - δ^2H, $^{87}Sr/^{86}Sr$
67	Eastern	Eastern	Non-migratory	Migratory	Migratory	(50%): Indeterminate (75%): Migratory
90	Eastern	Western	Migratory	Migratory	Migratory	Migratory
91	Eastern	Eastern	Non-migratory	Migratory	Migratory	Migratory
15	Western	Indeterminate	Indeterminate	Non-migratory	Non-migratory	Non-migratory
16	Western	Central	Migratory	Migratory	Non-migratory	Indeterminate
95	Western	Central	Migratory	Migratory	Migratory	Migratory
96	Western	Western	Non-migratory	Migratory	Migratory	Migratory
14	Western	Eastern	Migratory	Migratory	Migratory	Migratory
17	Western	Eastern	Migratory	Migratory	Non-migratory	Migratory
18	Western	Central	Migratory	Non-migratory	Non-migratory	Migratory
19	Western	Western	Non-migratory	Migratory	Migratory	Indeterminate
20	Western	Eastern	Migratory	Migratory	Migratory	Migratory
60	Western	Central	Migratory	Non-migratory	Non-migratory	Migratory
74	Western	Indeterminate	Indeterminate	Migratory	Migratory	Indeterminate (D):Migratory
100	Western	Western	Non-migratory	Non-migratory	Non-migratory	Non-migratory
101	Western	Indeterminate	Indeterminate	Migratory	Migratory	Indeterminate (D): Migratory
102	Western	Indeterminate	Indeterminate	Migratory	Migratory	Indeterminate (D): Migratory
50	Labrador	Indeterminate	Indeterminate	Migratory	Migratory	Migratory
98	Labrador	Indeterminate	Indeterminate	Non-migratory	Non-migratory	Indeterminate (D): Non-migratory
99	Labrador	Indeterminate	Indeterminate	Migratory	Migratory	Migratory

B. δ^{34}S results

The random forest regression isoscape made using the previously published δ^{34}S values of lichen in Newfoundland performed well in terms of explaining variability in the dataset ($r^2 = 0.60$) but performed less desirably in terms of accuracy of the model (Figure 3.4; $MAE = 1.4$; $RMSE = 2.0$). The low accuracy of the model was also reflected in the transfer function, which showed a weak, insignificant linear relationship between δ^{34}S$_{iso}$ and δ^{34}S$_{fur}$ (Figure 3.4; $p = 0.65$, $r^2 = 0.02$), with the standard deviation of the residuals being +1.56 ‰. Due to the nature of these results, we opted not to move forward with further analyses and migratory classifications using δ^{34}S.
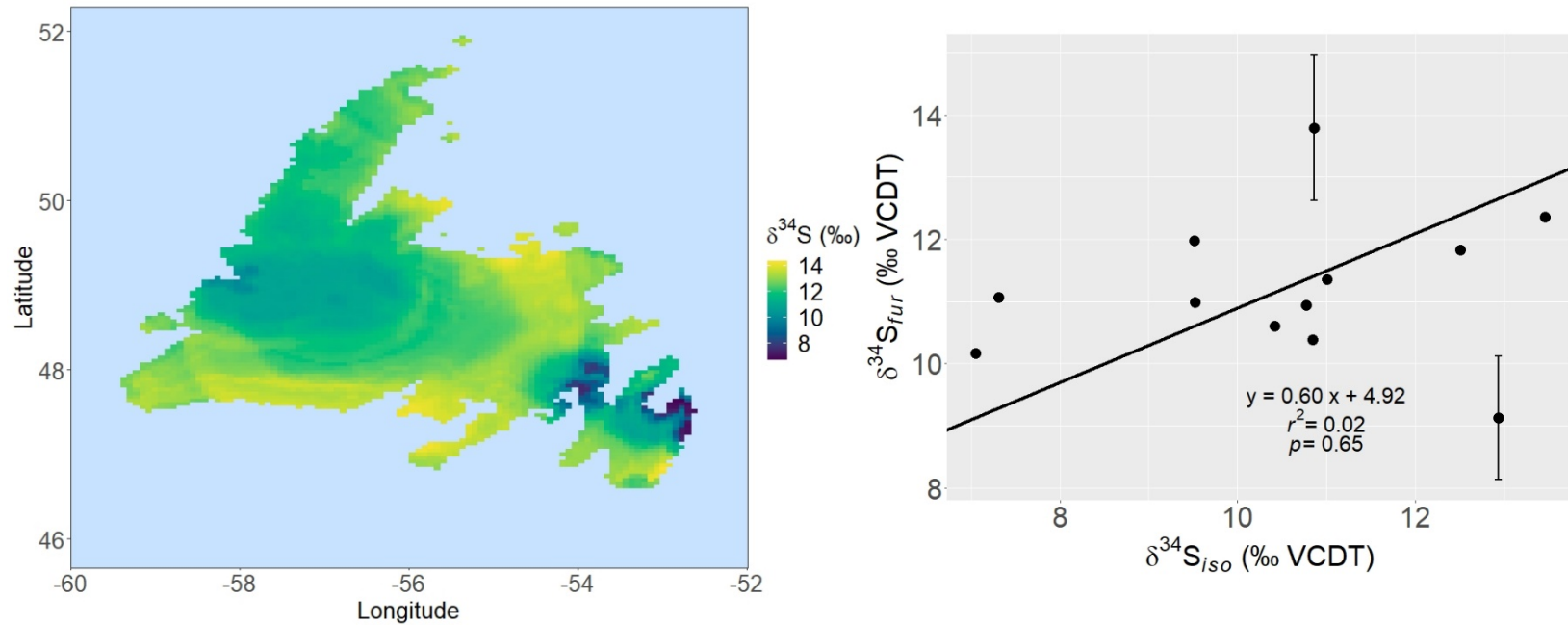
Figure 3.4. (Left) *Spatial distribution of $\delta^{34}S$ across insular Newfoundland ($\delta^{34}S_{iso}$). Modeled with $\delta^{34}S$ values recorded in lichen by Wadleigh and Blake (1999), interpolated with distance to pollutants, distance to the coast, dust aerosol deposition, the Bouguer anomaly, and sea salt deposition (wet and dry) using a random forest regression. **(Right)** Linear relationship between $\delta^{34}S$ values of* Myotis lucifugus *fur ($\delta^{34}S_{fur}$) and $\delta^{34}S_{iso}$ in insular Newfoundland. Variation in $\delta^{34}S_{fur}$ values of individuals sampled within the same raster cell is illustrated with error bars (± 1 SD). $\delta^{34}S$ values reported relative to Vienna-Canyon Diablo Troilite (VCDT).*

C. ^{87}Sr/^{86}Sr results

Before establishing a ^{87}Sr/^{86}Sr transfer function, we excluded one outlier (individual 43), as the offset between ^{87}Sr/^{86}Sr$_{iso}$ and ^{87}Sr/^{86}Sr$_F$ for this individual was large [^{87}Sr/^{86}Sr$_F$ = 0.707023, ^{87}Sr/^{86}Sr$_{iso}$ = 0.712596 (Bataille et al., 2020), ^{87}Sr/^{86}Sr$_{iso}$ = 0.713774 (Le Corre, 2023)]. Neither isoscape reflected the observed variation in ^{87}Sr/^{86}Sr values of bat fur throughout the province. The transfer function made using the global Sr isoscape (Bataille et al., 2020) explained very little of the variation in ^{87}Sr/^{86}Sr$_F$ values: p = 0.83, r^2 = 0.003, standard deviation of the residuals = 0.002232 (Figure 3.5). Comparatively, the transfer function made using the regional Sr isoscape (Le Corre, 2023) performed slightly better: p = 0.10, r^2 = 0.20, standard deviation of the residuals = 0.001720 (Figure 3.6).

As the ^{87}Sr/^{86}Sr values predicted by both isoscapes showed weak, insignificant linear relationships with observed ^{87}Sr/^{86}Sr$_F$ values, we did not move forward with probabilistic summer residency predictions (Figures 3.4 & 3.5). Instead, we used the same regional ^{87}Sr/^{86}Sr estimates as the previous chapter to predict summer residency region for all individuals of unknown origin (Figure 3.7). Using these predictions, 25 % (n = 5), 40 % (n = 8), and 35 % (n = 7) of individuals were classified as non-migratory, migratory, and indeterminate, respectively (Table 3.2). These migratory movements occurred at the same rate between neighboring regions (Eastern/Central and Western/Central; n = 4) and across the island (Eastern/Western, n = 4) (Table 3.2, Figure 3.7).

The high proportion of individuals classified as indeterminate was largely due to the high variation in ^{87}Sr/^{86}Sr$_F$ values across the body of a single individual. 57 % of

individuals classified as indeterminate were assigned this classification due to differences in the ^{87}Sr/^{86}Sr values between fur sampled from the dorsal and ventral surface of the individual (Table 3.2; Figure 3.7). The absolute difference between ^{87}Sr/^{86}Sr values of dorsal and ventral surfaces for all individuals was 0.001021 ± 0.001103 (mean ± sd, *n* = 9).
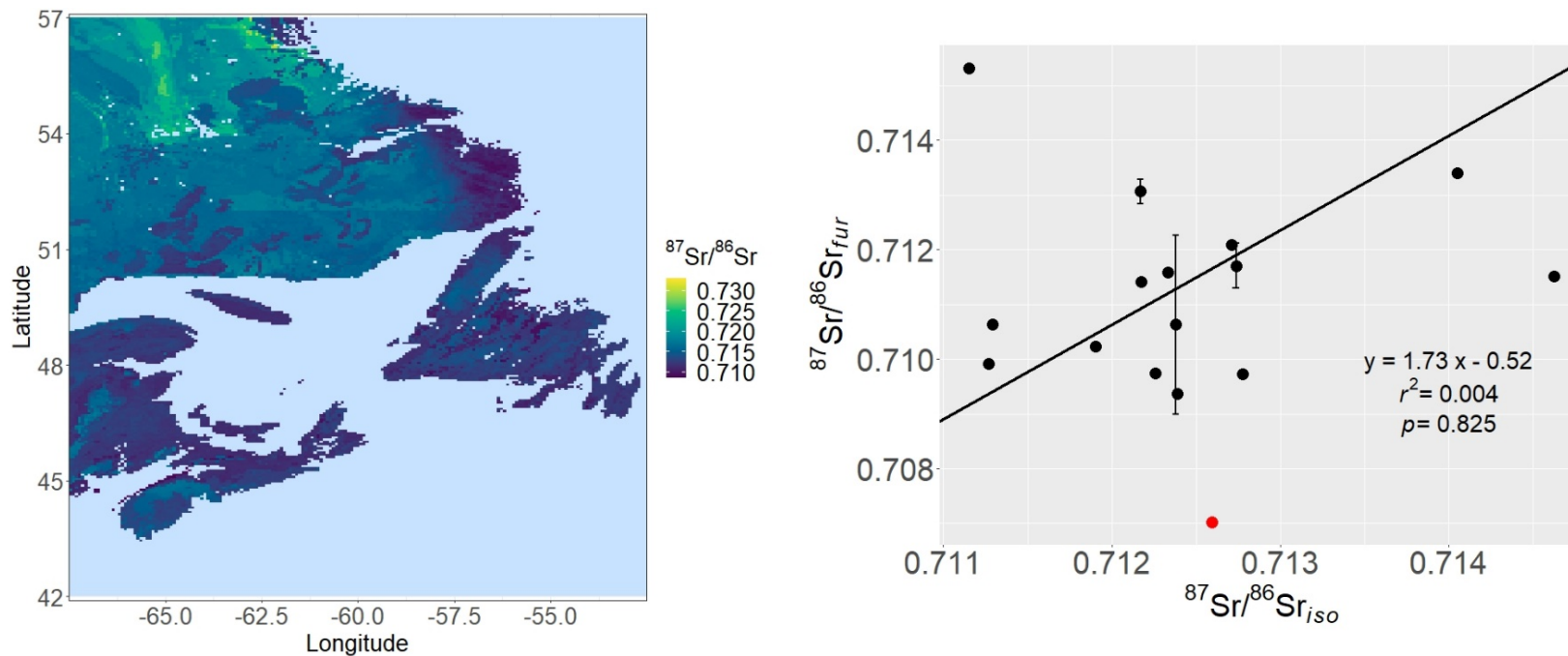
Figure 3.5. (Left) *Global distribution of $^{87}Sr/^{86}Sr$ values ($^{87}Sr/^{86}Sr_{iso}$) developed by Bataille et al. (2020).* **(Right)** *Linear relationship between $^{87}Sr/^{86}Sr$ values of* Myotis lucifugus *fur ($^{87}Sr/^{86}Sr_F$) and $^{87}Sr/^{86}Sr_{iso}$ in Newfoundland and Labrador. Variation in $^{87}Sr/^{86}Sr_F$ values of individuals sampled within the same raster cell is illustrated with error bars (± 1 SD). Outlier excluded from calculations is plotted in red.*
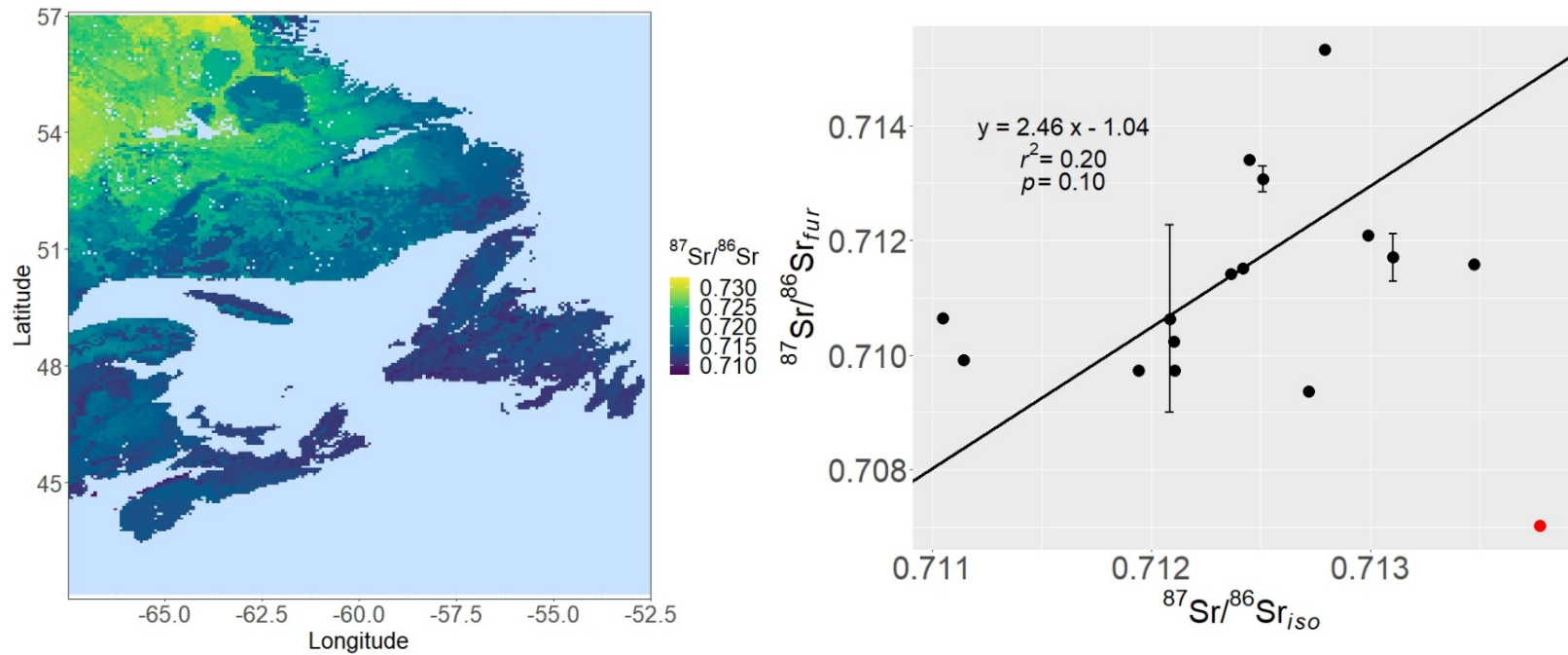
Figure 3.6. (Left) *Spatial distribution of $^{87}Sr/^{86}Sr$ values across Atlantic Canada ($^{87}Sr/^{86}Sr_{iso}$) developed by Le Corre et al. (2023).* **(Right)** *Linear relationship between $^{87}Sr/^{86}Sr$ values of* Myotis lucifugus *fur ($^{87}Sr/^{86}Sr_F$) and $^{87}Sr/^{86}Sr_{iso}$ in Newfoundland and Labrador. Variation in $^{87}Sr/^{86}Sr_F$ values of individuals sampled within the same raster cell is illustrated with error bars ($\pm$ 1 SD). Outlier excluded from calculations is plotted in red.*
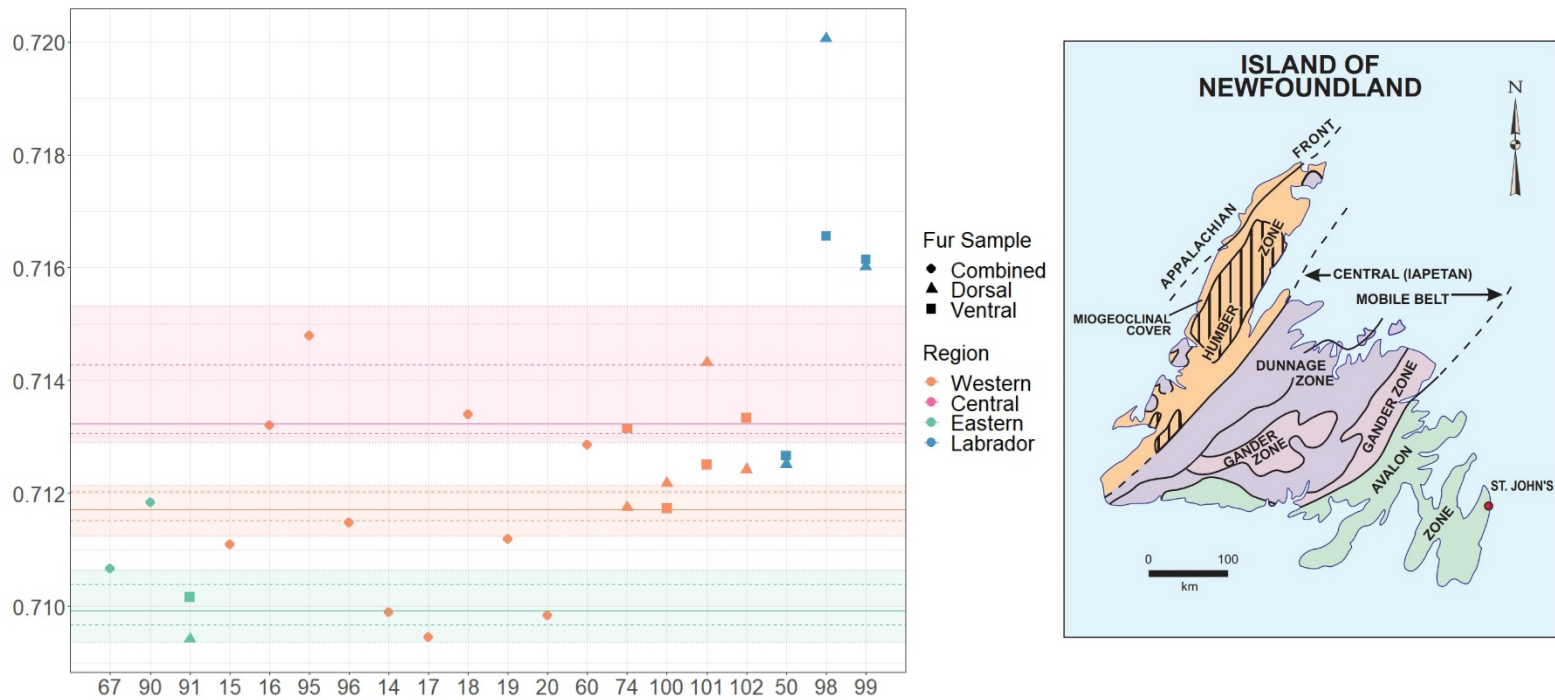
Figure 3.7. (Left) *Predictions of summer residency for individuals of unknown origin using regional estimates of* $^{87}Sr/^{86}Sr$ *values in the fur of known origin individuals. Solid lines represent the median, dashed lines represent the intra-quartile range, and shading represents the range of the known origin fur data. Note the absence of a regional estimate for Labrador due to limited sample availability in this region of the province. Points associated with each individual are showing* $^{87}Sr/^{86}Sr$ *values of fur sampled from the dorsal or ventral surface, or a combination of the two. Colors of each datapoint indicate region of mortality.* **(Right)** *Simplified geological map of Newfoundland showing tectonic zones for reference (Colman-Sadd et al., 2000). Western corresponds to the Humber Zone, Central to the Dunnage and Gander Zones, and Eastern to the Avalon Zone.*

D. Dual isotope migratory classification results

A high proportion of individuals were assigned to the same geographic area using the regional $^{87}Sr/^{86}Sr$ and probabilistic δ^2H predictions; in other words, we observed a high rate of agreement between assignments made using the two isotopic systems. Of the thirteen individuals with definitive $^{87}Sr/^{86}Sr$ predictions (i.e., migratory or non-migratory), ten (77 %) and eleven (85 %) showed agreement with assignments made using 50 % and 75 % probability thresholds for δ^2H assignments, respectively (Figure 3.8). The single individual that makes up the difference in agreement between δ^2H probability thresholds can be seen in Figure 3.3 (individual 67); more than likely, this individual originated from the easternmost tip of the Avalon peninsula (as shown in the 75 % probability threshold assignment; Figure 3.3).
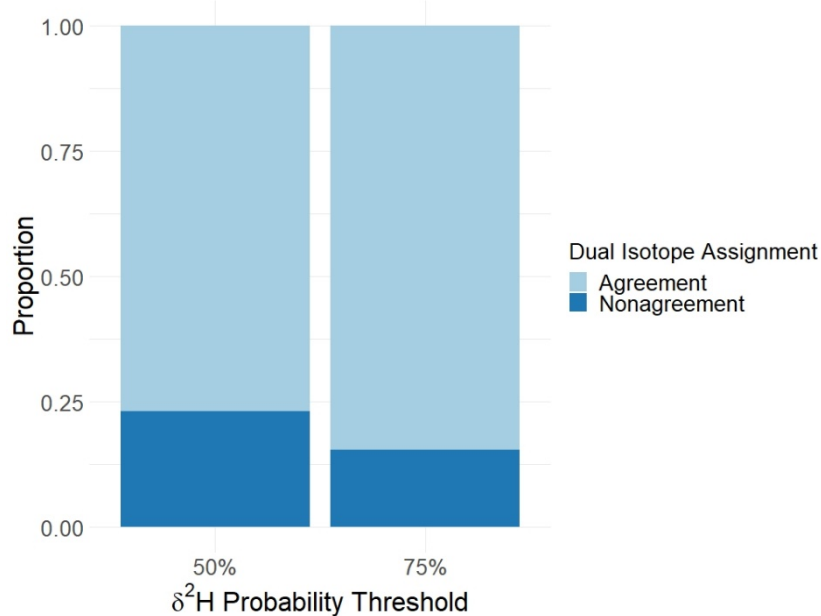
Figure 3.8. *Proportion of unknown origin individuals with definitive $^{87}Sr/^{86}Sr$ regional assignments (i.e., migratory or non-migratory; n = 13) that showed agreement and nonagreement with δ^2H summer residency predictions. The proportions of agreement between $^{87}Sr/^{86}Sr$ and δ^2H summer residency predictions are as follows: 0.77 (50% probability threshold) and 0.85 (75% probability threshold).*

Based on the combination of summer residency predictions using $^{87}Sr/^{86}Sr$ and the 50 % probability threshold for δ^2H, 10 % ($n = 2$), 55 % ($n = 11$), and 35 % ($n = 7$) of individuals were classified as non-migratory, migratory, and indeterminate, respectively (Table 3.2). Similarly, the combination of predictions made using $^{87}Sr/^{86}Sr$ and the 75 % probability threshold for δ^2H classified 10 % ($n = 2$), 60 % ($n = 12$), and 30 % ($n = 6$) of individuals as non-migratory, migratory, and indeterminate, respectively. Excluding individual 67 (which was the single discrepancy between classifications made using the 50 % and 75 % probability thresholds), ~36 % ($n = 4$) of migratory movements occurred within the region of mortality (including movements within Labrador), ~27 % ($n = 3$) of movements occurred between neighboring regions, and ~36 % ($n = 4$) occurred across the island (Table 3.2; Figure 3.7; Appendices VIII & IX, pg. 225 – 230). Three individuals saw agreement between summer residency predictions of fur sampled from the dorsal surface of the individual but were classified as indeterminate based on the large difference between dorsal and ventral $^{87}Sr/^{86}Sr$ values (Table 3.2; Figure 3.7; Appendices VIII and IX, pg. 225 – 230). Two individuals were classified as indeterminate due to disagreement between the predicted location of summer residency of δ^2H and $^{87}Sr/^{86}Sr$ (3.2; Figure 3.7; Appendices VIII & IX, pg. 225 – 230).

VI.   DISCUSSION

Using δ^2H, $\delta^{34}S$, and $^{87}Sr/^{86}Sr$ to investigate the migratory movements of *M. lucifugus* in Newfoundland, Canada, we highlighted the challenges of combining lesser-used isotopic systems to study the movements of a cryptic migratory species. The δ^2H_p isoscape was the only continuous model which reliably predicted geospatial isotopic

variation in bat fur for our study area. However, by quantifying variation in the $^{87}Sr/^{86}Sr_F$

values of geologically distinct regions on the island, we developed a categorical model

which was then used in combination with the δ^2H_p isoscape to improve precision and

accuracy of summer residency predictions for *M. lucifugus* on the island. The high

variation in $^{87}Sr/^{86}Sr$ values observed across the body of a single individual necessitates

further investigation into the molting timeline of *M. lucifugus* in Newfoundland.

A. Relating $\delta^{34}S_{iso}$ with $\delta^{34}S_{fur}$

The weak relationship observed in this study between $\delta^{34}S_{iso}$ and $\delta^{34}S_{fur}$ likely

results from characteristics of the calibration dataset used to build the random forest

regression. The data collected by Wadleigh and Blake (1999) targeted industrial areas

throughout the island, as their study aimed to understand major sources of atmospheric S

in Newfoundland. In doing so, the $\delta^{34}S$ data published in this study was inherently biased

towards active industrial areas from over 20 years ago, and likewise excluded more recent

industrial developments. Three industrial areas used in our distance-to-pollutants raster

file are no longer operational. Buchan's Mine closed in the 1980s (Thurlow, 2010); the

Grand Falls-Windsor Pulp and Paper Mill stopped production in 2009 (CBC News,

2009); the Come by Chance refinery, which stopped operations in 2020 and was sold in

2021, is in the process of being converted to a renewable fuel facility (now known as

Braya Renewable Fuels; CBC News, 2020; CBC News, 2021). Today, the primary

sources of atmospheric S pollution on the island are likely concentrated in the urban

centers of Newfoundland (i.e., the cities of St. John's and Corner Brook) and include the

Corner Brook Pulp and Paper Mill and Holyrood Thermal Generating Station.

Additionally, a recent increase in the number and severity of wildfires in Newfoundland

could introduce additional sources of atmospheric S pollution (CBC News, 2023).

However, it should be noted that the majority of SO_2 present in the atmosphere of

Newfoundland may be primarily sourced from urban areas outside of the province via

prevailing westerly winds (Wadleigh & Blake, 1999; ECCC, 2023).

Additionally, $\delta^{34}S$ values of epiphytic lichen tissues may not be strong predictors

of the $\delta^{34}S$ incorporated into the tissues of *M. lucifugus*. Most lichens source $\delta^{34}S$ from

atmospheric S and $\delta^{34}S$ values of lichen are known to reflect $\delta^{34}S$ values in atmospheric

SO_2 (Krouse, 1977). Thus, the $\delta^{34}S$ values in epiphytic lichen may be a good predictor of

$\delta^{34}S$ incorporated into lichenivorous insects and their predators, as fractionation of $\delta^{34}S$

between diet and animal tissues is typically low (Richards et al., 2003; Pinzone et al.,

2017; Webb et al., 2017; but see McCutchan et al., 2003). However, $\delta^{34}S$ deposited into

the fur of *M. lucifugus* may be sourced through the diet and drinking water of this species,

and *M. lucifugus* is known to consume many insect orders, foraging in both aquatic and

terrestrial environments (Broders et al., 2014; Clare et al., 2014). Thus, atmospheric

pollution will only be an important predictor of $\delta^{34}S$ values in the fur of *M. lucifugus* if it

influences the $\delta^{34}S$ values of the dietary sources for this species. Developing a $\delta^{34}S$

isoscape that reliably predicts the $\delta^{34}S_{fur}$ values of *M. lucifugus* requires the incorporation

of a diversity of insects; in lieu of these data, $\delta^{34}S$ values of plants taken from a diversity

of ecosystems – both terrestrial and aquatic – may provide a better baseline for those $\delta^{34}S$

values incorporated into the tissues of *M. lucifugus*.

B. Comparison of dorsal and ventral $^{87}Sr/^{86}Sr$ fur values

The difference in $^{87}Sr/^{86}Sr_F$ values recorded across the body of a single individual

raises intriguing questions related to the presumed molting timeline of *M. lucifugus* in

Newfoundland, particularly in the context of the results from the previous chapter. With the recent introduction of WNS to Newfoundland, and with our study area situated in boreal Canada, the energetic demands of survival after an individual becomes infected with WNS in this region are likely high. There is evidence that fur replacement is costly and can be delayed when energetic requirements are high (Fraser et al., 2013). Thus, the large difference in ^{87}Sr/^{86}Sr$_F$ values sampled from the dorsal and ventral surfaces of a single individual may provide evidence for *M. lucifugus* undergoing large movements (i.e., fall migration) during the process of new fur growth. Alternatively, and perhaps equally as likely, individuals could be undergoing small movements (i.e., between summer roosting sites) to nearby geologically distinct pockets during the summer residency period, resulting in a similar integration of multiple ^{87}Sr/^{86}Sr$_F$ values across the body of a single individual. This is not unexpected; researchers have reported *M. lucifugus* at northern latitudes undergoing frequent movements between maternity roosts (Norquay et al., 2013; Slough & Jung, 2020). Finally, juvenile *Perimyotis subflavus* have been shown to delay molting at northern latitudes, resulting in yearlings retaining their juvenile pelage and likely molting their coat during a different time period than adults (Davis, 1963, as cited in Fraser et al., 2013). For the purposes of this study, we had no way of distinguishing yearlings from adults, which could have resulted in a mismatch between the location of fur growth and the ^{87}Sr/^{86}Sr$_F$ value associated with these individuals.

No matter the cause, these results emphasize the importance of sampling fur from a single surface (we recommend the dorsal surface as it is likely grown first; Fraser et al., 2013). Still, sampling a single surface depends on the conditions of the carcasses

available, as we recommend using $10 - 12$ mg of fur per sample in Sr analysis. If the carcasses available are particularly deteriorated, it may be best to consider using an isotopic system that requires a smaller amount of keratinous tissue for analysis. Finally, these results highlight the increasing need for further investigation into the molting timeline of hibernating bats at northern latitudes and with the physiological effects of WNS in mind.

C. Correlating $^{87}Sr/^{86}Sr_{iso}$ with $^{87}Sr/^{86}Sr_F$

The weak relationship between predicted $^{87}Sr/^{86}Sr_{iso}$ values and observed $^{87}Sr/^{86}Sr_F$ values detected in this study has several possible explanations. One explanation relates to the isoscapes themselves; similar to $\delta^{34}S$, there may be a discrepancy between the calibration dataset and the observed $^{87}Sr/^{86}Sr_F$ values. A known limitation of this study is the lack of baseline bioavailable (i.e., $^{87}Sr/^{86}Sr$ values of plants and local animals) $^{87}Sr/^{86}Sr$ values; currently, limited data are available that quantify the $^{87}Sr^{86}Sr$ values of biological organisms (e.g., plants, animals) in Newfoundland and Labrador. The global and regional isoscapes were calibrated with data primarily from outside the province and therefore rely heavily on the covariates used in the model (i.e., geological variables, soil properties, climate, etc.) to predict $^{87}Sr/^{86}Sr$ values throughout Newfoundland and Labrador. Further, many authors caution against using a random forest regression modeling approach in data-poor regions (i.e., regions without a good record and distribution of bioavailable $^{87}Sr/^{86}Sr$ values); it is important to remember that the model is only as good as the data used to calibrate it (Hoogewerff et al., 2019; Bataille et al., 2020; Holt et al., 2021).

Additionally, as *M. lucifugus* is known to consume emergent aquatic insects, the $^{87}Sr/^{86}Sr$ values of surface waters may be an important predictor for $^{87}Sr/^{86}Sr$ values incorporated into the tissues of this study species. The $^{87}Sr/^{86}Sr$ values of surface waters are reflective of the surrounding geological formations that are exposed to weathering (Bataille et al., 2021), but differ substantially from those formations due to the combined contributions of multiple sources of Sr, and the differential weathering rates of rock (Blum et al., 1993). Thus, $^{87}Sr/^{86}Sr$ values sourced from surface waters would not be reflective of the $^{87}Sr/^{86}Sr$ values of the underlying geology and could contribute to a weak relationship between predicted $^{87}Sr/^{86}Sr_{iso}$ values and observed $^{87}Sr/^{86}Sr_{F}$ values. A better understanding of bioavailable Sr values throughout the province, including those values in surface waters, would improve future investigations which rely on $^{87}Sr/^{86}Sr$ values to predict the movements of organisms in Atlantic Canada.

A second explanation pertains to the large difference in $^{87}Sr/^{86}Sr$ values recorded across the body of a single individual. These results imply that the $^{87}Sr/^{86}Sr_{F}$ value associated with each individual whose dorsal and ventral fur was analyzed together may realistically represent an integrated signal of multiple values and their respective locations. Thus, the $^{87}Sr/^{86}Sr$ value associated with each known origin individual used to develop the transfer function may not accurately indicate the mortality location. These results are further complicated by the inherent nature of the low Sr concentration in keratinous tissues, which requires a large amount of sample (~12 mg of fur) compared to the stable isotopes of elements like H and S (which require 0.34 and 1 mg, respectively). Thus, it is not always possible to analyze fur sampled across the body of a single individual in separate batches for $^{87}Sr/^{86}Sr$. However, the results of this study highlight

the importance of collecting and analyzing fur samples collected from a standardized and constrained location on all bats' bodies.

D. The dual isotope approach

Despite the limitations of the regional $^{87}Sr/^{86}Sr$ estimates, we saw similar results between origin assignments using δ^2H and $^{87}Sr/^{86}Sr$. Thirteen individuals had definitive predictions of summer residency region using $^{87}Sr/^{86}Sr$, and there was high congruence between these assignments and those based on δ^2H_{fur} values (Figure 3.8). The two individuals' predictions that showed considerable incongruence between δ^2H and $^{87}Sr/^{86}Sr$ assignments were likely a result of the presence of geological pockets within the Western region of Newfoundland that have $^{87}Sr/^{86}Sr$ values which predominantly occur in the Central region. These results are not unexpected; as mentioned in the previous chapter, our estimates of $^{87}Sr/^{86}Sr$ baseline values for each region assume that Sr isotopes are homogenous when they are known to be heterogeneous (Faure & Powell, 1972; Bentley, 2006; Bataille et al., 2020). However, the high rate of agreement between summer residency predictions using δ^2H and $^{87}Sr/^{86}Sr$ suggests that using $^{87}Sr/^{86}Sr$ estimates of geologically distinct regions for origin assignments may be appropriate in cases where bioavailable Sr isoscapes underperform.

Nevertheless, the importance of using both isotope systems becomes clear when considering the migratory classifications made using $^{87}Sr/^{86}Sr$. By corroborating predictions with both isotopes, indeterminate assignments made using $^{87}Sr/^{86}Sr$ results have an alternative prediction using δ^2H results. Likewise, in the case of δ^2H, corroborating summer residency predictions from both isotope systems shows promise for improving accuracy (i.e., increasingly the likelihood that the true location of origin falls

within the probabilistic origin surface) and precision (i.e., decreasing the total geographic area of probable origin). When making predictions using continuous probability surfaces, there is always a trade-off between accuracy and precision (Campbell et al., 2020). As demonstrated in Figure 3.3, by increasing the accuracy of δ^2H predictions from 50 % to 75 %, a greater area of potential summer residency is generated (thus decreasing precision). However, by combining summer residency predictions of both isotopes, we can use a higher threshold (75 %) while maintaining precision of assignments by inferring migratory status from the overlap between summer residency predictions. Likewise, predictions made using a lower threshold (50 %) combined with $^{87}Sr/^{86}Sr$ were more precise than either prediction alone without implicating migratory status determinations, as the migratory status inferred from both probability thresholds was identical when combined with $^{87}Sr/^{86}Sr$.

E. Identifying seasonal movements of *Myotis lucifugus*

Results of the dual isotope approach using δ^2H and $^{87}Sr/^{86}Sr$ support a highly mobile population of *M. lucifugus* in Newfoundland. Similar proportions of migratory movements occurred within regions, between regions, and across the island. While there is not a clear pattern in date of mortality or sex that could explain decision-making for these movements, it is evident that *M. lucifugus* in Newfoundland and Labrador undergo regular migratory movements between distinct regions (i.e., Western, Eastern) and seemingly distinct populations (i.e., Labrador and insular Newfoundland). These results have implications for the spread of WNS to presently unaffected populations in Newfoundland. As WNS has been detected solely in the Western region of insular Newfoundland, these results suggest that a subset of the population could be spreading *P.*

destructans across the island. Thus, the dual isotope approach using δ^2H and ^{87}Sr/^{86}Sr could inform monitoring efforts in Newfoundland, especially in white nose absent regions that are in close proximity to areas where *P. destructans* has recently been detected.

The implications of these findings are also meaningful for future uses of intrinsic markers to study the migratory movements of terrestrial organisms with high accuracy and precision. Many organisms (i) are negatively affected by the attachment of extrinsic markers, (ii) are small in size, making attachment of markers difficult, or (iii) have low recapture rates, making inferences about population-level movement patterns difficult (Taylor et al., 2017; Hobson et al., 2019). The use of δ^2H and ^{87}Sr/^{86}Sr isotopes to infer migratory movements provides an alternative method for studying the movements of those organisms. In particular, this study shows promise for regions of the world with minimal knowledge of baseline ^{87}Sr/^{86}Sr values across the landscape, as we observed agreement between the majority of summer residency predictions using ^{87}Sr/^{86}Sr regional estimates and δ^2H probabilistic assignments.

VII. CONCLUSION

The overarching objective of this study was to use δ^2H, ^{87}Sr/^{86}Sr, and δ^{34}S to infer the movements of *M. lucifugus* in Newfoundland and Labrador, Canada. In doing so, we aimed to (i) contribute to a theoretical understanding of an emerging technique for the study of modern migratory movements, and (ii) infer the migratory movements and regional connectivity of *M. lucifugus* populations in Newfoundland and Labrador. To satisfy these objectives, we analyzed the fur of 43 *M. lucifugus* individuals collected throughout the province for δ^2H and ^{87}Sr/^{86}Sr, and 36 individuals for δ^{34}S. We used

previously published $^{87}Sr/^{86}Sr$ isoscapes, and developed our own $\delta^{34}S$ and δ^2H isoscapes, to evaluate the distribution of all three isotopes across the province. While the δ^2H_p isoscape exclusively explained variation in bat fur, we used previously developed regional $^{87}Sr/^{86}Sr$ estimates to infer summer residency region for all individuals of unknown origin. The combination of probabilistic summer origin predictions using δ^2H and regional predictions using $^{87}Sr/^{86}Sr$ proved promising for areas with minimal bioavailable $^{87}Sr/^{86}Sr$ data; we observed agreement between summer residency predictions using both isotopes for all but two unknown origin individuals. The combination of δ^2H and $^{87}Sr/^{86}Sr$ improved predictions of summer residency by corroborating migratory classifications and provided the opportunity to use a higher probability threshold for origin assignments without compromising the precision of migratory predictions. However, it should be noted that we observed high variation in $^{87}Sr/^{86}Sr_F$ values across the body of individuals for which we analyzed dorsal and ventral fur separately. Thus, future research can investigate both the molting timeline of *M. lucifugus* at northern latitudes and with the energetic demands of WNS in mind, as well as the discrimination of $^{87}Sr/^{86}Sr$ isotopes between diet and fur keratin. Additionally, investigations seeking to use probabilistic origin assignments of $^{87}Sr/^{86}Sr$ and $\delta^{34}S$ should consider developing models specific to the diet and behavior of the species of interest. Finally, the results of this study show promise for future investigations using intrinsic markers to infer the migratory movements of species. We acknowledge the current cost of Sr analysis is high, and large quantities of fur samples are required for this analysis. However, as technology continues to advance, there is great potential for these techniques

to illuminate many unanswered questions related to migratory theory and the protection of imperiled species.

VIII. REFERENCES

Bataille, C. P., von Holstein, I. C. C., Laffoon, J. E., Willmes, M., Liu, X.-M., Davies, G. R. (2018). A bioavailable strontium isoscape for Western Europe: A machine learning approach. *PLoS One, 13*(5), Article e0197386. https://doi.org/10.1371/journal.pone.0197386.

Bataille, C. P., Crowley, B. E., Wooller, M. J., & Bowen, G. J. (2020). Advances in global bioavailable strontium isoscapes. *Palaeogeography, Palaeoclimatology, Palaeoecology, 55*, Article 109849. https://doi.org/10.1016/j.palaeo.2020.109849.

Bataille, C. P., Jaouen, K., Milano, S., Trost, M., Steinbrenner, S., Crubézy, É., & Colleter, R. (2021). Triple sulfur-oxygen-strontium isotopes probabilistic geographic assignment of archaeological remains using a novel sulfur isoscape of western Europe. *PLoS One, 16*(5), Article e0250383. https://doi.org/10.1371/journal.pone.0250383.

Bentley, R. A. (2006). Strontium isotopes from the earth to the archaeological skeleton: A review. *Journal of Arcaheological Method and Theory, 13*(3), 135-187. https://doi.org/10.1007/s10816-006-9009-x.

Blum, J. D., Erel, Y., & Brown, K. (1993). $^{87}Sr/^{86}Sr$ ratios of Sierra Nevada stream waters: Implications for relative mineral weathering rates. *Geochimica et Cosmochimica Acta, 58*(21-22), 5019-5025. https://doi-org.qe2a-proxy.mun.ca/10.1016/S0016-7037(05)80014-6.

Blum, J. D., Taliaferro, E. H., & Holmes, R. T. (2001). Determining the sources of calcium for migratory songbirds using stable strontium isotopes. *Oecologia, 126*, 569-574. https://doi.org/10.1007/s004420000550.

Bowen, G. J., Liu, Z., Vander Zanden, H. B., Zhao, L., & Takahashi, G. (2014).

    Geographic assignment with stable isotopes in IsoMAP. *Methods in Ecology and*

    Evolution, 5(3), 201-206. https://doi.org/10.1111/2041-210X.12147.

Bowen, G. J., & West, J. B. (2019). Isoscapes for terrestrial migration research. In K. A.

    Hobson & L. I. Wassenaar (Eds.), *Tracking animal migration with stable isotopes*

    (pp. 53-84). Academic Press. https://doi.org/10.1016/B978-0-12-814723-8.00003-

    9.

Broders, H. G., Farrow, L. J., Hearn, R. N., Lawrence, L. M., & Forbes, G. J. (2014).

    Stable isotopes reveal that little brown bats have a broader dietary niche than

    northern long-eared bats. *Acta Chiropterologica, 16*(2), 315-325.

    https://doi.org/10.3161/150811014X687279.

Campbell, C. J., Fitzpatrick, M. C., Vander Zanden, H. B., & Nelson, D. M. (2020).

    Advancing interpretation of stable isotope assignment maps: Comparing and

    summarizing origins of known-provenance migratory bats. *Animal Migration,*

    7(1), 27-41. https://doi.org/10.1515/ami-2020-0004.

CBC News (2009, February 12). *AbitibiBowater production ends in Grand Falls-*

    Windsor. CBC. https://www.cbc.ca/news/canada/newfoundland-

    labrador/abitibibowater-production-ends-in-grand-falls-windsor-1.786086.

CBC News (2018, May 11). *Deadly white-nose syndrome confirmed in Newfoundland*

    bats. CBC. https://www.cbc.ca/news/canada/newfoundland-labrador/deadly-

    white-nose-syndrome-bats-1.4658578.

CBC News (2020, March 30). *Come By Chance refinery stopping production due to*

COVID-19, economic concerns. CBC.

https://www.cbc.ca/news/canada/newfoundland-labrador/come-by-chance-

refinery-shutting-down-1.5514499.

CBC News (2021, November 30). *Come By Chance refinery sold, will become biofuel*

operation by mid-2022. CBC. https://www.cbc.ca/news/canada/newfoundland-

labrador/nl-north-atlantic-refinery-1.6267625.

CBC News (2023, May 19). *It's a wild year for wildfires already in parts of*

Newfoundland. CBC. https://www.cbc.ca/news/canada/newfoundland-

labrador/wildfires-nl-1.6846769.

Chamberlain, C. P., Blum, J. D., Holmes, R. T., Feng, X., Sherry, T. W., & Graves, G. R.

(1997). The use of isotope tracers for identifying populations of migratory birds.

Oecologia, 109, 132-141. https://doi.org/10.1007/s004420050067.

Cheng, T. L., Reichard, J. D., Coleman, J. T. H., Weller, T. J., Thogmartin, W. E.,

Reichard, B. E., Bennett, A. B., Broders, H. G., Campbell, J., Etchison, K., Feller,

D. J., Geboy, R., Hemberger, T., Herzog, C., Hicks, A. C., Houghton, S., Humber,

J., Kath, J. A., King, R. A.,… Frick, W. F. (2021). The scope and severity of

white-nose syndrome on hibernating bats in North America. *Conservation*

Biology, 35(5), 1586-1597. https://doi.org/10.1111/cobi.13739.

Clare, E. L., Symondson, W. O. C., Broders, H., Fabianek, F., Fraser, E. E., MacKenzie,

A., Boughen, A., Hamilton, R., Willis, C. K. R., Martinez-Nuñez, F., Menzies, A.

K., Norquay, K. J. O., Brigham, M., Poissant, J., Rintoul, J., Barclay, R. M. R., &

Reimer, J. P. (2014). The diet of *Myotis lucifugus* across Canada: Assessing

foraging quality and diet variability. *Molecular Ecology,* 23(15), 3618-3632.

https://doi.org/10.1111/mec.12542.

Colman-Sadd, S. P., Hayes, J. P., & Knight, I. (2000). *Geology of the island of Newfoundland.* Newfoundland Department of Mines and Energy, Geological Survey, Map 2000-30, scale 1:1,000,000.

Crowley, B. E., Bataille, C. P., Haak, B. A., & Sommer, K. M. (2021). Identifying nesting grounds for juvenile migratory birds with dual isotope: An initial test using North American raptors. *Ecosphere, 12*(10), Article e03765. https://doi.org/10.1002/ecs2.3765.

Cryan, P. M., Bogan, M. A., Rye, R. O., Landis, G. P., & Kester, C. L. (2004). Stable hydrogen isotope analysis of bat hair as evidence for seasonal molt and long-distance migration. *Journal of Mammalogy, 85*(5), 995-1001. https://doi.org/10.1644/BRG-202.

Cryan, P. M., Meteyer, C. U., Boyles, J. G., & Blehert, D. S. (2010). Wing pathology of white-nose syndrome in bat suggests life-threatening disruption of physiology. *BMC Biology, 8*, Article 135. https://doi.org/10.1186/1741-7007-8-135.

Davis, W. H. (1963). Aging bats in winter. *Transactions of the Kentucky Academy of Science, 24*, 28-30.

Department of Environment and Climate Change Canada (ECCC). (2023). *2020-2022 Air Zone Management Report.* https://www.gov.nl.ca/ecc/files/2020-2022-Air-Zone-Management-Report.pdf.

Evans, J., & Bullman, R. (2009). ^{87}Sr/^{86}Sr isotope fingerprinting of Scottish and Icelandic

migratory shorebirds. *Applied Geochemistry, 24*(10), 1927-1933. https://doi.org/10.1016/j.apgeochem.2009.07.006.

Farmer, A., Abril, M., Fernández, M., Torres, J., Kester, C., & Bern, C. (2004). Using stable isotopes to associate migratory shorebirds with their wintering locations in Argentina. *Ornitologia Neotropical, 15*, 377-384.

Faure, G., & Powell, J. L. (1972). *Strontium Isotope Geology* (W. von Engelhardt, T. Hahn, R. Roy, & P. J. Wyllie, Eds.). Springer.

Fenton, M. B. (1969). Summer activity of *Myotis lucifugus* (Chiroptera:Vespertilionidae) at hibernacula in Ontario and Quebec. *Canadian Journal of Zoology, 47*(4), 597-602. https://doi.org/10.1139/z69-103.

Flockhart, D. T. T., Kyser, T. K., Chipley, D., Miller, N. G., & Norris, D. R. (2015). Experimental evidence shows no fractionation of strontium isotopes ($^{87}Sr/^{86}Sr$) among soil, plants, and herbivores: Implications for tracking wildlife and forensic science. *Isotopes in Environmental and Health Studies, 51*(3), 372-381. https://doi.org/10.1080/10256016.2015.1021345.

Font, L., van der Peijl, G., van Wetten, I., Vroon, P., van der Wagt, B., & Davies, G. (2012). Strontium and lead isotope ratios in human hair: Investigating a potential tool for determining recent human geographical movements. *Journal of Analytical Atomic Spectrometry, 27*(5), 719-732. https://doi.org/10.1039/c2ja10361c.

Fox, A. D., Hobson, K. A., De Jong, A., Kardynal, K. J., Koehler, G., & Heinicke, T. (2016). Flyway population delineation in Taiga Bean Geese *Anser fabalis fabalis* revealed by multi-element feather stable isotope analysis. *International Journal of Avian Science, 159*(1), 66-75. https://doi.org/10.1111/ibi.12417.

Fraser, E. E., Longstaffe, F. J., & Fenton, M. B. (2013). Moulting matters: The

importance of understanding moulting cycles in bats when using fur for

endogenous marker analysis. *Canadian Journal of Zology, 91*(8), 533-544.

https://doi.org/10.1139/cjz-2013-0072.

Fraser, E. E., Brooks, D., & Longstaffe, F. J. (2017). Stable isotope investigation of the

migratory behavior of silver-haired bats (*Lasionycteris noctivagans*) in eastern

North America. *Journal of Mammalogy, 98*(5), 1225-1235.

https://doi.org/10.1093/jmammal/gyx085.

Genuer, R., Poggi, J.-M., & Tuleau-Malot, C. (2019). *VSURF: Variable Selection Using

Random Forests*. R package version 1.1.0. https://CRAN.R-

project.org/package=VSURF.

Hijmans, R. J. (2022). *raster: Geographic Data Analysis and Modeling*. R package

version 3.5-29. https://CRAN.R-project.org/package=raster.

Hobson, K. A., & Wassenaar, L. (1996). Linking breeding and wintering grounds of

neotropical migrant songbirds using stable hydrogen isotopic analysis of feathers.

Oecologia, 109, 142-148. https://doi.org/10.1007/s004420050068.

Hobson, K. A. (1999). Tracing origins and migration of wildlife using stable isotopes: A

review. *Oecologia, 120*(3), 314-326.

Hobson, K. A. (2005). Stable isotopes and the determination of avian migratory

connectivity and seasonal interactions. *The Auk, 122*(4), 1037-1048.

https://doi.org/10.1093/auk/122.4.1037.

Hobson, K. A. (2019). Application of isotopic methods to tracking animal movements. In

K. A. Hobson & L. I. Wassenaar (Eds.), *Tracking animal migration with stable isotopes* (pp. 85-115). Academic Press. https://doi.org/10.1016/B978-0-12-814723-8.00004-0.

Hobson, K. A., Norris, D. R., Kardynal, K. J., & Yohannes, E. (2019). Animal migration: A context for using new techniques and approaches. In K. A. Hobson & L. I. Wassenaar (Eds.), *Tracking animal migration with stable isotopes* (pp. 1-23). Academic Press. https://doi.org/1016/B978-0-12-814723-8.00001-5.

Hobson, K. A., Kusack, J. W., Gootgarts, J., Longstaffe, F. J., & McNeil, J. N. (2022). Using stable isotopes (δ^2H, δ^{13}C) to identify natal origins and larval host plant use by western bean cutworm, *Striacosta albicosta* (Lepidoptera: Noctuidae) captured in southern Ontario. *Ecological Entomology, 47*(3), 347-356. https://doi.org/10.1111/een.13120.

Holt, E., Evans, J. A., & Madgwick, R. (2021). Strontium (^{87}Sr/^{86}Sr) mapping: A critical review of methods and approaches. *Earth-Science Reviews, 216*, Article 103593. https://doi.org/10.1016/j.earscirev.2021.103593.

Hoogewerff, J. A., Reimann, C., Ueckermann, H., Frei, R., Frei, K. M., van Aswegen, T., Stirling, C., Reid, M., Clayton, A., Ladenberger, A., & The GEMAS Project Team (2019). Bioavailable ^{87}Sr/^{86}Sr in European soils: A baseline for provenancing studies. *Science of the Total Environment, 672*, 1033-1044. https://doi.org/10.1016/j.scitotenv.2019.03.387.

Horacek, M. (2011). Backtracking the movements of a migratory bird: A case study of a white-fronted goose (*Anser albifrons*). *Rapid Communications in Mass Spectrometry, 25*(20), 3146-3150. https://doi.org/10.1002/rcm.5209.

Kabalika, Z., Morrison, T. A., McGill, R. A. R., Munishi, L. K., Ekwem, D., Mahene, W.
L., Lobora, A. L., Newton, J., Morales, J. M., Haydon, D. T., & Hopcraft, G. G. J.
C. (2020). Tracking animal movements using biomarkers in tail hairs: A novel
approach for animal geolocating from sulfur isoscapes. *Movement Ecology, 8*, 37.
https://doi.org/10.1186/s40462-020-00222-w.

Krouse, H. R. (1977). Sulphur isotope abundance elucidates uptake of atmospheric
sulphur emissions by vegetation. *Nature, 265*, 45-46.
https://doi.org/10.1038/265045a0.

Kruszynski, C., Bailey, L. D., Courtiol, A., Bach, L., Bach, P., Göttsche, Ma., Göttsche,
Mi., Hill, R., Lindecke, O., Matthes, H., Pommeranz, H., Popa-Lisseanu, A. G.,
Seebens-Hoyer, A., Tichomirowa, M., & Voigt, C. C. (2020). Identifying
migratory pathways of Nathusius' pipistrelles (*Pipistrellus nathusii*) using stable
hydrogen and strontium isotopes. *Rapid Communications in Mass Spectrometry,
35*(6). https://doi.org/10.1002/rcm.9031.

Kurta, A., & Smith, S. M. (2020). Changes in population size and clustering behavior of
hibernating bats in the Upper Peninsula of Michigan after arrival of white-nose
syndrome. *Northeastern Naturalist, 27*(4), 763-772.
https://doi.org/10.1656/045.027.0415.

Le Corre, M. (2023). [Manuscript in preparation]. Department of Archaeology,
University of Aberdeen.

Liaw, A., & Wiener, M. (2002). Classification and Regression by randomForest. *R News,
2*(3), 18-22.

Linglin, M., Amiot, R., Richardin, P., Porcier, S., Antheaume, I., Berthet, D., Grossi, V.,

Fourel, F., Flandrois, J.-P., Louchart, A., Martin, J. E., & Lécuyer, C. (2020). Isotopic systematics point to wild origin of mummified birds in Ancient Egypt. *Scientific Reports, 10*, Article 15463. https://doi.org/10.1038/s41598-020-72326-7.

Lott, C. A., Meehan, T. D., & Heath, J. A. (2003). Estimating the latitudinal origins of migratory birds using hydrogen and sulfur stable isotopes in feathers: Influence of marine prey base. *Oecologia, 134*, 505-510. https://doi.org/10.1007/s00442-002-1153-8.

Ma, C., Vander Zanden, H. B., Wunder, M. B., & Bowen, G. J. (2020). *assignR: An R package for isotope-based geographic assignment*. Methods in Ecology and Evolution. https://doi.org/10.1111/2041-210X.13426

Madgwick, R., Grimes, V., Lamb, A. L., Nederbrag, A. J., Evans, J. A., & McCormick, F. (2019). Feasting and mobility in Iron Age Ireland: Multi-isotope analysis reveals the vast catchment of Navan Fort, Ulster. *Scientific Reports, 9*, Article 19792. https://doi.org/10.1038/s41598-019-55671-0.

McArdle, B. H. (1988). The structural relationship: Regression in biology. *Canadian Journal of Zoology, 66*(11), 2329-2339. https://doi.org/10.1139/z88-348.

McCutchan, J. H., Lewis, W. M., Kendall, C., & McGrath, C. C. (2003). Variation in trophic shift for stable isotope ratios of carbon, nitrogen, and sulfur. *Oikos, 102*(2), 378-390. https://doi.org/10.1034/j.1600-0706.2003.12098.x.

Moran, P. A. P. (1948). The interpretation of statistical maps. *Journal of the Royal Static Society Series B, 10*(2), 243-251.

Nehlich, O. (2015). The application of sulphur isotope analyses in archaeological

research: A review. *Earth-Science Reviews, 142*, 1-17.

https://doi.org/10.1016/j.earscirev.2014.12.002.

Neuwirth, E. (2014). *RColorBrewer: ColorBrewer palettes*. R package version 1.1-2.

https://CRAN.R-project.org/package=RColorBrewer.

Norquay, K. J. O., Martinez-Nuñez, F., Dubois, J. E., Monson, K. M., & Willis, C. K. R.

(2013). Long-distance movements of little brown bats (*Myotis lucifugus*). *Journal

of Mammalogy, 94*(2), 506-515. https://doi.org/10.1644/12-MAMM-A-065.1.

Pinzone, M., Acquarone, M., Huyghebaert, L., Sturaro, N., Michel, L. N., Siebert, U., &

Das, K. (2017). Carbon, nitrogen and sulphur isotopic fractionation in captive

juvenile hooded seal (*Cystophora cristata*): Application for diet analysis. *Rapid

Communications in Mass Spectrometry, 31*(20), 1720-1728.

https://doi.org/10.1002/rcm.7955.

Popa-Lisseanu, A. G., Sörgel, K., Luckner, A., Wassenaar, L.I., Ibáñez, C., Kramer-

Schadt, S., Ciechanowski, M., Görföl, T., Niermann, I., Beuneux, G., Mysłajek, R.

W., Juste, J., Fonderflick, J., Kelm, D. H., & Voigt, C. C. (2012). A triple-isotope

approach to predict the breeding origins of European bats. *PLoS One, 7*(1),

e30388. https://doi.org/10.1371/journal.pone.0030388.

Pylant, C. L., Nelson, D. M., & Keller, S. R. (2014). Stable hydrogen isotopes record the

summering grounds of eastern red bats (*Lasiurus borealis*). *PeerJ*, Article e629.

https://doi.org/10.7717/peerj.629.

Pylant, C. L., Nelson, D. M., Fitzpatrick, M. C., Gates, J. E., & Keller, S. R. (2016).

Geographic origins and population genetics of bats killed at wind-energy facilities. *Ecological Applications, 26*(5), 1381-1395. https://doi.org/10.1890/15-0541.

R Core Team (2022). *R: A language and environment for statistical computing*. R Foundation for Statistical Computing, Vienna, Austria. https://www.R-project.org.

Rand, A. J., Matute, V., Grimes, V., Freiwald, C., Źrałka, J., & Koszkul, W. (2020). Prehispanic Maya diet and mobility at Nakum, Guatemala: A multi-isotopic approach. *Journal of Archaeological Science: Reports, 32*, Article 102374. https://doi.org/10.1016/j.jasrep.2020.102374.

Reeder, D. M., Frank, C. L., Turner, G. G., Meteyer, C. U., Kurta, A., Britzke, E. R., Vodzak, M. E., Darling, S. R., Stihler, C. W., Hicks, A. C., Jacob, R., Grieneisen, L. E., Brownlee, S. A., Muller, L. K., & Blehert, D. S. (2012). Frequent arousal from hibernation linked to severity of infection and mortality in bats with white-nose syndrome. *Public Library of Science One, 7*(6). https://doi.org/10.1371/journal.pone.0038920.

Reich, M. S., Flockhart, D. T. T., Norris, D. R., Hu, L., & Bataille, C. P. (2021). Continuous-surface geographic assignment of migratory animals using strontium isotopes: A case study with monarch butterflies. *Methods in Ecology and Evolution, 12*(12), 2445-2457. https://doi.org/10.1111/2041-210X.13707.

Richards, M. P., Fuller, B. T., Sponheimer, M., Robinson, T., & Ayliffe, L. (2003). Sulphur isotopes in palaeodietary studies: A review and results from a controlled feeding experiment. *International Journal of Osteoarchaeology, 13*(1-2), 37-45. https://doi.org/10.1002/oa.654.

Rubenstein, D. R., & Hobson, K. A. (2004). From birds to butterflies: Animal movement

    patterns and stable isotopes. *Trends in Ecology and Evolution, 19*(5), 256-263.

    https://doi.org/10.1016/j.tree.2004.03.017.

Sellick, M. J., Kyser, T. K., Wunder, M. B., Chipley, D., & Norris, D. R. (2009).

    Geographic variation of strontium and hydrogen isotopes in avian tissue:

    Implications for tracking migration and dispersal. *PLoS One, 4*(3), Article e4735.

    https://doi.org/10.1371/journal.pone.0004735.

Slough, B. G., & Jung, T. S. (2020). Little brown bats utilize multiple maternity roosts

    within foraging areas: Implications for identifying summer habitat. *Journal of*

    Fish and Wildlife Management, 11(1), 311-320. https://doi.org/10.3996/052019-

    JFWM-039.

Smith, W. H. F., & Wessel, P. (1990). Gridding with continuous curvature splines in

    tension. *Geophysics, 55*(3), 293-305. https://doi.org/10.1190/1.1442837.

Smith, R. J. (2009). Use and misuse of the reduced major axis for line-fitting. *American*

    Journal of Physical Anthropology, 140(3), 476-486.

    https://doi.org/10.1002/ajpa.21090.

Soto, D. X., Koehler, G., Wassenaar, L. I., & Hobson, K. A. (2017). Re-evaluating of the

    hydrogen stable isotopic composition of keratin calibration standards for wildlife

    and forensic science applications. *Rapid Communications in Mass Spectrometry,*

    31(14), 1193-1203. https://doi.org/10.1002/rcm.7893.

Sunga, J. S., Humber, J., Rodrigues, B., McGuire, L., & Broders, H. (2021). Long-

distance movement over a period of days by a female *Myotis lucifugus* in
Newfoundland, Canada. *Northeastern Naturalist, 28*(2), 24-26.
https://doi.org/10.1656/045.028.0214.

Taylor, P. D., Crewe, T. L., Mackenzie, S. A., Lepage, D., Aubry, Y., Crysler, Z., Finney,
G., Francis, C. M., Guglielmo, C. G., Hamilton, D. J., Holberton, R. L., Loring, P.
H., Mitchell, G. W., Norris, D. R., Paquet, J., Ronconi, R. A., Smetzer, J. R.,
Smith, P. A., Welch, L. J., & Woodworth, B. K. (2017). The motus wildlife
tracking system: A collaborative research network to enhance the understanding
of wildlife movement. *Avian Conservation & Ecology, 12*(1), Article 8.
https://doi.org/10.5751/ACE-00953-120108.

Thurlow, J. G. (2010). Great Mining Camps of Canada 3. The history and geology of the
Buchans Mine, Newfoundland and Labrador. *Geoscience Canada, 37*(4), 145-
173.

Vander Zanden, H. B., Soto, D. X., Bowen, G. J., & Hobson, K. A. (2016). Expanding the
isotopic toolbox: Applications of hydrogen and oxygen stable isotope ratios to
food web studies. *Frontiers in Ecology and Evolution, 4*, 20.
https://doi.org/10.3389/fevo.2016.00020.

Voigt, C. C., Lehmann, D., & Greif, S. (2015). Stable isotope ratios of hydrogen separate
mammals of aquatic and terrestrial food webs. *Methods in Ecology and Evolution,
6*(11), 1332-1340. https://doi.org/10.1111/2041-210X.12414.

Wadleigh, M. A., & Blake, D. M. (1999). Tracing sources of atmospheric sulphur using
epiphytic lichens. *Environmental Pollution, 106*(3), 265-271.
https://doi.org/10.1016/S0269-7491(99)00114-1.

Warton, D. I., Duursma, R. A., Falster, D. S., & Taskinen, S. (2012). smatr 3 - an R package for estimation and inference about allometric lines. *Methods in Ecology and Evolution*, *3*(2), 257-259. https://doi.org/10.1111/j.2041-210X.2011.00153.x.

Wassenaar, L., & Hobson, K. A. (2000). Stable-carbon and hydrogen isotope ratios reveal breeding origins of red-winged blackbirds. *Ecological Applications, 10*(3), 911-916. https://doi.org/10.1890/1051-0761(2000)010[0911:SCAHIR]2.0.CO;2.

Wassenaar, L. I., & Hobson, K. A. (2003). Comparative equilibration and online technique for determination of non-exchangeable hydrogen of keratins for use in animal migration studies. *Isotopes in Environmental and Health Studies, 39*(3), 211-217. https://doi.org/10.1080/1025601031000096781.

Webb, E. C., Newton, J., Lewis, J., Stewart, A., Miller, B., Tarlton, J. F., & Evershed, R. P. (2017). Sulphur-isotope compositions of pig tissues from a controlled feeding study. *Science and Technology of Archaeological Research, 3*(1), 71-79. https://doi.org/10.1080/20548923.2017.1368821.

Wickham, H. (2016). *ggplot2: Elegant graphics for data analysis*. Springer-Verlag New York. https://ggplot2.tidyverse.org.

Wickham, H., François, R., Henry, L., & Müller, K. (2022). *dplyr: A grammar of data manipulation*. R package version 1.0.8. https://CRAN.R-project.org/package=dplyr.

Wieringa, J. G., Nagel, J., Nelson, D. M., Carstens, B. C., & Gibbs, H. L. (2020). Using trace elements to identify the geographic origin of migratory bats. *PeerJ, 8,* Article e10082. https://doi.org/10.7717/peerj.10082.

Wilcox, A., & Willis, C., K. R. (2016). Energetic benefits of enhanced summer roosting

habitat for little brown bats (*Myotis lucifugus*) recovering from white-nose

syndrome. *Conservation Physiology, 4*(1).

https://doi.org/10.1093/conphys/cov070.

Wunder, M. B., & Norris, D. R. (2019). Design and analysis for isotope-based studies of

migratory animals. In K. A. Hobson & L. I. Wassenaar (Eds.), *Tracking animal

migration with stable isotopes* (pp. 191-206). Academic Press.

https://doi.org/10.1016/B978-0-12-814723-8.00008-8.

Zazzo, A., Monahan, F. J., Moloney, A. P., Green, S., & Schmidt, O. (2011). Sulphur

isotopes in animal hair track distance to sea. *Rapid Communications in Mass

Spectrometry, 25*(17), 2371-2378. https://doi.org/10.1002/rcm.5131.

CHAPTER IV. Summary and conclusions

I.   OVERALL SUMMARY

In an increasingly developed world, migratory species across taxa are facing a number of threats to their populations, translating to the adaptation of migration itself becoming increasingly at risk. In order to understand the evolutionary drivers of migration, and protect threatened and endangered migratory species, it is important to develop increasingly accurate and precise methods to study seasonal migration relative to birthplace. Here, we used multiple tissues and isotopic systems to understand how the combined use of δ^2H, $\delta^{34}S$, and $^{87}Sr/^{86}Sr$ can improve our understanding of relatively small landscape-level movements of species. Using the population of *Myotis lucifugus* in Newfoundland and Labrador as a case study, we approached this overall objective in two ways: by using $^{87}Sr/^{86}Sr$ analysis of multiple tissues to identify patterns in lifetime movements, and by using δ^2H, $\delta^{34}S$, and $^{87}Sr/^{86}Sr$ analysis of a single tissue to predict seasonal movements with improved accuracy and precision.

In the first data chapter, we sought to (i) determine whether bat fur retained high enough concentrations of strontium to allow for reliable $^{87}Sr/^{86}Sr$ values to be recorded, and further, to understand how the $^{87}Sr/^{86}Sr$ values of teeth, fur, and bone in juvenile bats differ. We then aimed to (ii) correlate the variation in $^{87}Sr/^{86}Sr$ values between geologically distinct regions in Newfoundland with the isotopic signatures in the fur of known origin individuals. Finally, we intended to (iii) identify lifetime movements for adult *M. lucifugus* individuals in insular Newfoundland. Despite the low concentration of strontium in fur tissue, we recorded consistent and reliable $^{87}Sr/^{86}Sr$ values for all 31 fur

samples analyzed. Additionally, none of these $^{87}Sr/^{86}Sr_F$ values exhibited evidence of exogenous strontium contamination. However, one of the three juvenile individual's $^{87}Sr/^{86}Sr_F$ value was distinct from its calciferous tissues and the $^{87}Sr/^{86}Sr$ baseline of its region of mortality – this was likely a result of the heterogenous nature of the distribution of $^{87}Sr/^{86}Sr$ across our landscape of interest, which could not be addressed by the methodology used in this chapter. Our comparison of the $^{87}Sr/^{86}Sr$ values of tissues sampled from adult *M. lucifugus* showed no evidence for sex-biased dispersal, and a high likelihood for both male and female individuals to return to their region of birth in late life. Intriguingly, our results demonstrated a bias of known origin individuals towards a philopatric classification whereby only unknown origin individuals were classified as dispersed. This pattern suggests the molt timeline of hibernating bats at northern latitudes may differ from previous assumptions.

In the second data chapter, our objectives were to (i) correlate the variation in environmental δ^2H, $\delta^{34}S$, and $^{87}Sr/^{86}Sr$ across Newfoundland and Labrador with the isotopic signatures in bat fur, and (ii) identify seasonal movements of *M. lucifugus* in the province using data from all three isotope systems. While our δ^2H_p isoscape reliably predicted geospatial isotopic variation in bat fur for our study area, the $^{87}Sr/^{86}Sr$ values predicted by both isoscapes showed weak, insignificant linear relationships with observed $^{87}Sr/^{86}Sr_F$ values, and the same was reflected in the $\delta^{34}S$ values predicted by our isoscape. However, using regional $^{87}Sr/^{86}Sr$ estimates, we predicted summer residency region for all individuals of unknown origin and combined these predictions with probabilistic origin assignments made using our δ^2H_p isoscape and transfer function. Our results showed increasing precise and accurate predictions of summer residency using both

160

isotopes as compared to either isotopic system alone. Using the combination of $^{87}Sr/^{86}Sr$ and δ^2H to predict seasonal migration of unknown origin individuals, we provide evidence for a highly mobile population of *M. lucifugus* in Newfoundland that undergoes regular movements between geologically distinct regions and seemingly distinct populations (i.e., Labrador and insular Newfoundland).

II.   DISCUSSION AND CONCLUSIONS

We demonstrate the utility of using a combination of tissue types and intrinsic marking techniques to offer meaningful inferences about species that regularly undergo regional migrations. In addition to our insights into the movements of *M. lucifugus* in Newfoundland as a case study, our findings offer implications for studies of migratory movements of organisms worldwide.

At the outset of this project, our primary objective was to determine if bat fur could be reliably analyzed for $^{87}Sr/^{86}Sr$. We were aware of several studies that successfully analyzed feathers and human hair for $^{87}Sr/^{86}Sr$ (e.g., Font et al., 2007; Font et al., 2012; Tipple et al., 2013; Shin et al., 2020), and several others which tracked movements using these techniques (e.g., Sellick et al., 2009; Kruszynski et al., 2020; Crowley et al., 2021). However, considering the small body size of insectivorous bats, we were initially curious about the applications of this technique in our specific study system. Considering the relatively low strontium concentration in keratin, our results are promising for future investigations seeking to use $^{87}Sr/^{86}Sr$ values of small mammal fur for tracking movements. It should be noted that the volume of fur used in this study (~12 mg) necessitated lethal and destructive sampling and, therefore, required predeceased

carcasses instead of sampling live individuals or museum specimens. However, Font et al. (2007) recorded similar ^{88}Sr intensity values to this study using $\sim 1 - 2$ mg of feather material and Thermal Ionization Mass Spectrometry (TIMS) for analysis as opposed to the MC-ICP-MS methodology of this study. Although TIMS is more time- and technique-intensive, it may be preferred by biologists who do not have access to pre-deceased carcasses and that, therefore, require non-lethal or non-destructive sampling.

In both chapters, we used ^{87}Sr/^{86}Sr values incorporated into the fur of known origin individuals to track movements of unknown origin individuals between geologically distinct regions in insular Newfoundland. This methodology was not without its limitations – it implied a homogenous distribution of ^{87}Sr/^{86}Sr values across the landscape and limited our ability to track movements of individuals whose fur, teeth, or bone value fell outside of a regional distribution of ^{87}Sr/^{86}Sr values. Despite these limitations, the regional ^{87}Sr/^{86}Sr predictions performed equally well compared to the probabilistic origin predictions using δ^2H. These results suggest that, in lieu of a reliable ^{87}Sr/^{86}Sr isoscape, a categorical ^{87}Sr/^{86}Sr model can be used in combination with a continuous δ^2H model, expanding the accessibility of this technique to regions without extensive sampling of bioavailable ^{87}Sr/^{86}Sr values across the landscape (e.g., Kruszynski et al. 2020).

Unfortunately, the isoscape we developed using δ^{34}S values of lichen sampled throughout the island did not perform well when compared to the δ^{34}S values of known origin bat fur. Further, we were unable to use δ^{34}S values incorporated into the fur of unknown origin individuals to differentiate location of origin relative to distance from the coast. However, this technique has been effective in other studies (e.g., Zazzo et al., 2011;

Crowley et al., 2021) and may be a viable alternative for areas that lack a reliable δ^{34}S isoscape but have a larger surface area to coastline ratio (i.e., inland areas with a single coastline) and predictable prevailing winds.

Despite the lack of reliable isoscapes for ^{87}Sr/^{86}Sr and δ^{34}S in this study, the combination of regional ^{87}Sr/^{86}Sr predictions and probabilistic δ^2H origin assignments improved the accuracy and precision of origin assignments when compared with predictions using either isotopic system alone. This is not a novel concept – it is common knowledge that using multiple isotopic systems to predict migratory origin improves the precision and accuracy of predictions (e.g., Horacek, 2011; Popa-Lisseanu et al., 2012; Bataille et al., 2021; Crowley et al., 2021; Hobson et al., 2022). However, this project used an alternative method to predict migratory origin in combination with probabilistic origin assignments – the results performed similarly in terms of accuracy and precision when compared with studies that overlaid multiple isoscapes to predict migratory origin. This has wide-reaching implications for studies of migration – here, we show that stable and radiogenic isotope systems can be used to predict migratory origin in areas of the world previously limited by the availability of reliable isoscapes.

Finally, this is the first study that we know of which used the combination of ^{87}Sr/^{86}Sr values of fur, bone, and teeth, and δ^2H values of fur, to predict seasonal migratory movements of modern vertebrates and relate those movements to birthplace. The results are inspiring for future investigations seeking to understand the behavior of migratory organisms, whether to protect those organisms in a changing climate, or to better understand the evolutionary drivers and decision-making of migratory organisms. For the *M. lucifugus* population in Newfoundland, our results offer two unique and

interesting glimpses into the movements of individuals throughout their life. Seasonally, we present evidence of a highly mobile population of *M. lucifugus* in Newfoundland that regularly undergoes movements between geologically distinct regions. When considering the region of birth, however, our results imply a high likelihood for both male and female *M. lucifugus* to return to their natal region. Together, these results imply that yearly movements of *M. lucifugus* in the province are widespread, but across their lifetime, individuals of this species will most likely return to their region of birth for the summer residency period. This highlights the importance of protecting areas with known maternity colonies and high-quality roosting habitat nearby, especially for species declining due to the effects of white-nose syndrome and an increasingly anthropomorphized world. Ultimately, this project demonstrates the profound ability of intrinsic marking techniques to illuminate questions of both a theoretical and applied nature.

III.   REFERENCES

Bataille, C. P., Jaouen, K., Milano, S., Trost, M., Steinbrenner, S., Crubézy, É., & Colleter, R. (2021). Triple sulfur-oxygen-strontium isotopes probabilistic geographic assignment of archaeological remains using a novel sulfur isoscape of western Europe. *PLoS One, 16*(5), Article e0250383. https://doi.org/10.1371/journal.pone.0250383.

Crowley, B. E., Bataille, C. P., Haak, B. A., & Sommer, K. M. (2021). Identifying nesting grounds for juvenile migratory birds with dual isotope: An initial test using North American raptors. *Ecosphere, 12*(10), Article e03765. https://doi.org/10.1002/ecs2.3765.

Font, L., Nowell, G. M., Pearson, D. G., Ottley, C. J., & Willis, S. G. (2007). Sr isotope analysis of bird feathers by TIMS: A tool to trace bird migration paths and breeding sites. *Journal of Analytical Atomic Spectrometry, 22*(5), 513-522. https://doi.org/10.1039/b616328a.

Font, L., van der Peijl, G., van Wetten, I., Vroon, P., van der Wagt, B., & Davies, G. (2012). Strontium and lead isotope ratios in human hair: Investigating a potential tool for determining recent human geographical movements. *Journal of Analytical Atomic Spectrometry, 27*(5), 719-732. https://doi.org/10.1039/c2ja10361c.

Hobson, K. A., Kusack, J. W., Gootgarts, J., Longstaffe, F. J., & McNeil, J. N. (2022). Using stable isotopes (δ^2H, δ^{13}C) to identify natal origins and larval host plant use by western bean cutworm, *Striacosta albicosta* (Lepidoptera: Noctuidae) captured in southern Ontario. *Ecological Entomology, 47*(3), 347-356. https://doi.org/10.1111/een.13120.

Horacek, M. (2011). Backtracking the movements of a migratory bird: A case study of a

white-fronted goose (*Anser albifrons*). *Rapid Communications in Mass

Spectrometry, 25*(20), 3146-3150. https://doi.org/10.1002/rcm.5209.

Kruszynski, C., Bailey, L. D., Courtiol, A., Bach, L., Bach, P., Göttsche, Ma., Göttsche,

Mi., Hill, R., Lindecke, O., Matthes, H., Pommeranz, H., Popa-Lisseanu, A. G.,

Seebens-Hoyer, A., Tichomirowa, M., & Voigt, C. C. (2020). Identifying

migratory pathways of Nathusius' pipistrelles (*Pipistrellus nathusii*) using stable

hydrogen and strontium isotopes. *Rapid Communications in Mass Spectrometry,

35*(6). https://doi.org/10.1002/rcm.9031.

Popa-Lisseanu, A. G., Sörgel, K., Luckner, A., Wassenaar, L.I., Ibáñez, C., Kramer-

Schadt, S., Ciechanowski, M., Görföl, T., Niermann, I., Beuneux, G., Mysłajek, R.

W., Juste, J., Fonderflick, J., Kelm, D. H., & Voigt, C. C. (2012). A triple-isotope

approach to predict the breeding origins of European bats. *PLoS One, 7*(1),

e30388. https://doi.org/10.1371/journal.pone.0030388.

Sellick, M. J., Kyser, T. K., Wunder, M. B., Chipley, D., & Norris, D. R. (2009).

Geographic variation of strontium and hydrogen isotopes in avian tissue:

Implications for tracking migration and dispersal. *PLoS One, 4*(3), e4735.

https://doi.org/10.1371/journal.pone.0004735.

Shin, W.-J., Jung, M., Ryu, J-S., Hwang, J., & Lee, K.-S. (2020). Revisited digestion

methods for trace element analysis in human hair. *Journal of Analytical Science

and Technology, 11*, 1. https://doi.org/10.1186/s40543-019-0200-6.

Tipple, B. J., Chau, T., Chesson, L. A., Fernandez, D. P., & Ehleringer, J. R. (2013).

Isolation of strontium pools and isotope ratios in modern human hair. *Analytica Chimica Acta, 798*, 64-73. https://doi.org/10.1016/j.aca.2013.08.054.

Zazzo, A., Monahan, F. J., Moloney, A. P., Green, S., & Schmidt, O. (2011). Sulphur isotopes in animal hair track distance to sea. *Rapid Communications in Mass Spectrometry, 25*(17), 2371-2378. https://doi.org/10.1002/rcm.5131.

Appendix I. *Pre-treatment Experiment*

We conducted an initial pre-treatment experiment to determine the most appropriate method to remove exogenous strontium contamination from fur samples. As not to waste valuable bat fur samples, we conducted this experiment using the primary author's hair (CBH) and two human hair standards [IAEA 086 (International Atomic Energy Agency, Vienna, Austria), NIES 13 (National Institute for Environmental Studies, Tsukuba-City, Japan)]. To obtain CBH samples, we removed $3 - 4$ full strands of hair at the scalp, trimming the hair to $2.5 - 5$ cm sections. We weighed all hair samples (CBH, IAEA 086, NIES 13) to $5 - 10$ mg, which represented a conservative estimate of the amount of fur that could be obtained from the bat carcasses. We stored the weighed samples in 2 mL plastic centrifuge tubes for pre-treatment.

We tested four chemical pre-treatments (mirroring Tipple et al., 2013) and included two replicates per treatment. These hair treatments included (1) no treatment, (2) $2 : 1$ chloroform : methanol treatment, (3) IAEA treatment, and (4) HCl treatment. One cycle of treatment included an ultrasonication step using 2 mL of reagent for 5 minutes, a centrifuge step for 4 minutes at 10,000 rpm, and a decant step which entailed removing the waste solution, or leachate, using a 1 mL glass Pasteur pipette. Category (1), samples remained untouched until strontium digestion. Category (2) samples were treated with one cycle using a $2 : 1$ chloroform : methanol solution and rinsed with one cycle of deionized water (DI H_2O). We treated Category (3) samples with one treatment cycle of acetone and a rinse cycle using 2 mL of DI H_2O following the same ultrasonication, centrifuge, decant steps. We then repeated these treatment and rinse cycles one additional time. Finally, Category (4) samples were treated with 0.1 M HCl using the same

ultrasonication, centrifuge, and decant cycle detailed above. This HCl treatment cycle was repeated two additional times before a rinse cycle using DI H_2O.

After pre-treatment, we transferred all samples to a clean hood, covered the vials with parafilm fitted with small condensation release holes, and dried the samples at room temperature for 48 hours, then on a hotplate set to 100 °C for 24 hours. Once all samples were dried, they were digested and analyzed using the same methodology as the bat fur samples.

To determine the most appropriate pre-treatment method for fur tissue moving forward, we graphically compared the four chemical pre-treatments by plotting the $^{87}Sr/^{86}Sr$ values and ^{88}Sr intensity (measured in V) for each hair sample (Figure A.1.1). We defined the most appropriate pre-treatment method as that which balanced precision and accuracy of analysis (i.e., minimal spread of $^{87}Sr/^{86}Sr$ values and those closest to reported values for IAEA 086 and NIES 13) with overall quantity of strontium in the sample (i.e., higher ^{88}Sr intensity) (Tipple et al., 2013). The reported relative concentrations of strontium in IAEA 086 and NIES 13 are 8.37 ± 0.12 µg/g and 2.9 ± 0.02 µg/g, respectively (Sahoo et al., 2014). Hu et al. (2020) report the ^{88}Sr intensity of SRM 987 at 100 ng/g to be 4.8 ± 1.5 V ($n = 37$) and the ^{88}Sr intensity of SRM 987 at 10 ng/g to be 0.53 ± 0.01 V ($n = 16$); we would expect the ^{88}Sr intensity of our samples and standards after pre-treatment to be similar, depending on the strength of the chemical used in pre-treatment (i.e., HCl vs. acetone). Tipple et al. (2013) and Tipple et al. (2018) report the $^{87}Sr/^{86}Sr$ value of NIES 13 as 0.70827 ± 0.00004 ($n = 6$); a published $^{87}Sr/^{86}Sr$ value for IAEA 086 was not available at the time of writing.

The mean absolute difference between $^{87}Sr/^{86}Sr$ values for each pre-treatment method was as follows: (1) None: 0.000532, (2) chloroform : methanol: 0.000261, (3) IAEA: 0.000184, (4) HCl: 0.001101. Alternatively, the mean ^{88}Sr intensity for each pre-treatment method was as follows: (1) None: 1.01 V, (2) chloroform : methanol: 0.91 V, (3) IAEA: 0.55 V, (4) HCl: 0.12 V. Ultimately, the IAEA pre-treatment method appeared to optimize ^{88}Sr intensity while minimizing spread of $^{87}Sr/^{86}Sr$ values. To further test the effectiveness of this pre-treatment method on the fur of *Myotis lucifugus*, we used a JEOL JSM 7100-F Scanning Electron Microscope (Tokyo, Japan) to visualize particles adhered to fur before and after pre-treatment. Fur was sampled from four representative individuals, and images were collected before and after pre-treatment of those fur samples (Figure A.1.2). According to this test, the IAEA pre-treatment method appeared largely effective, however, matted and partially degraded fur samples retained external particulates, as these particulates appeared to be adhered to the matrix of matted fur (Figure A.1.2). Ultimately, we moved forward with the IAEA procedure for pre-treating fur samples, but with the understanding that not all exogenous sources of strontium contamination could be reasonably removed from the fur of pre-deceased *M. lucifugus* carcasses.

REFERENCES

Hu, L. Fernandez, D. P., Cerling, T. E., & Tipple, B. J. (2020). Fast exchange of strontium between hair and ambient water: Implications for isotopic analysis in provenance and forensic studies. *PLoS One, 15*(5), e0233712. https://doi.org/10.1371/journal.pone.0233712.

Sahoo, S. K., Mishra, S., Žunić, Z. S., Arae, H., Gjergj, F., Stegnar, P., Benedik, L.,

Repinc, U., & Kritsananuwat, R. (2014). Distribution of uranium and selected trace metals in Balkan human scalp hair using inductively coupled plasma mass spectrometry. *International Journal of Mass Spectrometry, 373*, 15-21. https://doi.org/10.1016/j.ijms.2014.08.020.

Tipple, B. J., Chau, T., Chesson, L. A., Fernandez, D. P., & Ehleringer, J. R. (2013). Isolation of strontium pools and isotope ratios in modern human hair. *Analytica Chimica Acta, 798*, 64-73. https://doi.org/10.1016/j.aca.2013.08.054.

Tipple, B. J., Valenzuela, L. O., & Ehleringer, J. R. (2018). Strontium isotope ratios of human hair record intra-city variations in tap water source. *Scientific Reports, 8*. https://doi.org/10.1038/s41598-018-21359-0.
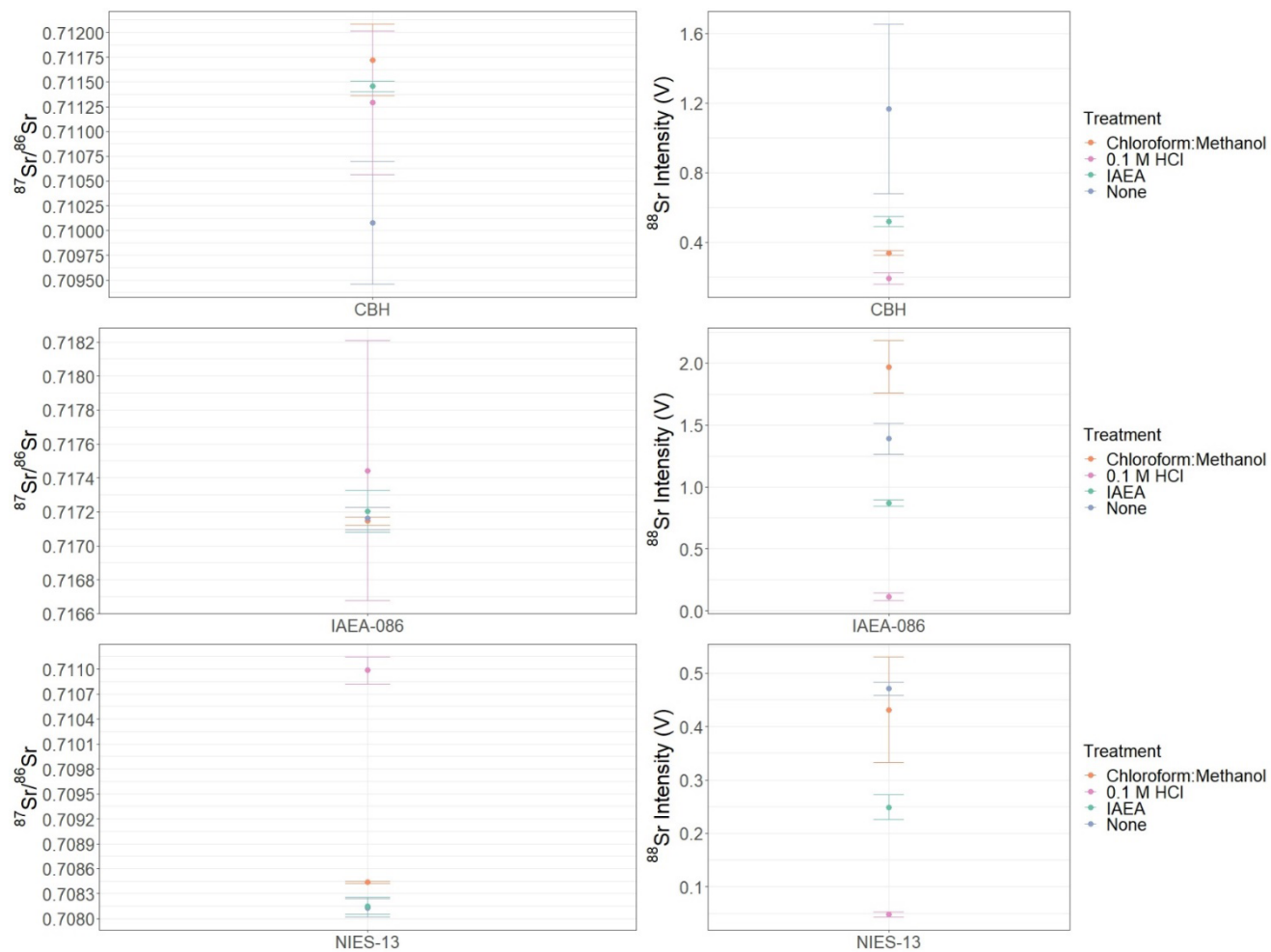
Figure A.1.1. *Spread of $^{87}Sr/^{86}Sr$ values and ^{88}Sr intensity according to each pre-treatment method and sample type. IAEA 086 (International Atomic Energy Agency, Vienna, Austria) and NIES 13 (National Institute for Environmental Studies, Tsukuba-City, Japan) are both homogenized keratin standards, while CBH hair offered for analysis from the primary author to approximate a less controlled keratin sample.*
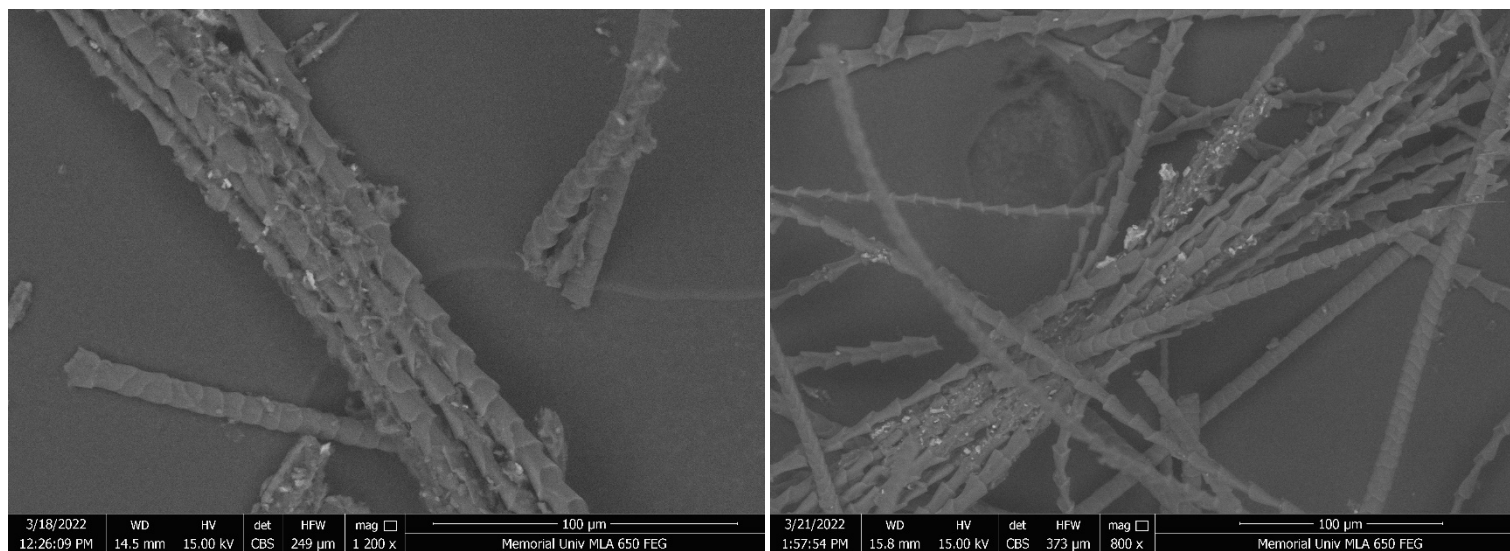
Figure A.1.2. *Scanning electron microscopic image of fur sampled from Individual 90 before* ***(left)*** *and after* ***(right)*** *pre-treatment using the IAEA procedure.*

Appendix II. *Detailed strontium analysis data – values are separated by tissue [i.e., fur (F), teeth (T), and bone (B)]. Fur values are reported with anatomical surface of the individual sampled [i.e., dorsal (D) and ventral (V)] when applicable.*

Sample ID	$^{87}Sr/^{86}Sr_F$	1 SE	$^{88}Sr_F$ V	$^{84}Sr/^{86}Sr_F$	$^{87}Sr/^{86}Sr_T$	1 SE	$^{88}Sr_T$ V	$^{84}Sr/^{86}Sr_T$	$^{87}Sr/^{86}Sr_B$	1 SE	$^{88}Sr_B$ V	$^{84}Sr/^{86}Sr_B$
41	0.710642	0.000023	1.039	0.055505	0.709999	0.000006	24.273	0.056448	0.710279	0.000007	20.749	0.056474
42	0.710237	0.000025	1.043	0.054741	0.710054	0.000005	33.222	0.056466	0.710148	0.000007	17.252	0.056434
44	0.710554	0.000019	1.095	0.055871	0.710253	0.000005	23.408	0.056447	0.710383	0.000005	26.251	0.056464
81	0.709915	0.000023	1.021	0.055207	–	–	–	–	–	–	–	–
66	0.709364	0.000018	1.401	0.055518	0.709231	0.000007	13.470	0.056442	0.709342	0.000006	27.380	0.056501
69	0.709484	0.000057	0.382	0.054407	–	–	–	–	–	–	–	–
79	0.709601	0.000010	3.511	0.056063	0.708691	0.000006	29.179	0.056400	0.709006	0.000007	23.983	0.056442
82	0.709738	0.000025	0.868	0.055368	–	–	–	–	–	–	–	–
83	0.709730	0.000027	0.795	0.054896	0.709657	0.000005	23.704	0.056427	0.709643	0.000006	26.163	0.056458
88	0.713456	0.000020	1.132	0.055278	0.710422	0.000005	30.536	0.056439	0.710421	0.000007	26.093	0.056475
76	0.715323	0.000010	3.441	0.056320	0.715244	0.000005	34.181	0.056476	0.715142	0.000009	17.086	0.056447
37	0.713227	0.000018	1.543	0.055532	0.713555	0.000009	10.987	0.056529	0.713400	0.000006	22.157	0.056461
38	0.712907	0.000015	1.812	0.056078	0.712907	0.000004	32.027	0.056444	0.712556	0.000006	20.075	0.056422
40	0.711416	0.000017	1.107	0.055779	0.712389	0.000009	9.393	0.056495	0.712142	0.000007	28.621	0.056460
39	0.711518	0.000050	0.379	0.054938	–	–	–	–	–	–	–	–
75	0.712140 (D) 0.712028 (V)	0.000018 (D) 0.000024 (V)	1.465 (D) 0.925 (V)	0.055915 (D) 0.055385 (V)	0.711540	0.000006	25.878	0.056470	0.711840	0.000009	15.914	0.056403
78	0.710065	0.000022	1.044	0.055309	–	–	–	–	–	–	–	–
84	0.712034	0.000015	1.905	0.056248	–	–	–	–	–	–	–	–
85	0.711844	0.000011	2.511	0.056129	–	–	–	–	–	–	–	–
86	0.711243	0.000012	2.466	0.056367	–	–	–	–	–	–	–	–
87	0.711586	0.000013	1.691	0.055928	–	–	–	–	–	–	–	–
97	0.713401	0.000035	0.618	0.055020	–	–	–	–	–	–	–	–
43	0.707023	0.000012	3.008	0.056186	0.706834	0.000005	27.589	0.056473	0.707104	0.000005	34.746	0.056459
67	0.710668	0.000017	1.311	0.055889	0.708854	0.000008	21.667	0.056438	0.708679	0.000007	22.947	0.056474
90	0.711833	0.000015	1.410	0.055622	–	–	–	–	–	–	–	–
91	0.709422 (D) 0.710160 (V)	0.000010 (D) 0.000009 (V)	2.611 (D) 3.264 (V)	0.056242 (D) 0.056159 (V)	–	–	–	–	–	–	–	–
15	0.711094	0.000042	0.480	0.055024	–	–	–	–	–	–	–	–
16	0.713208	0.000008	5.153	0.056155	0.710918	0.000005	32.339	0.056478	0.710775	0.000007	21.667	0.056458
95	0.714787	0.000025	0.982	0.054887	0.711772	0.000007	15.547	0.056441	0.711590	0.000007	22.734	0.056467
96	0.711478	0.000031	0.804	0.054931	0.711400	0.000007	26.962	0.056490	0.711688	0.000005	31.067	0.056456
14	0.709898	0.000013	2.072	0.056047	0.709494	0.000006	26.498	0.056454	0.709508	0.000006	23.656	0.056461
17	0.709450	0.000014	2.244	0.056087	0.709317	0.000007	22.359	0.056446	0.709351	0.000008	19.323	0.056443
18	0.713392	0.000048	0.397	0.053929	0.712352	0.000007	19.259	0.056482	0.712159	0.000007	30.489	0.056477

19	0.711193	0.000015	1.791	0.055807	–	–	–	–	–	–	–	–
20	0.709844	0.000030	0.770	0.055169	–	–	–	–	–	–	–	–
60	0.712860	0.000010	2.735	0.056083	0.711780	0.000005	36.270	0.056479	0.711781	0.000006	26.448	0.056465
74	0.711747 (D) 0.713147 (V)	0.000039 (D) 0.000020 (V)	0.562 (D) 1.146 (V)	0.054710 (D) 0.055785 (V)	–	–	–	–	–	–	–	–
100	0.712176 (D) 0.711733 (V)	0.000018 (D) 0.000017 (V)	1.353 (D) 1.798 (V)	0.055186 (D) 0.056016 (V)	–	–	–	–	–	–	–	–
101	0.714315 (D) 0.712507 (V)	0.000031 (D) 0.000014 (V)	0.673 (D) 2.056 (V)	0.054876 (D) 0.056141 (V)	–	–	–	–	–	–	–	–
102	0.712422 (D) 0.713338 (V)	0.000006 (D) 0.000009 (V)	6.850 (D) 4.268 (V)	0.056394 (D) 0.056428 (V)	–	–	–	–	–	–	–	–
50	0.712514 (D) 0.712662 (V)	0.000013 (D) 0.000010 (V)	2.084 (D) 2.767 (V)	0.056435 (D) 0.055819 (V)	–	–	–	–	–	–	–	–
98	0.720056 (D) 0.716555 (V)	0.000038 (D) 0.000017 (V)	0.522 (D) 1.916 (V)	0.054594 (D) 0.055721 (V)	–	–	–	–	–	–	–	–
99	0.716015 (D) 0.716141 (V)	0.000011 (D) 0.000016 (V)	2.128 (D) 1.721 (V)	0.056128 (D) 0.055663 (V)	–	–	–	–	–	–	–	–

Appendix III. *R code used to calculate the δ^2H transfer function and conduct origin assignment analysis.*

```
#AssignR workflow - Mylu Migration in Newfoundland

#Clear R's Brain
rm(list=ls())
#Where is R looking?
getwd()
#Tell R where to look
setwd("C:/Users/caral/Documents/Bats_NL/AssignR")
#Check where r is looking
getwd()

#Open packages used in AssignR workflow
library(assignR)
library(raster)
library(sf)
library(ggplot2)
library(maptools)
library(dplyr)
data("wrld_simpl")
library(smatr)
library(ggplot2)
library(rasterVis)
library(gridExtra)
library(rnaturalearth)
library(rnaturalearthdata)

#I'm calling up my isoscape from IsoMap
d2H_precip <- raster("predreg.tiff")
d2H_precip_sd <- raster("stdreg.tiff")
d2H_precip_all <- brick(d2H_precip,d2H_precip_sd)

#Now that we have our underlying precipitation isoscape,
#I'll call up my known origin data
Mylu_KO <- read.csv("d2H Analysis Results_KO.csv")
#I'm removing the Labrador bats
Mylu_KO <- Mylu_KO %>%
  filter(sample != "50")
Mylu_KO <- Mylu_KO %>%
  filter(sample != "98")
Mylu_KO <- Mylu_KO %>%
  filter(sample != "99")
```

```r
Mylu_KO <- Mylu_KO %>%
  filter(sample != "43")

#I need to make my data into a spatial points data frame
coordinates(Mylu_KO) <- c(3,4)
#We need to be sure the coordinate system is defined
is.projected(Mylu_KO)
#Here I'm defining it as WGS84
projection(Mylu_KO) <- CRS("+proj=longlat +ellps=WGS84
+datum=WGS84 +no_defs")
#Here we're checking the coordinate system of our raster
#brick from IsoMap
proj4string(d2H_precip_all)

#Here I'm doing some background work to change the isoscape
#to be rescaled using an SMA regression instead of a linear
#regression.

  nSample = nrow(Mylu_KO)
  null.iso = NULL
  tissue.iso = Mylu_KO$i..d2H.fur
  tissue.iso.sd = Mylu_KO$sd.d2H.fur
  tissue.iso.wt = 1/Mylu_KO$sd.d2H.fur^2
  isoscape.iso = raster::extract(d2H_precip_all, Mylu_KO,
  method = "simple")
  isoscape.iso[, 2] = pmax(isoscape.iso[, 2],
  cellStats(d2H_precip_all[[2]], min))
  if (any(is.na(isoscape.iso[, 1]))) {
    na = which(is.na(isoscape.iso[, 1]))
    wtxt = "NO isoscape values found at the following
    locations:\n"
    for (i in na) {
      wtxt = paste0(wtxt, Mylu_KO@coords[i, 1], ", ",
      Mylu_KO@coords[i,2], "\n")
    }
    tissue.iso = tissue.iso[!is.na(isoscape.iso[, 1])]
    tissue.iso.wt = tissue.iso.wt[!is.na(isoscape.iso[, 1])]
    isoscape.iso = isoscape.iso[!is.na(isoscape.iso[, 1]),]
    nSample = length(tissue.iso)
  }
  smaResult = sma(tissue.iso ~ isoscape.iso[, 1])
  summary(smaResult)
  smaresiduals<-residuals(smaResult)
  x = isoscape.iso[,1]
  y = tissue.iso
```

```r
  w = tissue.iso.wt
  xyw = data.frame(x, y, w)
  xl = max(x)
  yl = min(y) + 0.05 * diff(range(y))
  intercept = as.numeric(coef(smaResult)[1])
  slope = as.numeric(coef(smaResult)[2])
  isoscape.rescale = d2H_precip_all[[1]] * slope + intercept
  plot(isoscape.rescale)
  isoscape.sim = matrix(0, nrow = nSample, ncol = 100)
  for (i in seq_along(isoscape.iso[, 1])) {
    isoscape.sim[i,] = rnorm(100, isoscape.iso[i,1],
    isoscape.iso[i,2])
  }
  isoscape.dev = tissue.dev = double()
  for (i in 1:100) {
    sma.sim = sma(tissue.iso ~ isoscape.sim[, i])
    isoscape.dev = c(isoscape.dev, isoscape.sim[, i] -
    isoscape.iso[,1])
    sma.sim.residuals<-residuals(sma.sim)
    tissue.dev = c(tissue.dev, sma.sim.residuals)
  }
  ti.corr = cor(isoscape.dev, tissue.dev)^2
  sd = sqrt(d2H_precip_all[[2]]^2 + var(smaresiduals) * (1 -
  ti.corr))
  isoscape.rescale = disaggregate(isoscape.rescale,10)
  isoscape.rescale = mask(isoscape.rescale,wrld_simpl)
  sd = disaggregate(sd,10)
  sd = mask(sd,wrld_simpl)
  isoscape.rescale = stack(isoscape.rescale, sd)
  names(isoscape.rescale) = c("mean", "sd")
  names(xyw) = c("isoscape.iso", "tissue.iso",
  "tissue.iso.wt")
  result = list(isoscape.rescale = isoscape.rescale, lm.data
  = xyw, lm.model = smaResult)
  class(result) = c("rescale")
  plot(isoscape.rescale)
  plot(isoscape.rescale$mean)

#Here I'm plotting my isoscape
#Now mask the ocean for the mean raster
d2H_precip <- disaggregate(d2H_precip,10)
d2H_precip <- mask(d2H_precip,wrld_simpl)
plot(d2H_precip)

gglayers <-  list(geom_tile(aes(fill = value)),
```

```r
                     coord_equal(),theme_bw(),
                     scale_x_continuous(name = "Longitude",
                     expand = c(0,0)),
                     scale_y_continuous(name = "Latitude",
                     expand = c(0,0)))

lab1 <- list(gglayers, scale_fill_gradientn(name =
  expression(paste(delta^{2}, "H (\u2030)")), colours =
  hcl.colors(20, palette = "viridis"), na.value =
  "slategray1", breaks = waiver(), n.breaks = 6))

gridExtra::grid.arrange(gplot(d2H_precip) + lab1 +
                      theme(axis.title=element_text(size=20),
                            axis.text=element_text(size=20),
                          legend.text=element_text(size=20),
                        legend.title=element_text(size=20)))

#Here I'm plotting my transfer function
Mylu_KO_Precip <- read.csv("Mylu_KO_d2H_Fur_Precip.csv")
highlight_df <- Mylu_KO_Precip %>%
  filter(ï..sample=="43")
#First I'm removing my labrador bats
Mylu_KO_Precip <- Mylu_KO_Precip %>%
  filter(ï..sample != "50")
Mylu_KO_Precip <- Mylu_KO_Precip %>%
  filter(ï..sample != "98")
Mylu_KO_Precip <- Mylu_KO_Precip %>%
  filter(ï..sample != "99")
Mylu_KO_Precip <- Mylu_KO_Precip %>%
  filter(ï..sample != "43")
#Now I'm running the SMA
SMA <- sma(d2H.fur ~ Precip, data=Mylu_KO_Precip, V=v)
summary(SMA)
summary(smaResult)
smaresiduals<-residuals(SMA)
sd(smaresiduals)
d2H.transfer<-ggplot(data = Mylu_KO_Precip, aes(x=Precip,
  y=d2H.fur)) +
  geom_point(size=5) +
  geom_point(data=highlight_df,
             aes(x=Precip,y=d2H.fur),
             color='red',
             size=5) +
  theme(axis.title=element_text(size=25),
        axis.text=element_text(size=25),
```

```r
        plot.title = element_text(hjust=0.5, size=30,
        face="bold"),
        plot.margin = margin(1,1,1.5,1.2, "cm")) +
        geom_abline(aes(intercept=3.505939,slope=0.9428589),
            color = "black", size = 1.5) +
        ylab(expression(paste(italic(delta)^{2},
            'H'[italic(fur)], "(\u2030 VSMOW)"))) +
        xlab(expression(paste(italic(delta)^{2},
            'H'[italic(p)], "(\u2030 VSMOW)"))) +
        annotate("text", x = -80, y = -30, xmin = NULL, xmax
                = NULL, ymin = NULL, ymax = NULL,
                xend = NULL, yend = NULL, size = 8,
                label = "y = 0.94 x + 3.51") +
        annotate("text", x = -80, y = -34, xmin = NULL, xmax
                = NULL, ymin = NULL, ymax = NULL,
                xend = NULL, yend = NULL, size = 8,
                label = expression(paste(italic(r)^{2}, '=
                    0.354'))) +
        annotate("text", x = -80, y = -38, xmin = NULL, xmax
                = NULL, ymin = NULL, ymax = NULL,
                xend = NULL, yend = NULL, size = 8,
                label = expression(paste(italic(p), '=
                    0.032'))) +
        geom_errorbar(aes(x = -52.0435, ymin = -53.8, ymax =
                    -46.3), width = 0.5, size = 0.9) +
        geom_errorbar(aes(x = -63.5098, ymin = -54.1, ymax =
                    -37.9), width = 0.5, size = 0.9) +
        geom_errorbar(aes(x = -43.3736, ymin = -31.4, ymax =
                    -27.8), width = 0.5, size = 0.9) +
        geom_errorbar(aes(x = -43.2399, ymin = -43.2, ymax =
                    -32.5), width = 0.5, size = 0.9) +
        geom_errorbar(aes(x = -45.1704, ymin = -54.3, ymax =
                    -49.7), width = 0.5, size = 0.9) +
        geom_errorbar(aes(x = -61.9980, ymin = -56.0, ymax =
                    -44.4), width = 0.5, size = 0.9)
d2H.transfer

#Now I'm ready to make origin assignments! Woo hoo!
Mylu_UO <- read.csv("d2H Analysis Results_UO.csv")
Mylu_PO2 <- pdRaster(r=isoscape.rescale, unknown = Mylu_UO)
plot(Mylu_PO2)

#And can make origin assignment estimates with a given
#accuracy threshold
```

```r
##########Individual 14#########################

#Individual 14 with 50% Accuracy
Dist_14 <- qtlRaster(Mylu_PO2$F14, threshold=0.5,
          thresholdType = "prob")
xy_14 <- c(x,y)
DFP_14 <- distanceFromPoints(Dist_14, xy_14)
plot(DFP_14)
DFP_14_Mask <- mask(DFP_14, Dist_14)
plot(DFP_14_Mask)
DFP_14_Mask <- mask(DFP_14_Mask, Dist_14, maskvalue=0)
plot(DFP_14_Mask)
plot(Dist_14) #double check they match
Min_14 <- (DFP_14_Mask@data@min)
Min_14/1000 #177.7067 km <- migratory

#Individual 14 with 75% Accuracy
Dist_14.2 <- qtlRaster(Mylu_PO2$F14, threshold=0.75,
                       thresholdType = "prob")
plot(Dist_14.2)
DFP_14.2 <- distanceFromPoints(Dist_14.2, xy_14)
plot(DFP_14.2)
DFP_14.2_Mask <- mask(DFP_14.2, Dist_14.2, maskvalue=0)
DFP_14.2_Mask <- mask(DFP_14.2_Mask, Dist_14.2)
plot(DFP_14.2_Mask)
plot(Dist_14.2) #double check they match
Min_14.2 <- (DFP_14.2_Mask@data@min)
Min_14.2/1000 #11.42875 km <- migratory

#Individual 14 with 90% Accuracy
Dist_14.3 <- qtlRaster(Mylu_PO2$F14, threshold=0.9,
                       thresholdType = "prob")
plot(Dist_14.3)
DFP_14.3 <- distanceFromPoints(Dist_14.3, xy_14)
plot(DFP_14.3)
DFP_14.3_Mask <- mask(DFP_14.3, Dist_14.3, maskvalue=0)
DFP_14.3_Mask <- mask(DFP_14.3_Mask, Dist_14.3)
plot(DFP_14.3_Mask)
plot(Dist_14.3) #double check they match
Min_14.3 <- (DFP_14.3_Mask@data@min)
Min_14.3/1000 #0.2407427 km

#Plot
terra::plot(Dist_14, legend=FALSE, xlab="Longitude",
            ylab="Latitude")
```

```r
points(x = x,
       y = y,
       pch = 16,
       cex = 0.75,
       col = "black")
text(x=-60.3, y=48.3, labels = "14", cex = 1)

##########Individual 15#########################

#Individual 15 with 50% Accuracy
Dist_15 <- qtlRaster(Mylu_PO2$F15, threshold=0.5,
                     thresholdType = "prob")
xy_15 <- c(x,y)
DFP_15 <- distanceFromPoints(Dist_15, xy_15)
plot(DFP_15)
DFP_15_Mask <- mask(DFP_15, Dist_15, maskvalue=0)
DFP_15_Mask <- mask(DFP_15_Mask, Dist_15)
plot(DFP_15_Mask)
plot(Dist_15) #double check they match
Min_15 <- (DFP_15_Mask@data@min)
Min_15/1000 #7.931779 km <- non-migratory

#Individual 15 with 75% Accuracy
Dist_15.2 <- qtlRaster(Mylu_PO2$F15, threshold=0.75,
                       thresholdType = "prob")
DFP_15.2 <- distanceFromPoints(Dist_15.2, xy_15)
plot(DFP_15.2)
DFP_15.2_Mask <- mask(DFP_15.2, Dist_15.2, maskvalue=0)
DFP_15.2_Mask <- mask(DFP_15.2_Mask, Dist_15.2)
plot(DFP_15.2_Mask)
plot(Dist_15.2) #double check they match
Min_15.2 <- (DFP_15.2_Mask@data@min)
Min_15.2/1000 #7.931779 km <- non-migratory

#Individual 15 with 90% Accuracy
Dist_15.3 <- qtlRaster(Mylu_PO2$F15, threshold=0.9,
                       thresholdType = "prob")
DFP_15.3 <- distanceFromPoints(Dist_15.3, xy_15)
plot(DFP_15.3)
DFP_15.3_Mask <- mask(DFP_15.3, Dist_15.3, maskvalue=0)
DFP_15.3_Mask <- mask(DFP_15.3_Mask, Dist_15.3)
plot(DFP_15.3_Mask)
plot(Dist_15.3) #double check they match
Min_15.3 <- (DFP_15.3_Mask@data@min)
Min_15.3/1000 #7.931779 km
```

```r
#Plot
terra::plot(Dist_15, legend=FALSE, xlab="Longitude",
            ylab="Latitude")
points(x = x,
       y = y,
       pch = 16,
       cex = 0.75,
       col = "black")
text(x=-58.6, y=50.25, labels = "15", cex = 1)


##########Individual 16#######################

#Individual 16 with 50% Accuracy
Dist_16 <- qtlRaster(Mylu_PO2$F16, threshold=0.5,
                     thresholdType = "prob")
xy_16 <- c(x,y)
DFP_16 <- distanceFromPoints(Dist_16, xy_16)
DFP_16_Mask <- mask(DFP_16, Dist_16, maskvalue=0)
DFP_16_Mask <- mask(DFP_16_Mask, Dist_16)
plot(DFP_16_Mask)
plot(Dist_16)
Min_16 <- DFP_16_Mask@data@min
Min_16/1000 #7.798478 km <- migratory


#Individual 16 with 75% Accuracy
Dist_16.2 <- qtlRaster(Mylu_PO2$F16, threshold=0.75,
              thresholdType = "prob")
DFP_16.2 <- distanceFromPoints(Dist_16.2, xy_16)
DFP_16.2_Mask <- mask(DFP_16.2, Dist_16.2, maskvalue=0)
DFP_16.2_Mask <- mask(DFP_16.2_Mask, Dist_16.2)
plot(DFP_16.2_Mask)
plot(Dist_16.2)
Min_16.2 <- DFP_16.2_Mask@data@min
Min_16.2/1000 #0.4110647 km <- non-migratory


#Individual 16 with 90% Accuracy
Dist_16.3 <- qtlRaster(Mylu_PO2$F16, threshold=0.9,
                       thresholdType = "prob")
DFP_16.3 <- distanceFromPoints(Dist_16.3, xy_16)
DFP_16.3_Mask <- mask(DFP_16.3, Dist_16.3, maskvalue=0)
DFP_16.3_Mask <- mask(DFP_16.3_Mask, Dist_16.3)
plot(DFP_16.3_Mask)
plot(Dist_16.3)
Min_16.3 <- DFP_16.3_Mask@data@min
```

```r
Min_16.3/1000

#Plot
terra::plot(Dist_16.2, legend=FALSE, xlab="Longitude",
            ylab="Latitude")
points(x = x,
       y = y,
       pch = 16,
       cex = 0.75,
       col = "black")
text(x=-59, y=50.15, labels = "16", cex = 1)

##########Individual 17#########################

#Individual 17 with 50% Accuracy
Dist_17 <- qtlRaster(Mylu_PO2$F17, threshold=0.5,
                     thresholdType = "prob")
xy_17 <- c(x,y)
DFP_17 <- distanceFromPoints(Dist_17, xy_17)
DFP_17_Mask <- mask(DFP_17, Dist_17, maskvalue=0)
DFP_17_Mask <- mask(DFP_17_Mask, Dist_17)
plot(DFP_17_Mask)
plot(Dist_17)
Min_17 <- DFP_17_Mask@data@min
Min_17/1000 #80.9996 km <- migratory

#Individual 17 with 75% Accuracy
Dist_17.2 <- qtlRaster(Mylu_PO2$F17, threshold=0.75,
                       thresholdType = "prob")
DFP_17.2 <- distanceFromPoints(Dist_17.2, xy_17)
DFP_17.2_Mask <- mask(DFP_17.2, Dist_17.2, maskvalue=0)
DFP_17.2_Mask <- mask(DFP_17.2_Mask, Dist_17.2)
plot(DFP_17.2_Mask)
plot(Dist_17.2)
Min_17.2 <- DFP_17.2_Mask@data@min
Min_17.2/1000 #0.1418093 km <- non-migratory

#Individual 17 with 90% Accuracy
Dist_17.3 <- qtlRaster(Mylu_PO2$F17, threshold=0.9,
                       thresholdType = "prob")
DFP_17.3 <- distanceFromPoints(Dist_17.3, xy_17)
DFP_17.3_Mask <- mask(DFP_17.3, Dist_17.3, maskvalue=0)
DFP_17.3_Mask <- mask(DFP_17.3_Mask, Dist_17.3)
plot(DFP_17.3_Mask)
plot(Dist_17.3)
```

```r
Min_17.3 <- DFP_17.3_Mask@data@min
Min_17.3/1000 #0.1418093 km

#Plot
terra::plot(Dist_17.2, legend=FALSE, xlab="Longitude",
            ylab="Latitude")
points(x = x,
       y = y,
       pch = 16,
       cex = 0.75,
       col = "black")
text(x=-59.5, y=49.2, labels = "17", cex = 1)

##########Individual 18#######################

#Individual 18 with 50% Accuracy
Dist_18 <- qtlRaster(Mylu_PO2$F18, threshold=0.5,
                     thresholdType = "prob")
xy_18 <- c(x,y)
DFP_18 <- distanceFromPoints(Dist_18, xy_18)
DFP_18_Mask <- mask(DFP_18, Dist_18, maskvalue=0)
DFP_18_Mask <- mask(DFP_18_Mask, Dist_18)
plot(DFP_18_Mask)
plot(Dist_18)
Min_18 <- DFP_18_Mask@data@min
Min_18/1000 #0.2953059 km <- non-migratory

#Individual 18 with 75% Accuracy
Dist_18.2 <- qtlRaster(Mylu_PO2$F18, threshold=0.75,
                       thresholdType = "prob")
DFP_18.2 <- distanceFromPoints(Dist_18.2, xy_18)
DFP_18.2_Mask <- mask(DFP_18.2, Dist_18.2, maskvalue=0)
DFP_18.2_Mask <- mask(DFP_18.2_Mask, Dist_18.2)
plot(DFP_18.2_Mask)
plot(Dist_18.2)
Min_18.2 <- DFP_18.2_Mask@data@min
Min_18.2/1000 #0.2953059 km <- non-migratory

#Plot
terra::plot(Dist_18.2, legend=FALSE, xlab="Longitude",
            ylab="Latitude")
points(x = x,
       y = y,
       pch = 16,
       cex = 0.75,
```

```r
          col = "black")
text(x=-58.8, y=49.6, labels = "18", cex = 1)


##########Individual 19#######################

#Individual 19 with 50% Accuracy
Dist_19 <- qtlRaster(Mylu_PO2$F19, threshold=0.5,
                     thresholdType = "prob")
xy_19 <- c(x,y)
DFP_19 <- distanceFromPoints(Dist_19, xy_19)
DFP_19_Mask <- mask(DFP_19, Dist_19, maskvalue=0)
DFP_19_Mask <- mask(DFP_19_Mask, Dist_19)
plot(DFP_19_Mask)
plot(Dist_19)
Min_19 <- DFP_19_Mask@data@min
Min_19/1000 #226.8543 km <- migratory

#Individual 19 with 75% Accuracy
Dist_19.2 <- qtlRaster(Mylu_PO2$F19, threshold=0.75,
                       thresholdType = "prob")
DFP_19.2 <- distanceFromPoints(Dist_19.2, xy_19)
DFP_19.2_Mask <- mask(DFP_19.2, Dist_19.2, maskvalue=0)
DFP_19.2_Mask <- mask(DFP_19.2_Mask, Dist_19.2)
plot(DFP_19.2_Mask)
plot(Dist_19.2)
Min_19.2 <- DFP_19.2_Mask@data@min
Min_19.2/1000 #118.4022 km <- migratory

#Individual 19 with 90% Accuracy
Dist_19.3 <- qtlRaster(Mylu_PO2$F19, threshold=0.9,
                       thresholdType = "prob")
DFP_19.3 <- distanceFromPoints(Dist_19.3, xy_19)
DFP_19.3_Mask <- mask(DFP_19.3, Dist_19.3, maskvalue=0)
DFP_19.3_Mask <- mask(DFP_19.3_Mask, Dist_19.3)
plot(DFP_19.3_Mask)
plot(Dist_19.3)
Min_19.3 <- DFP_19.3_Mask@data@min
Min_19.3/1000 #84.16873 km

#Plot
terra::plot(Dist_19.2, legend=FALSE, xlab="Longitude",
            ylab="Latitude")
points(x = x,
       y = y,
       pch = 16,
```

```
        cex = 0.75,
        col = "black")
text(x=-59.6, y=49.25, labels = "19", cex = 1)


##########Individual 20#######################

#Individual 20 with 50% Accuracy
Dist_20 <- qtlRaster(Mylu_PO2$F20, threshold=0.5,
                     thresholdType = "prob")
xy_20 <- c(x,y)
DFP_20 <- distanceFromPoints(Dist_20, xy_20)
DFP_20_Mask <- mask(DFP_20, Dist_20, maskvalue=0)
DFP_20_Mask <- mask(DFP_20_Mask, Dist_20)
plot(DFP_20_Mask)
plot(Dist_20)
Min_20 <- DFP_20_Mask@data@min
Min_20/1000 #50.24711 km <- migratory


#Individual 20 with 75% Accuracy
Dist_20.2 <- qtlRaster(Mylu_PO2$F20, threshold=0.75,
                       thresholdType = "prob")
DFP_20.2 <- distanceFromPoints(Dist_20.2, xy_20)
DFP_20.2_Mask <- mask(DFP_20.2, Dist_20.2, maskvalue=0)
DFP_20.2_Mask <- mask(DFP_20.2_Mask, Dist_20.2)
plot(DFP_20.2_Mask)
plot(Dist_20.2)
Min_20.2 <- DFP_20.2_Mask@data@min
Min_20.2/1000 #2.155564 km <- migratory


#Individual 20 with 90% Accuracy
Dist_20.3 <- qtlRaster(Mylu_PO2$F20, threshold=0.9,
                       thresholdType = "prob")
DFP_20.3 <- distanceFromPoints(Dist_20.3, xy_20)
DFP_20.3_Mask <- mask(DFP_20.3, Dist_20.3, maskvalue=0)
DFP_20.3_Mask <- mask(DFP_20.3_Mask, Dist_20.3)
plot(DFP_20.3_Mask)
plot(Dist_20.3)
Min_20.3 <- DFP_20.3_Mask@data@min
Min_20.3/1000 #0.2961537 km


#Plot
terra::plot(Dist_20.2, legend=FALSE, xlab="Longitude",
            ylab="Latitude")
points(x = x,
       y = y,
```

```r
      pch = 16,
      cex = 0.75,
      col = "black")
text(x=-59.8, y=49, labels = "20", cex = 1)


##########Individual 60########################

#Individual 60 with 50% Accuracy
Dist_60 <- qtlRaster(Mylu_PO2$F60, threshold=0.5,
                      thresholdType = "prob")
xy_60 <- c(x,y)
DFP_60 <- distanceFromPoints(Dist_60, xy_60)
DFP_60_Mask <- mask(DFP_60, Dist_60, maskvalue=0)
DFP_60_Mask <- mask(DFP_60_Mask, Dist_60)
plot(DFP_60_Mask)
plot(Dist_60)
Min_60 <- DFP_60_Mask@data@min
Min_60/1000 #0.4110647 km <- non-migratory

#Individual 60 with 75% Accuracy
Dist_60.2 <- qtlRaster(Mylu_PO2$F60, threshold=0.75,
                        thresholdType = "prob")
DFP_60.2 <- distanceFromPoints(Dist_60.2, xy_60)
DFP_60.2_Mask <- mask(DFP_60.2, Dist_60.2, maskvalue=0)
DFP_60.2_Mask <- mask(DFP_60.2_Mask, Dist_60.2)
plot(DFP_60.2_Mask)
plot(Dist_60.2)
Min_60.2 <- DFP_60.2_Mask@data@min
Min_60.2/1000 #0.4110647 km <- non-migratory

#Plot
terra::plot(Dist_60.2, legend=FALSE, xlab="Longitude",
            ylab="Latitude")
points(x = x,
       y = y,
       pch = 16,
       cex = 0.75,
       col = "black")
text(x=-58, y=50.35, labels = "60", cex = 1)


##########Individual 67########################

#Individual 67 with 50% Accuracy
Dist_67 <- qtlRaster(Mylu_PO2$F67, threshold=0.5,
                      thresholdType = "prob")
```

```r
xy_67 <- c(x,y)
DFP_67 <- distanceFromPoints(Dist_67, xy_67)
DFP_67_Mask <- mask(DFP_67, Dist_67, maskvalue=0)
DFP_67_Mask <- mask(DFP_67_Mask, Dist_67)
plot(DFP_67_Mask)
plot(Dist_67)
Min_67 <- DFP_67_Mask@data@min
Min_67/1000 #620.8753 km <- migratory

#Individual 67 with 75% Accuracy
Dist_67.2 <- qtlRaster(Mylu_PO2$F67, threshold=0.75,
                        thresholdType = "prob")
DFP_67.2 <- distanceFromPoints(Dist_67.2, xy_67)
DFP_67.2_Mask <- mask(DFP_67.2, Dist_67.2, maskvalue=0)
DFP_67.2_Mask <- mask(DFP_67.2_Mask, Dist_67.2)
plot(DFP_67.2_Mask)
plot(Dist_67.2)
Min_67.2 <- DFP_67.2_Mask@data@min
Min_67.2/1000 #31.80325 km <- migratory

#Plot
terra::plot(Dist_67, legend=FALSE, xlab="Longitude",
            ylab="Latitude")
points(x = x,
       y = y,
       pch = 16,
       cex = 0.75,
       col = "black")
text(x=-54.3, y=47.75, labels = "67", cex = 1)

##########Individual 74####################

#Individual 74 with 50% Accuracy
Dist_74 <- qtlRaster(Mylu_PO2$D74, threshold=0.5,
                        thresholdType = "prob")
xy_74 <- c(x,y)
DFP_74 <- distanceFromPoints(Dist_74, xy_74)
DFP_74_Mask <- mask(DFP_74, Dist_74, maskvalue=0)
DFP_74_Mask <- mask(DFP_74_Mask, Dist_74)
plot(DFP_74_Mask)
plot(Dist_74)
Min_74 <- DFP_74_Mask@data@min
Min_74/1000 #110.0493 km <- migratory

#Individual 74 with 75% Accuracy
```

```r
Dist_74.2 <- qtlRaster(Mylu_PO2$D74, threshold=0.75,
                       thresholdType = "prob")
DFP_74.2 <- distanceFromPoints(Dist_74.2, xy_74)
DFP_74.2_Mask <- mask(DFP_74.2, Dist_74.2, maskvalue=0)
DFP_74.2_Mask <- mask(DFP_74.2_Mask, Dist_74.2)
plot(DFP_74.2_Mask)
plot(Dist_74.2)
Min_74.2 <- DFP_74.2_Mask@data@min
Min_74.2/1000 #10.96209 km <- migratory

#Individual 74 with 90% Accuracy
Dist_74.3 <- qtlRaster(Mylu_PO2$D74, threshold=0.9,
                       thresholdType = "prob")
DFP_74.3 <- distanceFromPoints(Dist_74.3, xy_74)
DFP_74.3_Mask <- mask(DFP_74.3, Dist_74.3, maskvalue=0)
DFP_74.3_Mask <- mask(DFP_74.3_Mask, Dist_74.3)
plot(DFP_74.3_Mask)
plot(Dist_74.3)
Min_74.3 <- DFP_74.3_Mask@data@min
Min_74.3/1000 #4.502458 km

#Plot
terra::plot(Dist_74.2, legend=FALSE, xlab="Longitude",
            ylab="Latitude")
points(x = x,
       y = y,
       pch = 16,
       cex = 0.75,
       col = "black")
text(x=-58.8, y=50.3, labels = "74 (D)", cex = 1)

##########Individual 90#######################

#Individual 90 with 50% Accuracy
Dist_90 <- qtlRaster(Mylu_PO2$F90, threshold=0.5,
                     thresholdType = "prob")
xy_90 <- c(x,y)
DFP_90 <- distanceFromPoints(Dist_90, xy_90)
DFP_90_Mask <- mask(DFP_90, Dist_90, maskvalue=0)
DFP_90_Mask <- mask(DFP_90_Mask, Dist_90)
plot(DFP_90_Mask)
plot(Dist_90)
Min_90 <- DFP_90_Mask@data@min
Min_90/1000 #105.1334 km <- migratory
```

```r
#Individual 90 with 75% Accuracy
Dist_90.2 <- qtlRaster(Mylu_PO2$F90, threshold=0.75,
                       thresholdType = "prob")
DFP_90.2 <- distanceFromPoints(Dist_90.2, xy_90)
DFP_90.2_Mask <- mask(DFP_90.2, Dist_90.2, maskvalue=0)
DFP_90.2_Mask <- mask(DFP_90.2_Mask, Dist_90.2)
plot(DFP_90.2_Mask)
plot(Dist_90.2)
Min_90.2 <- DFP_90.2_Mask@data@min
Min_90.2/1000 # 12.06433 km <- migratory

#Individual 90 with 90% Accuracy
Dist_90.3 <- qtlRaster(Mylu_PO2$F90, threshold=0.9,
                       thresholdType = "prob")
DFP_90.3 <- distanceFromPoints(Dist_90.3, xy_90)
DFP_90.3_Mask <- mask(DFP_90.3, Dist_90.3, maskvalue=0)
DFP_90.3_Mask <- mask(DFP_90.3_Mask, Dist_90.3)
plot(DFP_90.3_Mask)
plot(Dist_90.3)
Min_90.3 <- DFP_90.3_Mask@data@min
Min_90.3/1000 # 0.3734421 km

#Plot
terra::plot(Dist_90.2, legend=FALSE, xlab="Longitude",
            ylab="Latitude")
points(x = x,
       y = y,
       pch = 16,
       cex = 0.75,
       col = "black")
text(x=-51.7, y=48.5, labels = "90", cex = 1)

##########Individual 91#######################

#Individual 91 with 50% Accuracy
Dist_91 <- qtlRaster(Mylu_PO2$D91, threshold=0.5,
                     thresholdType = "prob")
xy_91 <- c(x,y)
DFP_91 <- distanceFromPoints(Dist_91, xy_91)
DFP_91_Mask <- mask(DFP_91, Dist_91, maskvalue=0)
DFP_91_Mask <- mask(DFP_91_Mask, Dist_91)
plot(DFP_91_Mask)
plot(Dist_91)
Min_91 <- DFP_91_Mask@data@min
```

```r
Min_91/1000 #105.9416 km <- migratory

#Individual 91 with 75% Accuracy
Dist_91.2 <- qtlRaster(Mylu_PO2$D91, threshold=0.75,
                       thresholdType = "prob")
DFP_91.2 <- distanceFromPoints(Dist_91.2, xy_91)
DFP_91.2_Mask <- mask(DFP_91.2, Dist_91.2, maskvalue=0)
DFP_91.2_Mask <- mask(DFP_91.2_Mask, Dist_91.2)
plot(DFP_91.2_Mask)
plot(Dist_91.2)
Min_91.2 <- DFP_91.2_Mask@data@min
Min_91.2/1000 #24.06622 km <- migratory

#Individual 91 with 90% Accuracy
Dist_91.3 <- qtlRaster(Mylu_PO2$D91, threshold=0.9,
                       thresholdType = "prob")
DFP_91.3 <- distanceFromPoints(Dist_91.3, xy_91)
DFP_91.3_Mask <- mask(DFP_91.3, Dist_91.3, maskvalue=0)
DFP_91.3_Mask <- mask(DFP_91.3_Mask, Dist_91.3)
plot(DFP_91.3_Mask)
plot(Dist_91.3)
Min_91.3 <- DFP_91.3_Mask@data@min
Min_91.3/1000 #0.3099001 km

#Plot
terra::plot(Dist_91.2, legend=FALSE, xlab="Longitude",
            ylab="Latitude")
points(x = x,
       y = y,
       pch = 16,
       cex = 0.75,
       col = "black")
text(x=-51, y=48.25, labels = "91 (D)", cex = 1)

##########Individual 95#######################

#Individual 95 with 50% Accuracy
Dist_95 <- qtlRaster(Mylu_PO2$F95, threshold=0.5,
                     thresholdType = "prob")
xy_95 <- c(x,y)
DFP_95 <- distanceFromPoints(Dist_95, xy_95)
DFP_95_Mask <- mask(DFP_95, Dist_95, maskvalue=0)
DFP_95_Mask <- mask(DFP_95_Mask, Dist_95)
plot(DFP_95_Mask)
plot(Dist_95)
```

```r
Min_95 <- DFP_95_Mask@data@min
Min_95/1000 #63.20354 km <- migratory

#Individual 95 with 75% Accuracy
Dist_95.2 <- qtlRaster(Mylu_PO2$F95, threshold=0.75,
                       thresholdType = "prob")
DFP_95.2 <- distanceFromPoints(Dist_95.2, xy_95)
DFP_95.2_Mask <- mask(DFP_95.2, Dist_95.2, maskvalue=0)
DFP_95.2_Mask <- mask(DFP_95.2_Mask, Dist_95.2)
plot(DFP_95.2_Mask)
plot(Dist_95.2)
Min_95.2 <- DFP_95.2_Mask@data@min
Min_95.2/1000 #4.48027 km <- migratory

#Individual 95 with 90% Accuracy
Dist_95.3 <- qtlRaster(Mylu_PO2$F95, threshold=0.9,
                       thresholdType = "prob")
DFP_95.3 <- distanceFromPoints(Dist_95.3, xy_95)
DFP_95.3_Mask <- mask(DFP_95.3, Dist_95.3, maskvalue=0)
DFP_95.3_Mask <- mask(DFP_95.3_Mask, Dist_95.3)
plot(DFP_95.3_Mask)
plot(Dist_95.3)
Min_95.3 <- DFP_95.3_Mask@data@min
Min_95.3/1000 #0.4110647 km

#Plot
terra::plot(Dist_95.2, legend=FALSE, xlab="Longitude",
            ylab="Latitude")
points(x = x,
       y = y,
       pch = 16,
       cex = 0.75,
       col = "black")
text(x=-58, y=50.4, labels = "95", cex = 1)


##########Individual 96#######################

#Individual 96 with 50% Accuracy
Dist_96 <- qtlRaster(Mylu_PO2$F96, threshold=0.5,
                     thresholdType = "prob")
xy_96 <- c(x,y)
DFP_96 <- distanceFromPoints(Dist_96, xy_96)
DFP_96_Mask <- mask(DFP_96, Dist_96, maskvalue=0)
DFP_96_Mask <- mask(DFP_96_Mask, Dist_96)
plot(DFP_96_Mask)
```

```r
plot(Dist_96)
Min_96 <- DFP_96_Mask@data@min
Min_96/1000 #157.4314 km <- migratory

#Individual 96 with 75% Accuracy
Dist_96.2 <- qtlRaster(Mylu_PO2$F96, threshold=0.75,
                       thresholdType = "prob")
DFP_96.2 <- distanceFromPoints(Dist_96.2, xy_96)
DFP_96.2_Mask <- mask(DFP_96.2, Dist_96.2, maskvalue=0)
DFP_96.2_Mask <- mask(DFP_96.2_Mask, Dist_96.2)
plot(DFP_96.2_Mask)
plot(Dist_96.2)
Min_96.2 <- DFP_96.2_Mask@data@min
Min_96.2/1000 #85.81359 km <- migratory

#Individual 96 with 90% Accuracy
Dist_96.3 <- qtlRaster(Mylu_PO2$F96, threshold=0.9,
                       thresholdType = "prob")
DFP_96.3 <- distanceFromPoints(Dist_96.3, xy_96)
DFP_96.3_Mask <- mask(DFP_96.3, Dist_96.3, maskvalue=0)
DFP_96.3_Mask <- mask(DFP_96.3_Mask, Dist_96.3)
plot(DFP_96.3_Mask)
plot(Dist_96.3)
Min_96.3 <- DFP_96.3_Mask@data@min
Min_96.3/1000 #4.48027 km

#Plot
terra::plot(Dist_96.2, legend=FALSE, xlab="Longitude",
            ylab="Latitude")
points(x = x,
       y = y,
       pch = 16,
       cex = 0.75,
       col = "black")
text(x=-58, y=50.4, labels = "96", cex = 1)

##########Individual 100#######################

#Individual 100 with 50% Accuracy
Dist_100 <- qtlRaster(Mylu_PO2$D100, threshold=0.5,
                      thresholdType = "prob")
xy_100 <- c(x,y)
DFP_100 <- distanceFromPoints(Dist_100, xy_100)
DFP_100_Mask <- mask(DFP_100, Dist_100, maskvalue=0)
DFP_100_Mask <- mask(DFP_100_Mask, Dist_100)
```

```r
plot(DFP_100_Mask)
plot(Dist_100)
Min_100 <- DFP_100_Mask@data@min
Min_100/1000 #0.5336292 km <- non-migratory

#Individual 100 with 75% Accuracy
Dist_100.2 <- qtlRaster(Mylu_PO2$D100, threshold=0.75,
                        thresholdType = "prob")
DFP_100.2 <- distanceFromPoints(Dist_100.2, xy_100)
DFP_100.2_Mask <- mask(DFP_100.2, Dist_100.2, maskvalue=0)
DFP_100.2_Mask <- mask(DFP_100.2_Mask, Dist_100.2)
plot(DFP_100.2_Mask)
plot(Dist_100.2)
Min_100.2 <- DFP_100.2_Mask@data@min
Min_100.2/1000 #0.3854591 km <- non-migratory

#Individual 100 with 90% Accuracy
Dist_100.3 <- qtlRaster(Mylu_PO2$D100, threshold=0.9,
                        thresholdType = "prob")
DFP_100.3 <- distanceFromPoints(Dist_100.3, xy_100)
DFP_100.3_Mask <- mask(DFP_100.3, Dist_100.3, maskvalue=0)
DFP_100.3_Mask <- mask(DFP_100.3_Mask, Dist_100.3)
plot(DFP_100.3_Mask)
plot(Dist_100.3)
Min_100.3 <- DFP_100.3_Mask@data@min
Min_100.3/1000 #0.3854591 km

#Plot
terra::plot(Dist_100.2, legend=FALSE, xlab="Longitude",
            ylab="Latitude")
points(x = x,
       y = y,
       pch = 16,
       cex = 0.75,
       col = "black")
text(x=-61.5, y=48.5, labels = "100 (D)", cex = 1)

##########Individual 101######################

#Individual 101 with 50% Accuracy
Dist_101 <- qtlRaster(Mylu_PO2$D101, threshold=0.5,
                      thresholdType = "prob")
xy_101 <- c(x,y)
DFP_101 <- distanceFromPoints(Dist_101, xy_101)
DFP_101_Mask <- mask(DFP_101, Dist_101, maskvalue=0)
```

```r
DFP_101_Mask <- mask(DFP_101_Mask, Dist_101)
plot(DFP_101_Mask)
plot(Dist_101)
Min_101 <- DFP_101_Mask@data@min
Min_101/1000 #139.4958 km <- Migratory

#Individual 101 with 75% Accuracy
Dist_101.2 <- qtlRaster(Mylu_PO2$D101, threshold=0.75,
                        thresholdType = "prob")
DFP_101.2 <- distanceFromPoints(Dist_101.2, xy_101)
DFP_101.2_Mask <- mask(DFP_101.2, Dist_101.2, maskvalue=0)
DFP_101.2_Mask <- mask(DFP_101.2_Mask, Dist_101.2)
plot(DFP_101.2_Mask)
plot(Dist_101.2)
Min_101.2 <- DFP_101.2_Mask@data@min
Min_101.2/1000 #100.9227 km <- Migratory

#Plot
terra::plot(Dist_101, legend=FALSE, xlab="Longitude",
            ylab="Latitude")
points(x = x,
       y = y,
       pch = 16,
       cex = 0.75,
       col = "black")
text(x=-59, y=49.75, labels = "101 (D)", cex = 1)

##########Individual 102#######################

#Individual 102 with 50% Accuracy
Dist_102 <- qtlRaster(Mylu_PO2$D102, threshold=0.5,
thresholdType = "prob")
xy_102 <- c(x,y)
DFP_102 <- distanceFromPoints(Dist_102, xy_102)
DFP_102_Mask <- mask(DFP_102, Dist_102, maskvalue=0)
DFP_102_Mask <- mask(DFP_102_Mask, Dist_102)
plot(DFP_102_Mask)
plot(Dist_102)
Min_102 <- DFP_102_Mask@data@min
Min_102/1000 #119.3444 km <- Migratory

#Individual 102 with 75% Accuracy
Dist_102.2 <- qtlRaster(Mylu_PO2$D102, threshold=0.75,
                        thresholdType = "prob")
DFP_102.2 <- distanceFromPoints(Dist_102.2, xy_102)
```

```r
DFP_102.2_Mask <- mask(DFP_102.2, Dist_102.2, maskvalue=0)
DFP_102.2_Mask <- mask(DFP_102.2_Mask, Dist_102.2)
plot(DFP_102.2_Mask)
plot(Dist_102.2)
Min_102.2 <- DFP_102.2_Mask@data@min
Min_102.2/1000 #45.53257 km <- migratory

#Plot
terra::plot(Dist_102.2, legend=FALSE, xlab="Longitude",
            ylab="Latitude")
points(x = x,
       y = y,
       pch = 16,
       cex = 0.75,
       col = "black")
text(x=-57, y=49.9, labels = "102 (D)", cex = 1)

##########Individual 50#######################

#Individual 50 with 50% Accuracy
Dist_50 <- qtlRaster(Mylu_PO2$D50, threshold=0.5,
                     thresholdType = "prob")
xy_50 <- c(x, y)
DFP_50 <- distanceFromPoints(Dist_50, xy_50)
DFP_50_Mask <- mask(DFP_50, Dist_50, maskvalue=0)
DFP_50_Mask <- mask(DFP_50_Mask, Dist_50)
plot(DFP_50_Mask)
plot(Dist_50)
Min_50 <- DFP_50_Mask@data@min
Min_50/1000 #275.3971 km <- migratory

#Individual 50 with 75% Accuracy
Dist_50.2 <- qtlRaster(Mylu_PO2$D50, threshold=0.75,
                       thresholdType = "prob")
DFP_50.2 <- distanceFromPoints(Dist_50.2, xy_50)
DFP_50.2_Mask <- mask(DFP_50.2, Dist_50.2, maskvalue=0)
DFP_50.2_Mask <- mask(DFP_50.2_Mask, Dist_50.2)
plot(DFP_50.2_Mask)
plot(Dist_50.2)
Min_50.2 <- DFP_50.2_Mask@data@min
Min_50.2/1000 #199.1041 km <- migratory

#Plot
terra::plot(Dist_50.2, legend=FALSE, xlab="Longitude",
            ylab="Latitude")
```

```r
points(x = x,
       y = y,
       pch = 16,
       cex = 0.75,
       col = "black")
text(x=-58, y=54.15, labels = "50 (D)", cex = 1)


##########Individual 98#######################

#Individual 98 with 50% Accuracy
Dist_98 <- qtlRaster(Mylu_PO2$D98, threshold=0.5,
                     thresholdType = "prob")
xy_98 <- c(x, y)
DFP_98 <- distanceFromPoints(Dist_98, xy_98)
DFP_98_Mask <- mask(DFP_98, Dist_98, maskvalue=0)
DFP_98_Mask <- mask(DFP_98_Mask, Dist_98)
plot(DFP_98_Mask)
plot(Dist_98)
Min_98 <- DFP_98_Mask@data@min
Min_98/1000 #0.1771997 km <- non-migratory

#Individual 98 with 75% Accuracy
Dist_98.2 <- qtlRaster(Mylu_PO2$D98, threshold=0.75,
                       thresholdType = "prob")
DFP_98.2 <- distanceFromPoints(Dist_98.2, xy_98)
DFP_98.2_Mask <- mask(DFP_98.2, Dist_98.2, maskvalue=0)
DFP_98.2_Mask <- mask(DFP_98.2_Mask, Dist_98.2)
plot(DFP_98.2_Mask)
plot(Dist_98.2)
Min_98.2 <- DFP_98.2_Mask@data@min
Min_98.2/1000 #0.1771997 km <- non-migratory

#Plot
terra::plot(Dist_98.2, legend=FALSE, xlab="Longitude",
            ylab="Latitude")
points(x = x,
       y = y,
       pch = 16,
       cex = 0.75,
       col = "black")
text(x=-67.9, y=54.5, labels = "98 (D)", cex = 1)


##########Individual 99#######################

#Individual 99 with 50% Accuracy
```

```r
Dist_99 <- qtlRaster(Mylu_PO2$D99, threshold=0.5,
                     thresholdType = "prob")
xy_99 <- c(x, y)
DFP_99 <- distanceFromPoints(Dist_99, xy_99)
DFP_99_Mask <- mask(DFP_99, Dist_99, maskvalue=0)
DFP_99_Mask <- mask(DFP_99_Mask, Dist_99)
plot(DFP_99_Mask)
plot(Dist_99)
Min_99 <- DFP_99_Mask@data@min
Min_99/1000 #106.121 km <- migratory

#Individual 99 with 75% Accuracy
Dist_99.2 <- qtlRaster(Mylu_PO2$D99, threshold=0.75,
                       thresholdType = "prob")
DFP_99.2 <- distanceFromPoints(Dist_99.2, xy_99)
DFP_99.2_Mask <- mask(DFP_99.2, Dist_99.2, maskvalue=0)
DFP_99.2_Mask <- mask(DFP_99.2_Mask, Dist_99.2)
plot(DFP_99.2_Mask)
plot(Dist_99.2)
Min_99.2 <- DFP_99.2_Mask@data@min
Min_99.2/1000 #3.718046 km <- migratory

#Individual 99 with 90% Accuracy
Dist_99.3 <- qtlRaster(Mylu_PO2$D99, threshold=0.9,
                       thresholdType = "prob")
DFP_99.3 <- distanceFromPoints(Dist_99.3, xy_99)
DFP_99.3_Mask <- mask(DFP_99.3, Dist_99.3, maskvalue=0)
DFP_99.3_Mask <- mask(DFP_99.3_Mask, Dist_99.3)
plot(DFP_99.3_Mask)
plot(Dist_99.3)
Min_99.3 <- DFP_99.3_Mask@data@min
Min_99.3/1000 #0.2190044 km

#Plot
terra::plot(Dist_99.2, legend=FALSE, xlab="Longitude",
            ylab="Latitude")
points(x = x,
       y = y,
       pch = 16,
       cex = 0.75,
       col = "black")
text(x=-61.3, y=54, labels = "99 (D)", cex = 1)
```

Appendix IV. *R code used to generate δ³⁴S isoscape. Obtained from Bataille et al., 2021, with small modifications for this project.*

```
#δ34S Isoscape – rf regression
#Clear R's brain and set directory
rm(list=ls())
setwd("C:/Users/caral/Documents/Bats_NL/Sulfur Isoscape")
getwd()
###Create a Figure folder in your directory
###Add Table S1 in your directory

#Open packages used in workflow
library(parallel)
library(doParallel)
library(raster)
library(randomForest)
library(readxl)
library(proj4)
library(rgdal)
library(gdalUtils)
library(exactextractr)
library("rnaturalearth")
library("rnaturalearthdata")
library(ggpubr)
library(cowplot)
library(rasterVis)
library(RColorBrewer)
library(colorRamps)
library(caret)
library(gridExtra)
library("ggspatial")
library(assignR)
library(gstat)
library(GSIF)
library(sp)
library("ranger")
library(dplyr)

#Start random forest regression
#Input observations

#Load sulfur data from compiled database
#Call the data
Lichen_NL <-read.csv("C:/Users/caral/Documents/
          Bats_NL/Sulfur Isoscape/LICHENlocations_2.csv")
```

```r
View(Lichen_NL)
#Clean up the data
Lichen_NL<-Lichen_NL[!is.na(Lichen_NL$Î.34S),]
d34S<-Lichen_NL[!is.na(Lichen_NL$Î.34S),]
coordinates(d34S) <- c(2,3)
proj4string(d34S) <- CRS("+init=EPSG:2962")
crs(d34S)

#Input covariates from Bataille et al. 2021
setwd("C:/Users/caral/Documents/Bats_NL/Sr
      Isoscape/Projected_rasters")
r.mat=raster("mat_reproj.tif")
r.fert=raster("nfert_reproj.tif")
r.dust = raster("dust_reproj.tif")
r.map = raster("map_reproj.tif")
r.salt = raster("salt_reproj.tif")
r.ai = raster("ai_reproj.tif")
r.pet = raster("pet_reproj.tif")
r.elevation = raster("elevation_reproj.tif")
r.clay = raster("rclay_reproj.tif")
r.ph = raster("rph_reproj.tif")
r.cec = raster("rcec_reproj.tif")
r.bulk = raster("rbulk_reproj.tif")
r.age =raster("basement_age_reproj.tif")
r.m1 = raster("rm1_reproj.tif")
r.maxage_geol=raster("agemax.tif")
r.minage_geol=raster("agemin.tif")
r.meanage_geol=raster("agemean.tif")
r.sr=raster("rf_plantsoilmammal1.tif")
r.bouger=raster("bouger_reproj.tif")
r.ssa=raster("ssa.tif")
r.ssaw=raster("ssaw.tif")
r.xx=raster("xx.tif")
#This is a distance to the coast raster file that we made
#for our study area
r.distance<-raster("dist_newfoundland.tif")
#This is a distance to point source pollutants raster file
#that we made for our study area
r.pollutant<-raster("dp.tif")

#Change the wd back to the original
setwd("C:/Users/caral/Documents/Bats_NL/Sulfur Isoscape")
getwd()

#Extract raster values at observations
```

```r
#Extract from raw and transformed rasters
Mode <- function(x) {
  ux <- unique(x)
  ux[which.max(tabulate(match(x, ux)))]
}

m1xy <- extract(r.m1,d34S,method='simple',
                buffer=7000,fun=Mode,na.rm=TRUE)
agexy <- extract(r.age,d34S,method='simple',na.rm=TRUE)
dustxy <- extract(r.dust,d34S,method='bilinear',na.rm=TRUE)
saltxy <- extract(r.salt,d34S,method='bilinear',na.rm=TRUE)
mapxy <- extract(r.map,d34S,method='simple',buffer=7000,
                 fun=mean,na.rm=TRUE)
aixy <- extract(r.ai,d34S,method='bilinear',buffer=7000,
                fun=mean,na.rm=TRUE)
petxy <- extract(r.pet,d34S,method='bilinear',buffer=7000,
                 fun=mean,na.rm=TRUE)
elevationxy <- extract(r.elevation,d34S,method='simple',
                       buffer=7000,fun=mean,na.rm=TRUE)
clayxy <- extract(r.clay,d34S,method='simple',buffer=7000,
                  fun=Mode,na.rm=TRUE)
phxy <- extract(r.ph,d34S,method='simple',buffer=7000,
                fun=Mode,na.rm=TRUE)
cecxy <- extract(r.cec,d34S,method='simple',buffer=7000,
                 fun=Mode,na.rm=TRUE)
bulkxy <- extract(r.bulk,d34S,method='simple',buffer=7000,
                  fun=Mode,na.rm=TRUE)
minage_geolxy <- extract(r.minage_geol,d34S,method='simple',
                         buffer=7000,fun=Mode,na.rm=TRUE)
maxage_geolxy <- extract(r.maxage_geol,d34S,method='simple',
                         buffer=7000,fun=Mode,na.rm=TRUE)
meanage_geolxy <- extract(r.meanage_geol,d34S,buffer=7000,
                          fun=Mode,method='simple',
                          na.rm=TRUE)
srxy <- extract(r.sr,d34S,method='simple',buffer=7000,
                fun=Mode,na.rm=TRUE)
bougerxy <- extract(r.bouger,d34S,method='simple',
                    buffer=7000,fun=mean,na.rm=TRUE)
matxy <- extract(r.mat,d34S,method='bilinear',buffer=7000,
                 fun=mean,na.rm=TRUE)
fertxy <- extract(r.fert,d34S,method='bilinear',buffer=7000,
                  fun=mean,na.rm=TRUE)
ssaxy <- extract(r.ssa,d34S,method='bilinear',buffer=7000,
                 fun=mean,na.rm=TRUE)
ssawxy <- extract(r.ssaw,d34S,method='bilinear',buffer=7000,
```

```r
                            fun=mean,na.rm=TRUE)
distancexy <- extract(r.distance,d34S,method='bilinear',
                        buffer=7000,fun=mean,na.rm=TRUE)
xxxy <- extract(r.xx,d34S,method='simple',buffer=7000,
                fun=Mode,na.rm=TRUE)
pollutxy <- extract(r.pollutant,d34S,method='bilinear',
                      buffer=7000,fun=mean,na.rm=TRUE)

#Append all extracted data into a summary table with the
#database
d34S_proj_xy <- data.frame(Lichen_NL$E,Lichen_NL$N,
                            Lichen_NL$Î.34S,Lichen_NL$S.ppm.,
                            m1xy,agexy,dustxy,mapxy,saltxy,
                            aixy,petxy,elevationxy,clayxy,
                            phxy,cecxy,bulkxy,minage_geolxy,
                            maxage_geolxy,meanage_geolxy,
                            srxy,bougerxy,matxy,fertxy,ssaxy,
                            ssawxy,xxxy,distancexy,pollutxy)

#Rename columns same as the rasters
colnames(d34S_proj_xy) <- c("Easting","Northing","d34S",
                            "S(ppm)","r.m1","r.age",
                            "r.dust","r.map","r.salt",
                            "r.ai","r.pet","r.elevation",
                            "r.clay","r.ph","r.cec",
                            "r.bulk","r.minage_geol",
                            "r.maxage_geol",
                            "r.meanage_geol","r.sr",
                            "r.bouger","r.mat","r.fert",
                            "r.ssa", "r.ssaw","r.xx",
                            "r.dist","r.pollut")

#Aggregate redundant lat/long
d34S_proj_xy <- d34S_proj_xy[complete.cases(d34S_proj_xy),]
d34S_agg<-d34S_proj_xy[complete.cases(d34S_proj_xy),]
write.csv(d34S_agg,file="regression_matrix.csv")

#Project subsetted dataset
coordinates(d34S_agg) <- c(1,2)
proj4string(d34S_agg) <- CRS("+init=EPSG:2962")
crs(d34S_agg)

#Select predictor using parallelized VSURF algorithm
library(VSURF)
set.seed(123)
```

```r
d34S_vsurf <- VSURF(d34S_proj_xy[,4:28],d34S_proj_xy$d34S,
                    RFimplem = "ranger",parallel = TRUE,
                    ncores = detectCores() - 1,clusterType =
                    "PSOCK")
d34S_vsurf$varselect.pred
plot(d34S_vsurf)
d34S_sub <- d34S_proj_xy[,1:3]
d34S_sub2 <- d34S_proj_xy[,4:28]

#automatic subsetting of selected variables
d34S_VSURF <- d34S_sub2[c(d34S_vsurf$varselect.pred)]
d34S_agg_VSURF <- cbind(d34S_sub, d34S_VSURF)

#Check the variables selected by VSURF
d34S_agg_VSURF
#Often VSURF still preserves some strong redundancies
#between variables that require some clean up

#Parallelize random forest modeling
cluster <- makeCluster(detectCores() - 1)
registerDoParallel(cluster)

# Splitting the data for repeated cross validation
fitControl <- trainControl(#10-fold crossvalidation
                           method="repeatedcv",
                           number=10,
                           #repeated ten times
                           repeats=5,
                           verboseIter=FALSE,
                           returnResamp="final",
                           savePredictions="all",
                           #with parallel backend
                           allowParallel=FALSE)

set.seed(124)

bestmtry <- tuneRF(training, training$d34S, stepFactor=1,
                   improve=1e-7, ntree=500)
mtry <- 2
tunegrid <- expand.grid(.mtry=mtry)
metric <- "Accuracy"

#Random forest training
RF_c <- train(d34S ~ r.pollut+r.dist+r.dust+r.bouger+r.ssaw,
```

```r
                    data=training,method="rf",importance=TRUE,
                    tuneGrid=tunegrid,trControl=fitControl)
RF_c

#Quantile random forest training
qrf_c <- ranger(d34S ~ r.bouger+r.ssaw+r.ssa,data=training,
                quantreg=TRUE,num.trees=500,seed=1)

#FIGURE Cross-Validation#
pdf("CV.pdf",width=6,height=6)
par(mfrow=c(1,1))
plot(RF_c$pred$pred,RF_c$pred$obs,pch=15,cex=0.4,
     xlab="d34Smod",ylab="d34Sobs",cex.lab=1,cex.axis=1)
lm2 <- lm(RF_c$pred$obs~RF_c$pred$pred)
abline(lm2)
dev.off()

#FIGURE Variable Importance#
pdf("\Importance.pdf",width=6,height=6)
par(mfrow=c(1,2))
varImpPlot(RF_c$finalModel,type=1)
varImpPlot(RF_c$finalModel,type=2)
plot(RF$finalModel,main='Error vs No. of trees plot: Base
     Model')
dev.off()


#FIGURE Model Residuals#
pred_RF_c_final <- predict(RF_c,d34S_agg)
residuals <- d34S_agg$d34S -pred_RF_c_final
train <- d34S_agg
train$resid <- residuals
train$absresid <- abs(residuals)
train$pred <- pred_RF_c_final

pdf("Residuals.pdf",width=6,height=4)
par(mfrow = c(1,2))
plot(train$pred,train$resid,pch=15,cex=0.4,log="x")
plot(train$pred,train$absresid,pch=15,cex=0.4,log="y")
dev.off()


#FIGURE Partial Dependence Plot#
#Combined plant, soil and local animals
pdf("PD.pdf",width=6,height=6)
```

```r
par(mfrow = c(2,2))
par(oma = c(1,1,1,1))
partialPlot(RF_c$finalModel,training,x.var="r.clay",main=NA)
partialPlot(RF_c$finalModel,training,x.var="r.m1",main=NA)
dev.off()


#Apply best model spatially
#Create a raster stack with all predictors
world_stack <- stack(r.dust,r.bouger,r.ssa)
names(world_stack) <- c("r.dust","r.bouger","r.ssa")
crs(world_stack)
r.dist <- projectRaster(r.distance,crs=crs(world_stack))
r.pol <- projectRaster(r.pollutant,crs=crs(world_stack))
crs(r.dist)
crs(r.pol)
extent(world_stack)
extent(r.dist)
extent(r.pol)


#Clip raster stack to smallest extent
e <- as(extent(-5125237,-3893187,5627237,6489317),
        'SpatialPolygons')
crs(e) <- crs(r.dist)
crs(e)
r_stack <- crop(world_stack,e)
r_dist <- crop(r.dist,e)
extent(r_stack)
extent(r.dist)
r_stack_resample <- terra::resample(r_stack,r_dist,
                                    method="bilinear")
pol_resample <- terra::resample(r.pol, r_dist,
                                method="bilinear")
extent(r_stack_resample)
extent(r.dist)
NL_stack <- stack(r_stack_resample,r_dist,pol_resample)
names(NL_stack)<-c("r.dust","r.bouger","r.ssa","r.dist",
                   "r.pollut")
crs(NL_stack)

#Create a grid to apply model extent
#Generate gridded area of NL
CAN <- ne_states(country="Canada",returnclass="sp")
plot(CAN)
```

```
proj4string(CAN)
e <- as(extent(-64,-30,30,54),'SpatialPolygons')
crs(e) <- "+proj=longlat +datum=WGS84 +no_defs"
NL <- crop(CAN,e)
plot(NL)
proj4string(NL)

#Generate grid within area of NL, resolution 100 m
grid <- makegrid(NL,cellsize=0.1) #cellsize in map units!
#grid is a data.frame. We need to change it to a spatial
#data set
grid <- SpatialPoints(grid,proj4string=CRS(proj4string(NL)))
plot(NL)
plot(grid,pch=".",add=T)

#Tranform the grid
grid <- spTransform(grid,crs(NL_stack))
proj4string(grid)

#only extract the points in the limits of Newfoundland and
#Labrador
#NL.grid<-(NL_stack$r.clay/NL_stack$r.salt)*r.m1/r.m1
#crs(NL.grid)

#Apply random forest model spatially
rf2 <- predict(NL_stack,RF_c,ext=grid,na.rm=TRUE,
               overwrite=TRUE,progress='text')

#Save the isoscape raster
writeRaster(rf2,filename="rf_d34S_5",format="GTiff",
            overwrite=TRUE)

#Apply quantile random forest model spatially
sp_NL_stack <- as(NL_stack,"SpatialPixelsDataFrame")
sr.rfd_low <- predict(NL_stack,qrf_c,ext=NL.grid,
                      type="quantiles",quantiles=0.15,
                      fun=function(model, ...)
                      predict(model, ...)$predictions)
sr.rfd_high <- predict(NL_stack,qrf_c,ext=NL.grid,
                       type="quantiles",quantiles=0.841,
                       fun=function(model, ...)
                       predict(model, ...)$predictions)

#Calculate uncertainty raster for random forest model
sr.se <- sr.rfd_high-sr.rfd_low
```

```
sr.se <- sr.se/2
writeRaster(sr.se,filename="Output\\srse",format="GTiff",
            overwrite=TRUE)

#FIGURE Isoscape#
#Create breakpoints for random forest prediction map

library(maptools)
data("wrld_simpl") #from maptools package
wrld_simpl_p <- spTransform(wrld_simpl,crs(rf2))
crs(wrld_simpl_p)
crs(rf2)
nl_rf_e <- extent(rf2)
wrld_simpl_p <- crop(wrld_simpl_p, extent(NL_stack))
breakpoints<-c(0,2,4,6,8,10,12,14,16)
d34S_agg$Col <- matlab.like2(13)[as.numeric(cut(
                                  d34S_agg$d34S,breaks =
                                  breakpoints))]

pdf("d34S_isoscape.pdf",width=7,height=5)
par(mfrow=c(1,1))
plot(rf2,col=matlab.like2(13),breaks=breakpoints,axes=FALSE)
plot(wrld_simpl_p,add=TRUE)
points(d34S_agg$Easting,d34S_agg$Northing,pch=21,col="black"
,bg=d34S_agg$Col,cex=1.1)
#scaleBar(crs(na.dH_Hobson2012$mean),"topright",cex=1,
          seg.len=2,box.color = NULL)
dev.off()
```

Appendix V. *R code used to calculate the $\delta^{34}S$ transfer function and plot isoscape.*

```r
#Generating d34S TF and plotting isoscape

#Clear R's Brain
rm(list=ls())
#Check where R is looking
getwd()
#Tell R where to look
setwd("C:/Users/caral/Documents/Bats_NL/Sulfur Isoscape")
getwd()
#Open necessary packages
library("raster")
library("akima")
library(maptools)
library(ggplot2)

#Call up my rf model
d34S_rf <- raster("rf_d34S_5.tif")
crs(d34S_rf)

#Reproject to another coordinate system
NL_crs <- "+proj=longlat +datum=WGS84 +no_defs +ellps=WGS84"
NL_rf <- projectRaster(d34S_rf, crs=NL_crs)
plot(NL_rf)
extent(NL_rf)

p <- spPolygons(rbind(c(-60,45), c(-60,50), c(-57,51.3),
                      c(-55,52.3), c(-52,52), c(-52,45)))
plot(p, add=TRUE, lwd=4, border='red')

NL_rf <- crop(NL_rf, p)
NL_rf <- mask(NL_rf, p)
plot(NL_rf)

#Now I can extract d34S values at my bat locations
#Then I'll extract the d34S prediction values
d34S_rf_Prediction <- raster::extract(NL_rf, d34S_Predict)
#Bind these values to the original dataframe
KO_Bats_NL_rf <- cbind(KO_Bats, d34S_rf_Prediction)
#And save the data
write.csv(KO_Bats_NL_rf, "d34S_Bats_NL_rf.csv")

#Create an SMA that relates predicted values to bat fur
library(smatr, quietly=TRUE)
```

```r
regression_data_rf <- read.csv("C:/Users/caral/Documents/
                               Bats_NL/Sulfur Isoscape/
                               d34S_Bats_NL_rf.csv")
regression_data_rf_2 <- regression_data_rf[2:13,]
SMA_rf <- sma(d34S.Fur~d34S.Predict,
              data=regression_data_rf)
plot(SMA_rf, pch = 16, col = "black", cex = 0.75)
summary(SMA_rf)
#fur = 0.5997693(isoscape) + 4.8742955 / p=0.64 / r2=0.02
smaresiduals_rf<-residuals(SMA_rf)
plot(smaresiduals_rf)
abline(a=0, b=0)
sd(smaresiduals_rf)

SMA_rf_2 <- sma(d34S.Fur~d34S.Predict,
                data=regression_data_rf_2)
plot(SMA_rf_2, pch = 16, col = "black", cex = 0.75)
summary(SMA_rf_2)
# fur = 0.5441464(isoscape) + 5.741454 / p=0.14  / r2=0.20

#Here I'm plotting my TF

#d34S using rf
d34S.transfer.rf <- ggplot(data = regression_data_rf,
                           aes(x=d34S.Predict, y=d34S.Fur))
                           + geom_point(size=5) +
                           theme(axis.title=element_text(
                                 size=30),
                           axis.text=element_text(size=30),
                           plot.title =
                           element_text(hjust=0.5, size=40,
                                        face="bold")) +
                           geom_abline(data=SMA_rf$data,
                           aes(intercept=4.9190935,
                               slope=0.5987294), color =
                               "black", size = 1.5) +
                           ylab(expression(paste(
                                     italic(delta)^
                                     {34},'S'
                                     [italic(fur)],
                                     '(\u2030
                                     VCDT)'))) +
                      xlab(expression(paste(
                                italic(delta)^
                                {34}, 'S'
```

```
                                      [italic(iso)],
                                      '(\u2030
                                      VCDT)'))) +
                      annotate("text", x = 11, y = 9.5,
                              xmin = NULL, xmax =
                              NULL, ymin = NULL,
                              ymax = NULL, xend =
                              NULL, yend =
                              NULL, size = 8, label =
                              "y = 0.60 x + 4.92") +
                      annotate("text", x = 11, y = 9.1,
                              xmin = NULL, xmax =
                              NULL, ymin = NULL, ymax
                              = NULL, xend = NULL,
                              yend = NULL, size = 8,
                              label = expression(
                              paste(italic(r)^{2}, '=
                              0.02'))) +
                      annotate("text", x = 11, y = 8.7,
                              xmin = NULL, xmax =
                              NULL, ymin = NULL,
                              ymax = NULL, xend =
                              NULL, yend =
                              NULL, size = 8, label =
                              expression(paste(
                              italic(p), '=
                              0.65'))) +
                      geom_errorbar(aes(x = 10.86, ymin
                              = 12.62, ymax =
                              14.96), width =
                              0.08, size =
                              0.9) +
                      geom_errorbar(aes(x = 12.94, ymin
                              = 8.14,
                              ymax = 10.12),
                              width = 0.08,
                              size = 0.9)
d34S.transfer.rf

#Here I'm plotting my isoscape

#d34S using random forest
library(rasterVis)
gglayers <-  list(geom_tile(aes(fill = value)),
                coord_equal(),theme_bw(),
```

211

```r
                      scale_x_continuous(name = "Longitude",
                      expand = c(0,0)),
                      scale_y_continuous(name = "Latitude",
                      expand = c(0,0)))

lab1 <- list(gglayers, scale_fill_gradientn(name =
             expression(paste(delta^{34}, "S (\u2030)")),
             colours = hcl.colors(20, palette = "viridis"),
             na.value = "slategray1"))

gridExtra::grid.arrange(gplot(NL_rf) + lab1 +
                    theme(axis.title=
                          element_text(size=20),
                          axis.text=
                          element_text(size=20),
                          legend.text=
                          element_text(size=20),
                          legend.title=
                          element_text(size=20)))
```

Appendix VI. *R code used to calculate the $^{87}Sr/^{86}Sr$ transfer functions and plot isoscapes.*

```r
#Generating 87Sr/86Sr TF and plotting isoscape

#Clear R's Brain
rm(list=ls())
#Where is R looking?
getwd()
#Tell R where to look
setwd("C:/Users/caral/Documents/Bats_NL/AssignR")
#Check where r is looking
getwd()

#Open packages
library(assignR)
library(raster)
library(smatr)
library(rasterVis)
library(ggplot2)

#Here is the strontium isoscape from Bataille et al., 2020
Sr_B20 <- raster("rf_plantsoilmammal1.tif")
proj4string(Sr_B20)
Sr_B20_proj <- projectRaster(Sr_B20,
                             crs=crs("+init=epsg:4326"))
plot(Sr_B20_proj)

#Here I'm cropping the raster to the same extent as the d2H
#precipitation raster
e <- as(extent(-67.5, -52.5, 42, 57), 'SpatialPolygons')
crs(e) <- "+proj=longlat +datum=WGS84 +no_defs"
Sr_B20_NL <- crop(Sr_B20_proj, e, snap='near')
plot(Sr_B20_NL)

#Now I can plot the isoscape the way that I like it
gglayers <-  list(geom_tile(aes(fill = value)),
                  coord_equal(),theme_bw(),
                  scale_x_continuous(name = "Longitude",
                                     expand = c(0,0),
                                     breaks = waiver(),
                                     n.breaks = 6),
                  scale_y_continuous(name = "Latitude",
                                     expand = c(0,.1)))
```

```r
lab1 <- list(gglayers, scale_fill_gradientn(name =
                                        expression(
                                        paste({}^{87},
                                        "Sr/" ^{86},
                                        "Sr")), colours
                                        = hcl.colors(20,
                                        palette =
                                        "viridis"),
                                        na.value =
                                        "slategray1"))

gridExtra::grid.arrange(gplot(Sr_B20_NL) + lab1 +
                        theme(axis.title=
                                element_text(size=20),
                                axis.text=
                                element_text(size=20),
                                legend.text=
                                element_text(size=20),
                                legend.title=
                                element_text(size=20)))

#I need to extract data for each of my KO individuals
Mylu_Sr <- read.csv("Sr_latlong.csv")
coordinates(Mylu_Sr) <- c(2,3)
crs(Mylu_Sr) <- "+proj=longlat +ellps=WGS84 +datum=WGS84
                +no_defs"
Mylu_Sr_proj <- spTransform(Mylu_Sr,crs(proj4string
                                        (Sr_B20)))
crs(Sr_B20)
crs(Mylu_Sr_proj)
Sr_value <- extract(Sr_B20, Mylu_Sr_proj)
Mylu_Sr <- read.csv("Sr_latlong.csv")
Sr_all <- cbind(Mylu_Sr, Sr_value)
write.csv(Sr_all, file = "KO_GlobalIsoscape_Sr.csv")

#Now that I have the precip values I can run the regression
regression_data <- read.csv("KO_GlobalIsoscape_Sr.csv")
highlight_df <- regression_data %>%
  filter(Sample=="43")
regression_data <- regression_data %>%
  filter(Sample != "43")
SMA <- sma(Fur~Isoscape, data=regression_data)
plot(SMA, pch = 16, col = "black", cex = 0.75)
summary(SMA)
```

```r
# fur = 1.6579252(precip) - 0.4697068 <- r2 = 0.004 / p=0.83
smaresiduals<-residuals(SMA)
sd(smaresiduals)
plot(smaresiduals)
abline(a=0, b=0)
sd(smaresiduals)

#Now I can do my TF plot
library(dplyr)
highlight_df <- regression_data %>%
  filter(Sample=="43")

Sr.transfer.B20 <-ggplot(data = regression_data,
                   aes(x=Isoscape, y=Fur)) +
                   geom_point(size=5) +
                   geom_point(data=highlight_df,
                             aes(x=Isoscape,y=Fur),
                             color='red', size=5) +
                   theme(axis.title=
                       element_text(size=30),
                       axis.text=
                       element_text(size=30),
                       plot.title=
                       element_text(hjust=0.5,
                       size=40, face="bold")) +
                    geom_abline(data = SMA$data,aes(
                            intercept =
                            -0.5195452,
                            Slope = 1.7277899),
                            color = "black",
                            size = 1.5) +
                    ylab(expression(paste({}^{87},
                               'Sr/'^{86},
                               'Sr'[italic
                                  (fur)]))) +
                    xlab(expression(paste({}^{87},
                               'Sr/'^{86},
                               'Sr'[italic
                                  (iso)]))) +
                    scale_y_continuous(breaks =
                                waiver(),
                                n.breaks = 6) +
                    scale_x_continuous(breaks =
                                waiver(),
                                n.breaks = 6) +
```

```r
              annotate("text", x = 0.714, y =
                      0.710, xmin = NULL, xmax
                      = NULL, ymin = NULL, ymax
                      = NULL, xend = NULL, yend
                      = NULL, size = 8, label =
                      "y = 1.73 x - 0.52") +
              annotate("text", x = 0.714, y =
                      0.70945, xmin = NULL,
                      xmax = NULL, ymin =
                      NULL, ymax = NULL,
                      xend = NULL, yend =
                      NULL, size = 8, label =
                      expression(paste(italic
                              (r)^{2}, '=
                              0.004'))) +
              annotate("text", x = 0.714, y =
                      0.7088, xmin = NULL, xmax
                      = NULL, ymin = NULL, ymax
                      = NULL, xend = NULL, yend
                      = NULL, size = 8,
                      label =
                      expression(paste(
                              italic(p), '=
                              0.825'))) +
              geom_errorbar(aes(x = 0.712379754,
                      ymin = 0.708997725,
                      ymax = 0.712266275),
                      width = 0.00004, size
                      = 0.9) +
              geom_errorbar(aes(x = 0.712169707,
                      ymin = 0.712840726,
                      ymax = 0.713293274),
                      width = 0.00004, size
                      = 0.9) +
              geom_errorbar(aes(x = 0.712736905,
                      ymin = 0.711294087,
                      ymax = 0.712120),
                      width = 0.00004, size
                      = 0.9)
Sr.transfer.B20

#Here is the first strontium isoscape from Mael
Sr_LC <- raster("rf_alldata_pred_jan23.tif")
proj4string(Sr_LC)
plot(Sr_LC)
```

```r
Sr_LC_proj <- projectRaster(Sr_LC,crs=crs(
                                   "+init=epsg:4326"))
plot(Sr_LC_proj)

#Here I'm cropping the raster to the same extent as the d2H
#precipitation raster
e <- as(extent(-67.5, -52.5, 40, 57), 'SpatialPolygons')
crs(e) <- "+proj=longlat +datum=WGS84 +no_defs"
Sr_LC_NL <- crop(Sr_LC_proj, e, snap='near')
crs(Sr_LC_NL)
plot(Sr_LC_NL)

#Now I can plot the isoscape the way that I like it
gglayers <-  list(geom_tile(aes(fill = value)),
                  coord_equal(),theme_bw(),
                  scale_x_continuous(name = "Longitude",
                                     expand = c(0,0),
                                     breaks = waiver(),
                                     n.breaks = 6),
                  scale_y_continuous(name = "Latitude",
                                     expand = c(0,.1)))

lab1 <- list(gglayers, scale_fill_gradientn(name =
                                     expression(
                                     paste({}^{87},
                                     "Sr/" ^{86},
                                     "Sr")), colours
                                     = hcl.colors(20,
                                     palette =
                                     "viridis"),
                                     na.value =
                                     "slategray1"))

gridExtra::grid.arrange(gplot(Sr_B20_NL) + lab1 +
                        theme(axis.title=
                              element_text(size=20)
                              axis.text=
                              element_text(size=20),
                              legend.text=
                              element_text(size=20),
                              legend.title=
                              element_text(size=20)))

#I need to extract data for each of my KO individuals
```

```r
Mylu_Sr <- read.csv("Sr_latlong.csv")
coordinates(Mylu_Sr) <- c(2,3)
crs(Mylu_Sr) <- "+proj=longlat +ellps=WGS84 +datum=WGS84
                 +no_defs"
Mylu_Sr_proj <- spTransform(Mylu_Sr,
                             crs(proj4string(Sr_LC)))
crs(Sr_LC)
crs(Mylu_Sr_proj)
Sr_value <- extract(Sr_LC, Mylu_Sr_proj)
Mylu_Sr <- read.csv("Sr_latlong.csv")
Sr_all <- cbind(Mylu_Sr, Sr_value)
write.csv(Sr_all, file = "KO_Isoscape_Sr.csv")

#Now that I have the precip values I can run the regression
regression_data <- read.csv("KO_Isoscape_Sr.csv")
regression_data <- regression_data %>%
  filter(Sample != "43")
SMA <- sma(Fur~Isoscape, data=regression_data)
plot(SMA, pch = 16, col = "black", cex = 0.75)
summary(SMA)
#fur = 2.464693(precip) - 1.0443663 <- r2=0.20 / p=0.10
Smaresiduals <- residuals(SMA)
sd(smaresiduals)
plot(smaresiduals)
abline(a=0, b=0)
sd(smaresiduals)

#Now I can do my TF plot
library(dplyr)
highlight_df <- regression_data %>%
  filter(Sample=="43")
Sr.transfer.LC <- ggplot(data = regression_data,
                         aes(x=Isoscape, y=Fur)) +
                         geom_point(size=5) +
                         geom_point(data=highlight_df,
                                    aes(x=Isoscape,y=Fur),
                                    color='red',
                                    size=5) +
                         theme(axis.title=
                               element_text(size=30),
                               axis.text=
                               element_text(size=30),
                               plot.title =
                               element_text(hjust=0.5,
                               size=40, face="bold")) +
```

218

```r
geom_abline(data=SMA$data,
            aes(intercept=
                -1.0443663,
                slope=2.464693),
                color="black",
                size=1.5) +
ylab(expression(paste({}^{87},'Sr/'
                ^{86},
                'Sr'[italic
                    (fur)]))) +
xlab(expression(paste({}^{87},
                'Sr/'^{86},
                'Sr'[italic
                    (iso)]))) +
scale_y_continuous(breaks =
                waiver(),
                n.breaks = 6) +
scale_x_continuous(breaks =
                waiver(),
                n.breaks = 3) +
annotate("text", x = 0.7116, y =
        0.714, xmin = NULL, xmax =
        NULL, ymin = NULL, ymax =
        NULL, xend = NULL, yend =
        NULL, size = 8, label = "y
        = 2.46 x - 1.04") +
annotate("text", x = 0.7116, y =
        0.7135, xmin = NULL, xmax
        = NULL, ymin = NULL, ymax
        = NULL, xend = NULL, yend
        = NULL, size = 8, label =
        expression(paste(
        italic(r)^{2},
        '= 0.20'))) +
annotate("text", x = 0.7116, y =
        0.713, xmin = NULL, xmax =
        NULL, ymin = NULL, ymax =
        NULL, xend = NULL, yend =
        NULL, size = 8, label =
        expression(paste(
        italic(p),
        '= 0.10'))) +
geom_errorbar(aes(x = 0.71208483,
                ymin = 0.7089977,
```

```
                                              ymax = 0.712266),
                                     width = 0.00004,
                                     size = 0.9) +
                    geom_errorbar(aes(x = 0.712508619,
                                              ymin = 0.7128407,
                                              ymax = 0.713293),
                                     width = 0.00004,
                                     size = 0.9) +
                    geom_errorbar(aes(x = 0.713103771,
                                              ymin = 0.7112941,
                                              ymax = 0.712120),
                                     width = 0.00004,
                                     size = 0.9)
Sr.transfer.LC
```

Appendix VII. *R code used to conduct regional fur assignments.*

```r
#Regional Fur Origin Assignments - NL Mylu 87Sr/86Sr values

#First I'll clear R's brain and tell it where to look
rm(list=ls())
getwd()
setwd("C:/Users/caral/Documents/Bats_NL/Sr Data")
getwd()

library(lattice)
library(gmodels)
library(car)
library(DescTools)
library(gridExtra)
library(forcats)
library(RColorBrewer)
library(ggpubr)
library(vctrs)

#Then I'll load the data
KO <- read.csv("C:/Users/caral/Documents/Bats_NL/Sr
                Data/Tissue Comparison.csv")
KO$Region.Found<-as.factor(KO$Region.Found)

#I'll subset the data
library(dplyr)
KO_Western <- KO %>% filter(Region.Found=="Western")
KO_Central <- KO %>% filter(Region.Found=="Central")
KO_Eastern <- KO %>% filter(Region.Found=="Eastern")

#Produce descriptive statistics by group
Western <- KO_Western %>%
  summarise(n = n(),
            mean = mean(Sr.Fur, na.rm = TRUE),
            sd = sd(Sr.Fur, na.rm = TRUE),
            stderr = sd/sqrt(n),
            LCL = mean - qt(1 - (0.05 / 2), n - 1) * stderr,
            UCL = mean + qt(1 - (0.05 / 2), n - 1) * stderr,
            median = median(Sr.Fur, na.rm = TRUE),
            min = 0.7112428,
            max = 0.7121400,
            IQR = IQR(Sr.Fur, na.rm = TRUE),
            Q3 = 0.7120340,
            Q1 = 0.7115176)
```

```r
Eastern <- KO_Eastern %>%
  summarise(n = n(),
            mean = mean(Sr.Fur, na.rm = TRUE),
            sd = sd(Sr.Fur, na.rm = TRUE),
            stderr = sd/sqrt(n),
            LCL = mean - qt(1 - (0.05 / 2), n - 1) * stderr,
            UCL = mean + qt(1 - (0.05 / 2), n - 1) * stderr,
            median = median(Sr.Fur, na.rm = TRUE),
            min = 0.7093641,
            max = 0.7106420,
            IQR = IQR(Sr.Fur, na.rm = TRUE),
            Q3 = 0.7103952,
            Q1 = 0.7096656)
Central <- KO_Central %>%
  summarise(n = n(),
            mean = mean(Sr.Fur, na.rm = TRUE),
            sd = sd(Sr.Fur, na.rm = TRUE),
            stderr = sd/sqrt(n),
            LCL = mean - qt(1 - (0.05 / 2), n - 1) * stderr,
            UCL = mean + qt(1 - (0.05 / 2), n - 1) * stderr,
            median = median(Sr.Fur, na.rm = TRUE),
            min = 0.7129070,
            max = 0.7153225,
            IQR = IQR(Sr.Fur, na.rm = TRUE),
            Q3 = 0.7142747,
            Q1 = 0.7130669)
Region_Data <- bind_rows(list("Western" = Western, "Eastern"
                              = Eastern, "Central" =
                              Central), .id= "Region")

#Produce Boxplots and visually check for outliers
library(ggplot2)
library(ggsignif)
Boxplot <- ggplot(KO, aes(x = Region.Found, y = Sr.Fur)) +
              stat_boxplot(geom = "errorbar", width =
                              0.5) +
              geom_boxplot(fill = "light blue") +
              theme_bw() + theme(legend.position=
                              "none",
                              axis.title=element_text
                              (size=25),
                              legend.title=
                              element_text
                              (size=20),
                              axis.text=element_text
```

```
                                      (size=20, hjust=0.5)) +
              scale_y_continuous(breaks = c(0.710,
                                  0.711, 0.712, 0.713,
                                  0.714, 0.715, 0.716)) +
              ylab(expression(paste({}^{87},'Sr/',
                              {}^{86},'Sr'))) +
              xlab("Region")

Boxplot + scale_x_discrete(limits = c("Western", "Central",
                              "Eastern")) +
        geom_signif(comparisons = list(c("Western",
                                      "Central")),
                              test="wilcox.test",
                              map_signif_level=TRUE,
                              y_position = 0.7153,
                              tip_length = .015, vjust
                              = 0.4, textsize = 7) +
        geom_signif(comparisons = list(c("Western",
                                      "Eastern")),
                              test="wilcox.test",
                              map_signif_level=TRUE,
                              y_position = 0.716,
                              tip_length = .015, vjust
                              = 0.4, textsize = 7) +
        geom_signif(comparisons = list(c("Eastern",
                                      "Central")),
                              test="wilcox.test",
                              map_signif_level=TRUE,
                              y_position = 0.7156,
                              tip_length = .015, vjust
                              = 0.4, textsize = 7)

        geom_signif(stat="identity", data=
                    data.frame(x=c(0.875,1.875),
                    xend=c(1.125, 2.125),y=c(5.8, 8.5),
                    annotation=c("**", "NS")),
                    aes(x=x,xend=xend, y=y, yend=y,
                    annotation=annotation)) +
        geom_signif(comparisons=list(c("S1", "S2")),
                    annotations="***",y_position = 9.3,
                    tip_length = 0, vjust=0.4)

Boxplot_data <- ggplot_build(Boxplot)
```

```r
ggplot(AbsDiff, aes(x=Age, y=Diff.TB)) +
        stat_boxplot(geom="errorbar", width = 0.5) +
        geom_boxplot(fill= "light blue") +
        stat_summary(fun=mean, geom="point", shape=10,
                     size=3.5, color="black") +
        ggtitle("Tissue Comparison") +
        theme_bw() + theme(legend.position="none") +
        ylab("Abs Diff T/B")

#Plotting Sr Fur Origin Assignments
Sr_UO <- read.csv("SrFur_UO.csv")
Sr_UO <- Sr_UO %>%
  rename(c("Region" = "Region.Found", "Sample" =
           "ï..Sample", "Location Found" = "Location.Found",
           "Fur Sample" = "Fur.Sample"))

UO_plot <- ggplot(Sr_UO, aes(x = as.character(Sample), y =
                             X87Sr.86Sr, shape = `Fur
                             Sample`, color=Region)) +
                scale_color_manual(values = c("Western" =
                                              "#FC8D62",
                                              "Central" =
                                              "#f768a1",
                                              "Eastern" =
                                              "#66C2A5",
                                              Labrador =
                                              "#4393C3"))+
                annotate(geom="rect", fill = "#f768a1",
                         xmin = 0, xmax = 21, ymin =
                         0.7129070, ymax = 0.7153225,
                         Alpha = .1) +
                annotate(geom="rect", fill = "#66C2A5",
                         xmin = 0, xmax = 21, ymin =
                         0.7093641, ymax = 0.7106420,
                         alpha = .1) +
                annotate(geom="rect", fill = "#FC8D62",
                         xmin = 0, xmax = 21, ymin =
                         0.7112428, ymax = 0.7121400,
                         alpha = .1) +
                geom_point(size = 4) +
                scale_y_continuous(n.breaks = 8) +
                ylab(expression(paste({}^{87},'Sr/',
                                {}^{86},'Sr'))) +
                theme_bw() +
                theme(axis.title.y =
```

```
                    element_blank(),
                    axis.title=element_text(size=25),
                    legend.text=element_text(size=20),
                    legend.title=element_text(size=20),
                    axis.text=element_text(size=20,
                    hjust=0.5), axis.title.x =
                    element_blank()) +
            geom_hline(data=Region_Data,
                    aes(yintercept=median,
                    color=Region), linetype="solid") +
            geom_hline(data=Region_Data,
                    aes(yintercept=min, color=Region),
                    linetype = "dotted") +
            geom_hline(data=Region_Data,
                    aes(yintercept=max, color=Region),
                    linetype = "dotted") +
            geom_hline(data=Region_Data,
                    aes(yintercept=Q1, color=Region),
                    linetype = "dashed") +
            geom_hline(data=Region_Data,
                    aes(yintercept=Q3, color=Region),
                    linetype = "dashed")

UO_plot_spec <- UO_plot +
            scale_x_discrete(limits =
                        c("67","90","91","15",
                          "16","95","96","14",
                          "17","18","19","20",
                          "60","74","100","101",
                          "102","50","98","99"))

UO_plot_spec
```

Appendix VIII. *Summer residency predictions for all individuals of unknown origin based on $\delta^2 H_{\text{fur}}$ values and using the "qtlRaster" function in AssignR. Results indicate 50% probability of origin. Point denotes location of mortality with label specifying sample ID.*

228
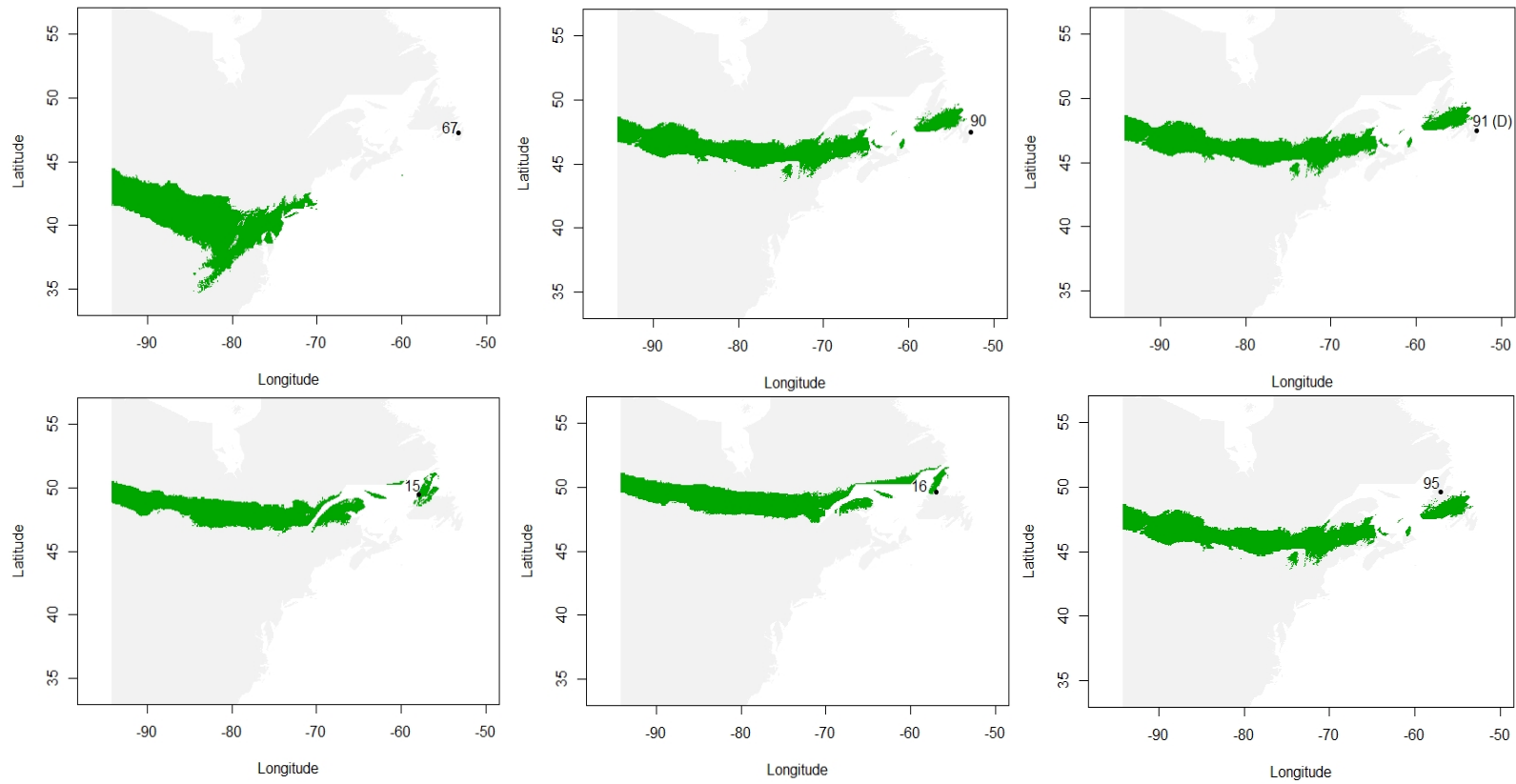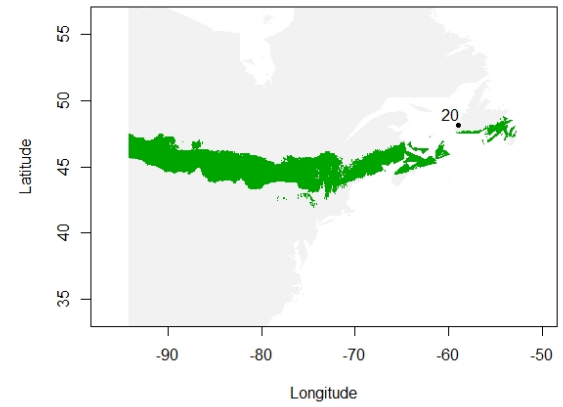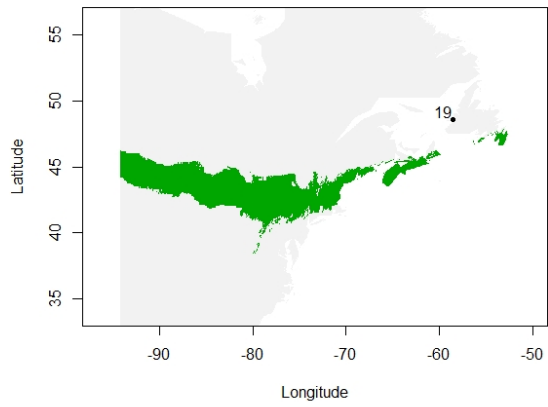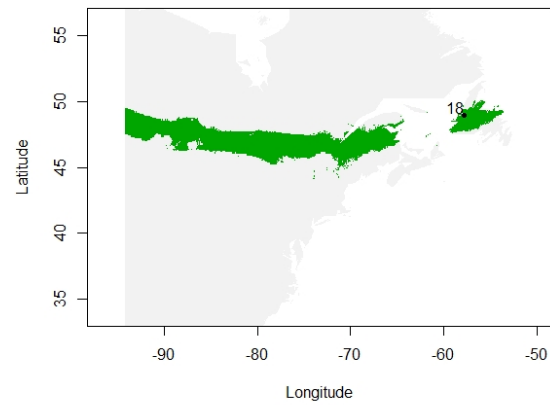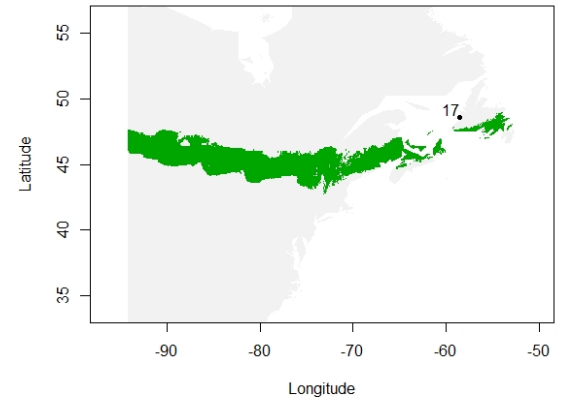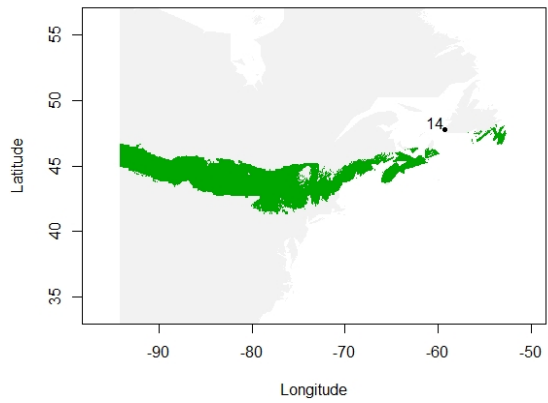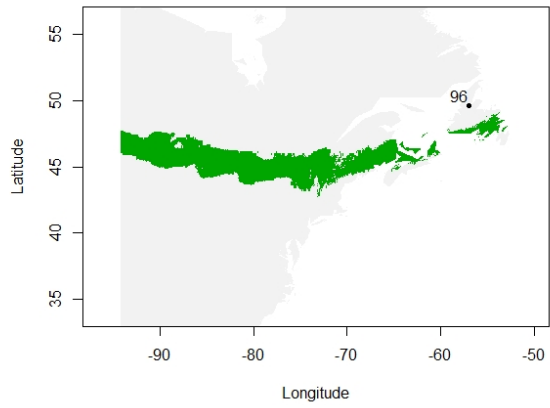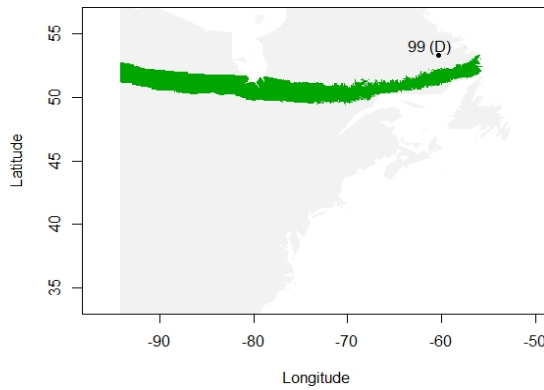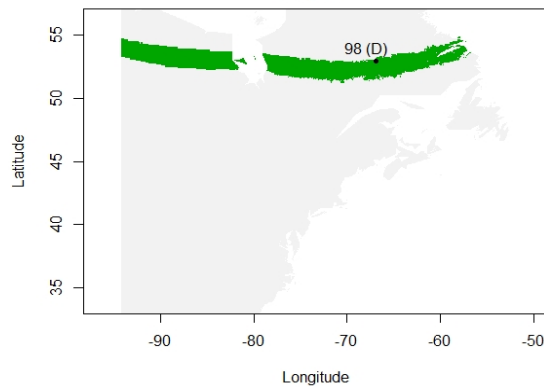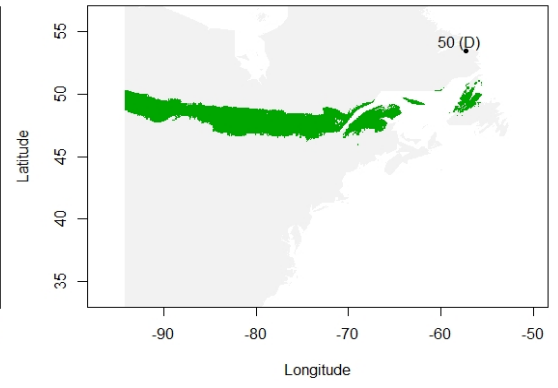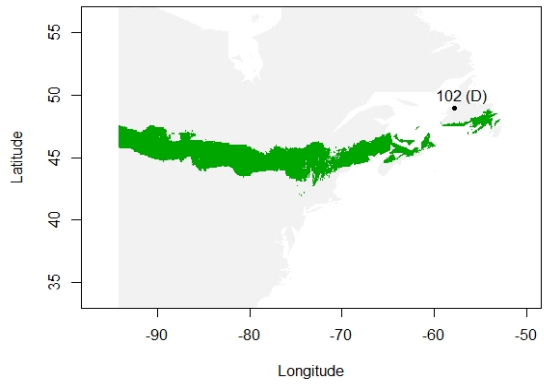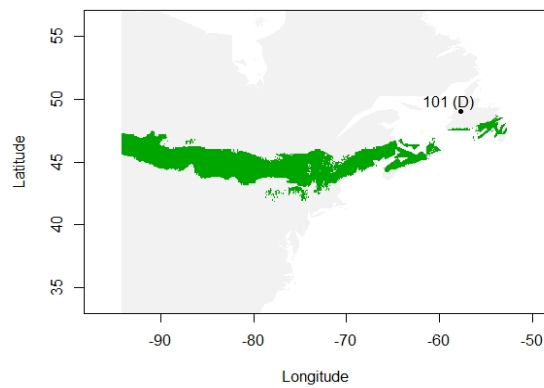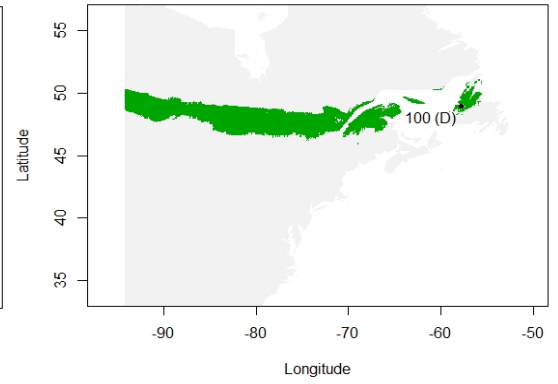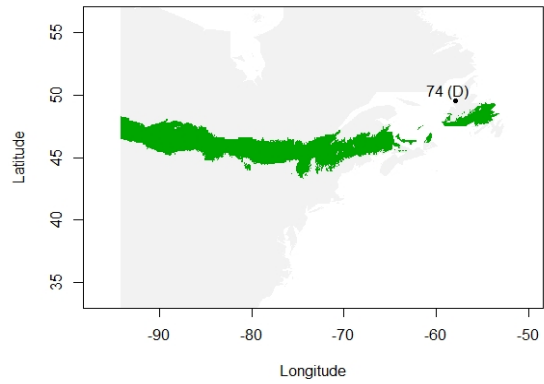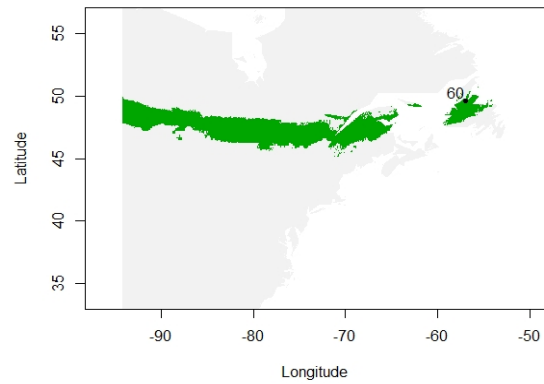
Appendix IX. *Summer residency predictions for all individuals of unknown origin based on δ²Hₑfur values and using the "qtlRaster" function in AssignR. Results indicate 75% probability of origin. Point denotes location of mortality with label specifying sample ID.*

231